VIETNAM JOURNAL OF HYDRO - METEOROLOGY

ISSN 2525 - 2208

VIETNAM METEOROLOGICAL AND HYDROLOGICAL ADMINISTRATION

No 09
12-2021

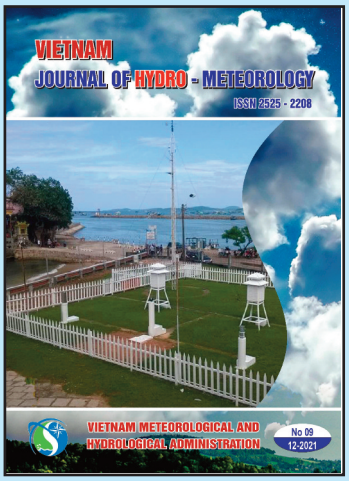

Publishing licence
No: 166/GP-BTTTT - Ministry of Information and Communication dated 17/04/2018

Editorial office
No 8 Phao Dai Lang, Dong Da, Ha Noi
Tel: 024.39364963
Email: tapchikttv@gmail.com

Engraving and printing
Vietnam Agriculture Investment Company Limited
Tel: 0243.5624399

VIETNAM JOURNAL OF HYDROMETEOROLOGY
Volume 09 - 12/2021

TABLE OF CONTENT

VIETNAM JOURNAL OF HYDROMETEOROLOGY

Rerearch paper

The assessment of visual acuity for low socioeconomic status kids by their environmental factors

Yu-Ting Hsiao[1,2], Yi-Ching Chen[3*]

[1] Department of Environmental Engineering, Da-Yeh University, Taiwan; a0908819180@gmail.com
[2] Public Healthcare Center of Tianwei Town, Taiwan; a0908819180@gmail.com
[3] Department of Environmental Engineering, Da-Yeh University, Taiwan; yiching@mail.dyu.edu.tw

*Corresponding author: yiching@mail.dyu.edu.tw; Tel.: +886–939107419

Received: 12 July 2021; Accepted: 25 August 2021; Published: 25 December 2021

Abstract: Although many studies have discussed visual acuity (VA), the childhood myopia epidemic has not been alleviated and requires further investigation. In this study, investigations were carried out on the difference in kids' VA by their environmental factors, such as various family structures, the effect of visual health attitudes (VHA) and visual health behaviours (VHB) on VA. The research subjects are selected for kids in low socioeconomic status (SES) families in Changhua County, Taiwan. This study conducted purposive sampling based on a questionnaire survey and combining a VA examination. There were 260 questionnaires collected, and significantly over 60% of the samples of low SES elementary school kids were not living with their both parents. Of these kids, the highest proportion (33.5%) lived with their mothers, sequentially, 32.7% with their grandparents and 30.0% with their fathers. In fact, 48.8% of these low SES kids' visions were below 0.9, which is 2.7% higher than the defective vision rate in Taiwan. These kids with poor VA mostly in worse VHA can lead to unhealthy VHB and ultimately to myopia. Some parents at low SES families were busy at making money rather than taking care of kids. Thus, kids addicted to playing 3C products at home without participating in leisure sports result in the rapid increase of myopia. According to the results of the study, "correct" VHA can lead to "correct" VHB; nevertheless, leisure sports participation (LSP) can lead to "correct" VHB for ensuring good VA for kids.

Keywords: Visual acuity (VA); Visual health attitudes (VHA); Visual health behaviours (VHB); Low socioeconomic status (SES).

1. Introduction

1.1. Prelude of study for visual acuity

The World Health Organization (WHO) estimates that there are 246 million visually impaired people worldwide and, in which, 90% of these people are of low socioeconomic status (SES) [1]. According to the WHO, 43% of moderate to severe visual impairment is caused by uncorrected refractive errors, such as myopia, hyperopia, astigmatism and presbyopia. Although, the WHO reports that worldwide socioeconomic development and concerted public health action have brought about a general decrease in visual impairment worldwide, there is a scholarly consensus that myopia is increasing worldwide and is approaching epidemic proportions in the industrialized nations of East Asia [2-5]. A strong negative association between prevalence rates of moderate-to-severe visual impairment

(MSVI) and blindness and socioeconomic level of development was observed [6]. Also, one recent study reports a prevalence of myopia as high as 86.1% among young Taiwanese men aged 18 to 24 years [7], and their visual impairment may happen early in kid age. Although myopia and other refractive error can be corrected with the aid of glasses, contact lenses and refractive surgeries, myopes will likely suffer to some degree from lost educational and employment opportunities, lost economic gain, and impaired quality of life [8–9]. Moreover, myopes are at a higher risk of blindness in old age. The increased prevalence of myopia is likely to lead to increases in the numbers of blind people, whose health care poses a serious socioeconomic burden to families and societies.

An observation was commonly found in children with visual impairment who resort to repetitive behaviour when the environment becomes too visually complex for them to cope with. Therefore, theory of Planned Behaviour (TPB) [10] can be applied to suggest that low-SES kids' behaviour can be predicted based on their attitudes under different environmental factors. The Theory of Planned Behavior (TPB) was developed by social psychologists and has been widely employed as a tool to aid our understanding of a variety of behaviors including health behaviors [11–12].

In this study, investigations were carried out on the difference in kids' VA by their environmental factors, such as various family structures, the effect of visual health attitudes (VHA) and visual health behaviours (VHB) on visual acuity (VA). Here, a model of TPB was formed to analyze VA for 260 kids in low SES families in Changhua County, Taiwan. VA is controlled by VHB which guided by attitude to the VHA and perceived behavioural control with leisure sports participation (LSP), too. The designed questionnaire was conducted on students counselled by social welfare organizations. A purposive sampling study and an examination of VA were also conducted as part of the preliminary study.

1.2. Environmental factors affecting visual acuity

More researches are needed to investigate whether unhealthy visual behaviours such as not doing sufficient daytime outdoor activity and obsessively watching electronic devices (e.g. smartphones, computer monitors or TV screens) are environmental factors in the development of myopia.

1.2.1. Myopia and outdoor activities

Myopia has traditionally been considered a hereditary condition, and many previous studies indicate that kids with myopia are more likely to have a family history of myopia [13–14]. However, there is a growing scholarly consensus that both environmental and hereditary factors play a role in the development of myopia. [15] reported that, in China, school kids in urban settings exhibit a higher prevalence of myopia than kids in rural settings, suggesting that environmental factors are involved in the kid's myopia development. A research in Japan by [16] mentioned that visual acuity of kids is influenced by hereditary and environmental factors. The lifestyle of kids has changed. Video games have become popular; kids must study hard in order to enter first-rank schools and they often stay up till late at night. Such circumstances might have some influence on their visual acuity. [17] found that a lower prevalence of myopia in Chinese kids raised in Sydney than in Chinese kids living in Singapore was associated with increased hours of outdoor activities.

1.2.2. Recent studies about childhood myopia

Many studies have shown that near work may be a significant factor in the development of childhood myopia. In Singapore, kids who read more than two books per week had a 1.43 and 3.05 higher incidence of low/ moderate myopia and high myopia than kids who read less than two books per week [18]. Besides reading books, the definition of near work might be expanded to include watching TV, playing computer games and using mobile devices, such

as smartphones and tablet computers. Many studies of myopia in industrialized East Asian countries have suggested that the problem is most acute among kids of higher socioeconomic status parents [19]. These studies may suggest that white collar parents pressurize their kids to do more near work at a younger age, putting their kids at greater risk of developing myopia.

2. Materials and methods

2.1. Hypotheses

The hypothesis that white-collar kids spend longer hours doing near work than blue collar kids do, might become somewhat less plausible, because it seems unlikely that white collar parents would put pressure on their kids to use electronic devices. More researches are needed before scholars can hypothesize confidently about the relationship between SES, near work and electronic devices. Based on the widely utilized TPB, which suggests that people's behaviour can be predicted based on their attitudes. The purpose of this study is to investigate the relationship between VHB and VHA. The study's hypotheses follow.

- H1: The low SES elementary school students' VHA will have a positive impact on VHB.
- H2: The low SES kids' LSP will have a positive impact on VHB.
- H3: VHB will have a positive impact on VA.

A TPB model as Figure 1 is created where VHB is guided by VHA and perceived behavioural control LSP. Finally, behaviour (VA) is controlled by VHB.

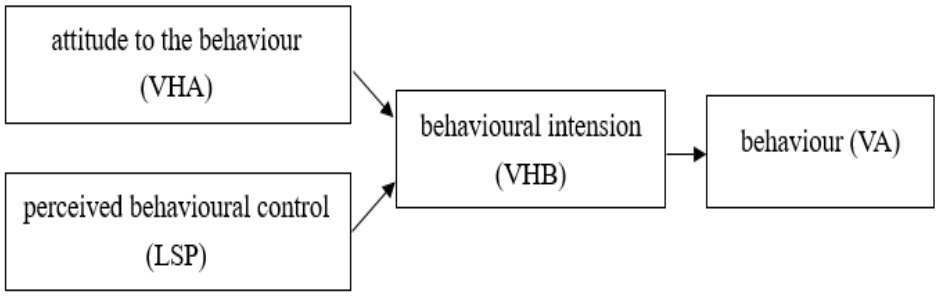

Figure 1. The framework of TPB model about visual acuity with visual health behaviour.

2.2. Research subjects and scope

The kids in low SES families counselled by social welfare organizations (one Taiwanese fund for kids and families and two charity foundations based in Changhua County) are the research subjects. Most of these kids were in low-SES families, single-parent families, foster families, or families in which parental responsibility fell on grandparents, relatives, foreign spouses, and parents with physical or mental disorders.

2.3. Questionnaire collection

To anticipate the reliability of the questionnaire, a preliminary test using the questionnaire was conducted on students counselled by social welfare organizations. A purposive sampling study and an examination of VA were also conducted as part of the preliminary study. There were 50 questionnaires returned in total with test results indicating that Cronbach's on research variables were over 0.8 which show a reliable result and a high interior consistency. Later, there were 330 formal questionnaires distributed and 260 questionnaires returned. The scale reliability of Cronbach's was higher than 0.80, also showing high consistency.

3. Results and discussion

3.1. Samples structural analysis

Structural analysis was carried out by SPSS software package. The demographic statistics in the basic data of the sample are shown by gender. There are 116 (44.6%) males and 144 (55.4%) females. 104 (40.0%) kids live with their both parents and 156 (60.0%) kids do not, among whom, the highest proportion live with the mother (25.4%). Of the low SES students, the highest proportion (33.5%) are raised by their mothers, the second highest proportion (32.7%), by their grandparents, and the third highest (30.0%), by their fathers.

3.2. Visual acuity testing

The study conducted a questionnaire and performed a VA examination on low SES elementary school kids. The VA examination used a standard visual scale to measure uncorrected defective VA. Any uncorrected VA less than 0.9 without other eye diseases was regarded as poor VA. The worst eye would be measured if both eyes exhibited poor VA, and the right eye would be measured if the eyes were of the same VA. The result of the examination is shown in Table 1. Approximately 48.8% of the student's VA is under 1.0.

Table 1. Eyes classified by unaided VA on low SES elementary school kids.

VA	No.	%	Accumulated %
over 1.0 (normal)	133	51.2	51.2
0.8-0.9 (mild vision loss)	28	10.8	62.0
0.4-0.7 (ametropia)	57	22.0	84.0
under 0.3 (severe ametropia)	42	16.0	100.0
Total	**260**	**100.0**	

3.3. Data analysis

For questionnaire a Likert's 4-point scale is applied from most disagree in 1 to most agree in 4. The children whose VA was over 1.0 and between 0.4 to 0.7 had significant differences in 3 questions related to VHB, as shown in table 2. The children with good VA had established the habit of resting the eyes by taking a 10-minute break after 30 minutes reading, but the children whose VA was between 0.4 to 0.7 did not pay attention to resting the eyes. The children with good VA had "correct" VHA and would do outdoor sports everyday. Also, the children with good VA could keep reading distance of over 35 cm while some other whose VA was between 0.4 to 0.7 could not good eye care habits on reading or doing homework. There is a turning point of agree level about the children whose VA was under 0.3. It was assumed that children whose VA under 0.3 might show strong self-examination in mind to change their eye care habits to avoid deterioration of vision. However, this assumption is not significant.

Table 2. ANOVA of the differences environmental factors in VHB for various VA.

VHB	VA	Agree Level	Mean	Standard deviation	PostHoc (Scheffe)
A. I look into the distance and rest for 10 minutes after reading for 30 minutes.	(1) over 1.0	2.625	1.099	2.994*	(1) > (3)
	(2) 0.8-1.0	2.313	1.026		
	(3) 0.4-0.7	2.012	1.006		
	(4) under 0.3	2.236	0.980		
B. I spend at least 120 minutes outdoors every day.	(1) over 1.0	2.968	1.031	4.814*	(1) > (3)
	(2) 0.8-1.0	2.525	1.003		
	(3) 0.4-0.7	2.189	1.013		

VHB	VA	Agree Level	Mean	Standard deviation	PostHoc (Scheffe)
	(4) under 0.3	2.454	0.959		
C. I maintain a reading distance of over 35 cm while reading or doing homework.	(1) over 1.0	2.968	0.999	3.695*	(1) > (3)
	(2) 0.8-1.0	2.606	0.966		
	(3) 0.4-0.7	2.303	1.078		
	(4) under 0.3	2.436	0.976		

*Significant $p < 0.05$

Also, an ANOVA significant difference between the various family structures emerged regarding the questionnaire item "I look into the distance and rest for 10 minutes after reading, watching TV or playing computer for 30 minutes". As shown in Table 3 kids who live with their parents have poorer VHB than those who do not live with their parents in significant difference.

Table 3. ANOVA of the differences between various family structures in questionnaire.

Question	Family Structure	Mean	F-value	PostHoc (Scheffe)
"I look into the distance and rest for 10 minutes after reading, watching TV or playing computer for 30 minutes"	(1) Live with parents	2.278	3.539*	(4) > (1)
	(2) Live with fathers	2.578		
	(3) Live with mothers	2.318		
	(4) others	2.800		

*Significant $p < 0.05$

The overall structure model was evaluated according to comparison with judgment index of multivariate data analysis [20], yielding the following results: AGFI = 0.93, GFI = 0.91, IFI = 0.95, TLI = 0.94, CFI = 0.95, RMSEA = 0.05, RMR = 0.04. All judgment indexes were within standard value. The sample estimation data and the content of the visual health and vision overall model (Structural Equation Model) are shown in Table 4 and Figure 2. According to the results of regression analysis, "correct" VHA, LSP affected VHB, and ultimately affected the test result. Besides, participating in more leisure sports also positively affected VHB and VA.

Table 4. ANOVA of the differences between various family structures in questionnaire.

Variable path relationship	regression coefficient	*p*-value
VHB ← VHA	0.466***	0.000
VHB ← LSP	0.282**	0.003
VA ← VHB	0.200*	0.031

*significant p < 0.05 **high significant p < 0.01 ***very high significant p < 0.001

$$VHB = 0.466\ VHA + 0.282LSP \quad (1)$$

$$VA = 0.200\ VHB \quad (2)$$

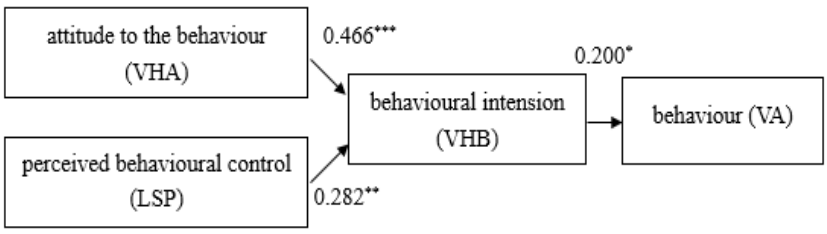

Figure 2. Path analysis of the overall structural relation TPB model.

For more specific questions referring VHA, VHB and LSP in regression analysis Table 5 shows that: the B3 "I don't want to get myopia, so I need to take care of my eyes" was the most effective question regarding VHA (regression coefficient 0.775 in a very high

significance level). The C7 "I read, do my homework, watch TV and play computer with good illumination indoors" was the most effective question regarding VHB (regression coefficient 0.727 in a very high significance level). The A9 "The number of times I participated in leisure sports in a week" was the most effective question regarding LSP (regression coefficient 0.707 in a very high significance level).

Table 5. Regression analysis for overall model regression coefficient.

Variable path relationship	regression coefficient	*p*-value
B1: Although glasses are expensive, I still need to wear glasses if I have myopia. ← VHA	0.660***	0.000
B2: Although wearing glasses looks good, I don't want to get myopia. ← VHA	0.602***	0.000
B3: I don't want to get myopia, so I need to take care of my eyes. ← VHA	0.775***	0.000
B5: I think I need to see an ophthalmologist when I can't see clearly. ← VHA	0.771**	0.006
B7: I think it is necessary to ask my family to take me to have my eyes examined. ← VHA	0.522***	0.000
B9: I want to avoid getting myopia even though my family has myopia. ← VHA	0.710***	0.000
C1: I use television, computer and smartphone for less than 2 hours per day. ← VHB	0.575***	0.000
C2: I look into the distance and rest for 10 minutes after reading, watching TV or playing computer for 30 minutes. ← VHB	0.692***	0.000
C4: I keep a 35 cm reading distance while reading or doing homework. ← VHB	0.679***	0.000
C7: I read, do my homework, watch TV and play computer with good illumination indoors. ← VHB	0.727***	0.000
C8: I have a balanced diet and am not a picky eater. ← VHB	0.542***	0.000
A9: The number of times I participated in leisure sports in a week. ← LSP	0.707***	0.000
A10: The average minutes I participated in leisure sports each time. ← LSP	0.695***	0.000

*significant $p < 0.05$ **highly significant $p < 0.01$ ***very highly significant $p < 0.001$

3.4. Discussions

According the analysis in Table 2 children with good VA had established the habit of resting the eyes by taking a 10-minute break after reading for 30 minutes, but the children whose VA was between 0.4 to 0.7 did not pay attention to resting the eyes. The children with good VA had "correct" VHA and would do outdoor sports more than 2 hours everyday. Due to unhealthy reading distance children whose VA was between 0.4 to 0.7 would squint their eyes to read clearly, making it harder for the ciliary muscles of they eye to adjust.

The results relating hypotheses test are discussed below:

- H1: Kid's VHA will have a positive impact on VHB. As shown in Table 4, the regression coefficient of VHA to VHB was 0.466 which achieved a very high significance level; thus, H1 was feasible.

- H2: kid's LSP will have a positive impact on VHB. As shown in Table 4, the regression coefficient of LSP to VHB was 0.282 which achieved a high significance level; thus, H2 was feasible.

- H3: VHB will have a positive impact on VA. As shown in Table 4, the regression coefficient of VHB to VA was 0.200 which achieved a significance level; thus, H3 was feasible.

For questions referring VHA, VHB and LSP in regression analysis in Table 5 with a very high significance level it could be found that children knew the relationship between myopia and well care of eyes, importance of indoor illumination, and regular leisure sports for strong healthy body and wider field of vision.

3.5. Limitations of study

Because the questionnaire and VA examination needed to have a parent or guardian's agree and signature before filling in and testing, it was not possible to obtain test results from all the low SES elementary school students in whole county. Also, Those VA examination of the low SES children were counseled by social welfare organizations only. Data collection for those who were not counseled by social welfare organizations were not included. Furthermore, it is necessary that a guidance counselor had to read the questions and helped each of the children to complete the questionnaire. It was possible that error crept into the results due to misunderstanding through bad communication.

4. Conclusion

There was 48.8% of the low SES kids' vision below 0.9, which is an increase of 2.7% on the defective vision rate in Taiwan (46.1%) [21]. A failure to maintain a healthy book-to-eye distance when reading seemed to be the main cause of myopia onset. The students with poor VA had worse VHA, leading to unhealthy VHB and ultimately to myopia shown by analysis in Table 2. This study also found that students participated in leisure sports, had positively affected VHB. Participating in leisure sports can reduce the usage time which has great help on the visual health care. Beside questionnaire study interviews with some low SES elementary school kids had been done, too. Facts were found that some parents in low SES families were busy at making money rather than taking care of students. Thus, students addicted to playing 3C (computer, communications, and consumer-electronics) products at home result in the rapid increase of myopia. Most low SES children did not have a dedicated desk lamp and only turned on a lamp to write or read under weak light to save money, forcing them to maintain an unhealthy reading distance. According to the results of the study, "correct" VHA led to "correct" VHB; LSP led to "correct" VHB and "correct" VHB ensured good VA for students. The low SES students need more care and assistance to change the situation of low SES and prevent the deteriorating of VA.

Author contribution statement: Conceived and designed the questionnaire; Analyzed and interpreted the data; wrote the draft manuscript: Y.T.S.; Manuscript editing, analyzed and interpreted the data: Y.C.C.

Acknowledgements: This article was part of MS thesis research by Ms. Yu-Ting Hsiao. The authors would like to thank the members of the Department of Sport and Health Management and Department of Environmental Engineering, Da-Yeh University for discussions that improved the quality of the publication.

Competing interest statement: The authors declare no conflict of interest.

References

1. World Health Organization. Visual impairment and blindness, Fact Sheet No. 282 **2014**. Retrived from: http://www.who.int/mediacentre/factsheets/fs282/en/
2. Lin, L.L.K.; Shih, Y.F.; Hsiao, C.K.; Chen, C.J. Prevalence of myopia in Taiwanese schoolchildren: 1983 to 2000. *Ann. Acad. Med.* **2004**, *33(1)*, 27–33.
3. Wu, P.C.; Tsai, C.L.; Wu, H.L.; Yang, Y.H.; Kuo, H.K. Outdoor activity during class

recess reduces myopia onset and progression in school children. *Ophthalmology* **2013**, *120(5)*, 1080–1085.
4. Lyu, Y.; Zhang, H.; Gong, Y.; Wang, D.; Chen, T.; Guo, X.; Yang, S.; Liu, D.; Kang, M. Prevalence of and factors associated with myopia in primary school students in the Chaoyang district of Beijing, China. *Jpn. J. Ophthalmol*. **2015**, *59(6)*, 421–429.
5. Tsai, D.C.; Lin, L.J.; Huang, N.; Hsu, C.C.; Chen, S.Y.; Chiu, A.W.H.; Liu, C.J.L. Study design, rationale and methods for a population-based study of myopia in schoolchildren: The Myopia Investigation study in Taipei. *Clin. Exp. Ophthalmol.* **2015**, *43(7)*, 612–620.
6. Wang W.; Yan, W.; Müller, A.; Keel, S.; He, M. Association of Socioeconomics With Prevalence of Visual Impairment and Blindness. *JAMA Ophthalmo.* **2017**, *135(12)*, 1295–1302.
7. Lee, Y.Y.; Lo, C.T.; Sheu, S.J.; Yin L.T. Risk factors for and progression of myopia in young Taiwanese men. *Ophthalmic Epidemiology* **2015**, *22(1)*, 66–73.
8. Holden, B.; Sankaridurg, P.; Smith, E.; Aller, T.; Jong, M.; He, M. Myopia, an underrated global challenge to vision: Where the current data takes us on myopia control. *Eye* **2014**, *28(2)*, 142–146.
9. Ramamurthy, D.; Lin Chua, S. Y.; Saw, S. M. A review of environmental risk factors for myopia during early life, childhood and adolescence. *Clin. Exp. Optometry* **2015**, *98(6)*, 497–506.
10. Fishbein, M.; Ajzen, I. Predicting and changing behavior: The Reasoned Action Approach. Taylor & Francis, New York, 2010.
11. Ajzen, I. The Theory of Planned Behavior. *Organizational Behav. Hum. Decis. Processes* **1991**, *50*, 179–211.
12. Godin, G.; Kok, G. The Theory of Planned Behavior: A Review of Its Applications to Health-related Behaviors. *Am. J. Health Promot.* **1996**, *11*, 87–98.
13. Morgan, I.; Rose, K. How genetic is school myopia? *Prog. Retinal Eye Res.* **2005**, *24(1)*, 1–38.
14. Lim, L.T.; Gong, Y.; Ah-kee, E.Y.; Xiao, G.; Zhang, X.; Yu, S. Impact of parental history of myopia on the development of myopia in Mainland China school-aged children. *Ophthalmol. Eye Dis.* **2014**, *6*, 31–35.
15. He, M.; Zheng, Y.; Xiang, F. Prevalence of myopia in urban and rural children in Mainland China. *Optometry Vision Sci.* **2009**, *86(1)*, 40–44.
16. Nishi, M., Miyake, H.; Shikai, T.; Takeuchi, M.; Tanaka, H.; Minagawa, N.; Morimoto, Y.; Wada, M. Factors influencing the visual acuity of primary school pupils. *J. Epidemiol.* **2000**, *10(3)*,179–182.
17. Rose, K.A.; Morgan, I.G.; Smith, W.; Burlutsky, G.; Mitchell, P.; Saw, S.M. Myopia, lifestyle, and schooling in students of Chinese ethnicity in Singapore and Sydney. *Arch. Ophthalmol.* **2008**, *126(4)*, 527–530.
18. Saw, S.M.; Chua, W.H.; Hong, C.Y.; Wu, H.M.; Chan, W.Y.; Chia, K.S.; Stone, R.A.; Tan, D. Near work in early-onset myopia. *Clin. Epidemiologic Res.* **2002**, *43(2)*, 332–339.
19. You, Q.S.; Wu, L.J.; Duan, J.L.; Luo, Y.X.; Liu, L.J.; Li, L.; Gao, Q.; Wang, W.; Xu, L.; Jonas, J.B.; Guo, X.H. Factors associated with myopia in school children in China: The Beijing Childhood Eye Study. *PLoS ONE* **2012**, *7(12)*, e52668.
20. Hair, J.F.J.; Anderson, R.E.; Tatham, R.L.; Black, W.C. Multivariate data analysis: Prentice-Hall, New Jersey, 1998.
21. Wu, P.C.; Chang, L.C.; Niu, Y.Z.; Chen, M.L.; Liao, L.L.; Chen, C.T. Myopia prevention in Taiwan. *Ann. Eye Sci.* **2018**, *3(12)*, 1–4.

VIETNAM JOURNAL OF HYDROMETEOROLOGY

Research paper

Comparative results of the average daily net radiation (R_{nd}) from meteorological observation data and Landsat–8 remote sensing imagery areas of Hoa Binh province

Le Hung Chien[1], Doan Ha Phong[2]*, Tran Xuan Truong[3]

[1] Viet Nam National University of Forestry; chienlh@vnuf.edu.vn
[2] Vietnam Institute of Meteorology, Hydrology and Climate Changer; doanhaphong.imhen@gmail.com
[3] Hanoi University of Mining and Geology; tranxtruong75@gmail.com

*Correspondence: doanhaphong.imhen@gmail.com; Tel: +84–913212325

Received: 12 July 2021; Accepted: 21 September 2021; Published: 25 December 2021

Abstract: Net radiation (Rn) is the solar energy absorbed by vegetation and land and water surfaces as a key driving force for evapotranspiration. Therefore, the accuracy of the Rn value affects the determination of evapotranspiration from different models. The article presents the results of calculating the average daily net radiation value according to the FAO–56 model, IRMAK model, and Remote sensing model. The results of calculating the average daily net radiation value at the Hoa Binh province's meteorological and hydrological monitoring stations according to the FAO–56, IRMAK, and Remote Sensing models have the value of 17.593 MJ/m^2/day, 16.389 MJ/m^2/day, and 18.531 MJ/m^2/day, respectively. The difference of R_{nd} between the FAO–56 model and the IRMAK model is –1.20 (MJ/m^2/day), corresponding to 6.84%, and the difference of R_{nd} between the FAO–56 model and the Remote sensing model is 0.94 (MJ/m^2/day), corresponding to 5.58%. The largest and smallest difference between R_{nd}_FAO–56 and R_{nd}_IRM values at Lam Son hydrological station and Hoa Binh meteorological station is –1.885 (MJ/m^2/day) match up 10.10%, and –0.31 (MJ/m^2/day) match up 1.75%, respectively. In addition, the largest and smallest difference between R_{nd}_FAO–56 and R_{nd}_VT values at Lac Son meteorological station and Lam Son hydrological station is 2.80 (MJ/m^2/day), corresponding to 17.49%, and 0.23 (MJ/m^2/day), corresponding to 1.18%, respectively. The average daily net radiation value due to percentage at meteorological and hydrological monitoring stations between R_{nd}_FAO and R_{nd}_VT: the difference of 0–5% is 5/8 stations, 5–10% is 1/8 stations, 10–15% is 1/8 stations and 15–20% is 1/8 stations, accounting for 62.5%, 12.5%, 12.5% and 12.5%, respectively.

Keywords: Net Radiation; FAO–56; Irmak; Sebal Manual; Jackson; Hoa Binh.

1. Introduction

Net radiation (Rn) is defined as the difference between the incoming and outgoing radiation fluxes including both long and shortwave radiation at the surface of Earth. It is a key quantity for the estimation of surface energy budget and is used for various applications including climate monitoring, weather prediction and agricultural meteorology. Remote sensing provides an unparalleled spatial and temporal coverage of land surface attributes, thus several studies have attempted to estimate net radiation (or its components) by combining remote sensing observations with surface and atmospheric data [1–4]. Rn

(coupled with soil heat flux, as available energy) serves as a key driving force for evapotranspiration (ET). Over the years, various ET models have been developed that use remote sensing and ancillary surface and ground-based observations [5–7]. Several of the recent ET models primarily use remote sensing data for ET estimation [8–10]. Yet, all these ET models require estimates of R_n.

In Vietnam, several typical research works use satellite image data in determining net radiant energy for evapotranspiration, such as: According to [11] the researchers calculated the amount of evapotranspiration from solar radiation extracted from the Modis remote sensing image with an average absolute error of not more than 10% for the northern region of Vietnam. Calculating evapotranspiration by the hour using Priestley–Taylor method from net radiant energy extracted from Modis satellite images applied to the topography of North Vietnam with average absolute error not greater than 10% [12]. Comparing the average daily net irradiance estimate extracted from the Modis satellite image with the results from the meteorological observations, the calculation of the net radiant energy from the Modis image has an average absolute error of 6% [13]. However, the studies mainly used Modis satellite images without experimenting with other types of optical satellite images.

This paper presents the results of extraction of net radiant energy from Landsat–8 satellite images according to the SEBAL model based on the principle of solar radiation balance to estimate evapotranspiration in Hoa Binh province.

2. Materials and Methods

2.1. Description of study site

Hoa Binh is a mountainous province in the Northwest region, adjacent to the Red River Delta, located 73 km away from Hanoi on the National Highway 6 Hanoi–Hoa Binh–Son La. The whole province has an area of about 4,578.1 km^2. It borders Phu Tho province to the north, Ha Nam and Ninh Binh provinces to the south, Hanoi to the east and northeast, Son La province to the west and northwest, and Thanh Hoa province to the southwest. The outstanding features of Hoa Binh's topography are low and medium-high mountains, complicatedly divided, steep slopes and stretching in the direction of Northwest–Southeast, divided into two distinct regions: The average high mountain area in the northwest has an average altitude of 600–700 m, the highest place is the top of Phu Canh (Da Bac) 1,373 m. The average slope is from 20–35^o, some places are over 40^o, accounting for about 46% of the province's area. Low mountains and hills (Southeast) have an area of 246,895 hectares, accounting for 54% of the province's area, with an average slope of 10–25^o, an average altitude of 100–200 m. Alternating mountainous terrain, there are low valleys, narrow valleys stretching along large rivers and streams.

Hoa Binh is located in a tropical monsoon climate with typical weather: hot, humid and cold winters. The average temperature in the year is 23^{o}C; average rainfall is 1,800 mm/year; relative humidity 85%; average annual evaporation of 704 mm. The climate of the year is divided into two distinct seasons. Summer starts in April and ends in September, the average temperature is above 25^{o}C, on some days it can reach 43^{o}C. The average monthly rainfall is over 100 mm, with the highest time of 680 mm (1985). Rain usually concentrates in July and August, which accounts for 85–90% of the whole year's rainfall. Winter begins in October of the previous year and ends in March of the following year, the average temperature in the month fluctuates between 16–20^{o}C, the lowest temperature is 3^{o}C, average monthly rainfall is 10–20 mm. Due to topographical features, Hoa Binh also has a Northwest climate with dry and cold winters, hot and humid summers (in the Northwest high mountains); the climate in the Northern Delta is more temperate (in the low mountainous areas) [14].

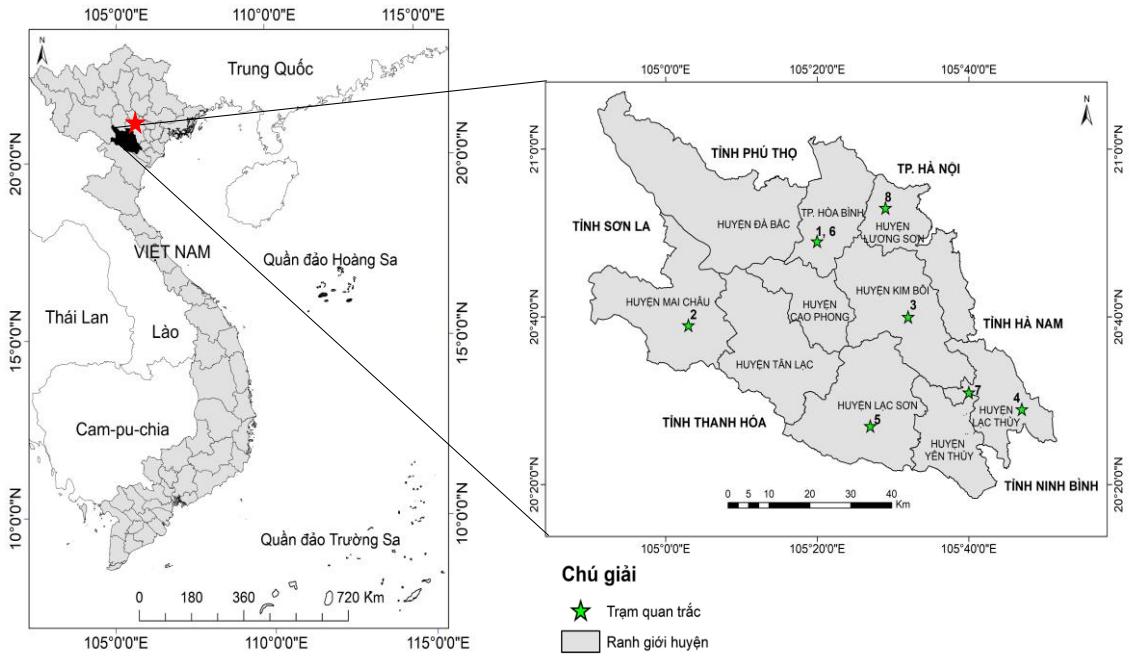

Figure 1. Research area and monitoring stations.

2.2. Meteorological data

Meteorological data for the calculation of evapotranspiration from various methods were collected from Hoa Binh hydrometeorological stations on June 4, 2017, provided by the Center for hydrometeorology of Hoa Binh Province (Table 1). According to Table 1, the wind speed of the monitoring points ranges from 4 m/s to 8 m/s, the average humidity is from 50% to 71%, the total number of sunshine hours is from 9.3 to 12.3 hours and the amount of actual water evaporation from 4.6 mm to 9.6 mm.

Table 1. Hydrometeorological data at meteorological monitoring stations in Hoa Binh area on June 4, 2017.

No.	Station Name	Coordinates			Strongest wind (m/s)		Average humidity (%)	Sunshine duration (hours)	Temperature (ºC)		Actual water evaporation (mm)
		Longitude	Latitude	Altitude (m)	Direction	Wind speed			T (max)	T (min)	
1	Hoa Binh Meteorology	105.20	20.49	22.7	Southwest	5	50	12.1	41.0	31.0	9.6
2	Mai Chau Meteorology	105.03	20.39	165.5	Northwest	8	65	10.0	40.0	25.3	5.7
3	Kim Boi Meteorology	105.32	20.40	61.1	Northwest	4	64	10.6	40.9	27.5	7.0
4	Chi Ne Meteorology	105.47	20.29	11.3	Northwest	6	71	11.6	40.3	29.6	7.8
5	Lac Son Meteorology	105.27	20.27	41.2	Northwest	4	69	9.3	40.1	27.2	4.6
6	Hoa Binh Hydrological	105.20	20.49	22.6	Southwest	6	52	12.0	40.8	30.7	9.5

No.	Station Name	Coordinates			Strongest wind (m/s)		Average humidity (%)	Sunshine duration (hours)	Temperature (ºC)		Actual water evaporation (mm)
		Longitude	Latitude	Altitude (m)	Direction	Wind speed			T (max)	T (min)	
7	Hung Thi Hydrological	105.40	20.31	20.1	Northwest	5	70	11.4	40.5	30.0	8.0
8	Lam Son Hydrological	105.29	20.53	25.4	Southwest	7	67	12.3	40.9	30.5	9.2

2.3. Satellite image material

Landsat–8 satellite image obtained on June 4, 2017 [15]. The image was geometrically corrected according to the administrative map of Hoa Binh province, reference system VN–2000.

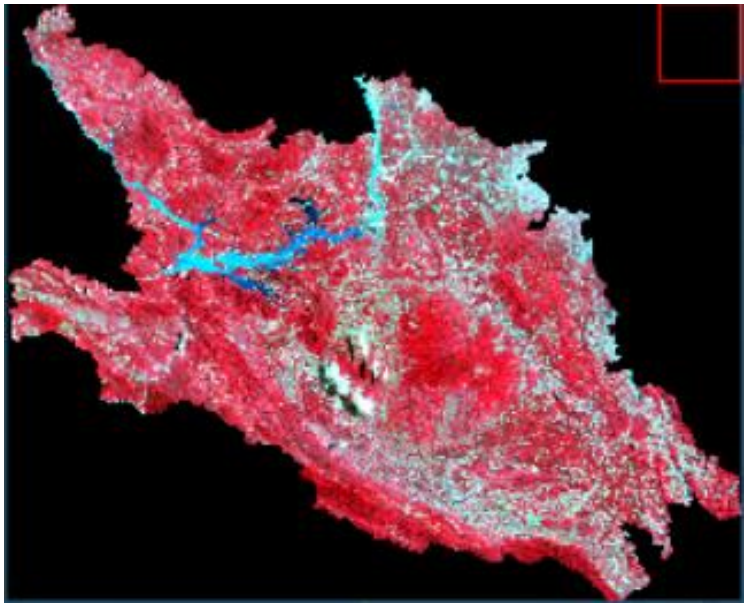

Figure 2. Landsat satellite image on June 4, 2017 adjusted and cut according to the administrative boundaries of Hoa Binh province.

2.3. Net radiant (Rn) from the meteorological observations calculation method

2.3.1. FAO –56 net radiation (R_{nd}) method

The daily net radiant energy value (R_{nd}) calculated according to the FAO–56 model [16–17] is a physical model, using directly observed data at hydrometeorology such as daily temperature (T_{mean}), sunshine duration hours (n), air humidity (RH), wind speed (u), and combination of geographical coordinates, altitude at meteorological monitoring stations. The FAO–56 model proposes the following formula for calculating net radiant energy:

$$R_{nd} = R_{nS} – R_{nL} \quad (1)$$

where R_{nd} is the net radiant per day (MJ/m^2/day); R_{nS} is the short wave net radiant (MJ/m^2/day); R_{nL} is the long wave net radiated (MJ/m^2/day).

The short wave net radiant (R_{nS}) [16] is calculated by the formula:

$$R_{nS} = (1 – \alpha)R_S \quad (2)$$

where α is the soil surface difference (albedo), α = 0.15 for soil surface; α = 0.23 for green cover and α = 0.05 for all other surfaces; R_S is incoming solar radiant energy (MJ/m^2/day).

The long wave net radiant (R_{nL}) [16] is calculated by the formula:

$$R_{nL} = \sigma\left[\frac{T_{maxK}^4 + T_{minK}^4}{2}\right]\left(0.34 - 0.14\sqrt{e_a}\right)\left(1.35\frac{R_S}{R_{SO}} - 0.35\right) \quad (3)$$

where R_{nL} is a long wave net radiated energy (MJ/m^2/day); σ is the Stefan–Boltzmann constant (4.903 10^{-9} MJ/K^4/m^2/day); $T_{max\,K}$ is the highest temperature of the day ^oK (^oK = ^oC + 273.15); $T_{min\,K}$ is the lowest temperature of the day ^oK (^oK = ^oC + 273.15); e_a is the steam pressure [kPa]; R_S is incoming solar radiant energy (MJ/m^2/day); R_{SO} is the solar radiant energy when the sky is clear (MJ/m^2/day).

2.3.2. IRMAK net radiation (R_{nd}) method

The regression model [18] was proposed by the Environmental and Water Resources Institute (EWRI) of The American Society of Civil Engineers (ASCE) to calculate the average daily net irradiance Rnd of the form R_{nd} after:

$$R_{nd} = -0.054T_{max} + 0.111T_{min} + 0.462R_s - 49.243d_r + 50.831 \quad (4)$$

where T_{max}, T_{min} is the highest and lowest air temperature of the day (^oC); R_S is incoming solar radiant energy (MJ/m^2/day); d_r is the inverse of the relative distance between the Sun and the Earth.

2.4. Method of extracting net radiant from remote sensing images

Extraction of net radiant energy absorbed by the ground at time i (R_{ni}) according to the SEBAL model [19] is calculated by the formula (5):

$$R_{ni} = R_{S\downarrow} - \alpha R_{S\downarrow} + R_{L\downarrow} - R_{L\uparrow} - (1-\varepsilon_o)R_{L\downarrow} \quad (5)$$

where R_{ni} is the earth surface net radiation (W/m^2); $R_{S\downarrow}$ is incoming short–wave radiation (W/m^2); $R_{L\downarrow}$ is incoming longwave radiation (W/m^2); $R_{L\uparrow}$ is outgoing longwave radiation (W/m^2); ε_o is the broad–spectrum heat emission; α is the differential rate of the soil surface.

The modules for calculating the net absorbed radiation by the ground (R_{ni}) are proposed to be implemented according to the diagram of figure 3.

2.4.1. Calculate pixel value from numeric DN to spectral radiant energy value $\boldsymbol{L_\lambda}$

According to United States Geological Survey (USGS) (2013) [15], the spectral radiant energy value for each image channel L_λ is calculated according to the following formula (F01):

$$L_\lambda = M_L * Q_{CAL} + A_L \quad (6)$$

where L_λ is the spectral radiant energy value (W/m^2); M_L is the radiance Multiplier; Q_{CAL} is the quantized and calibrated standard product pixel values (DN); A_L is the radiance add.

2.4.2. Convert pixel value from numeric (DN) to surface reflectance (Reflectance)

When taking satellite images, the sensor converts the wavelength of light into a brightness value (DN value) and converts it to an integer unit. Each image pixel corresponds to a DN value. Therefore, in order to get closer to the actual information, many factors must be corrected to bring back the surface reflectance (SR reflectance), till then the application

of satellite images has practical significance. According to the United States Geological Survey (USGS) (2013) [15] the reflectance value for each image channel P_λ is calculated according to the following formula (F02):

$$\rho_\lambda = \frac{M_\rho Q_{cal} + A_\rho}{\sin(\theta_{SE})} \quad (7)$$

where M_ρ is band-specific multiplicative rescaling factor from the metadata; A_ρ is band-specific additive rescaling factor from the metadata; Qcal is quantized and calibrated standard product pixel values (DN); θ_{SE} is local sun elevation angle. The scene center sun elevation angle in degrees is provided in the metadata (SUN_ELEVATION).

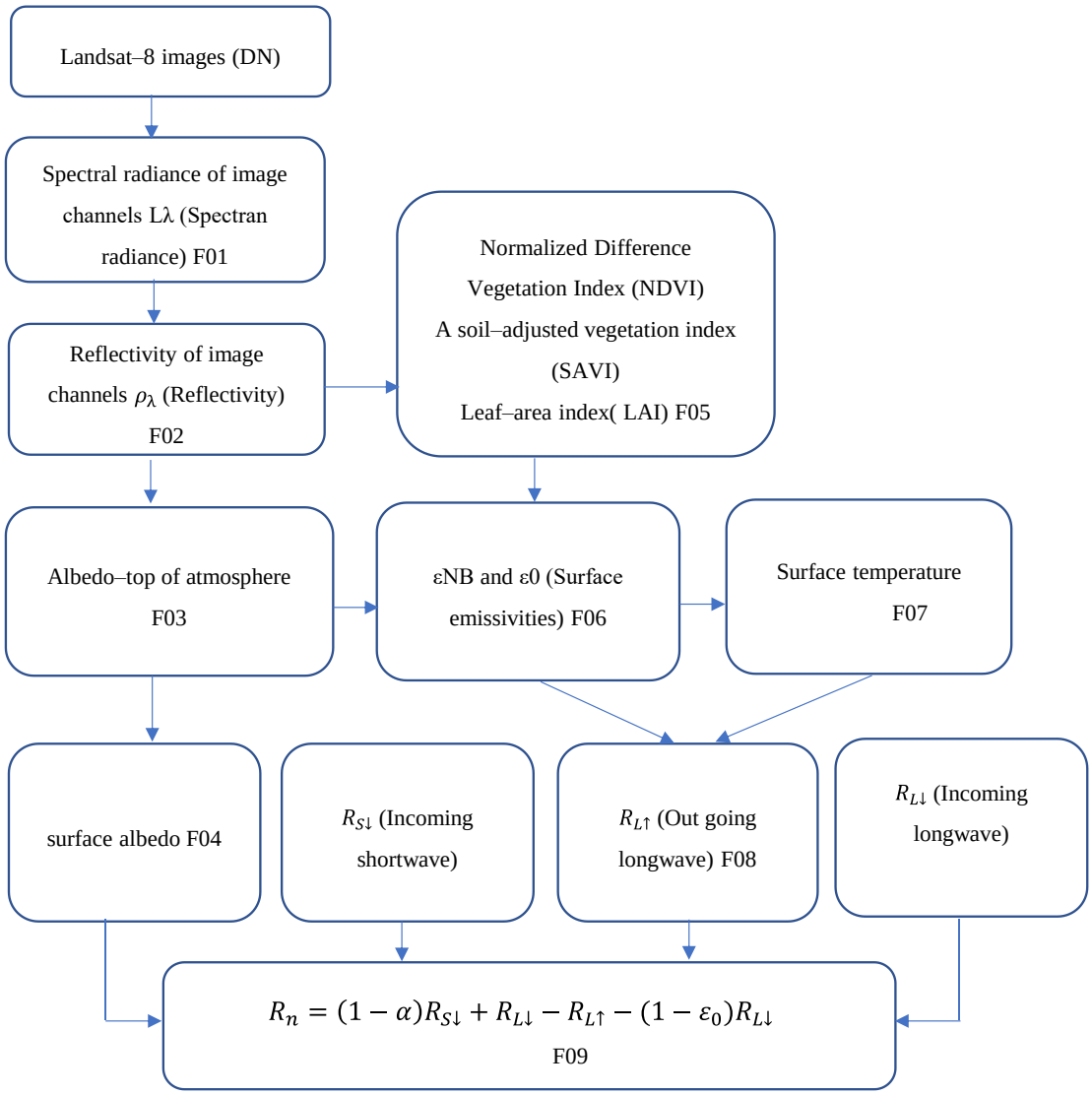

Figure 3. Calculation diagram of the net radiation absorbed by the ground R_n.

2.4.3. Calculate the surface difference (α)

The land surface differential (α) is calculated by correcting the top–atmospheric differential α_{toa} for atmospheric transmission (F04).

$$\alpha = \frac{\alpha_{toa} - \alpha_{path\_radiance}}{\tau_{SW}^2} \quad (8)$$

where α_{toa} is the difference at the top of the atmosphere; $\alpha_{path\_radiance}$ is the average portion of the incoming solar radiation across all bands that are backscattered to the satellite before

it reaches the earth's surface; τ_{sw}^2 is the atmospheric transmissivity. The value $\alpha_{path\_radiance}$ ranges from 0.025 to 0.04 for the SEBAL model and suggests a value of 0.03 [19].

2.4.4. Calculate the incoming shortwave radiation value ($R_S\downarrow$)

Incoming shortwave radiation is the direct flow of diffuse solar radiation to the earth's surface (W/m^2). It is calculated under clear sky conditions, which is a constant for the time using the image:

$$R_{S\downarrow} = G_{sc} \times \cos\theta \times d_r \times \tau_{sw} \quad (9)$$

where G_{sc} is the solar constant (1367 W/m^2); τ_{sw}^2 is the atmospheric transmissivity calculated by the formula; d_r is the inverse of the relative distance between the Sun and the Earth; θ is the local sun elevation angle (SUN_ELEVATION). Usually $R_{S\downarrow}$ is in the range of 200–1000 W/m^2 depending on the location and time of taking pictures.

2.4.5. Calculate outgoing longwave emission value ($R_L\uparrow$)

The longwave emission $R_{L\uparrow}$ is calculated in (F08**)**, calculated by the Stefan–Boltzmann formula as follows:

$$R_{L\uparrow} = \varepsilon_o \times \sigma \times T_s^4 \quad (10)$$

where σ is the Stefan–Boltzmann constant (5.67×10^{-8} W/m^2/K^4); T_s is the soil surface temperature (°K); ε_o surface emissivity coefficient used to calculate the total longwave energy emission from the surface. $R_{L\uparrow}$ values are in the range of 200–700 W/m^2 depending on the location and time the image was taken.

2.4.6. Calculate the incoming longwave radiation value ($R_{L\downarrow}$)

The incoming longwave radiation value $R_{L\downarrow}$ is the stream of thermal radiation descending from the atmosphere (W/m^2). It is calculated according to the Stefan–Boltzmann formula as follows:

$$R_{L\downarrow} = 0.85 \times (-\ln \tau_{sw})^{0.09} \times \sigma \times T_{cold}^4 \quad (11)$$

where σ is the Stefan–Boltzmann constant (5.67×10^{-8} W/m^2/K^4); τ_{sw} is the atmospheric transmissivity; T_{cold} gives a cold score according to the near-ground temperature field. Typical $R_{L\downarrow}$ values are in the range of 200–500 W/m^2 depending on the location and time taken to take pictures.

2.4.7. Calculate the value of the net radiant energy reaching the earth's surface (R_{ni})

The net radiation reaching the ground surface is calculated according to formula (5) of the SEBAL model. R_n values are in the range of 100–800 W/m^2 depending on the topographical surface.

2.4.8. Calculate the average daily value of net radiant reaching the land surface (R_{nd})

According to [20] Solar radiation at time i, R_i (W/m^2/h) is calculated by the formula:

$$R_i = R_{max} \sin(\pi . t/DL) \quad (12)$$

where R_{max} is the solar radiation at noon (12:00 PM); DL is the length of day (from sunrise to sunset); t is the time from sunrise to time i. To calculate the average daily radiation use the following integral formula:

$$R_{nd} = \int_0^{DL} R_{max} \sin(\pi . t/DL) = J . R_i \quad (13)$$

where J is the coefficient; R_i is the net radiation at time i.

3. Results and discussion

3.1. Results of calculating net radiant (Rn) from meteorological observations data

3.1.1. FAO–56 net radiation (R_n) calculating results

Using the formula (1), (2), (3) and directly measured data at meteorological monitoring stations in Hoa Binh province. The results of calculating R_{nd} according to FAO–56 are shown in Table 2.

Table 2. Results of calculation of average daily net radiation according to the FAO–56 model.

No.	Monitoring stations	A= σ*(T^4maxK + T^4minK)/2	B = 0.34–0.14(ea)1/2	C = 1.35*(Rs/Rso)–0.35	Rnl (MJ/m^2/d)	Rns = (1–α) Rs (MJ/m^2/d)	Rnd–FAO 56 = (R_{nS}–R_{nL}) (MJ/m^2/d)
1	Hoa Binh Meteorology	44.8617	0.0987	0.9236	4.0900	21.6421	17.552
2	Mai Chau Meteorology	43.0300	0.0893	0.7769	2.9862	19.2066	16.220
3	Kim Boi Meteorology	43.8821	0.0802	0.8229	2.8977	19.8794	16.982
4	Chi Ne Meteorology	44.2660	0.0607	0.8912	2.3932	21.0519	18.659
5	Lac Son Meteorology	43.5602	0.0744	0.7335	2.3771	18.3895	16.012
6	Hoa Binh Hydrological	44.7183	0.0956	0.9168	3.9199	21.5264	17.606
7	Hung Thi Hydrological	44.4355	0.0603	0.8772	2.3515	20.8217	18.470
8	Lam Son Hydrological	44.6937	0.0630	0.9369	2.6370	21.8757	19.239
	Mean						**17.593**

From Table 2, it is clear that the average daily net radiation of value R_{nd} according to FAO–56 at Hoa Binh hydrometeorological monitoring stations on June 4, 2017 is 17,593 MJ/m^2/day. The value of R_{nd}_FAO–56 varies from 16,012 MJ/m^2/day (at Lac Son meteorological station) to 19,239 MJ/m^2/day (at Lam Son hydrological station).

3.1.2. IRMAK net radiation (R_{nd}) calculating results

Using the formula (4) and directly measured data at meteorological monitoring stations in Hoa Binh province to calculate net radiant energy according to IRMAK. The results are shown in Table 3.

From Table 3, it is clear that the average daily net radiation value of R_{nd} calculated by IRMAK (R_{nd}_IRM) at Hoa Binh hydrometeorological monitoring stations on June 4, 2017 is 16,389 MJ/m^2/day. Rnd_IRM value varies from 14,921 MJ/m^2/day (at Lac Son meteorological station) to 17,336 MJ/m^2/day (at Lam Son hydrological station).

Table 3. IRMAK daily average net radiation (R_{nd}) calculating results (Rn_IRM).

No.	Monitoring stations	A= –0.054* T_{max}	B = 0.111* T_{min}	C = 0.462*Rs	D = 49.243*d_r +50.831	R_{nd}–IRM (MJ/m^2/d)
1	Hoa Binh Meteorology	–2.2140	3.4410	12.9853	3.0333	17.246
2	Mai Chau Meteorology	–2.1600	2.8083	11.5239	3.0333	15.206
3	Kim Boi Meteorology	–2.2086	3.0525	11.9276	3.0333	15.805
4	Chi Ne Meteorology	–2.1762	3.2856	12.6312	3.0333	16.774
5	Lac Son Meteorology	–2.1654	3.0192	11.0337	3.0333	14.921
6	Hoa Binh Hydrological	–2.2032	3.4077	12.9158	3.0333	17.154
7	Hung Thi Hydrological	–2.1870	3.3300	12.4930	3.0333	16.669
8	Lam Son Hydrological	–2.2086	3.3855	13.1254	3.0333	17.336
	Mean					**16.389**

3.2. Results of calculating daily net radiant (Rnd) using Landsat–8 remote sensing image data

3.2.1. Calculate net radiant at time i (R_{ni}) using Landsat–8 remote sensing image data

Applying formula (5) to calculate net radiation value using Landsat–8 remote sensing image data and intermediate formulas (8), (9), (10), (11) to calculate values soil surface differential rate (α); broad-spectrum heat emission (ε_0); incoming shortwave radiation value ($R_{S\downarrow}$); outgoing longwave radiation ($R_{L\uparrow}$); incoming longwave radiation ($R_{L\downarrow}$). The results are shown in figure 4.

$$R_{S\downarrow} = G_{sc} \times \cos\theta \times d_r \times \tau_{sw} = 926.28 \ (W/m^2)$$

$$R_{L\downarrow} = 0.85 \times (-\ln \tau_{sw})^{0.09} \times \sigma \times T_{cold}^4 = 325.87 \ (W/m^2)$$

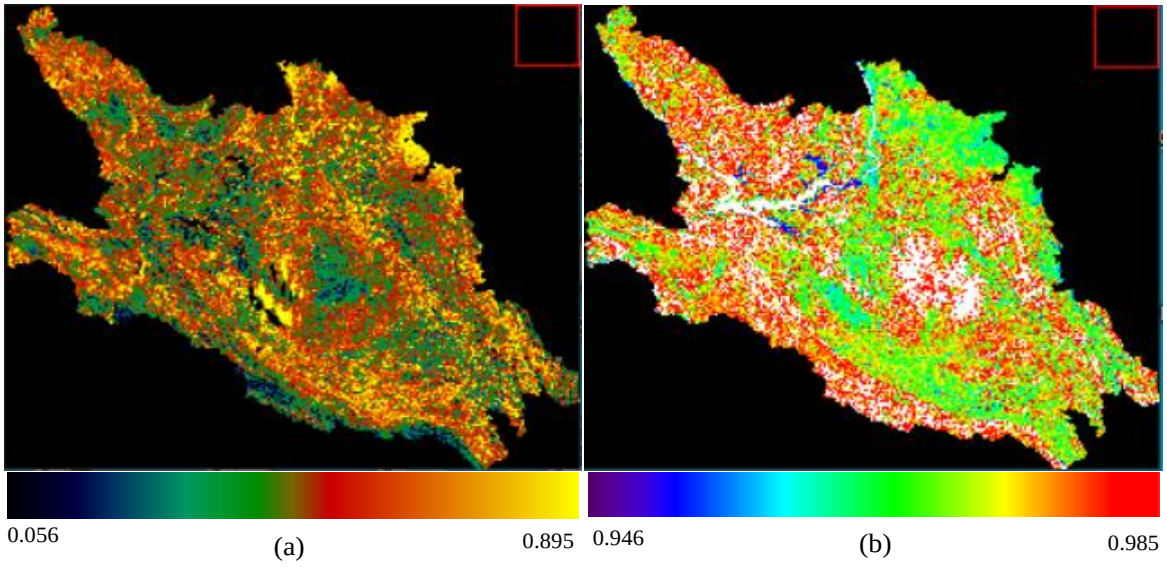

(a) (b)

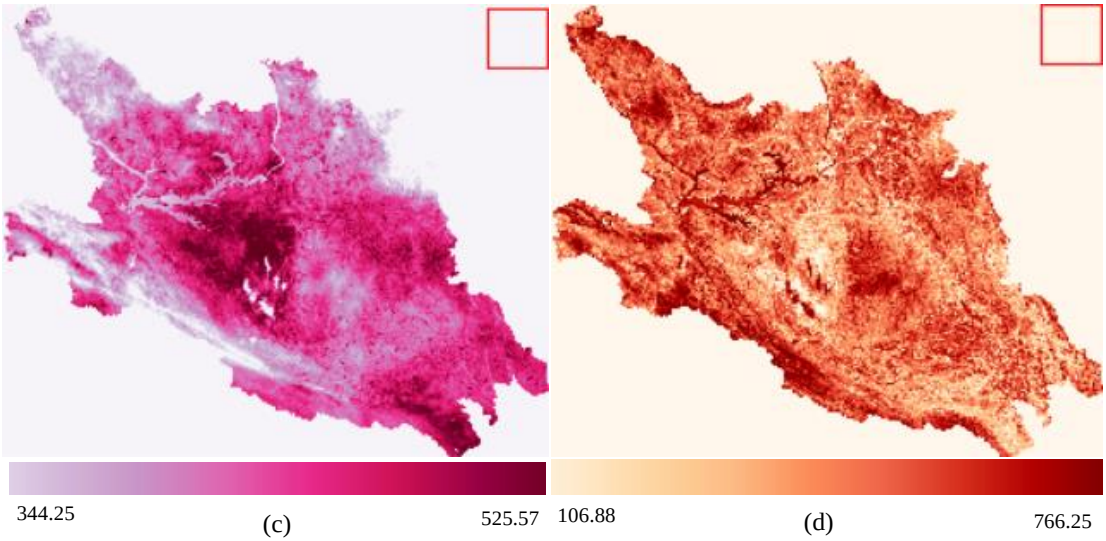

Figure 4. Results of calculating net radiation at time i (R_{ni}) from satellite image on 04/06/2017: (a) The surface difference (α) calculated from the satellite image on 04/06/2017; (b) Broad-spectrum heat emission (ε_0) calculated from satellite image on 04/06/2017; (c) Value of outgoing longwave radiation (RL↑) calculated from satellite image on 04/06/2017; (d) Value of Earth surface net radiation R_{ni} (W/m^2) calculated from satellite images on 04/06/2017.

3.2.2. Calculating average daily net radiant energy (R_{nd}) from Landsat–8 using remote sensing image data

After calculating the net radiation value at time i (R_{ni}) from satellite images using formula (13) to calculate the average daily net radiation value (R_{nd}_VT) at meteorology monitoring stations statue of Hoa Binh province. The results are shown in Table 4.

Table 4. Results of calculating average daily net radiation R_{nd} at meteorological observation stations using satellite images on 04/6/2017.

No.	Monitoring stations	Rni (W/m^2/h)	Latitude	ω_s degree	ω_s (rad)	a	b	N	2NRni	t	J coefficient	Rnd_VT (MJ/m^2/d)
1	Hoa Binh Meteorology	601.64	20.817	99.0739	1.7283	10.743	2.527	12.487	15024.956	6.321	7.9508	17.221
2	Mai Chau Meteorology	647.54	20.650	98.9943	1.7269	10.754	2.506	12.477	16158.951	6.314	7.9447	18.520
3	Kim Boi Meteorology	615.58	20.667	98.7172	1.7221	10.753	2.508	12.478	15362.578	6.310	7.9451	17.607
4	Chi Ne Meteorology	705.59	20.483	98.9149	1.7255	10.765	2.484	12.468	17594.207	6.308	7.9386	20.165
5	Lac Son Meteorology	658.4	20.450	98.8990	1.7252	10.767	2.480	12.466	16415.020	6.307	7.9374	18.814
6	Hoa Binh Hydrological	601.65	20.817	99.0739	1.7283	10.743	2.527	12.487	15025.206	6.321	7.9508	17.221
7	Hung Thi Hydrological	672.82	20.517	98.9308	1.7258	10.763	2.488	12.470	16779.619	6.310	7.9398	19.231
8	Lam Son Hydrological	679.89	20.883	99.1058	1.7288	10.739	2.536	12.490	16984.281	6.323	7.9532	19.466
	Mean											**18.531**

As shown in Table 4, the daily average value of net radiation R_{nd}_VT using Landsat–8 remote sensing images at Hoa Binh meteorological and hydrological monitoring stations on 04/6/2017 is 18,531 MJ/m^2/day. R_{nd}_VT value varies from 17,221 MJ/m^2/day (at Hoa Binh meteorological and Hoa Binh hydrology station) to 20,165 MJ/m^2/day (at Chi Ne meteorological station).

3.3. Compare the net radiation calculation results from other methods

The daily average net radiation value calculated according to the FAO–56 model is a physical model, using directly observed data at meteorological and hydrological stations such as average daily temperature, sunshine duration, relative humidity (RH), wind speed combined with geographical coordinates, the altitude at meteorological and hydrological monitoring stations. Therefore, the value of R_{nd}–FAO–56 is considered as the standard value to compare the results of R_{nd} calculation according to Irmak model (R_{nd}–IRM) and REMOTE SENSING model (R_{nd}–RS). The results of daily average net radiation calculation at 8 meteorological and hydrological monitoring stations according to 3 models R_{nd}–FAO–56, R_{nd}–IRM and R_{nd}–VT are shown in the Table 5.

Table 5. Comparison results of calculating net radiation by day Rnd between three models R_{nd}–FAO–56, R_{nd}–IRM and R_{nd}–RS.

No.	Monitoring stations	$R_{nd\_FAO–PM}$ (MJ/m^2/d)	R_{nd_IRM} (MJ/m^2/d)	R_{nd_VT} (MJ/m^2/d)	Differences between$R_{nd_FAO–PM}$ and R_{nd_IRM} (MJ/m^2/d)	Percentage %	Differences between$R_{nd_FAO–PM}$ and R_{nd_VT} (MJ/m^2/d)	Percentage %
1	Hoa Binh Meteorology	17.552	17.246	17.221	–0.31	–1.75	–0.33	–1.89
2	Mai Chau Meteorology	16.220	15.206	18.520	–1.01	–6.26	2.30	14.18
3	Kim Boi Meteorology	16.982	15.805	17.607	–1.18	–6.93	0.63	3.68
4	Chi Ne Meteorology	18.659	16.774	20.165	–1.88	–10.10	1.51	8.07
5	Lac Son Meteorology	16.012	14.921	18.814	–1.09	–6.82	2.80	17.49
6	Hoa Binh Hydrological	17.606	17.154	17.221	–0.45	–2.57	–0.39	–2.19
7	Hung Thi Hydrological	18.470	16.669	19.231	–1.80	–9.75	0.76	4.12
8	Lam Son Hydrological	19.239	17.336	19.466	–1.90	–9.89	0.23	1.18
Mean		**17.593**	**16.389**	**18.531**	**–1.20**	**6.76**	**0.94**	**5.58**
Mean square error					**1.43**		**1.54**	

Table 5 shows that the average difference of R_{nd} value between the FAO–PENMAN model and the IRMAK model is –1.20 (MJ/m^2/d) corresponds to 6.76% and the difference in Rnd value between the FAO–PENMAN model and REMOTE SENSING model is 0.94 (MJ/m^2/d) equivalent to 5.58%. The largest difference between Rnd_FAO–PM and Rnd–IRM values at Lam Son hydrological station is –1.90 (MJ/m^2/d) respectively 9.89% and the smallest at Hoa Binh meteorological station is –0.31 (MJ/m^2/d) respectively 1.75%. The largest difference between Rnd_FAO–PM and Rnd–VT values at Lac Son meteorological station is 2.80 (MJ/m^2/d) as 17.49% and the smallest at Lam Son hydrological station is 0.23 (MJ/m^2/d) as 1.18%. The difference in daily average net radiation value as a percentage at meteorological and hydrological monitoring stations between Rnd_FAO and Rnd_RS: in the range of 0–5%, with 5/8 stations accounting for 62.5%; in the range of 5–10 % is 1/8 stations accounting for 12.5%; in range of 10–15% is 1/8 stations accounting for 12.5% and the difference in the range of 15–20% is 1/8 stations accounting for 12.5%. Therefore, with the advantages of remote sensing image data and the difference between Rnd calculation results according to REMOTE SENSING model and FAO–56 model, it can be confirmed that remote sensing data is used to determine Rnd with the average difference of 5.58% is

sufficient to ensure the reliability to calculate the average daily radiation from remote sensing images instead of using directly observed data from meteorological stations.

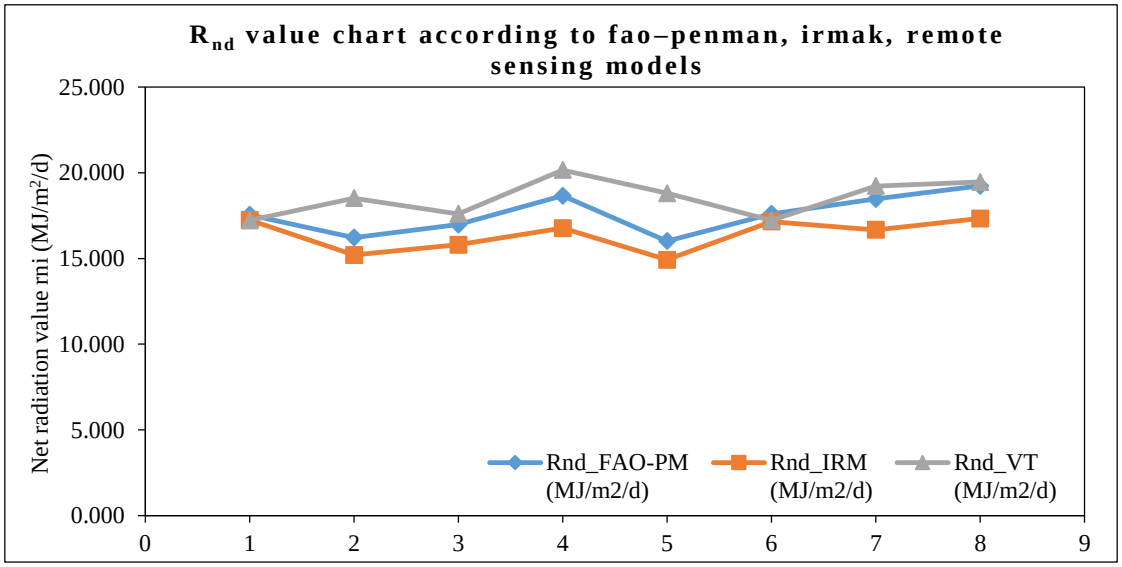

Figure 5. Daily average net radiation from three models: FAO–56, IRMAK and Remote Sensing model.

Figure 5 shows that the average net radiation per day calculated according to the IRMAK model (Rnd–IRM) is lower (–1.20 MJ/m^2/day) than the FAO–56 model. On another hand, the mean daily average net radiation calculated by the REMOTE SENSING model (R_{nd}_RS) is higher (0.94 MJ/m^2/day) than the mean daily net irradiance value according to the FAO model –56 (R_{nd}_FAO–56).

4. Conclusion

The research calculated the average daily net radiation value according to the FAO–56 model, IRMAK model from direct observation data at meteorological and hydrological stations and REMOTE SENSING models from Landsat–8 satellite images taken on June 4, 2017. The average daily net radiation value at hydrometeorological and hydrological monitoring stations calculated according to FAO–56, IRMAK, and REMOTE SENSING models is 17,593 MJ/m^2/day, 16,389 MJ/m^2/day and 18,531 MJ/m^2/day, respectively. The mean difference of R_{nd} between the FAO–56 model and the IRMAK model is –1.20 (MJ/m^2/d) as 6.84%, and the mean difference of R_{nd} between the FAO–56 model and the REMOTE SENSING is 0.94 (MJ/m^2/d) as to 5.58%. The largest difference between R_{nd} _FAO–56 and R_{nd}_IRM at Lam Son hydrological station is –1.885 (MJ/m^2/day) accounting for 10.10% and the smallest difference at Hoa Binh meteorological station is –0.31 (MJ/m^2/day) respectively 1.75%. The largest difference between the calculated values of Rnd_FAO–56 and Rnd_RS at Lac Son meteorological station is 2.80 (MJ/m^2/day) as 17.49% and the smallest at Lam Son hydrological station is 0.23 (MJ/m^2/day) equivalent to 1.18%. The difference in average daily net radiation value as a percentage at meteorological and hydrological monitoring stations between Rnd_FAO and Rnd_VT: in the range of 0–5%, with 5/8 stations accounting for 62.5%; in the range of 5–10 % is 1/8 stations accounting for 12.5 %; in the range of 10–15% is 1/8 stations accounting for 12.5% and the difference in the range of 15–20% is 1/8 stations accounting for 12.5%. Therefore, with the advantages of remote sensing image data and the difference between R_{nd} calculation results according to REMOTE SENSING and FAO–56 model, it is not exaggeragted to say that the use of remote sensing image data to determine R_{nd} with the average difference average 5.58% is reliable to

calculate the average daily radiation from remote sensing images instead of using directly observed data from meteorological stations.

Author contribution statement:

Conceptualization and methodology: H.C.L., H.P.D.; validation, formal analysis: H.C.L.; investigation and project administration: C.H.L., T.X.T.; resources, data curation, software, draft: H.C.L., H.P.D.; preparation and writing–original: H.C.L., writing–review, and editing, visualization: H.P.D., T.X.T. All authors have read and agreed to the published version of the manuscript.

Acknowledgments: This article is part of Mr. Le Hung Chien's doctoral thesis research. The authors would like to thank members of the Department of Imaging–Remote Sensing, University of Mining and Geology for discussions aimed at improving the quality of the publication.

Competing interest statement: The authors declare no conflict of interest.

Reference

1. Diak, G.R.; Gautier, C. Improvements to a simple physical model for estimating insolation from GOES data. *J. Clim. Appl. Meteorol.* **1983**, *22*, 505–508.
2. Gautier, C.; Diak, G.; Masse, S. A simple physical model to estimate incident solar radiation at the surface from GOES satellite data. *J. Appl. Meteorol.* **1980**, *19*, 1005–1012.
3. Jacobs, J.M.; Myers, D.A.; Anderson, M.C.; Diak, G.R. GOES surface insolation to estimate wetlands evapotranspiration. *J. Hydrol.* **2000**, *266*, 53 – 65
4. Ma, Y.; Su, Z.; Li, Z.; Koike, T.; Menenti, M. Determination of regional net radiation and soil heat flux over a heterogeneous landscape of the Tibetan Plateau. *Hydrol. Processes* **2002**, *16*, 2963–2971.
5. Bastiaanssen, W.G.M.; Pelgrum, H.; Menenti, M.; Feddes, R.A. Estimation of surface resistance and Priestley - Taylor a parameter at different scales. In Stewart, J.; Engman, E.; Feddes, R.; Kerr, Y. (Eds.). Scaling up in hydrology using remote sensing. New York' Wiley, 1996, pp. 93–111.
6. Jackson, R.D.; Reginato, R.J.; Idso, S.B. Wheat canopy temperature: A practical tool for evaluating water requirements. *Water Resour. Res.* **1977**, *3*, 651–656.
7. Seguin, B.; Assad, E.; Freaud, J.P.; Imbernon, J.P.; Kerr, Y.; Lagouarde, J.P. Use of meteorological satellite for rainfall and evaporation monitoring. *Int. J. Remote Sens.* **1989**, *10*, 1001–1017.
8. Jiang, L.; Islam, S. Estimation of surface evaporation map over southern Great Plains using remote sensing data. *Water Resour. Res.* **2001**, *37(2)*, 329–340.
9. Nishida, K.; Nemani, R.R.; Running, S.W.; Glassy, J.M. An operational remote sensing algorithm of land evaporation. *J. Geophys. Res.* **2003**, *108(D9)*, 4270.
10. Norman, J.M.; Anderson, M.C.; Kustas, W.P.; French, A.N.; Mecikalski, J.; Torn, R.; Diak, G.R.; Schmugge, T.J.; Tanner, B.C.W. Remote sensing of surface energy fluxes at 101-m pixel resolutions. *Water Resour. Res.* **2003**, *39(8)*, 1221.
11. Ke, L.C. Evaluating the accuracy of surface evapotranspiration according to Makkink model based on solar radiation data extracted from Modis satellite images. Proceedings of the Science and Technology Conference, University of Hanoi Natural Resources and Environment, 2013.
12. Tuong, T.N.; Manh, P.V.; Ke, L.C. Surveying hourly surface evapotranspiration on the Priestley–Taylor model by net radiation extracted from Modis satellite images. Proceedings of the Society Science and Technology Workshop, Institute of Geodesy and Cartography, Hanoi, 2014.

13. Ke, L.C.; Tuong, T.N.; Manh, P.V. Comparing the average daily net radiation estimate extracted from Modis satellite images with the results from meteorological observation data. Reported in the conference proceedings. Science and Technology, University of Ho Chi Minh City Natural Resources and Environment, 2014.
14. People's Committee of Hoa Binh province, 2018 statistical yearbook.
15. http://landsat.usgs.gov/landsat8.php/. Detailed information about the Landsat 8 satellite provided by the US Geological Survey (USGS).
16. Allen, G.R.; Pereira, L.S.; Raes, D.; Smith, M. Crop Evapotranspiration–Guidelines for computing crop water requirements. FAO Irrigation and Drainage Paper 56. FAO, Rome, Italy, 1998, pp. 78–86.
17. Allen, G.R.; Pereira, L.S.; Raes, D.; Smith, M. Crop Evapotranspiration–Guidelines for computing crop water requirements. FAO Irrigation and Drainage Paper 56. FAO, Rome, Italy, 1998, 78–86.
18. Irmak, S.; Irmak, A.; Allen, R.G.; Jones, J.W. Solar and net radiation-based equations to estimate reference evapotranspiration in humid climates. *J. Irrig. Drain. Eng. ASCE* 2003, *129(5)*, 336–347.
19. Allen, R.; Tasumi, M.; Trezza, R. Advanced Training and Users Manual SEBAL Surface Energy Balance Algorithms for Land, University of Idaho, 2002, pp.1–98.
20. Jackson, R.D.; Hatfield, J.L.; Reginato, R.J.; Idso, S.B.; Jr Pinter, P.J. Estimation of daily evapotranspiration from one-time-of-day measurements. *Agric. Water. Manage.* **1983**, *7(3)*, 351–362.

VIETNAM JOURNAL OF HYDROMETEOROLOGY

Research paper

Forecasting saline intrusion under the influence of the northeast monsoon in the Mekong Delta

Nguyen Van Hong[1]*, Nguyen Thao Hien[1], Nguyen Thi Thanh Minh[1], Ho Cong Toan[1]

[1] Sub-Institute of Hydrometeorology and Climate Change; nguyenvanhong79@gmail.com; nthien2710@gmail.com; minhmminh0419@gmail.com; hocongtoanhdh@gmail.com;

*Correspondence: nguyenvanhong79@gmail.com; Tel: +84–913613206

Received: 05 September 2021; Accepted: 03 October 2021; Published: 25 December 2021

Abstract: Saline intrusion is one of the most frequently occurring natural disasters in a coastal area, posing the most serious impact in the Vietnamese Mekong Delta (MD). With the characteristics of the region as an open and low system, located at the end of the Mekong River basin and part of the Vam Co River system, this region is strongly affected by the tidal regime, and therefore saline intrusion is a feature of the region and has become familiar to the people living here in the dry season. The degree of deep penetration into the inland area depends on several factors. These factors contribute to the determination of the depth of salinity penetration into the MD. Therefore, the paper will focus on the 3 factors having the greatest impacts on the salinity penetration, including the influence of upstream flow, high tide, and the northeast monsoon season in the application of a combined assessment model to forecast saline intrusion in 2021 in the Mekong Delta. The reliability of the salinity propagation module is greater than 0.7%, based on the data series observed and calculated daily for 3 months during the dry season. The location of the measuring stations from the estuary to the inland field is about 20–50 km, showing a suitable range to calculate the salinity forecast to support livelihood models in the Mekong River.

Keywords: Saline intrusion; Upstream flow; Tide; Southeast wind; Vietnamese Mekong Delta.

1. Introduction

The saline intrusion in the Mekong Delta (MD) has caused several disadvantages to water sources for production and people's life, in the context of flourishing development of hydropower plants on the Mekong mainstream with higher intensity and frequency due to climate change (CC) [1]. The MD has a flat–hollow–open–low terrain with a ground elevation of 2m lower than the sea level, under the influence of uneven semidiurnal tidal regimes in the East Sea and diurnal tidal regimes in the West Sea [2-4]. In addition, the MD is also located in the active monsoon region. Especially during the northeast monsoon with the prevailing direction of the east–southeast, the water source at the upstream of the Mekong River flowing to the downstream at the lowest level, together with the wind direction parallel to the estuaries, resulting in the tide level rise and causing the deeper saline intrusion into the river [5].

Serious saline intrusion in MD in 1977, 1993, 1998, 2005, and 2010 caused heavy damage to the economy, society, and environment. Especially, there have been 2 times of historical saline intrusion with the earlier occurrence and deeper intrusion in the river and canal system [6] in the last 5 years. Notably, a salinity limit of 4 g/l can approach as deep as

80 kilometers into the main rivers, leading to 10/13 provinces affected by saltwater in 2016. By 2020, a salinity limit of 4 g/l can approach as deep as approximately 100km inland, an increase compared to the same period in 2016, causing damage to the coastal provinces up to 100,000 ha of productive land and about 95 households are in lack of freshwater [7-10]. It can be seen that the occurrence of the last two historical events in a short period has been clear evidence of the increasing severity of saline intrusion in the MD.

Studies on calculation or forecasts and early warning of salinity intrusion in the MD are quite abundant. These studies have evaluated the combined impacts of climate change and the rapid development of an upstream hydropower dam system, with the variation of precipitation, sea-level rise, and upstream flows. These studies are approached with different methods such as (a) hydrological models to assess salinity concentrations in river basins [3, 8, 15, 16]; (b) hydrodynamic modeling and combination with meteorological and tidal forecast models, to clarify salinity intrusion and hydraulic regime in the estuaries [2]; (c) using deep learning method based on artificial neural network platform [17–18], in the MD, publications on this issue are rather scarce in general. In addition, the study [21] proposed a method different from the above methods for early warning of saline intrusion in the MD, which is a simple linear seasonal forecasting model based on ENSO and SSI (standardized streamflow index) predictors. With a dense river network and many irrigation works, while input data and computational capacity are limits, hence the one–dimensional model has been widely used for the study area, considered as a feasible method to apply flow simulation and saline intrusion for the entire river system in the MD [15].

For example, recent studies on simulating and forecasting saline intrusion in the MD may be cited [11], has applied modeling (MIKE 11–MIKE11 GIS) to calculate and forecasted salinity based on Google Earth software at coastal stations and upstream flow fluctuations at Tan Chau, Chau Doc stations. The model is currently serving forecasting work at the National Center for Hydrometeorological Forecasting. Another study [12] has built a tool to assess the socio-economic effects of saline intrusion to estimate the damage caused by the saltwater intrusion on people, economy, and society with the historical salinity event in 2016 for 4 provinces (Ca Mau, Bac Lieu, Kien Giang, Soc Trang, Ben Tre), the level of visual impact is shown on a map and calculated by the exposure, hazard and vulnerability functions based on human objects using water in production, aquaculture and cultivation.

With international cooperation studies on the harmful effects of saltwater intrusion and solutions for the MD region, [13] has analyzed data on perceptions of the adverse impacts of salinity intrusion on rice farming, through the process of interviewing households and workers to investigate the people’s understanding of the extent and how to respond to natural disasters, to give recommendations and solutions to the increasing saltwater intrusion in the MD. For the study [14] has calculated the Socio-ecological resilience of mangrove–shrimp models under various threats exacerbated from salinity intrusion in the coastal area. This study utilized a Motivation and Ability framework in combination with a sustainable livelihood framework to measure the perceived values and resilience of mangrove–shrimp farming systems, based on a broad interview with farmers, scientists.

Summarizing the latest articles related to the problem in the MD, saline intrusion is one of the types of natural disasters that have a terrific and strong impact on people’s lives and perceptions. Since then, it has led to studies from basic to advanced levels on the evolution of saline intrusion to its damage potential and measures to adapt to its increase over time. Simultaneously, the studies also provide pilot models of livelihoods for improving people's material and spiritual lives in response to saline intrusion and lack of freshwater.

However, at present, there are no specific studies on the northeast monsoon or other bases to forecast or have a warning of the extent and speed of wind impacting the saline intrusion. Thus, it is very necessary and essential to forecast the impact of saline intrusion

in the MD quickly and accurately. In this study, the authors will focus on analysis and evaluation of the process of salinity transmission in the main rivers, under the influence of the upstream flows and tidal regime in combination with the northeast monsoon with mathematical modeling method.

2. Materials and methods

2.1. Study area

2.1.1. Advantages

The MD is located at the end of the Mekong River basin with an area of over 39,000 km^2, accounting for 79% of the delta area and equal to 5% of the Mekong River basin area. The MD has a large system of rivers and canals, including the Tien and Hau river systems, the Vam Co river system, the Cai Lon–Cai Be river system, the Giang Thanh River, and many other tributaries and canals (Figure 1). Geographical location and natural conditions not only create advantages in irrigation and drainage for agriculture, industry, fishery, and forestry, etc. But also play an important role in transportation for economic and social activities. The MD is located in the humid & tropical, sub-equatorial monsoon area, favorable for the development and diversification of crops and livestock. Several valuable aquatic species can be cultivated in the coastal areas which are affected by saline intrusion [1–4].

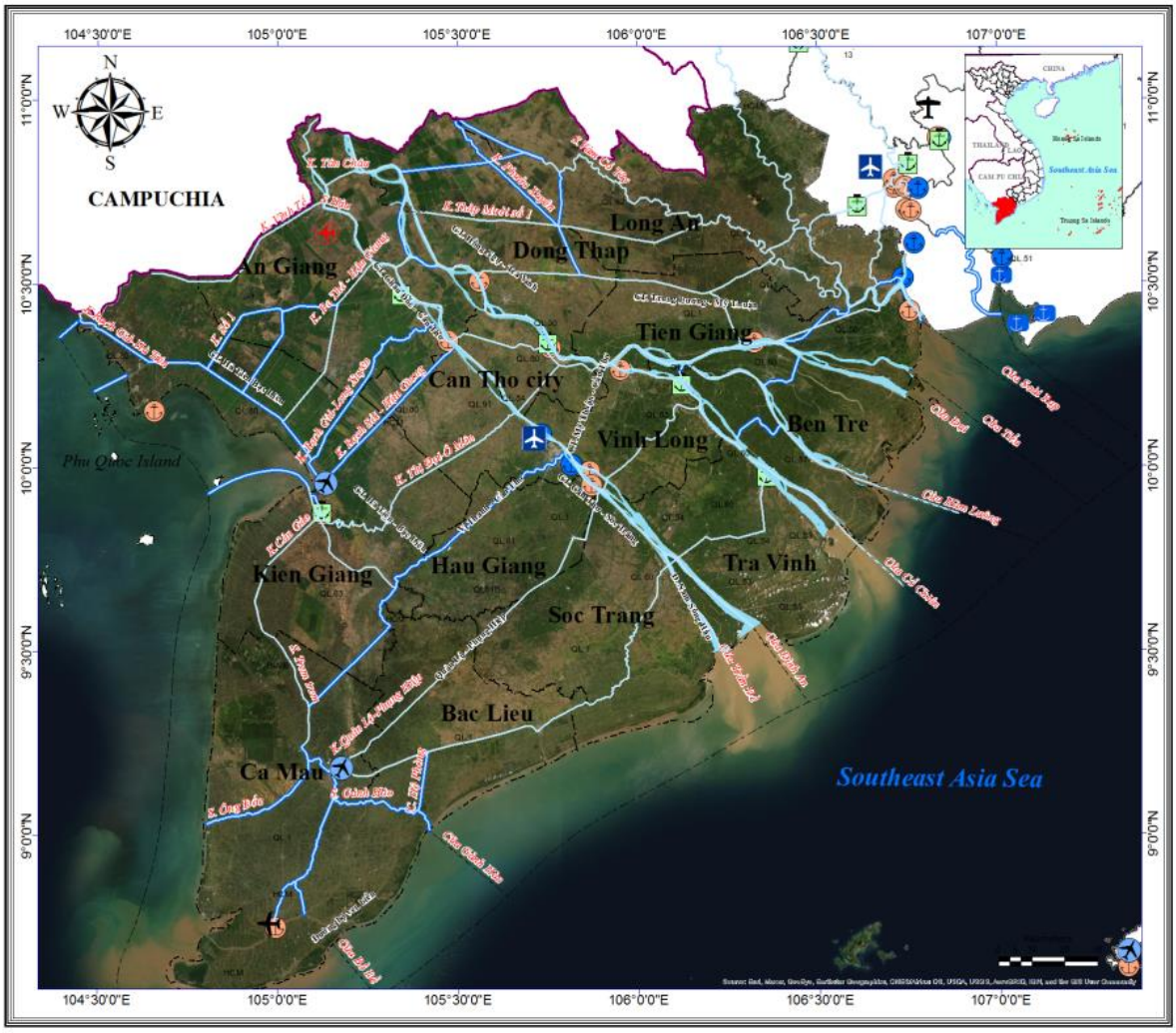

Figure 1. The Mekong Delta region.

2.1.2. Disadvantages

Two important upstream factors affecting water resources in the MD are the amount of water stored in TonleSap, which helps to regulate and limit flood flows in the MD during the flood season and increases the water source in the dry season; and the flow to the Kratie station (at the beginning of the MD) which is located about 300km upstream from the Vietnam–Cambodia border, representing the starting point of the lower Mekong River [19].

Depending on the above conditions, there are great changes in the flow to the delta in nature, the change could be from a tendency to flow naturally to being regulated in both the flood and dry seasons. While the large floods become less frequent, the number of the small and medium floods increases and floodplains in the upper delta become "eager and eager for the flood", leading to a lack of mud and sand in the MD for sedimentation, the lack of water to push salt back into the sea; making the saline intrusion more and more complicated to be forecasted. The northeast wind can become a negative factor in the lives of the residents in the MD.

2.2. Setup hydrodynamic and advection-dispersion models

MIKE 11 model, a mathematical model, is used in this study as the main method. MIKE 11 is a one-dimensional unsteady flow modeling for the detailed analysis, design, management, and operation of both simple and complex river and channel systems. In the MIKE 11 model, the river/channel flow process is calculated based on the Saint Venant Equations that are solved by the Abbott–Ionescu six-point implicit difference method. This model and MIKE Zero have been applied widely in several types of research and projects in Vietnam. Besides, the MIKE 11 model set is also used in annual forecasting at the Sub–Institute of Hydrometeorology and Climate Change.

In this study, two modules in MIKE 11 (i.e. Hydrodynamic (HD) and Advection – Dispersion (AD) modules) were applied to simulate and forecast the saline intrusion in the MD. The methodological framework in this study is described in Figure 2, including the data collection step, calculation scenarios, model reliability assessment, and the impacts on the increase of saline intrusion and transmission in the MD.

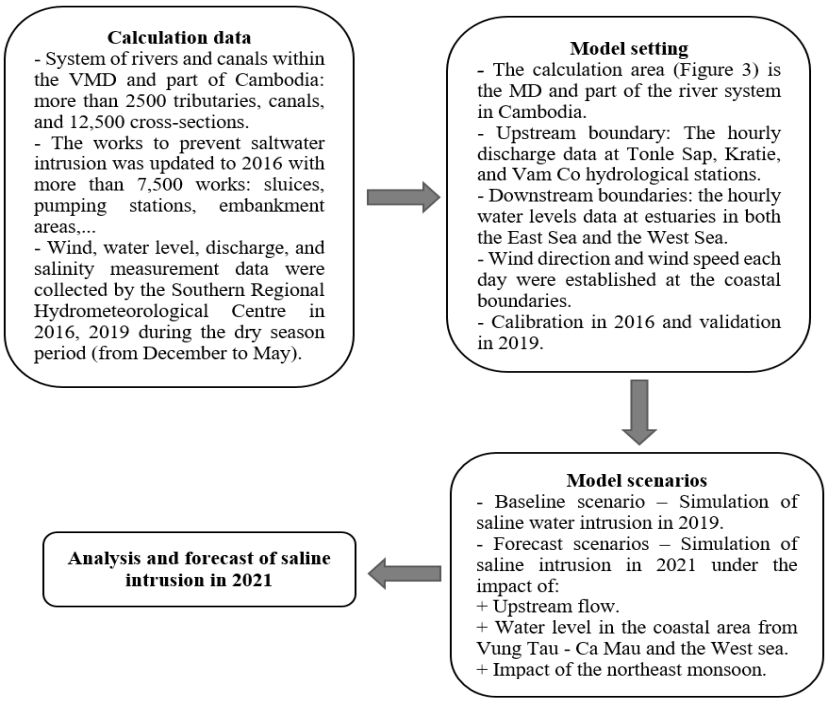

Figure 2. The methodological framework for salinity forecast.

The MD and part of the river system in Cambodia with more than 2,500 tributaries, canals, and 12,500 cross-sections are the area for calculation. There are more than 7,500 works, including the culverts, pumping stations, embankment areas as of 2016.

Boundary data for the model:

- Flow boundaries at Tonle Sap, Kratie and Vam Co;
- Tidal level boundaries at tributaries in both East Sea and West Sea;
- The parameters showing wind direction and wind speed at the coastal boundaries.

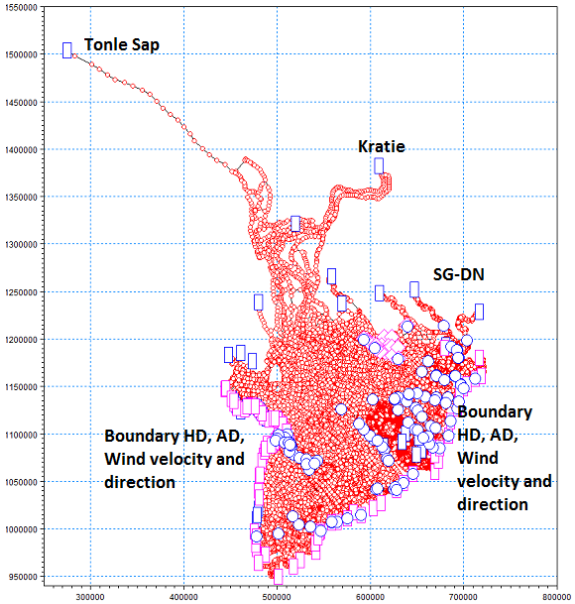

Figure 3. River network in modeling saline intrusion: including boundaries and hydrological stations.

2.3. Data acquisition for forecast scenarios in 2021

The salinity in the MD depends on many factors such as a) the water flow upstream of the Mekong River, b) the volume of water accumulated from the flood season of the previous year and rainfall, c) the tidal regime in combination with the northeast wind and d) the groundwater extraction for production and daily life [4].

This task is applied to a mathematical model in consideration of the factors causing the significant increase in the salinity over time in river basins, showing the process of the river–sea interaction, the complexity of river flows, tides, and meteorological conditions in the dry season.

a) Upstream flow

Two upstream factors that significantly affect freshwater reserves and saline intrusion in the lower MD are the water stored in Tonle Sap and the flow at the Kratie station. According to the statistical report updated to April 2016 by the Southern Institute of Water Resources Research, the evolution of water in Tonle Sap (Figurea) is extremely low (about 1.23 m on average) compared with the average data series from 1980 to 2031, and this was lower than an average level of 0.69 m at the same period in 2014–2015. As can be seen, the flow of Tonle Sap to the Delta is extremely limited [24].

The annual flow at the Kratie station (Figureb) was very low from the beginning of the dry season until March started to increase from the end of the month to the beginning of April, and remained stable. It can be seen that the serious shortage of fresh water occurs when the saline intrusion approaches inland the deepest. According to the data series of the flow path in Kratie for the period 1980–2016, there are fluctuations in a certain value range at the time of the driest month of the year [24].

Flow material was collected in 2011, 2012, 2013, 2016, and 2019 at Kraite station. The boundary-value of the two upstream locations is the average flow of the years, thereby determining the forecast flow and calculating saltwater intrusion for the dry season of 2021.

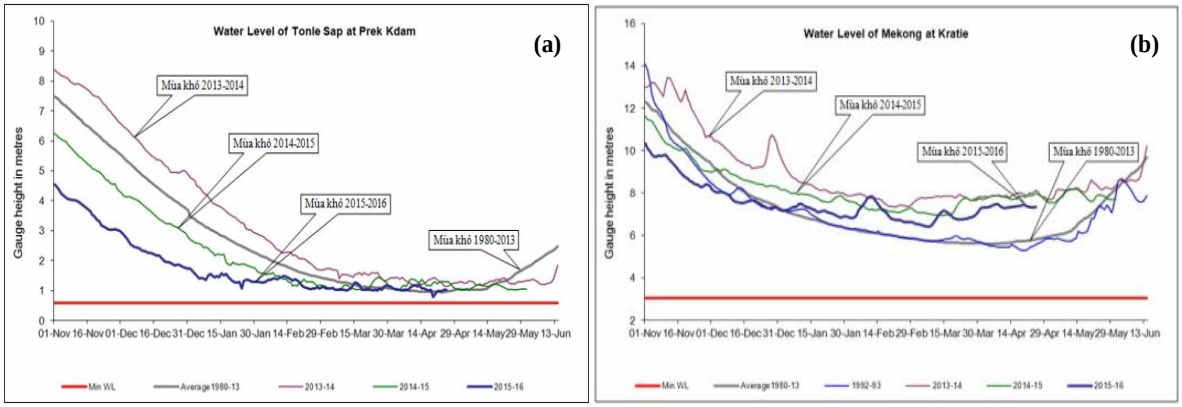

Figure 4. Daily discharges in the upper Mekong River over the years: a) The water level in the dry season 1980-2016 of Tonle Sap; b) The water level in the dry season 1980-2016 at Kratie station.

b) Forecasting the water level

To forecast the coastal tide level, the U–Tide calculation software by analyzing the harmonic constant set is applied to this task. "U–Tide consists of a pair of Matlab functions designed to be easy to understand and implement: ut_solv: for analysis in two-dimensions (e.g., tidal currents) and one-dimension (e.g. sea level); ut_reconstr: to use the analysis results for reconstruction of a time sequence for a hind-cast or forecast/prediction if needed" [22]. The software has become widely accepted in the study of physical oceanography. The results of the water level forecast at estuary stations in the Southern region using U–TIDE are shown in Figure.

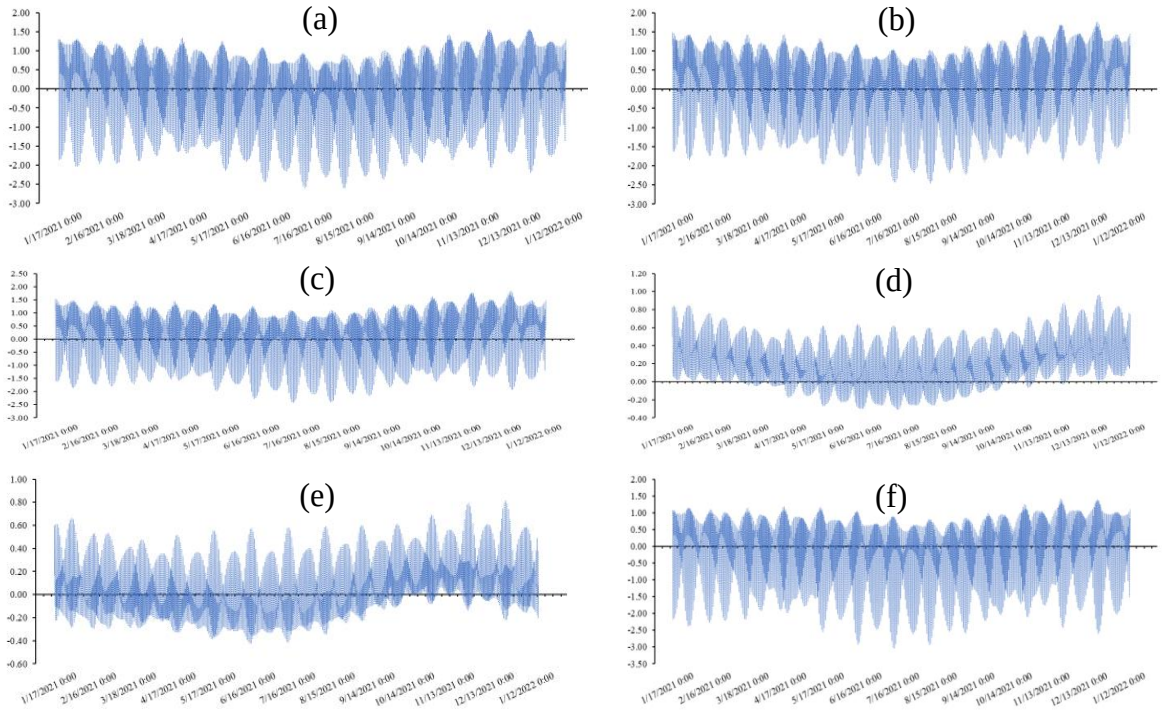

Figure 5. Forecasted water levels in 2021 at coastal stations in the Southern region: (a) Vam Kenh; (b) An Thuan; (c) Ben Trai; (d) Song Doc; (e) Rach Gia; (f) Vung Tau.

Tide peaks can reach over 1.5 m starting in early January and ending in late March.

Table 1. Forecasted high and low tides at coastal stations in the Southern region from January to March 2021.

Name of station	Highest day	High tide				Low tide			
		H (m)	Hour xh	H (m)	Hour xh	H (m)	Hour xh	H (m)	Hour xh
Vam Kenh	February 31, 2021	1.34	5:00	1.19	17:00	–1.17	11:00	–1.4	23:00
An Thuan	February 3, 2021	1.42	5:00	1.23	18:00	–1.48	12:00	–0.71	23:00
Ben Trai	February 3, 2021	1.46	5:00	1.27	18:00	–1.46	12:00	–0.48	23:00
Song Doc	January 14, 2021	0.85	4:00			0.04	11:00		
Rach Gia	January 14, 2021	0.66	5:00	0.15	17:00	–0.13	13:00	–0.28	22:00
Vung Tau	February 3, 2021	1.14	4:00	1.01	17:00	–1.84	11:00	–1.02	23:00

c) The northeast monsoon wind

In the middle and late months of the dry season in the MD, wind components with a direction from Northeast to Southeast often appear, most notably the wind with Southeast direction, which raises the water level, contributing to the transfer of salinity inland, affecting agricultural production, which is called "Gio Chuong". This type of wind is formed from the Asian continent's high pressure in the East Sea and the development and expansion of the Pacific subtropical high pressure to the west. Specifically, from 5 a.m. to 12 p.m., the prevailing wind direction between East and East-Northeast roughly coincides with the wind direction at sea. From 2 p.m. to 2 a.m., influenced by sea-continental winds, the main wind direction will be Southeast [5].

In the Southern region, at the beginning of the season, the wind only accounts for 20–30% of all windy days, but this rate gradually increases and by February, the rate will account for 73%. Under the influence of "Gio Chuong", all wind levels can exceed the level of over 5 - 6m/s (the level of wind obstruction affects saline intrusion).

The wind charts (Figure 6, Figure 7) as follows show characteristics of wind direction and speed in the northeast monsoon time (from February to April) at Soc Trang and My Tho stations in 2015 and 2016.

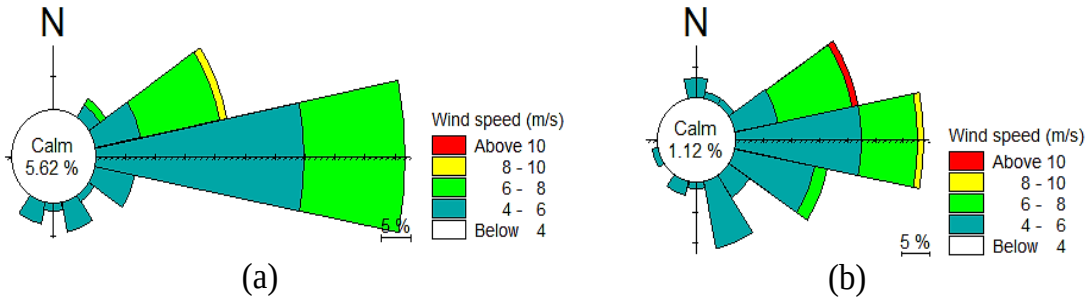

Figure 6. Wind charts at Soc Trang station in the dry season in 2015 (a) and 2016 (b).

It is shown in the wind chart of the Soc Trang station that the prevailing wind direction in 2015 is from the East and East–Northeast (Figure). By 2016, the wind direction blowing from the southeast appears more with a frequency of 15%. Therefore, it can be assumed that the wind direction blowing from the East–Southeast may cause disadvantages and increase the salinity in coastal areas such as Tran De, Dinh An (Hau river), My Thanh river (Soc Trang province).

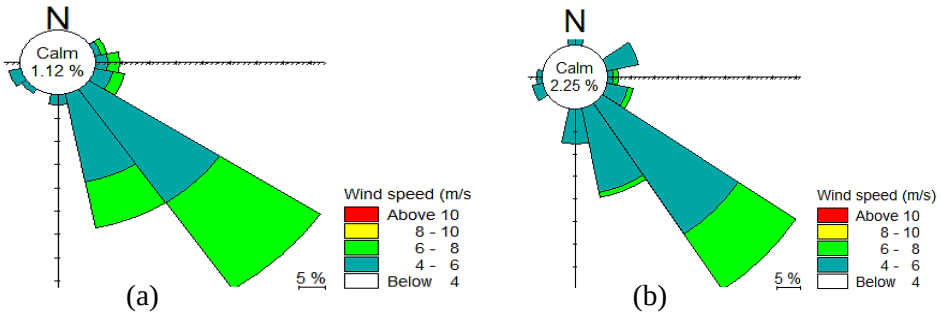

Figure 7. Wind charts at My Tho station in the dry season in 2015 (left) and 2016 (right).

Based on the wind chart at My Tho station over the years 2015 and 2016 (Figure), the prevailing wind direction is the Southeast direction with the direction perpendicular to the estuary cross-section at major tributaries such as Tien and Co Chien rivers, Ba Lai, Ham Luong River, and Vam Co river systems with common wind speeds of 4–8 m/s.

The northeast monsoon is one of the specific meteorological factors that cause many disadvantages to freshwater sources in the MD. To forecast saline intrusion most effectively, it is necessary to include the influencing factors in the saline simulation. Although it occurs every year and is considered a typical feature of the region, there is no software model to forecast it or quantify its morphological trends. As the result, the wind data in 2016 shall be used to forecast, due to the similarity between the wind direction blowing at My Tho and Soc Trang stations.

3. Results and discussion

3.1. Model calibration and validation

Based on the data after 2012: the Saline intrusion in the MD estuaries tends to be about 1 a month earlier than in the previous period; salinity has been affected since late December of the previous year in the year with the low flow, and can reach the highest salinity from February to mid–March; and tend to decrease rapidly from the end of March because of the increase in the low flows thanks to the flow regulation at the upstream. The maximum salinity limit of 4 g/l in the dry season can approach more than 70 km; In the past, it could only approach 60km in years of high salinity in several estuaries, now it occurs more often [3]. Therefore, the data used for calibration & validation is calculated from February to April. The final results of salinity concentration at various stations are presented in Table 2.

Table 2. Results of salinity testing at the Mekong Delta stations.

	The MD river basin	**Saigon–Dong Nai River basin**
The proposed options to calculate the salinity transmission, are: - Adjusting the salinity value on an hourly basis of February 2016; - Testing with the highest salinity value of the day	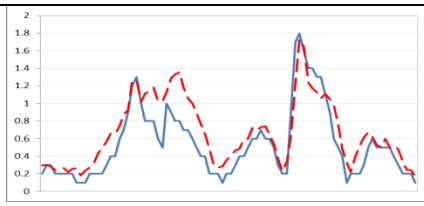	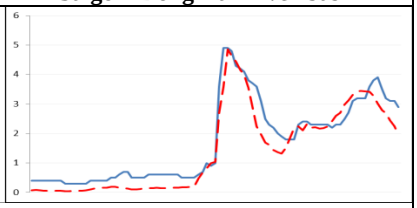
	My Hoa Station – Ham Luong river NSE = 0.681	Tan An Station –Vam Co river NSE = 0.62

from February to April 2019.

Thus, to focus on analyzing the important factors, the table presents the final results (testing the model) at the salinity measurement stations in the MD.

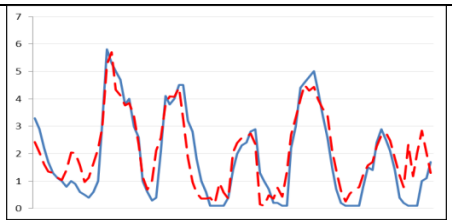

Tra Vinh Station – Co Chien river

NSE = 0.778

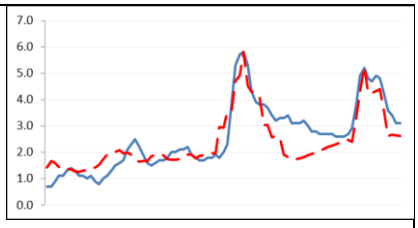

Ben Luc Station – Vam Co river

NSE = 0.725

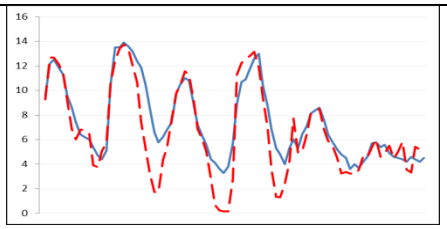

Tra Kha Station – Hau river

NSE = 0.76

According to the simulation results of salinity at the MD estuaries, in the dry season of 2019, the salinity came earlier from the beginning of December last year and reached the highest salinity in February and March, then gradually decreased. Compared to the 2016 period, the level of salinity difference between the measuring stations is much more significant. In Vam Co rivers, the salinity rate in 2016 was 5‰ higher than in 2019 at each station. Particularly for the MD rivers, the difference in salinity concentration is obvious (5–10‰). Especially for large rivers (Tien River, Hau River) with large and wide estuaries, flat terrains along with other factors have made saltwater intruded deeper into the inland. Therefore, to forecast saline intrusion for the main river systems in the MD, it is necessary to consider the negative factors causing more saline intrusion.

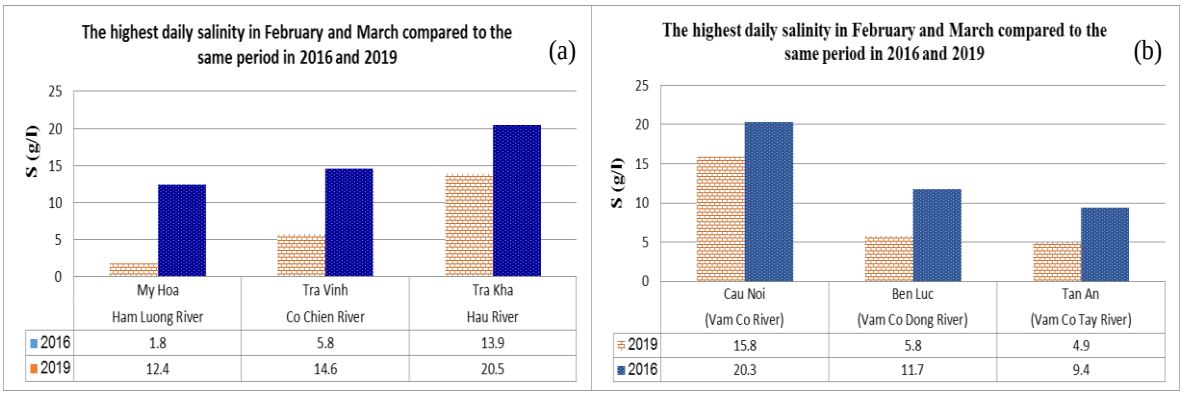

Figure 8. Maximum daily salinity concentrations from February to March 2016 and 2019: (a) The MD river basin; (b) Saigon–Dong Nai river basin.

Results and discussion: According to the assessment results in the graph of the salinity process at the MD salinity measurement stations, the index presents the reliability and accuracy of the model parameters in application in the forecast and have warning on the saline intrusion in the main rivers of the MD such as Hau River, Tien River, Vam Co, Co Chien, Ham Luong, etc. At the same time, the salinity assessment chart at 6 stations (Figure) has also shown the impact of natural factors on the extent of salinity penetration, salinity magnitude, and time of occurrence in the inland area. Therefore, it is necessary to study and include in the forecasting process the influence of negative factors on the formation of salinity to forecast the saline intrusion for the main river systems of the MD provinces.

3.2. Forecasting results

The average flow in the dry season tends to decrease. In recent years, there have been changes in the time of occurrence of the highest water level: the average tidal peak in the last 10 years is about 2–6 cm higher than the average of several years.

The trend of saline intrusion in the MD will be more complicated and the MD will have to cope with the saline intrusion and "eager for flooding" in the lower Mekong as shown in the forecast table of salinity values from February to April 2021 (Table 3) and the map of the maximum salinity in the dry season in 2021 (Figure). Among 13 provinces in the MD, there are 9 ones subject to the impacts of the saline intrusion. Especially the red area, it is forecasted that Ca Mau and the West Sea will have the highest salinity from 15–25‰ according to the map. The estuaries are subject to the influence of the northeast wind such as Tran De, Dinh An, Dai, Tieu, and Thi Vai river, etc., belonging to the main rivers such as Hau, Tien, and Vam Co river will have good conditions for saline intrusion into the inland. In coastal provinces and provinces along major rivers such as Tra Vinh, Soc Trang, Vinh Long, Ben Tre, and Long An, the salinity is forecast at 10–25‰.

With increased and prolonged salinity, saline intrusion will affect the mangrove ecosystem along with the sea level rise, which has risks causing negative impacts on the vegetation and biodiversity of Melaleuca forest ecosystems in coastal provinces such as Ca Mau, Kien Giang, etc.

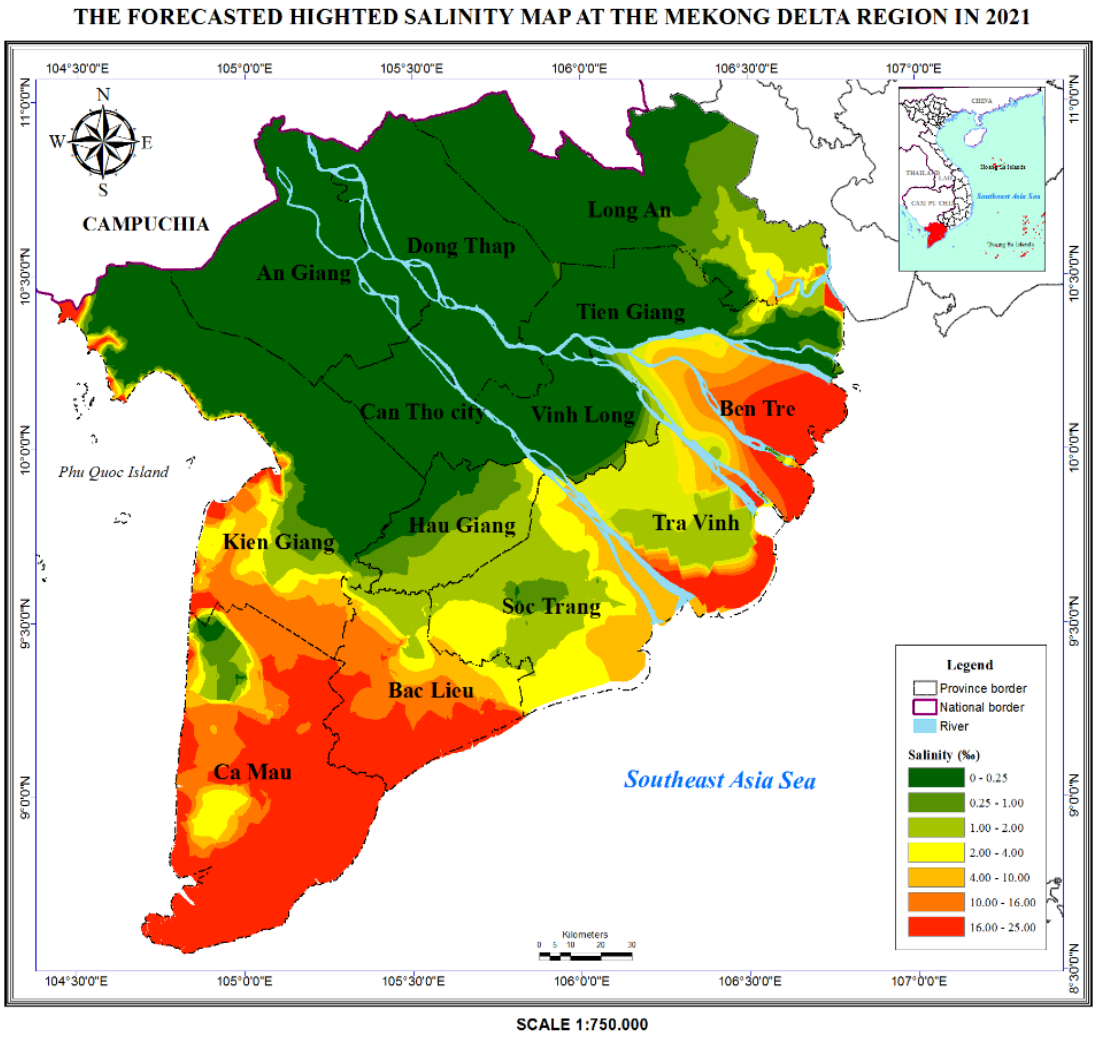

Figure 9. The forecasted highest salinity in 2021.

Table 3. Forecast of the highest salinity range from February to April 2021 at hydrological stations in the MD.

No.	Name of the station	River	The highest salinity range (‰)		
			February	March	April
1	Bnh Dai	Cua Dai	24 – 26	24 – 26	22 – 24
2	My Hoa	Ham Luong	8 – 10	7 – 9	9 – 11
3	Tra Vinh	Co Chien	14 – 16	9 – 11	14 – 16
4	Ben Trai	Co Chien	24 – 26	21 – 23	20 – 22
5	Dai Ngai	Hau	14 – 16	10 – 12	15 – 17
6	Tra Kha	Hau	23 – 25	25 – 27	21 – 23
7	Tran De	Hau	25 – 27	25 – 27	21 – 23
8	Ca Mau	Ganh Hao	27 – 29	25 – 27	27 – 29
9	Xeo Ro	Cai Lon	18 – 20	18 – 20	14 – 16
10	Rach Gia	Bien Tay	15 – 17	23 – 25	24 – 26
11	Ben Luc	Vam Co Dong	5 – 6	7 – 8	4 – 6
12	Cau Noi	Vam Co	12 – 14	15 – 17	14 – 16

Based on the measured and predicted salinity results in April 2021 (Table 3 and Figure), it is revealed that:

In the Vam Co river system, the measured salinity is all within the forecast range, such as Ben Luc station with the measured salinity value of 4.8‰, which is consistent with the forecast range of 4–6‰. At Cau Noi station, the measured salinity is 16.8‰, corresponding to the forecasted salinity in the range of 14–16‰.

In the MD river system, the results at the estuary and inland salinity measurement stations are as follows:

+ At coastal stations: Tran De station and Xeo Ro station with measured salinity of 22.4‰ and 13.8‰ respectively, both stations are within the predicted value; Binh Dai station has a measured salinity higher than the forecasted value of 0.5‰; Ben Trai station with measured salinity is 16.4‰, smaller than the forecasted value of 3‰.

+ Regarding the inland stations, the predicted salinity tends to be higher than the measured value from 3–6‰. In particular, My Hoa station has measured salinity of 6.3‰ (–3‰); Dai Ngai station has measured salinity of 7.3‰ (–6‰), and Ca Mau station has measured salinity of 34.5‰ (+5‰). ("–" Smaller value; "+": value larger than the forecast range).

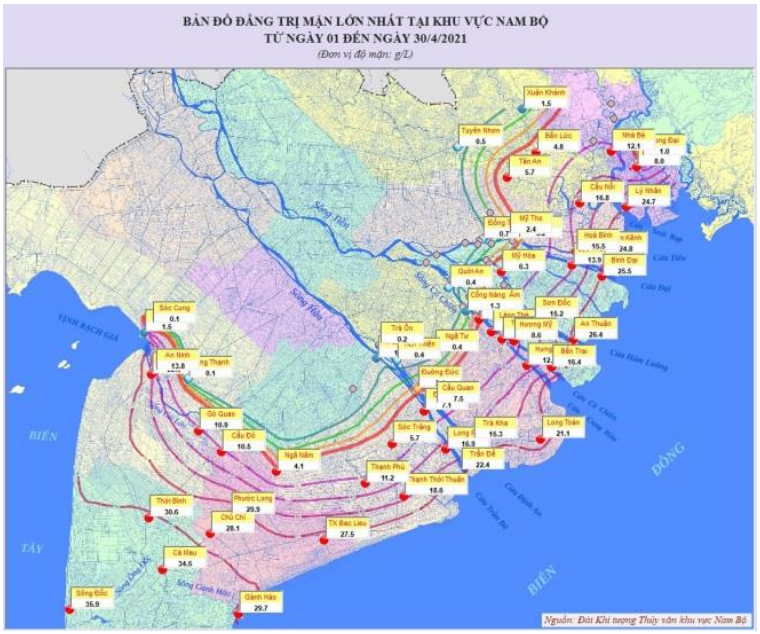

Figure 10. Map of the max salinity contour in the Southern region from April 1 to 30, 2021 (Southern Regional Hydrometeorological Centre).

According to the results of analysis and assessment of saline intrusion, the monthly salinity forecast value based on the salinity trends in the Vam Co river system, Rach Gia, and Cua Tran De areas is more consistent with the measured values. In the inland area, forecasts of salinity are still limited due to the complexity of the canal system and saltwater–prevention sluices,... but the deviation is incurable and can be improved thanks to the long–term monitoring and adjustment of the model closer to reality and continuously forecasting in the conditions of climate change and sea-level rise in the MD.

4. Conclusion

The integrated model is applied in the paper for saline intrusion forecast in the Mekong Delta and Saigon–Dong Nai River. From the results of water level verification at hydrological stations and the U–tide model, it is indicated that the model parameters are appropriate for tidal prediction simulation for the study area.

Thus, the forecast results will support providing early warning information for people and local authorities to adjust the cultivation schedule, propose solutions to limit the situation of saline intrusion affecting' lives of residents.

However, the study of factors influencing saline intrusion in the MD remains limited. Especially the flow from the upstream Mekong River. This factor necessitates a long-term research complex because of the climate change of the current period and is influenced by inter-reservoir regulation upstream. Application of this study, the authors desire to operate the annual saline forecasting model to better adjust the model parameters and achieve the best results for the livelihood of the population in the MD.

Author contribution statement: Conceptualization and methodology: Hong. V.N., Hien. T.N.; validation, formal analysis: Minh. T.T.N.; investigation and project administration: Hien. T.N., Toan. C.H.; resources, data curation, software, draft: Hong. V.N., Hien .T.N.; preparation and writing–original: Hong. V.N., Hien. T.N., Minh. T.T.N. writing–review, and editing, visualization: Hong. V.N., Hien. T.N., Toan. C.H. All authors have read and agreed to the published version of the manuscript.

Acknowledgments: This research is completed in the program of regular assignment by the functions of the Sub–Institute of Hydrometeorology and Climate Change in 2021, specifically Task 9: "Forecasting tides and saline intrusion in the main rivers of the Southern region".

Competing interest statement: The authors declare no conflict of interest.

Reference

1. Binh, D.V.; Kantoush, S.; Sumi, T.; Mai, N.T.; Trung, L.V. Study on the impacts of river–damming and climate change on the Mekong Delta of Vietnam. *Disaster Prev. Res. Inst. Annuals* **2017**, *60(B)*, 804–826.
2. Duong, T.A.; Bui, M.D.; Rutschmann, P. Impact of Climate Change on Salinity Intrusion in the Mekong Delta. Presented at the 14th International Conference on Environmental Science and Technology (CEST2015), Rhodes, Greece, 2015.
3. Dat, T.Q.; Likitdecharote, K.; Srisatit, T.; Trung, N.H. Modeling The Influence of River Discharge and Sea Level Rise on Salinity Intrusion in Mekong Delta. In First Environment Asia International Conference on "Environmental Supporting in Food and Energy Security: Crisis and Opportunity", 2011, 685–701.
4. Tuan, T.V.; Thuong, T.V.; Phat, H.P.D.; Hung, D.N. Assessing the Combined Impacts of Dams Upstream, Climate Change, Drought, Tide, and Sea Level Rise on the Temporal Variation of Paddy Land in Tien Giang Province. IOP Conf. Ser. *Earth Environ. Sci*. **2019**, 338.
5. Ba, L.H.; Drought, saline intrusion in the Mekong Delta: Theoretical and Practical

Basis. Ho Chi Minh City National University Publishing House, **2017**, pp. 525, ISBN: 978604735283.

6. Mai, N.P.; Kantoush, S.; Sumi, T.; Thang, T.D.; Trung, L.V.; Van Binh, D. Assessing and Adapting The Impacts of Dams Operation and Sea Level Rising on Saltwater Intrusions into The Vietnamese Mekong Delta. *J. Jpn. Soc. Civ. Eng*. *Ser.* B1, **2018**, *74(5)*, I_373–I_378.
7. Dung, N.T.; Thuan, P.; Lan, N.T. Livelihoods of residents in drought–salt areas in the Mekong Delta – Situation and solutions. *J. Political Sci. Inf.* **2020**, *4*, 77–80.
8. Kantoush, S.; Binh, D.V.; Sumi, T.; Trung, L.V. Impact of Upstream Hydropower Dams and Climate Change on Hydrodynamics of Vietnamese Mekong Delta. Annu. *J. Hydraul. Eng. JSCE* **2017**, *61*, I_109–I_114.
9. Khang, D.K.; Kotera, A.; Sakamoto, T.; Yokozawa, M. Sensitivity of Salinity Intrusion to Sea Level Rise and River Flow Change in Vietnamese Mekong Delta–Impacts on Availability of Irrigation Water for Rice Cropping. *J. Agric. Meteorol*. **2008**, *64*, 167–176.
10. Le, T.N.; Tran, D.X.; Tran, T.V.; Gyeltshen, S.; Lam, T.V.; Luu, T.H.; Nguyen, D.Q.; Dao, T.V. Estimating Soil Water Susceptibility to Salinization in the Mekong River Delta Using a Modified DRASTIC Model. *Water* **2021**, *13*, 1636. https://doi.org/10.3390/w13121636.
11. Hai, Đ.V.; Hue, L.T.; Tri, D.Q. Researching and applying modeling software to forecast floods and saltwater intrusion in the Mekong River and display the results of saltwater forecasting on Google Earth. *VN J. Hydrometeorol.* **2020**, *710*, 33–42. https://doi.org/10.36335/VNJHM.2020(710).33-42.
12. University of Science and Vietnam Institute for Advanced Studies in Mathematics, develop a tool to assess the effects of saltwater intrusion on socio–economic and apply experimental properties to the Mekong Delta. *J. Clim. Change Sci*. **2021,** *17(3), 21-29*.
13. Tien, K.D.; Adam, L.; Micheal, D.Y. Perceptions and responses to rising salinity intrusion in the Mekong River Delta: What drives a long–term community–based strategy. *Sci. Total Environ.* **2020**, *711*, 134759.
14. Nguyen, H.Q.; Wyatt, A. Socio–ecological resilience of mangrove–shrimp models under various threats exacerbated from salinity intrusion in coastal area of the Vietnamese Mekong Delta. *Int. J. Sustainable Dev. World Ecol.* **2020**, *27(7)*, 638–651.
15. Hai, T.X.; Van Nghi, V.; Hung, V.H.; Tuan, D.N.; Lam, D.T.; Van, C.T. Assessing and Forecasting Saline Intrusion in the Vietnamese Mekong Delta Under The Impact of Upstream Flow and Sea Level Rise. *J. Environ. Sci. Eng. B*, **2019**, *8*, 174.
16. Toan, T.Q. Climate Change and Sea Level Rise in the Mekong Delta: Flood, Tidal Inundation, Salinity Intrusion, and Irrigation Adaptation Methods. Coastal Disasters and Climate Change in Vietnam: Engineering and Planning Perspectives, 2014, 199–217.
17. Roehl Jr, E.A.; Daamen, R.C.; Cook, J.B. Estimating seawater intrusion impacts on coastal intakes as a result of climate change. *J. AWWA* **2013**, *105(11)*, E642–E650. https://doi.org/10.5942/jawwa.2013.105.0131.
18. Rohmer, J.; Brisset, N. Short–term forecasting of saltwater occurrence at La Comté River (French Guiana) using a kernel–based support vector machine. *Environ. Earth Sci.* **2017**, *76*, 246. https://doi.org/10.1007/s12665–017–6553–5.
19. Climate Change Adaptation Project for Sustainable Agriculture and Rural Development in the coastal provinces of the Mekong Delta in Vietnam. Southern Institute of Water Resources Planning, 2013.
20. Duyen, M.T.; Minh, N.M. Strengthen forecasting and warning of hydro–

meteorological disasters in response to climate change, saline intrusion and sea level rise in the Mekong Delta. *Environ. Magazine* **2021**, *4*, 58–60.

21. Apel, H., Khiem, M., Quan, N.H. and Toan, T.Q. Brief Communication: Seasonal Prediction of Salinity Intrusion in The Mekong Delta. *Nat. Hazards Earth Syst. Sci.* **2020**, *20(6)*, 1609–1616.
22. Codiga, D. L. Unified tidal analysis and prediction using the UTide Matlab functions, *GSO Tech. Rep.* Graduate School of Oceanography, Univ. of Rhode Island Narragansett, RI, 2011.
23. Southern Institute of Water Resources Research – Vietnam Academy for Water Resources, Investigating and forecasting the flood water levels inland and monitoring saline intrusion in the Mekong Delta in service of directing and operating agricultural production, 2019.
24. Southern Institute of Water Resources Research. The report "Forecasting saline intrusion at estuaries in the coastal area of the Mekong Delta and proposing solutions to combat drought", 2016.

VIETNAM JOURNAL OF HYDROMETEOROLOGY

Research Article

The application of the cumulative drawdown method in designing of groundwater lowering system - Golden Hill project

Le Thi Thuy Duong[1]*, Can Thu Van[1]

[1] Ho Chi Minh University of Natural Resources and Environment; duongltt@hcmunre.edu.vn; ctvan@hcmunre.edu.vn

*Corresponding author: duongltt@hcmunre.edu.vn; Tel.: +84–905777755

Received: 08 September 2021; Accepted: 02 November 2021; Published: 25 December 2021

Abstract: The presence of groundwater can lead to troublesome conditions when construction operations are to take place below the original groundwater level. There are several techniques or methods available for designing of groundwater lowering systems for a construction project. The selection of a technique or techniques appropriate to a particular project at a particular site or country will depend on many factors. The basic designer's "tool kit" – the formulae and concepts used in routine designs – are presented and their application discussed. By the case of Golden Hill project, the author has analyzed the details of the conceptual model, then selected the cumulative drawdown method to design of groundwater lowering system for particular engineering geological – hydrogeological at District 1, Ho Chi Minh City, Viet Nam. The paper does not merely cover the numerical aspects of design, but also discuss some of the issues over which "engineering judgement" must be exercised.

Keywords: Groundwater lowering; Dewatering; Pumped well; Cumulative drawdown method.

1. Introduction

Man has been aware of groundwater since prehistory, long before Biblical times. Over the centuries the mysteries of groundwater have been solved, and man has developed an increasing capability to manipulate it to his will. The control of groundwater is a practical problem, where theory is only part of the picture – how the theory is put into practice is vital. There are several techniques or methods available for controlling groundwater flow for a construction project. The various dewatering techniques are studied [1]. It will be seen from study "Typical applications", that only a few methods are suitable for use in all types of soils. The ranges of soils that are suitable for treatment by the various dewatering methods are shown in the traditional form of particle size distribution curves. These curves are taken from CIRIA Report 113 [2] and are based on the earlier work of Glossop and Skempton (1945) and others [3]. Similarly, the ranges of soils suitable for treatment by the various exclusion methods are shown [4]. The selection of a technique or techniques appropriate to a particular project at a particular site or country will depend on many factors. These are tentative economic and physical limits. The emphasis is on the word tentative.

In Vietnam, the use of underground space is considered an optimal solution in now, so the control of groundwater in the construction is a very important and necessary technical.

Many authors are studied to find out the best solution to controlling groundwater for construction projects. However, the philosophy and the selection of a technique methods for the design of groundwater lowering systems are too sketchy, sometimes illogical to deal simplistic at common situations, while not providing advice on the approach to more complex problems yet [5–6]. The uncertainty inherent in any ground engineering process, requires a "questioning" or "testing" approach be adopted in design, where nothing is taken for granted. Sometimes as work proceeds, the actual soil and groundwater conditions encountered may differ from what was expected and design is fail finally. As a good example at construction of Van Coc culvert, Ha Tay Province: the target drawdown is 11.6m depth, the first designer gave 105 wells with 14.6 m depth, and well spacing is 2.7 m, but after a long time of dewatering pumping, the groundwater is not gotten target drawdown be like expected. So, the contractor had to changed other design. Final output design parameters are 84 wells, 14.5 m depth and well spacing is 3.4 m [7]. It has been costly to the client.

Many engineering projects, especially major ones, entail excavations into water-bearing soils. For all such excavations, appropriate system(s) for the management and control of the groundwater, should be planned before the start of each project. In practice this can only be done with knowledge of the ground and groundwater conditions likely to be encountered by reference to site investigation data. Golden Hill project at 87 Cong Quynh Street, Nguyen Cu Trinh ward, District 1, HCMC. The plan dimensions of the well array will be 93.2 by 77.35 m, 50 floors with 4 basements. The deepest basement is located at 17.5 m depth. The target drawdown is to lower the groundwater level around to 1 m below formation level. This is 18.5m depth, or a drawdown of 14.2 m below the original piezometric level (–4.3 m). The main emphasis of the study is the basic designer's "tool kit" – the formulae and concepts used in routine designs are presented and their application discussed. Methods for estimation of steady-state discharge flow rate, and for selection of well yield and spacing are described in detail. Other design issues (such as time to achieve drawdown) are also outlined. The basic tenets of groundwater modelling are discussed in relation to more complex problems.

Figure 1. Location of project.

2. Materials and methods

2.1. Materials

2.1.1. Geological and hydrogeological of the area data

From the results of engineering geological and hydrogeological investigation to a depth of –50.0 m [8–9], based on the distribution depth, petrographic composition, water capacity, the water storage units can be classified:

a. Clay and sandy clay layers, very poor water

This layer is widely distributed throughout the survey area, it is located just below the fill soil layer, the roof layer is from 0.5–1.2 m depth, the bottom layer is from 7.0–8.0 m depth. The composition includes clay, sandy clay and clay containing laterite gravel, poor water capacity. From the hydrogeological point of view, this is an impermeable layer, and maximum piezometric level in the aquifer is –4.3 m below ground level.

b. Clayey sand, consisting of a sandy gravel

The roof floor is at the depth from 7.0 m to 8.0 m, the bottom floor is at an average depth of 45.0 m. This is the main aquifer in the entire survey area and is distributed throughout the Ho Chi Minh city. There are divided into two layers: The upper layer of clayey sand with average water capacity, the depth of the bottom layer is 26.0 m and the layer of sand with gravel lying next, with rich water storage. Analysis of field permeability test data gave an aquifer permeability k of 2.25×10^{-4} m/s (19.4 m/d) at 15 depth and a storage coefficient S of 0.005 [10–15]. This is a confined aquifer with a pressure height of 41.7 m.

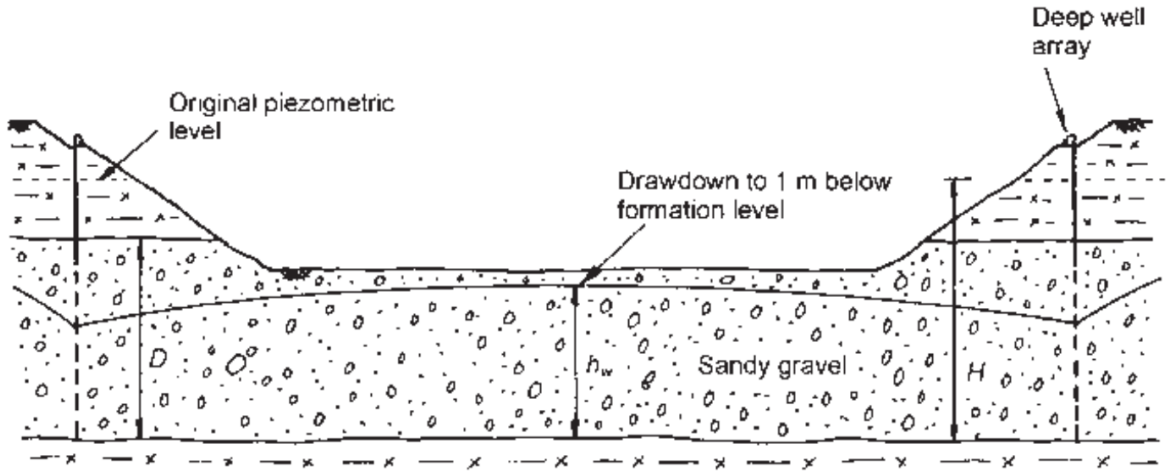

Figure 2. Conceptual model.

2.2. Methodology

2.2.1. Selection of method

The excavation extends through the stiff clay aquiclude (8 m) and into the upper 10.5 meters of the confined aquifer. The piezometric level in the confined aquifer will need to be lowered prior to excavation to prevent base heave during excavation through the clay, and then to provide a workable excavation when the excavation penetrates into the top of the aquifer.

The target drawdown is to lower the groundwater level to 1.0 m below formation level [16]. This is 18.5 m depth (B4), or a drawdown of around 14.2 m below the original piezometric level (4.3 m depth) [9–10].

For a drawdown of 14.2 m and the design permeability of 2.25×10^{-4} m/s, inspection of Figure 3 suggests that deep wells method would be suitable for this combination of drawdown and permeability [1–4]. In addition, in this case the contractor wishes to excavate rapidly to full depth [10].

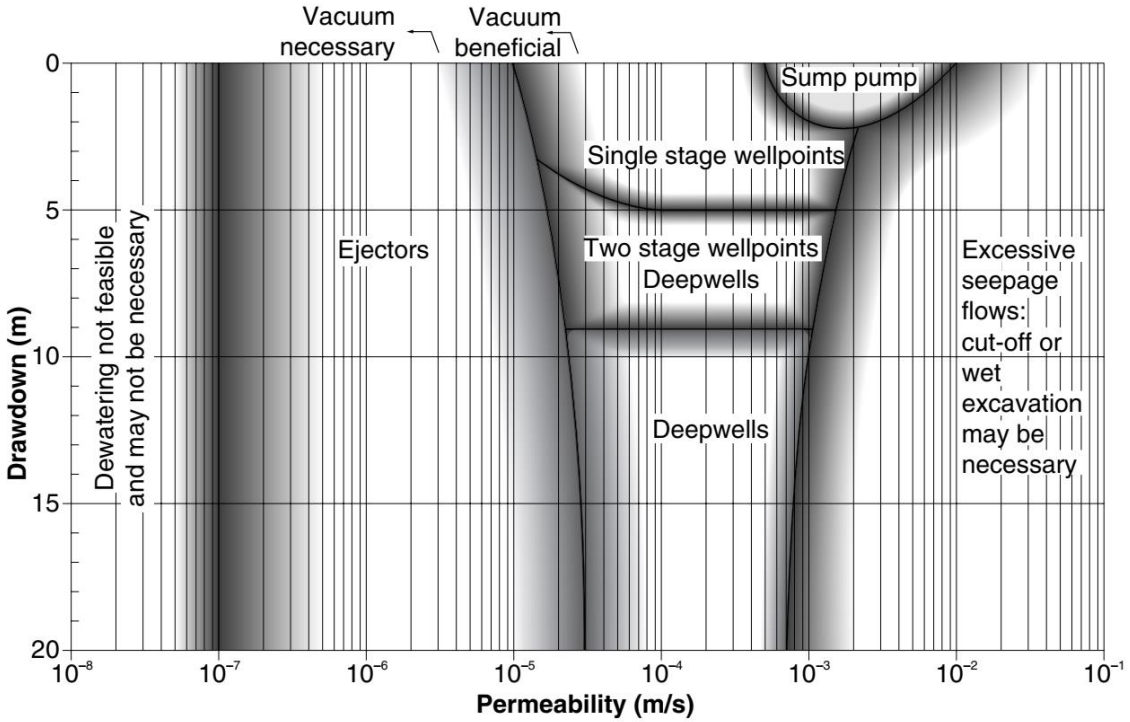

Figure 3. Range of application of pumped well groundwater control techniques – adapted from Rorberts and Preene (1994) and modified after Cashman (1994).

2.2.2. Estimation of steady-state discharge flow rate and estimation of number of wells

The cumulative drawdown method (using the Cooper–Jacob simplification) can be used in confined aquifers [16]. This method takes the advantage of the mathematical property of superposition applied to drawdowns in confined aquifers. In essence, the total (or cumulative) drawdown at a given point in the aquifer, resulting from the action of several pumped wells, is obtained by adding together (or superimposing) the drawdown from each well taken individually (Figure 4).

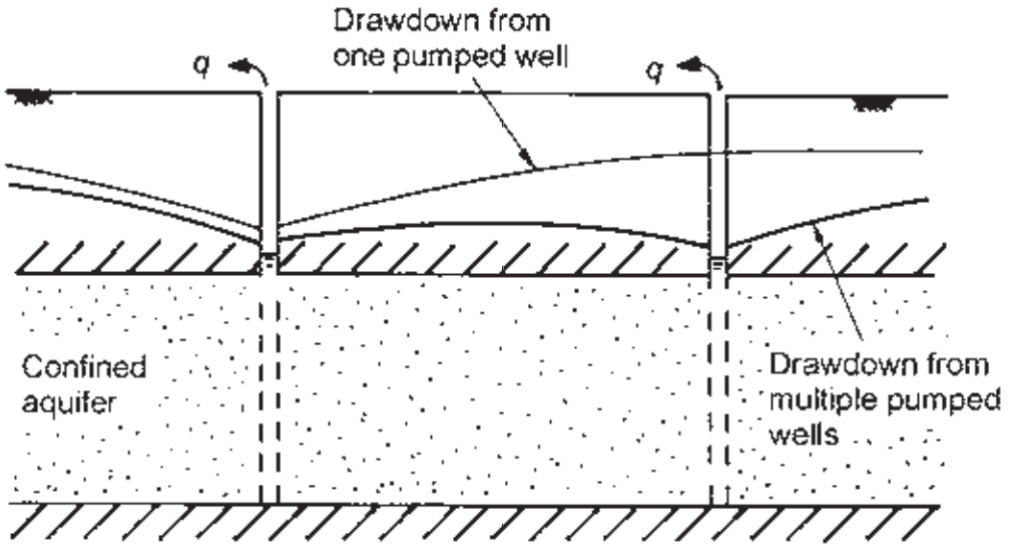

Figure 4. Superposition of drawdown from multiple wells.

This approach is theoretically correct in confined aquifers, but is invalid in unconfined aquifers where the changes in saturated thickness that occur during drawdown complicate the interaction of drawdowns. It has also been successfully applied in unconfined aquifers where the final drawdown is less than around 30 percent of the initial saturated aquifer thickness [16–17].

In this case, because drawdown is required to 18.5 m depth compared with the top of the aquifer at 8 m depth, the initially confined aquifer will become unconfined. The aquifer thickness will be reduced by 10.5 m out of 37 m, or 28 per cent. Therefore, this problem will be analyzed assuming confined behavior throughout. The cumulative drawdown is calculated using equation [17–20].

$$(\mathrm{H}-\mathrm{h_w}) = \sum_{i=1}^{n}(H - h_w)_\mathrm{i}$$

$$(\mathrm{H}-\mathrm{h_w}) = \sum_{\mathrm{i}=1}^{\mathrm{n}} \frac{\mathrm{q_i}}{4\pi \mathrm{kD}} \left\{ -0.5772 - \ln\left[\frac{\mathrm{r_i^2 S}}{4\mathrm{kDt}}\right]\right\} \quad (1)$$

where $(H–h_w)$ is the cumulative drawdown (at the point under consideration) resulting from n wells each pumped at constant flow rate q_i; k is the aquifer permeability: k is taken as $2.25.10^{-4}$ m/s; S is the aquifer storage coefficient: S is taken as 0.005; D is the original aquifer saturated thickness: D = 45–8 = 37m; t is the time since pumping began. In this case the target drawdown is required within fourteen days. It is always prudent to design to obtain the drawdown a little quicker than planned – this allows for minor problems during commissioning. In design, we will aim to achieve the target drawdown within ten days. T = 10×86.400 seconds will be used in calculations; r_i is the distance from each pumped well to the point where drawdown is being estimated.

The method requires that the plan layout of the well array be sketched, and the x–y co-ordinates of each well be determined [17–18]. The co-ordinates then allow the radial distances r_i (from each well to the point where drawdown is being checked) to be calculated. An initial guess is made of the number of wells and well spacing and the resulting x–y co-ordinates determined. In this case the initial guess was twenty-two wells evenly spaced at 15 m centres (Figure 5).

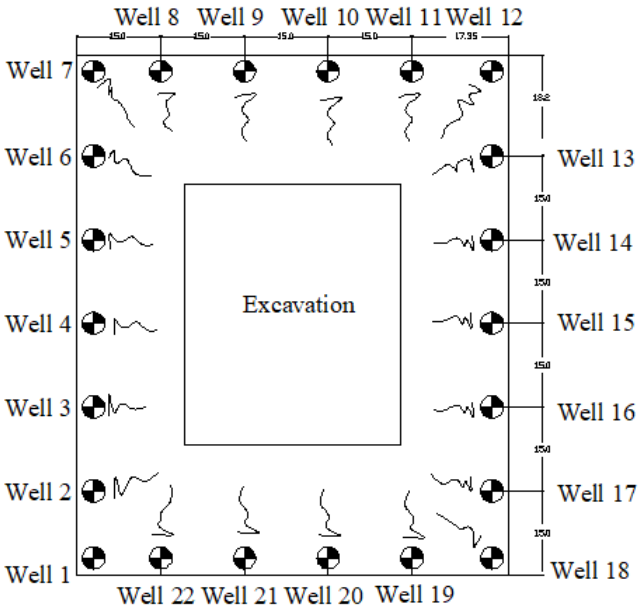

Figure 5. Schematic plan of twenty-two wells system (with xc=39, yc=47).

A spreadsheet program is then used to evaluate equation (1) for the cumulative drawdown at selected locations within the excavation [16–21]. For circular or rectangular excavations with evenly–spaced wells it is normally sufficient to determine the drawdown

in the center of the excavation, because drawdown everywhere else will be greater. This is the method used here. If the well array is irregular in shape (or if the depth of excavation is not constant) it will be necessary to determine the drawdown in a number of locations, to ensure the target drawdown is achieved at all critical locations [17–18].

The results from a spreadsheet calculating the drawdown in the center of the excavation for a twenty-two well system is shown below. The radial distance r_i, from each well (at location x_i, y_i) to the location (x_c, y_c) where the drawdown is being determined [18], is calculated from:

$$r_i = \sqrt{([x_i - x_c]^2 + [y_i - y_c]^2)} \quad (2)$$

For simplicity, the flow rate q_i from each well has been assumed to be the same, but if it was intended to use pumps of different sizes in certain wells this can easily be incorporated in the calculation. In the spreadsheet different values of qi were tried until the target drawdown of 14.2 m is just achieved in the center of the excavation. The total flow rate is simply the sum of all the well flow rates.

Table 1. The total flow rate is simply the sum of all the well rates flow.

Well	**x_i** (m)	**y_i** (m)	**q_i** (m/s)	**r_i** (m)	**H-h_w** (m)
1	0	0	8.10^{-4}	60.56	0.62
2	0	15	8.10^{-4}	49.94	0.64
3	0	30	8.10^{-4}	42.09	0.66
4	0	45	8.10^{-4}	38.71	0.67
5	0	60	8.10^{-4}	40.93	0.67
6	0	75	8.10^{-4}	47.98	0.64
7	0	93.2	8.10^{-4}	60.56	0.62
8	15	93.2	8.10^{-4}	52.27	0.64
9	30	93.2	8.10^{-4}	47.40	0.64
10	45	93.2	8.10^{-4}	47.03	0.65
11	60	93.2	8.10^{-4}	51.25	0.64
12	77.35	93.2	8.10^{-4}	60.56	0.62
13	77.35	75	8.10^{-4}	47.98	0.64
14	77.35	60	8.10^{-4}	40.93	0.68
15	77.35	45	8.10^{-4}	38.71	0.68
16	77.35	30	8.10^{-4}	42.09	0.67
17	77.35	15	8.10^{-4}	49.94	0.64
18	77.35	0	8.10^{-4}	60.56	0.62
19	60	0	8.10^{-4}	51.25	0.64
20	45	0	8.10^{-4}	47.03	0.65
21	30	0	8.10^{-4}	47.40	0.64
22	15	0	8.10^{-4}	52.27	0.64
Total			***0.176***		***14.21***

This calculation indicates that a system of twenty-two wells, each discharging 8.10^{-4} m/s (total flow rate 0.176 m/s) will achieve the target drawdown in the center of the excavation after ten days. During the pumping test could have yielded more if a larger pump has been used. It therefore makes sense to repeat the above calculations assuming fewer wells of greater discharge rate [18–22]. The results of these calculations are summarized below:

Table 2. The calculations assuming fewer wells of greater discharge rate.

No of Wells	**Well spacing** (m)	**Well flow of rate** (l/s)	**Drawdown in center of excavation (**m)	**Total flow rate (l/s)**
22	15	8	14.21	176
18	20	10	14.41	180
14	25	13	14.51	182

It is apparent that the target drawdown can be achieved by various combinations of well numbers and yields, but that the total flow rate remains approximately constant.

3. Results and discussion

The number and yield of wells chosen for the final design will depend on a number of factors, including:

The need for redundancy in a well system. Any system relying on relatively few wells is vulnerable to one or two wells suffering from damage or pump failure, leading to loss of drawdown and flooding or instability of the excavation. A system consisting of a greater number of wells will lose proportionately less drawdown if one or two wells are lost.

Each well must be able to yield the discharge flow rate qi assumed in design. However, in practice, problems can occur if the dewatering wells are not designed, installed and developed in exactly the same way as the test well – this may cause the production wells to have lower yields than the test wells. Some wells can have high yields and yet others, poorly connected into fissures, may be almost "dry". Thus, drawdown method needs to be applied with care.

In this case it is assumed that, due to the availability of pumps of suitable capacity, the nominal system of eighteen wells, each discharging 10 l/s each will be adopted (Table 2). It is normal practice to apply an empirical superposition factor J of 0.8–0.95; the system capacity is increased by a factor of 1/J ($Q=\frac{1}{J}\sum_{i=1}^{n} q_i$) [19, 21, 22]. This empirical factor allows for interference between wells, and also provides some allowance for additional drawdown around the wells and water released from storage when the aquifer becomes unconfined. Where aquifers become unconfined, and drawdowns are small (less than 30 per cent of the initial saturated aquifer thickness), the empirical superposition factor J is normally taken as 0.8 to 0.95. In this case, because the drawdown will reduce the thickness of the aquifer by almost 30 per cent, the maximum superposition factor of 0.8 will be applied, so the system capacity (and hence the number of wells) will need to be increased by 1/0.8 = 1.25.

The final system design is, therefore for twenty-two wells (18×1.25 = 22.5), of 10 l/s capacity each. Total system capacity is 220 l/s. The pump manufacturer's catalogue will list the minimum internal diameter of well screen necessary to accommodate the pump to be used, assuming the wells are perfectly straight and plumb. In practice, most wells deviate from the ideal alignment, and using a slightly larger screen diameter reduces the risk of a pump getting stuck down a well [19, 21, 22]. Some general guidance on well screen diameters is given in Table 3. The recommended minimum well screen diameters are generally larger than those quoted by the pump manufacturers. Even so, if a well has a large amount of deviation, even a very small pump may become jammed at the tight points in the well. Table 3 indicates that, to accommodate a pump of suitable capacity, a minimum well bore diameter of 300 mm is required. The corresponding well screen and liner diameter is 152 mm.

Table 3. Recommended well screen and casing diameters.

Maximum submersible pump discharge rate (l/s)	**Recommended minimum internal diameter of well screen and casing[a] (**mm)	**Recommended minimum internal diameter of boring[b]** (l/s)
5	125-152	250-275
10	152-203	300-325
15	165-250	300-375
20	180-250	300-375
25	203-300	325-425
44	250-350	375-475

Notes: [a] Diameter will depend on external dimensions of pump used. [b] Minimum diameter of boring in based on nominal filter pack thickness of 50 mm. Slightly smaller diameters may be feasible if natural filter can be developing in the aquifer.

4. Conclusion

Solution drawdown in the center of the excavation to dry the foundation pit by cumulative drawdown analysis from the well system arranged around the excavation is a superior solution because it has a logical theoretical approach, ensuring active lowering lower the groundwater level to the required depth, creating reverse seepage gradient overcomes the phenomenon underground erosion, flowing sand destabilizes the roof of the hole foundation, overcome the phenomenon of background flare, does not interfere with the construction of the foundation pit. For a drawdown of 14.2 m below the original piezometric level, the final system design (the methods used in combined theoretical and empirical approaches) is twenty-two wells (18×1.25 = 22.5), of 10 l/s capacity each. Total system capacity is 220 l/s, a minimum well bore diameter of 300 mm is required. The corresponding well screen and liner diameter is 152 mm.

The best design approaches incorporate elements of both the theoretical and empirical methods. The theoretical method requires a "conceptual model" of the ground and groundwater regime to be developed, following which calculations are carried out. Simple and fairly basic calculations are perfectly acceptable, and may be preferred in many cases, provided they are compared with an empirical approach. The empirical method should be used as a "sanity check" to ensure that the proposed groundwater lowering system is realistic and practicable. Any groundwater lowering system will need, to some degree, monitoring and maintenance measures to ensure effective operation. Once in operation, a groundwater lowering system is the end result of a lot of effort by a lot of people. It is a complex system dependent on a diverse range of hydrogeological, hydraulic, chemical, mechanical and human factors, but it will have a clear aim to lower groundwater levels sufficiently to allow the construction works to proceed. So that is the need for monitoring to measure the target drawdown by pumping groundwater to check back design.

Author contribution statement: D.L.T.T. devised the project, the main conceptual ideas and designed of groundwater lowering system. V.C.T. wrote the manuscript. Both authors contributed to the final version of the manuscript.

Acknowledgements: The authors would also like to thank Bach Khoa Ho Chi Minh City Science Technology Joint Stock Company (BKTECHS), Solar system foundation & Geotechnics J.S.C for providing documentation to complete the study.

Competing interest statement: The authors declare no conflict of interest.

References

1. Preene, M; Roberts, T.O.L.; Powrie, W.; Dyer, M.R. Groundwater Control – Design and Practice. *CIRIA Report C515*, London, 2000.

2. Somerville, S.H. Control of Groundwater for Temporary Works. *CIRIA Report 113*, London, 1986.
3. Glossop, R.; Skempton, A.W. Particle-size in silts and sands. *J. Inst. Eng*. **1945**, *25*, 81–105.
4. Roberts, T.O.L.; Preene, M. Range of application of construction dewatering systems. Groundwater Problems in Urban Areas (Wilkinson, W.B. Eds.). Thomas Telford, London, **1994**, pp. 415–423.
5. Anh, T.H. Research on solutions to lower groundwater in the construction of deep excavation pits in Hai Phong. Master's thesis in civil and industrial construction engineering, 2007.
6. Ba, K.N. Deep Foundation Design and Construction. Ha noi constuction publishing company, **2010**, pp. 576. (In Vietnamese)
7. Anh, L.V. Method of calculation for the ground water falling by well system. Journal of Water Resources & Evironmental Engineering. **2016**, *1*, 33-37. (In Vietnamese).
8. Research center of technology and industrial equipment (Rectie). Soil investigation report for Golden Hill project– 87 Cong Quynh, Nguyen Cu Trinh ward , Dict.1, HCMC.
9. Research center of technology and industrial equipment (Rectie). Report on hydrographic geologic investigation result to serve design lower water level borehole system during basement foundation working for Golden Hill project– 87 Cong Quynh, Nguyen Cu Trinh ward , Dict.1, HCMC.
10. Solar system foundation & Geotechnics J.S.C. Dewatering Proposal for Golden Hill project– 87 Cong Quynh, Nguyen Cu Trinh ward , Dict.1, HCMC.
11. Van, P.L.; Minh, T.T.; Van, T.T. Determination of hydro-geological parameters by the pumping test method at Tra Noc industrial zone - Can Tho city: A preliminary result. *J. Sci. Can Tho University Environ. Clim. Change.* **2017**, *1*, 31–38.
12. Ty, T.V.; Minh, H.V.T.; Ngan, L.H.B.; Nhan, D.T.; Luan, T.C. Pumping test for determinating hydrogeological parameter for goundwater flow simulation in Can Tho city, Vietnam. Vietgeo Proceedings, **2019**, 433–438.
13. Viet, K.N.; Van, N.D. Practical guide to hydrogeology. HCMC National University, **2013**, pp. 166.
14. TCVN 9903:2014 – Hydraulic structures - Requirements for design, construction and acceptance of decreasing groundwater level, 2014.
15. Viet, V.T. Geotechnical engineer's Handbook. **2010**, 409–438. (In Vietnamese)
16. Cooper, H.H.; Jacob, C.E. A generalised graphical method for evaluating formation constants and summarising well field history. *Trans. Am. Geophys. Union* **1946**, *27*, 526–534.
17. Powrie, W.; Preene, M. Equivalent well analysis of construction dewatering systems. *Géotechnique* **1992**, *42(4)*, 635–639.
18. Cashman P.M.; Preene, M. A practical guide Groundwater Lowering in Construction. Spon Press 2001, pp. 476.
19. Driscoll, F.G. Groundwater and Wells. Johnson Division. Saint Paul, Minnesota, 1986.
20. Powrie, W.; Preene, M. Time-drawdown behaviour of construction dewatering systems in fine soils. *Géotechnique.* **1994**, *44(1)*, 83–100
21. Powers, J.P. Construction Dewatering: New Methods and Applications, 2nd edition. Wiley, New York, 1992. p. 11.
22. Chapman, T.G. Groundwater flow to trenches and wellpoints. *J. Inst. Eng.* **1959**, 275–280.

VIETNAM JOURNAL OF HYDROMETEOROLOGY

Research Article

Distribution of perfluoroalkyl substances (PFASs) in the water of the Bac Hung Hai River, Van Giang district, Hung Yen province, Vietnam

Huu Tuan Do[1*], Lan Anh Phan Thi [2], Ngoc Lam Bui[1]

[1] Faculty of Environmental Sciences, VNU University of Science, Vietnam National University, Hanoi; tuandh@vnu.edu.vn; buingoclamhy1999@gmail.com
[2] VNU Key Laboratory of Analytical Technology for Environmental Quality and Food Safety Control (KLATEFOS), VNU University of Science, Vietnam National University, Hanoi; lananh@vnu.edu.vn

*Correspondence: tuandh@vnu.edu.vn; Tel: +84–2438584995

Received: 12 October 2021; Accepted: 05 November 2021; Published: 25 December 2021

Abstract: This study investigated and evaluated the quality of PFASs in the water of the Bac Hung Hai River passing through Van Giang district, Hung Yen, Vietnam. PFASs concentration in the river water samples were detected by using LC-MS/MS spectrum. The results showed that the studied river region contaminated PFASs. PFASs concentration ranged from 0.10 to 3.88 ng/l. The average concentrations of individual PFASs were PFBA 5.5, PFPeA 6.8, PFHxA 0.8, PFHpA 0.34, PFOA 0.16, PFNA 0.19, PFDA 0.036, PFHxA 1.34, PFOS 0.074, PFDS 0.037. The research results show that distribution of PFASs in the Bac Hung Hai River are not uniform and depend on the of discharge sources.

Keywords: PFASs contaminants; PFOA, PFOS, Bac Hung Hai; River pollution.

1. Introduction

Per– and polyfluoroalkyl substances (PFASs) are a group of anthropogenic compounds as new persistent organic pollutants (POPs) with special surface–active properties [1]. Their molecular contains both lipophilic and hydrophilic groups at both sides. PFASs are a diverse group of human-made chemicals used in a wide range of consumer and industrial products. Some PFASs, such as perfluorooctanoic acid (PFOA) and perfluorooctane sulfonate (PFOS), have been more widely used and studied chemicals in the PFASs group. Many PFASs are resistant to grease, oil, water, and heat. For this reason, PFASs have been manufactured since the late 1940s [1–2] and used in a variety of applications including in stain and water–resistant fabrics and carpeting, cleaning products, paints, and fire–fighting foams, refrigerants, surfactants, and polymers and as components of pharmaceuticals, fire retardants, lubricants, adhesives, cosmetics, paper coatings, and insecticides. Certain PFASs are also authorized by the Food and Drug Administration (FDA) for limited use in cookware, food packaging, and food processing equipment. The concern about their presence in the environmental and potential human exposure is rising all over the world. A great number of studies have been available on the contaminations of PFASs in rivers, lakes, and ocean waters [3], and even in air [4–5], in dust [6]. PFASs have been investigated widely in fish of Europe and Asia, such as: Spain [7] Norway [8], Greece [9], Italy [10], Korea [11], and China [12]. The median PFOS contamination was found in river

water 14.4 ng/L (England), 5.5 ng/L (Singapore), 3.2 ng/L (Japan), and 1.7 ng/L (China). PFOA contamination (median) in river water was in the order of Japan (30.7 ng/L), England (10.6 ng/L), China (7.4 ng/L), Singapore (5.6 ng/L), and Vietnam (0.7 ng/L) [13]. PFASs found in ocean water were range from hundreds to thousands pg/L, such as in South China Sea 980–2640 pg/L [14].

PFASs related to environmental water in Vietnam have been concerned recently [15–18]. The occurrence of PFASs in surface water near waste recycling and disposal sites in Vietnam was reported [15–16]. The significant PFASs concentrations were found in leachate from the municipal dumping site and ambient water from the e-waste recycling site, suggesting such sites as potential contamination sources of PFASs in Vietnam. In Hanoi, PFASs contamination in river systems was studied at Nhue, To lich, Yen So, and Ho Tay Lake.

Van Giang district is located in the north of Hung Yen province, on the left bank of the Red River, 40 km from Hung Yen city to the north, 20 km from the center of Hanoi capital to the southeast. Wastewater sources such as wastewater and some solid wastes that may contain PFASs from domestic activities as well as industrial activities and pottery villages of residents here are concentrated into the Bac Hung Hai River. This is considered as one of the potential sources of PFASs pollution in the surface water environment. This research investigates the occurrence of PFASs in Bac Hung Hai River water. The PFASs in pretreated samples were analyzed using high performance liquid chromatography-tandem mass spectrometry (LC/MS-MS). The obtained results showed a sufficient picture of the distribution PFASs in river water and initial identification of contamination sources.

2. Materials and methods

2.1. Materials

The mixture of PFASs (PFACMXB0614) and the mixture of Mass-Labeled PFASs (MPFACMXA0714) were purchased from Wellington Laboratories, Canada. HPLC-grade methanol was purchased from Merck, Germany, and other chemicals were of analytical reagent grade. Ammonium acetate was obtained from Wako Chemicals, Japan. Ultrapure water was delivered by a Direct-Q water purification system (Millipore, Japan).

2.2. Sample collection and preparation

Figure 1 shows the location of sampling sites. Fifteen river water samples were taken along the Bac Hung Hai River in March 2021. The water sample was pretreated according to the international standard ISO 25101:2009 with minor modifications [19]. Briefly, the water sample (500 mL) was filtered through a 47 mm glass fiber filters to separate suspended solids. An Oasis HLB (200mg) cartridge was preconditioned with 4mL of MeOH containing 0.1% ammonia followed by 4 mL of MeOH and 4 mL of deionized water. The water sample was then loaded through a WAX cartridge with a flow rate of 10 mL/min. The SPE cartridge was washed with 4 mL of 25 mM ammonium acetate and dried for 15min. Next, the target compounds in the cartridge were eluted with 4 mL of MeOH and 4 mL of 0.1% ammonia solution at a rate of 1 drop per second. The extract was concentrated to 1 under a gentle nitrogen stream. A 0.2 μm nylon membrane filter was used to filter the final eluate before LC-MS/MS analysis.

Figure 1. Sampling site in Bac Hung Hai River.

2.3. PFASs analysis

PFASs were analyzed by LC-MS/MS 8040, Shimadzu, Japan. The LC system was equipped with a column (Poroshell 120, EC.C18 (2.1 mm I.D. × 150 mm L, 2.7 µm) and guard column EC-C18, Agilent, USA. The mobile phase consisted of a binary mixture of A (2 $mM.L^{-1}$ ammonium acetate in water with methanol in a ratio of volume is 9 and 1) and solvent B (methanol) at flow rate of 0.25 $ml.min^{-1}$. The gradient, the start with 50% B in 2 min increased to 95% B for 18 min and linearly at 95% B for 4 min then ramped to 50%A for 5 min. Total running time was 29 min. The inject volume was 2µL. The MS system was running with an electrospray ionization source in negative mode (ESI) at 3.5kV.

3. Results and Discussions

3.1. PFASs concentrations in water samples

Figure 2 showed the total PFASs concentrations in all river water samples. They were detected in all studied samples in range from 1 ng/L to 38.8 ng/L. Comparison to PFASs concentration in the wastewater from the rivers which belong to the drainage systems of Hanoi city including Lu, Set, To Lich, Kim Nguu and Nhue Rivers and two urban large lakes as West Lake and Yen So Lake, was collected. The concentrations of PFASs were in arranged of 0.93 and 28 ng/L [20]. In Ha Dong silk weaving wastewater, the concentrations of PFASs were in arranged 2.94–12.64 ng/L, and those at Hoi Quan silk weaving wastewater were 4.77 to 17.66 ng/L [21]. The concentration of PFASs in surface water samples along the Bac Hung Hai River is slightly high.

There is a great difference between different sampling points. It proves that the water of Bac Hung Hai River is the reservoir of many waste sources with high concentration of pollution. Samples W1, W2, W3 with the appearance of PFASs were low because the location of these samples is the first part of Bac Hung Hai River, there are very few sources of impact but going deeper along the river. When we see the appearance of residential areas, restaurants, leather manufacturing companies, packaging... the more PFOA and PFOS appear and the concentration also varies.

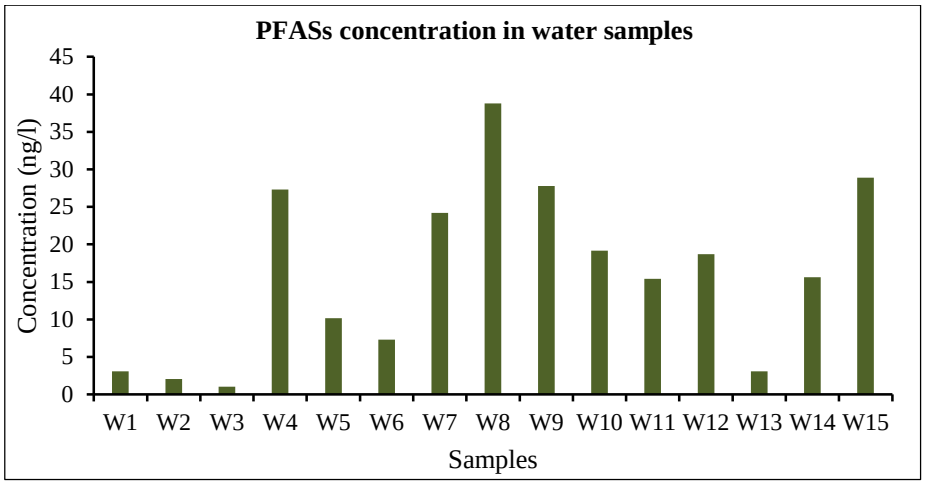

Figure 2. PFASs concentration in Bac Hung Hai River water samples.

It is the production activities of people, companies, industrial parks, and daily life that are not strictly managed, so the discharge of wastewater directly into the Bac Hung Hai River has led to the presence of toxic compounds. The highest concentration at position W8 reached 38.8 ng/L and then samples W4, W7, W9, W10, W11, W12, W14 and W15 also had high concentrations. The lowest at position W3 reached 1 ng/L.

3.2. PFOA and PFOS concentrations

The occurrence of PFOA showed frequency in all studied samples. There are many locations where PFOS is not found but PFOA is present, even PFOA is at high concentration. At sample W15, the highest occurrence of 2 substances was PFOA 0.42 ng/L and PFOS 0.38 ng/L. PFOS and PFOA concentration in other locations were showed in Table 1. In this study, the compound concentration of PFOA reached 0.044–0.42 ng/L and PFOS reached 0.06–0.38 ng/L. The surface water in Da Nang, Ho Chi Minh City and Bui Dau e-waste recycling craft village have much higher PFOA content than the study area of Bac Hung Hai River flowing through Van Giang district area.

For surface water in Hue, there are very small concentrations of PFOA and PFOS, indicating that there are very few impact sources containing this compound at those sampling locations. For the low PFOS concentration in Hanoi and Hung Yen, the PFOA concentration in the Bac Hung Hai River water flowing through the Van Giang district area was four times higher than the PFOA concentration in the river water in the Hanoi area.

The concentration of PFOA in the surface water of a waste recycling craft village in Hung Yen is nearly 90 times higher than the concentration of PFOA in the water of Bac Hung Hai River that we obtained.

Table 1. PEOS and PFOA concentrations through studies in provinces/cities.

Location	Samples	PFOS (ng/L)	PFOA (ng/L)	Ref.
Hanoi	River water	ND – 0.14	ND – 1.00	[22]
	Urban lake water	0.17–0.81	1.4 – 6.6	
	Wastewater channel	ND – 1.3	ND – 6.1	
Hung Yen	Surface water	ND – 0.8	ND – 4.1	[16]
	Surface water of Dong Mai craft village	ND – 2.7	2.5 – 5.6	
	Surface water of Bui Dau craft village	ND – 1.8	3.3 – 35	
Da Nang	Surface water	ND – 3.8	ND–104.5	[23]

Location	Samples	PFOS (ng/L)	PFOA (ng/L)	Ref.
Ho Chi Minh	Surface water	ND – 5.3	0.21 – 18	[18]
Hue	Surface water	ND – 0.19	0.09–0.32	

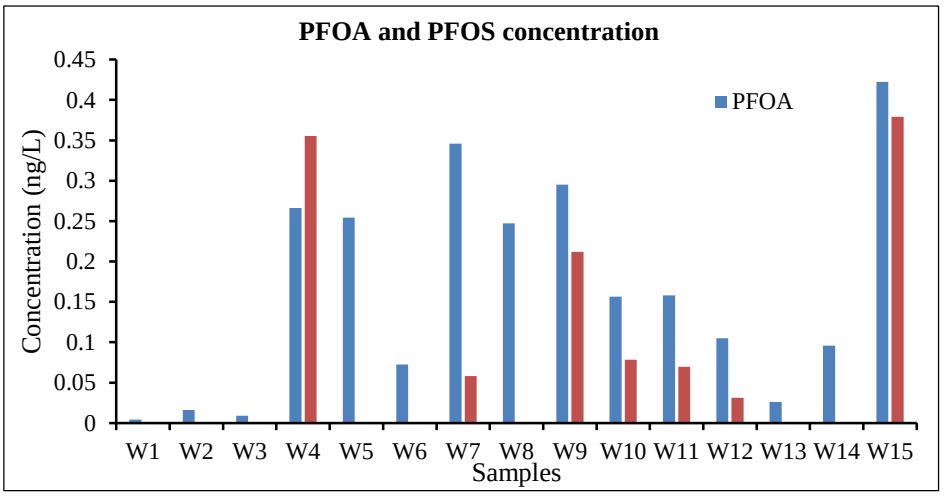

Figure 3. PFOA and PFOS concentration in Bac Hung Hai River water samples.

3.3. Composition profiles of various PFASs in water samples

PFASs were detected mostly in water samples. The composition profiles of PFASs are presented in figure 4, 5. Six perfluoroalkylcarboxylic acids (PFBA, PFPeA, PFHxA, PFHpA, PFOA, and PFNA) were found in all studied samples. The content of PFBA and PFPeA were found with the highest concentration among PFASs compounds. The difference between the content of PFASs compounds was explained for the composition of wastewater from industrial, production, business, domestic, medical, and livestock zones in different locations.

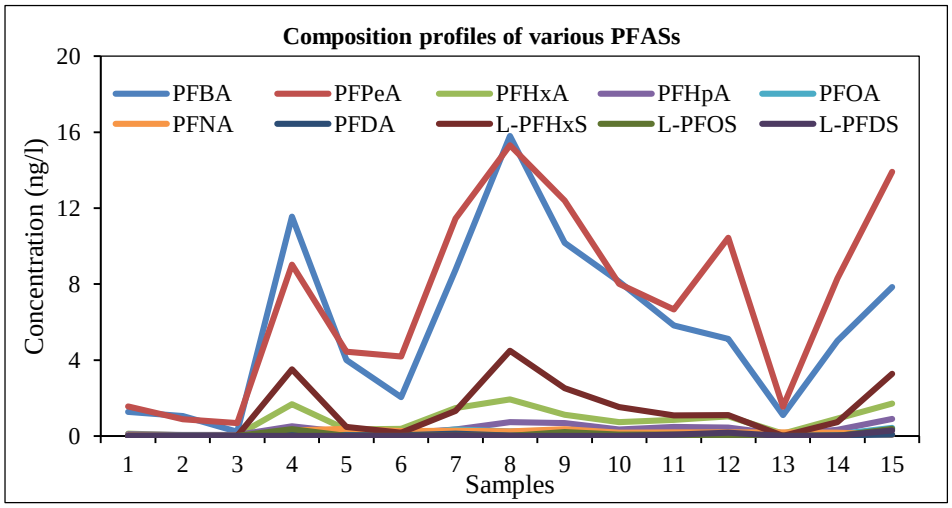

Figure 4. Composition profiles of various PFASs in Bac Hung Hai River water samples.

The PFASs that accounted for the highest percentage among the 10 analytes were PFBA at 36.4%, PFPeA 44.7%, PFDA 8.3%, PFHxA 5.1%. In general, the components detected with high content are pefloankyl acids with low number of carbon atoms in the molecule from C4, C5, indicating that the PFASs are from wastewater of residential and industrial zones.

Most of the compounds PFBA and PFPeA account for a high proportion and they occur at sample locations affected by many sources of direct discharge into the Bac Hung

Hai River. Typically, at sample location W4, W7, W8, W9, W10, the presence of these two compounds was very high due to waste sources from industrial parks, people's livelihoods, craft villages and many other sources. Short-chain PFASs were much more dominant than long-chain PFASs in Bac Hung Hai River water. Comparison with EU regulations for 25 ng/L PFOA threshold, PFASs contamination in the studied region is mostly within the threshold [24].

Aquatic studies and data for surface water in Denmark and other European countries most of the data are for PFOS, PFOA and other long-chain PFAS and some data are available for compounds short chains such as PFBS, PFHxS, PFBA, PFPeA and PFHxA were detected in many seafood samples. Usually, concentrations range from levels similar to PFOS or PFOA to one order of magnitude lower. The presence of shorter-chain compounds in the medium is explained by replacing long-chain compounds with shorter-chain substitutes.

In the Atlantic, PFASs concentrations were significantly higher in the North Atlantic than in the Central and South Atlantic. ΣPFAS concentrations decreased from 2007 to 2010 in the North and Mid-Atlantic mainly due to decreased PFOA/PFOS concentrations while such short-chain PFAS such as PFBS, PFHxA and PFHxS showed no such trend.

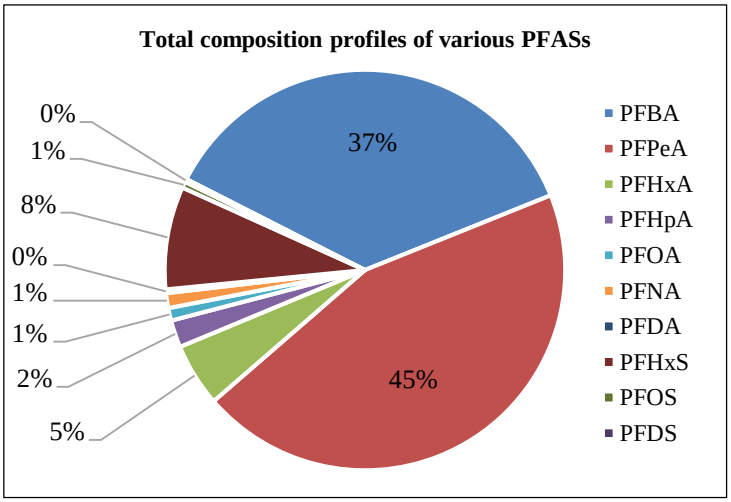

Figure 5. Percentage of various PFASs in Bac Hung Hai River water samples.

3.4. Identification of pollution sources

According to the actual survey, from the beginning of the river to the end point where samples are taken in Van Giang district, there are many sources of pollution affecting the river water. Main sources of pollution: industrial waste, services, healthcare, agricultural production, livestock, daily life activities, Kieu Ky landfill.

At the sample location W1, W2, W3 is affected by the waste source of the people of Xuan Quan commune and the people of Bat Trang Village. Sample location W4 is the main source of pollution originating from industrial, service, craft villages and people's wastewater along the Cau Bay River basin flowing through Xuan Thuy culvert along with about 50 facilities in the area discharging wastewater into Bac Hung Hai channel and Kieu Ky landfill. Sample W5 is affected by medical waste from Bay Hospital and from Cau Chua residential area. The location of the W6 sample is influenced by the waste source from the plastic and paint industry. At the sample location W7 is affected by waste sources of Tan Quang industrial cluster, service restaurants. The location of the sample W8 is affected by wastewater from industrial parks producing paper, paperboard, plastic, carton packaging, animal feed, mechanical engineering and waste sources from residential areas. Sample W9 is affected by residential waste, seafood processing, motor vehicle maintenance and repair, and waste from Dong Than market. Sample W10 is affected by wastes from

plastic, neoprene, scrap recycling and residential areas. Sample W11 is affected by wastewater from Bao Dap residential area and wastewater from Cau Kenh. Sample W12 is the wastewater of the whole Bao Da area, including all business and production activities of the people. Sample W13 is less affected by domestic waste. Sample W14 was the waste source of residential area and Bat Trang pottery village. Sample W15 was taken at the Xuan Cau bridge where it is affected by domestic waste, agricultural production, animal husbandry and services.

Thereby, it is found that the source of wastewater pollution from industrial parks and wastewater from residential areas is mainly along the Bac Hung Hai River in Van Giang district, Hung Yen province.

4. Conclusion

The distribution of PFASs concentration along the Bac Hung Hai River is uneven, which showed that each location and each area has different waste sources, leading to different concentrations of PFASs. The average ng/L concentrations of PFBA 5.5, PFPeA 6.8, PFHxA 0.8, PFHpA 0.34, PFOA 0.16, PFNA 0.19, PFDA 0.036, PFHxA 1.34, PFOS 0.074, PFDS 0.037 compared with EU regulations are mostly within the threshold for EU regulations. Bac Hung Hai River water flowing through Van Giang district, Hung Yen province contains mainly PFBA and PFPeA compounds. The total content of PFCs in water samples collected along the Bac Hung Hai River, the section running through Van Giang district, Hung Yen province ranged from 1 ng/L to 38.8 ng/L. This finding shows that it is the waste sources from production activities, industrial parks and domestic activities that are the main causes for the presence of these PFASs.

Author Contributions: The experiment was conducted by L.A.P.T., B.V.L., H.T.D. The paper was written by H.T.D., L.A.P.T.

Conflicts of Interest: The authors declare no conflict of interest.

References

1. Yong, Q. Study on treatment technologies for perflorochemicals in wastewater. Ph.D Dissertation, Kyoto University, Japan, 2007.
2. Yin, G.Z.; Hin, T.W.; Alice, Y.S.L.; Xi, W.; Ye Q.H.; John, P.G.; Ming, H.W.; Chris K.C.W. Risk assessment for human consumption of perfluorinated compound-contaminated freshwater and marine fish from Hong Kong and Xiamen. *Chemosphere* **2011**, *85(2)*, 277–283.
3. Kaboré, H.A.; Sung, V.D.; Munoz, G.; Méité, L.; Desrosiers, M.; Liu, J.; Sory T.K.; Sauvé, S. Worldwide drinking water occurrence and levels of newly-identified perfluoroalkyl and polyfluoroalkyl substances. *Sci. Total Environ.* **2018**, *616–617*, 1089–1100.
4. Goosey, E.; Harrad, S. Perfluoroalkyl substances in UK indoor and outdoor air: Spatial and seasonal variation, and implications for human exposure. *Environ. Int.* **2012**, *45*, 86–90.
5. Vestergren, R.; Herzke, D.; Wang, Thanh.; Cousins, I.T. Are imported consumer products an important diffuse source of PFASs to the Norwegian environment? *Environ. Pollut.* **2015**, *198*, 223–230.
6. D'Hollander, W.; Roosens, L.; Covaci, A.; Cornelis, C.; Reynders, Hans.; Campenhout, K.V.; Voogt, P.D.; Bervoets, L. Brominated flame retardants and perfluorinated compounds in indoor dust from homes and offices in Flanders, Belgium. *Chemosphere* **2010**, *81(4)*, 478–487.
7. Domingo, J.L.; Jogsten, I.E.; Eriksson, U.; Martorell, I.; Perelló, G.; Nadal, M.; Bavel, B.V. Human dietary exposure to perfluoroalkyl substances in Catalonia, Spain. Temporal trend. *Food Chem.* **2012**, *135(3)*, 1575–1582.

8. Haug, L.S.; Salihovic, S.; Jogsten, I.E.; Thomsen, C.; Bavel, B.V.; Lindström, G.; Becher, G. Levels in food and beverages and daily intake of perfluorinated compounds in Norway. *Chemosphere* **2010**, *80(10)*, 1137–1143.
9. Vassiliadou, I.; Costopoulou, D.; Kalogeropoulos, N.; Karavoltsos, S.; Sakellari, A.; Zafeiraki, E.; Dassenakis, M.; Leondiadis, L. Levels of perfluorinated compounds in raw and cooked Mediterranean finfish and shellfish. *Chemosphere* **2015**, *127*, 117–126.
10. Guerranti, C.; Perra, G.; Corsolini, S.; Focardi, S.E. Pilot study on levels of perfluorooctane sulfonic acid (PFOS) and perfluorooctanoic acid (PFOA) in selected foodstuffs and human milk from Italy. *Food Chem.* **2013**, *140(1)*, 197–203.
11. Heo, J.J.; Lee, J.W.; Kim, S.K.; Oh, J.E. Foodstuff analyses show that seafood and water are major perfluoroalkyl acids (PFAAs) sources to humans in Korea. *J. Hazard. Mater.* **2014**, *279*, 402–409.
12. Zhang, T.; Sun, H.; Lin, Y.; Wang, L.; Zhang, X.; Liu, Y.; Geng, X.; Zhao, L.; Li, F.; Kannan, K. Perfluorinated Compounds in Human Blood, Water, Edible Freshwater Fish, and Seafood in China: Daily Intake and Regional Differences in Human Exposures. *J. Agric. Food. Chem.* **2011**, *59(20)*, 11168–11176.
13. Isobe, T.; Kim, J.W.; Nguyen, M.T.; Misaki, K.; Takahash, S.; Pham, H.V.; Tanabe, S. Determination of Perfluoroalkyl Compounds in Aqueous Samples from Northern Vietnam. *Interdiscip. Studies Environ. Chem. Environ. Pollut. Ecotoxicol.* **2012**, 239–244.
14. Kim, J.W.; Nguyen, M.T.; Isobe, T.; Misaki, K.; Takahashi, S.; Pham, H.V.; Tanabe, S. Contamination by perfluorinated compounds in water near waste recycling and disposal sites in Vietnam. *Environ. Monit. Assess.* **2013**, *185(4)*, 2909–2919.
15. Nguyen, H.L.; Choa, C.R.; Kannan, K.; Choa, H.S. A nationwide survey of perfluorinated alkyl substances in waters, sediment and biota collected from aquatic environment in Vietnam: Distributions and bioconcentration profiles. *J. Hazard. Mater.* **2017**, *323*, 116–127.
16. Duong, H.T.; Kadokami, K.; Shirasaka, H.; Hidaka, R.; Chau, T.C.H.; Kong, L.; Nguyen, Q.T.; Nguyen, T.T. Occurrence of perfluoroalkyl acids in environmental waters in Vietnam. *Chemosphere* **2015**, *122*, 115–124.
17. ISO 2009. Water Quality-Determination of Per-fluorooctanesulfonate (PFOS) and Perfluorooctanoate(PFOA)-Method for Unfiltered Samples Using Solid Phase Extraction and Liquid Chromatography/mass Spectrometre, 2014.
18. Nguyen, T.N, P.T.V., Phan, D.Q, Le, H.T.; Truong, T.K.; Nguyen, T.Q.; Phan, T.L.A.; Duong, H.A.; Pham, H.V. Perfuorinated compounds (PFCs) in urban wastewater of river and lake system in Hanoi. *VN J. Chem.* **2018**, 272–277. (In Vietnamese)
19. Phung, T.V.; Le, H.T.; Nguyen, T.N.; Phan, D.Q.; Pham, T.C.; Nguyen, T.T.H.; Duong, H.A.; Pham, H.V. Preliminary Survey of Perfluorinated Chemicals (PFCs) in Surface Water from Textile Villages in Northern Vietnam. *VNU J. Sci. Nat. Sci. Technol*. **2015**, *31(4)*, 90–97. (In Vietnamese)
20. OECD. Synthesis paper on per- and polyfluorinated chemicals (PFCs), Environment, Health and Safety. Environment Directorate, OECD. OECD/UNEP Global PFC Group, 2013.
21. Dinh, Q.H. Development of a Rapid and Easy Measurement Protocol for Perfluorinated Carboxylic Acids (PFCAs) by a Continuous Flow Analysis. Kyoto Univeristy, 2016.

VIETNAM JOURNAL OF HYDROMETEOROLOGY

Research Article

Research on assessment of surface water quality of Hau river in An Giang province on the basis of physicochemical parameters and zooplankton system

Phu Huynh[1*], Ngoc Thao Nguyen Ly[1], Ngoc Han Huynh Thi[2], Ngoc Nu Tran[3]

[1] HUTECH University; h.phu@hutech.edu.vn; nln.thao@hutech.edu.vn;
[2] Hochiminh City University of Nature Resources & Environment; htnhan_ctn@hcmunre.edu.vn;
[3] Researcher: tngocnu043@gmail.com

*Correspondence: h.phu@hutech.edu.vn; Tel.: +84–966687548

Received: 05 October 2021; Accepted: 28 November 2021; Published: 25 December 2021

Abstract: Research on water quality assessment of Hau river in An Giang province was conducted in 2019 in the upper Hau river (SH–T) and downstream Hau river adjacent to Can Tho (SH–H) through the following physico–chemical parameters, heavy metals: temperature, pH, Dissolved Oxygen (DO), COD, BOD_5, Total Suspended Solids (TSS), Nitrate (NO_3^- by N), Phosphate (PO_4^{3-} by P), Coliform, Arsenic (As), Lead (Pb), Mercury (Hg), Ammonium (NH_4^+ by N) and zooplankton system. Research results showed that: (1) Surface water quality in the area showed signs of pollution, DO content: 3.02–5.97 mg/l, lower than the standard (≥ 6 mg/l); TSS parameters: 35–90 mg/l, 1.75–4.5 times higher than standard; COD: 10–23 mg/l, 1.1–2.2 times higher than standard; BOD_5: 7–14 mg/l, 1.75–3.5 times higher than standard; Ammonium: 0.039–1.14 mg/l higher than standard 1.63 times in March and 3.83 times in September; Coliform: 2.100–24.000 MNP/100ml, not guaranteed well according to QCVN 08–MT:2015/BTNMT (level A1); (2) Surface water quality in the upper Hau river area according to diversity index H': 0.91 in March at "Heavily polluted" and H': 1.89 in September, at "Moderately polluted"; (3) The results of statistical analysis and PCA showed that the water quality parameters had significant differences between the two seasons, the rainy season showed signs of Coliform pollution and TSS more than the dry season.

Keyword: An Giang; Water quality; Diversity index H'; Tu Giac Long Xuyen.

1. Introduction

An Giang is one of four provinces and cities belongs to the key economic region of the Mekong Delta [1]. This locality is not only a province with a particularly important strategic position in terms of military and defense of the Southwest region; An Giang also has a border with Cambodia nearly 100 km, with an interlaced system of rivers and canals, fertile land, abundant natural resources [2]. All these advantages have contributed to making An Giang become a key agricultural production province of the country. In addition, An Giang is also a strategic agricultural and aquatic product export source, and is the global source of rice and pangasius agricultural products.

In addition to the economic successes, regional water environment has been and is being affected by increasing agricultural, industrial and daily–life wastes. Water pollution is a global problem, not just one country, or any one territory. To take specific measures to protect water resources, it is essential to assess the current state of water quality. Currently, there are

many methods to assess water quality such as: environmental monitoring, WQI water quality index, modeling, etc. The task of protecting water sources must be based on the results of water quality assessment. In Vietnam, the application of WQI water quality assessment index is quite popular [3–4], when applied in the study area, it shows that the water quality is polluted and needs to be treated appropriately before being put into use. However, besides comparing water quality parameters with QCVN 08–MT:2015/BTNMT–National technical regulation on surface water quality or calculating WQI index, the assessment of water quality pollution needs to be more comprehensive, to recognize pollution trends, the correlation between water quality pollution components, or to be able to assess water quality from species diversity or detection frequency of aquatic organisms. The method of water quality analysis by H' index, statistical analysis and PCA can better meet this requirement.

2. Materials and methods

2.1. Description of study area

Hau river is one of two distributaries of the Mekong river flowing into Vietnam's territory and flows through Chau Doc, Long Xuyen (An Giang), Vinh Long, Can Tho City, Chau Thanh (Hau Giang), Soc Trang, and flows into the East Sea from Dinh An and Tran De estuaries (Figure 1). For An Giang province, the Hau river is the waterway that goes through the center of the province from upstream to downstream, and is the main source of water and alluvium for the low–lying area of the Long Xuyen Quadrangle in daily life, agricultural production and aquaculture and seafood processing.

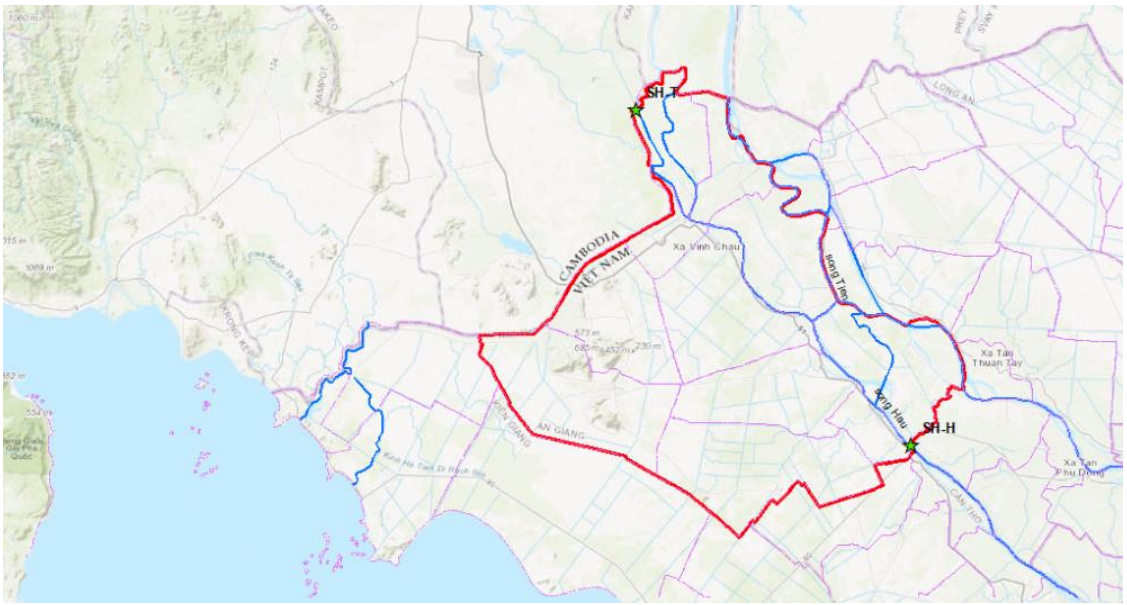

Figure 1. Sampling locations map.

SH–T: the upstream area of Hau river; SH–H: downstream area of Hau river

2.2. Methods of collecting and inheriting data

Data collection and inheritance about water environment monitoring data in the area, the study of the history and evolution of the aquatic environment to have a process of comparison and assessment.

2.3. Methods of observation, measurement and analysis

Monitoring in the upstream area of Hau River, An Phu District (SH–T) and downstream area of Hau River bordering Can Tho (SH–H), measured parameters of temperature, pH, DO,

TSS, COD, BOD_5, Nitrate (NO_3^- by N), Phosphate (PO_4^{3-} by P) and Coliform, Ammonium (NH_4^+ by N), As, Pb, Hg.

The variation of the flow greatly affects the water quality, so the flow data at the hydrological measurement stations need to be stored for analysis and evaluation of the results. The characteristics of flow change of the Hau river are different in the rainy and dry seasons, and the selection of sampling time in the rainy and dry seasons must take into account the characteristics of the rainfall distribution of the region. Therefore, sampling location, sampling time and frequency of water quality monitoring of Hau River were conducted continuously for 12 months in 2019 at 2 locations: upstream of Hau River (SH–T) and end of Hau river adjacent to Can Tho (SH–H) through the physico–chemical parameters, heavy metals.

Research was conducted to assess water quality parameters in the rainy season (July, August, September, October, November, and December in 2019) and the dry season (January, February, March, April, May, and June in 2019), there were 4 observation times each month, especially in December, there were 2 observation times. The zooplankton parameters were performed with a frequency of 2 times/at SH–T in March and September in 2019. The data analysis was performed after removing the outliers of each water quality parameter and the data was normalized to continue the test of statistical significance of variables.

2.4. Methods of sampling and preservation of samples

Sampling according to the following standards: TCVN 66631:2011, TCVN 6663–3:2008, TCVN 59941995, TCVN 66636:2008 and preserving samples according to standard TCVN 66633:2008.

2.5. Analytical and comparative methods

The study compared the monitoring results with QCVN 08–MT:2015/BTNMT (level A1)–National technical regulation on surface water quality. In addition, the study conducted statistical analysis and analysis of the main components of water quality parameters to evaluate the spatial trend of pollution at the sampling locations, according to the correlation between physico–chemical parameters, by the rainy season and the dry season.

The study used the Shannon and Weiner diversity index (H') to assess the diversity corresponding to the pollution degree of the water environment. The results of the analysis of biological indicators that were compared with the rating scales of Stau et al (1970) are presented in Table 1 by the formula:

$$H' = -\sum_{i=1}^{R} p_i \ln p_i \quad (1)$$

where p_i is the proportion of characters belonging to the ith type of letter in the string of interest. In ecology, p_i is often the proportion of individuals belonging to the ith species in the dataset of interest. Then the Shannon entropy quantifies the uncertainty in predicting the species identity of an individual that is taken at random from the dataset.

Table 1. Water Quality Rating by Diversity Index H'.

Range of ID	Class of water pollution
0 < H' < 1	Heavily polluted
1 < H' < 2	Moderately polluted
2 < H' < 3	Lowly polluted
3 < H' < 4	Slightly polluted
> 4–5	Good

Pearson analysis was performed to establish a correlation matrix and p–values to evaluate the statistical significance of water quality parameters in 2 seasons. Pearson correlation coefficient (symbol r), is a test metric that measures the relationship between water quality parameters fluctuating in the continuous range from –1 to +1,

where r = 0: Two variables have no linear correlation; r = 1; r = –1: The two variables have an absolute linear relationship; r < 0: Negative correlation coefficient. That is, the value of variable X increases, the value of variable Y decreases, and vice versa, the value of variable Y increases, the value of variable X decreases; r > 0: The correlation coefficient is positive. That is, the value of variable X increases, the value of variable Y increases and vice versa, the value of variable Y increases, the value of variable X also increases.

Pearson results are determined to be significant only if and only if the observed significance level is less than the significance level $\alpha = 5\%$. The confirmed degree of correlation with respect to r is as follows:

- If r is between 0.50 and ± 1; it is called the strong correlation.
- If r is between 0.30 and ± 0.49; it is called the average correlation.
- If r is less than ± 0.29; it is called the weak correlation.

2.6. Data processing methods

The data of the study were processed by using Microsoft Excel software, R software for statistical analysis and principal component analysis.

3. Results and discussion

3.1. Physicochemical parameters

3.1.1. Temperature

The temperature was measured at different times of the year at two locations upstream of the Hau river (SH–T) and the end of the Hau river (SH–H) fluctuated between 26.5^{o}C–32.8^{o}C and 27.8^{o}C–33.2^{o}C, respectively. The highest temperature was the 2nd observation in June at SH–T and the 3rd observation in July at SH–H. The lowest temperature was the 2nd observation in December at SH–T and the 3rd observation in September at SH–H (Figure 2a). In general, the temperature at the monitoring locations was consistent with the temperature of the general environment, without affecting the aquatic life of the area.

3.1.2. pH

The results of pH changes in 2019 by 12 observations at SH–T and SH–H locations showed that the pH was relatively stable, ranged from 6.03–7.64 and 6.81–7.86, respectively (Figure 2b). All of these values reached the allowable standards according to QCVN 08–MT:2015/BTNMT, leve A1 (68.5), met the quality of water for people's daily life and ensured aquatic life in the area.

3.1.3. Dissolved oxygen (DO)

Concentrations of DO at locations SH–T and SH–H ranged from 3.12–6.39 mg/l and 3.02–5.97 mg/l, respectively (Figure 2c). Particularly, DO at the location SH–T was the lowest in the 4th observation in November and only 04/48 monitoring times had values that reached the allowed standards according to QCVN 08–MT:2015/BTNMT (leve A1)–National technical regulation on quality surface water (≥ 6 mg/l). The lowest value of DO at the location SH–H was the 1st observation in August, the remaining values were lower than QCVN 08–MT:2015/BTNMT.

3.1.4. Suspended solids (TSS)

The monitoring results at SH–T and SH–H locations showed that concentrations of TSS ranged from 31–120 mg/l and 35–90 mg/l, respectively. All of these values exceeded the allowed standards according to QCVN 08–MT:2015/BTNMT, level A1 (20 mg/l) from 1.55–6 times and 1.75–4.50 times with the highest pollution in the second sampling in September (Figure 2d). Concentrations of TSS in water was mainly affected by the amount of alluvium upstream, plus the amount of soil and rock, waste caused by overflowing rainwater washed into the river, contributing to a significant increase in concentrations of TSS.

3.1.5. Chemical Oxygen Demand (COD)

The monitoring results at SH–T and SH–H locations showed that the COD concentration by the monitoring times ranged from 10–22 mg/l and 10–23 mg/l, respectively. Except for the 3rd observation in May and June, the values of COD concentration reached the allowed standards according to QCVN 08–MT:2015/BTNMT, leve A1 (10 mg/l); the remaining monitoring times were 1.10–2.20 times higher than the allowed standards, the highest pollution value was the 4th observation in November (Figure 2e).

3.1.6. Biochemical Oxygen Demand (BOD_5)

The monitoring results showed that the SH–T and SH–H locations showed that the concentrations of BOD_5 by the monitoring times did not reach the allowable standards according to QCVN 08–MT:2015/BTNMT, leve A1 (4 mg/l). The values of BOD_5 concentration at SH–T ranged from 7–14 mg/l, which were 1.75–3.50 times higher than the standard; the value of BOD_5 at SH–H ranged from 7–15 mg/l (Figure 2f), which exceeded the standard by 1.75–3.75 times.

3.1.7. Nitrate

The monitoring results at SH–T and SH–H locations showed that the concentrations of nitrate (NO_3^- by N) ranged from 0.015–0.340 mg/l and from undetectable to 0.916 mg/l, respectively. The value of the highest nitrate concentration was the 2nd observation in November (Figure 2g) but this value still reached the allowable standard according to QCVN 08–MT:2015/BTNMT, leve A1 (2 mg/l).

3.1.8. Phosphate

Monitoring results at SH–T and SH–H locations showed that the values of Phosphate concentrations (PO_4^{3-} by P) ranged from undetectable to 0.266 mg/l and from undetectable to 0.365 mg/l, respectively. The concentrations of Phosphate at the two locations fluctuated continuously through each monitoring period and were not according to the rules, typically at SH–T, the values of phosphate increased to the highest during the 3rd observation in November; at SH–H, the values of phosphate was highest during the 4th observation in October (Figure 2h). In general, most of the Phosphate concentrations reached QCVN 08–MT:2015/BTNMT, leve A1 (0,1 mg/l). However, at SH–T, there were only 11/48 observations with values exceeding from 1.01–2.66 times and at SH–H, there were 15/48 observations with values exceeding the allowable standards from 1.03–3.65 times.

3.1.9. Ammonia

The monitoring results at SH–T and SH–H locations showed that the values of ammonium concentration (NH_4^+ by N) ranged from 0.039–1.140 mg/l and from undetectable

to 1.150 mg/l, respectively. At SH–T, the values of ammonium exceeded the allowable standards according to QCVN 08–MT:2015/BTNMT, leve A1 (0.3 mg/l), these values were 1.75 times higher in March and 3.80 times higher in September (Figure 2j); At SH–H, the ammonium values exceeded the allowed standards according to QCVN 08–MT:2015/BTNMT, leve A1 (0.3 mg/l), these values were 1.68 times higher in March and 3.83 times higher in September.

3.1.10. As, Pb and Hg

The concentrations of As, Pb, and Hg were not found at both locations at all monitoring periods in 2019 (Figure 3), the values of the concentrations of these parameters reached QCVN 08–MT:2015/ BTNMT, leve A1 (As: 0.01 mg/l; Hg: 0.001 mg/l; Pb: 0.02 mg/l).

3.1.11. Coliform

Monitoring results at SH–T and SH–H locations in 2019 showed that the Coliform bacteria density ranged from 430–24.000 MPN/100 ml and 2.100–24.000 MPN/100 ml, respectively. Except for the 4th observation in January and the 1st observation in July at SH–T; and the 1st observation in January, the 3rd observation in May and the 2nd observation in June at SH–H (Figure 2i) reached the standard value, the values of Coliform in the remaining observations were higher than QCVN 08–MT:2015/BTNMT, leve A1 (2500 MPN/100 ml) from 1.72–9.60 times.

Figure 2. Water quality parameters: (a) Temperature; (b) Values of pH; (c) Concentrations of DO (mg/l); (d) Concentrations of TSS (mg/l); (e) Concentrations of COD (mg/l); (f) Concentrations of BOD_5 (mg/l).

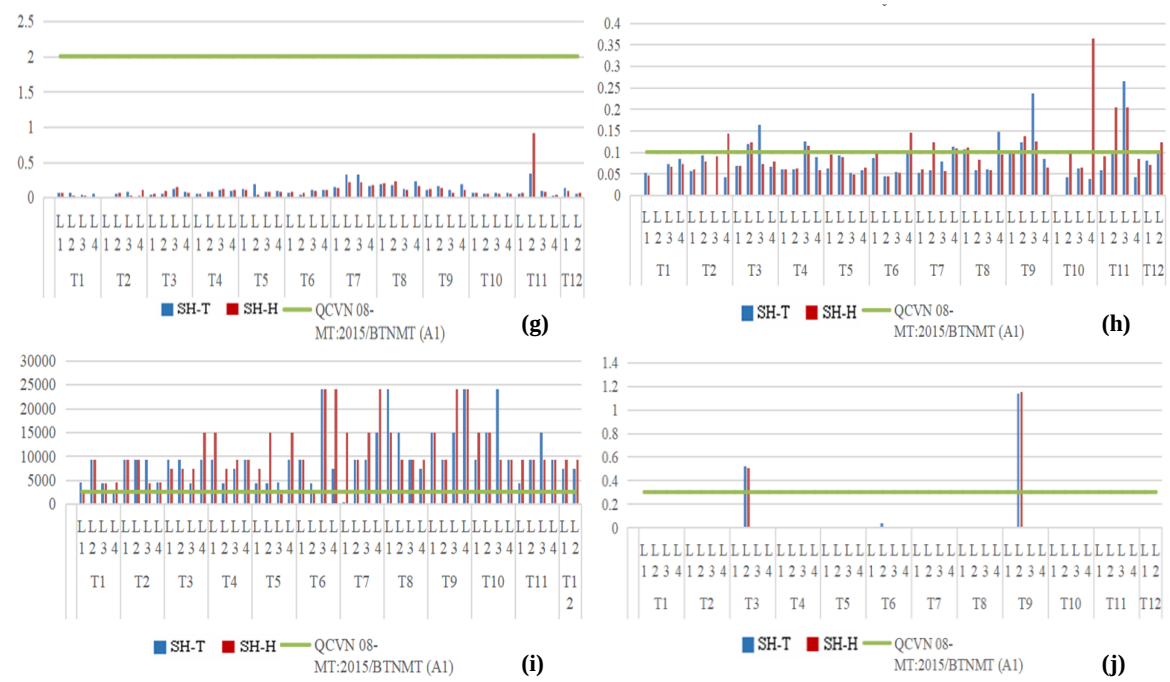

Figure 2. Water quality parameters: (g) Concentrations of Nitrat (mg/l); (h) Concentrations of Phosphate (mg/l); (i) Coliform (MPN/100ml); (j) Concentrations of Ammonia (mg/l) (continute).

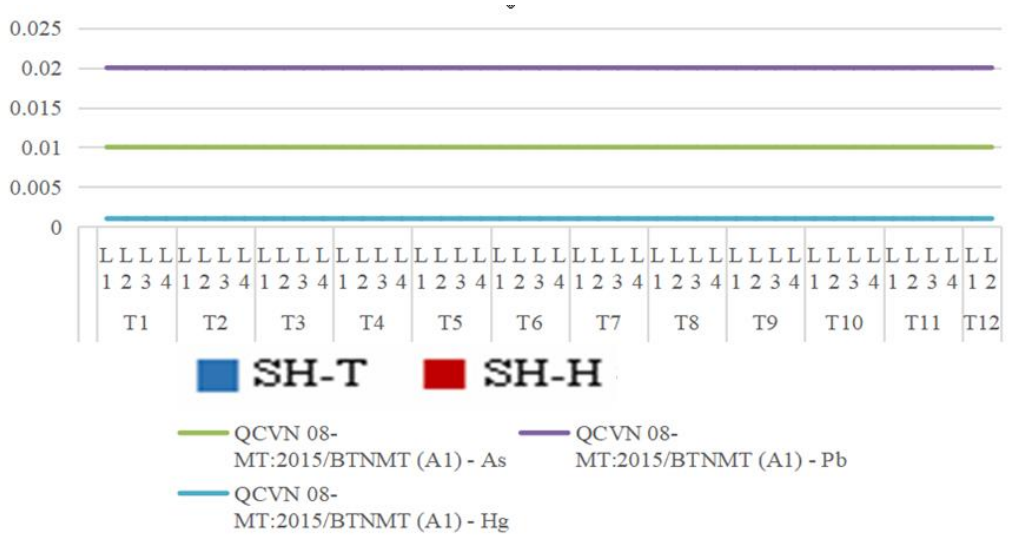

Figure 3. Concentrations of As, Pb, Hg (mg/l).

3.2. Components of the zooplankton system

3.2.1. Density of zooplankton

The results of monitoring parameters of phytoplankton in the upstream area of the Hau river in March (dry season) and September (rainy season) in 2019 are as follows:

- Structure of species composition: The composition of zooplankton species had a low diversity, only a total of 18 species belonging to 5 phylums had been identified. The structure of species composition during the year did not change significantly. In the dry season, the study recorded a more diverse species composition than in the rainy season (Figure 4 and Figure 5).

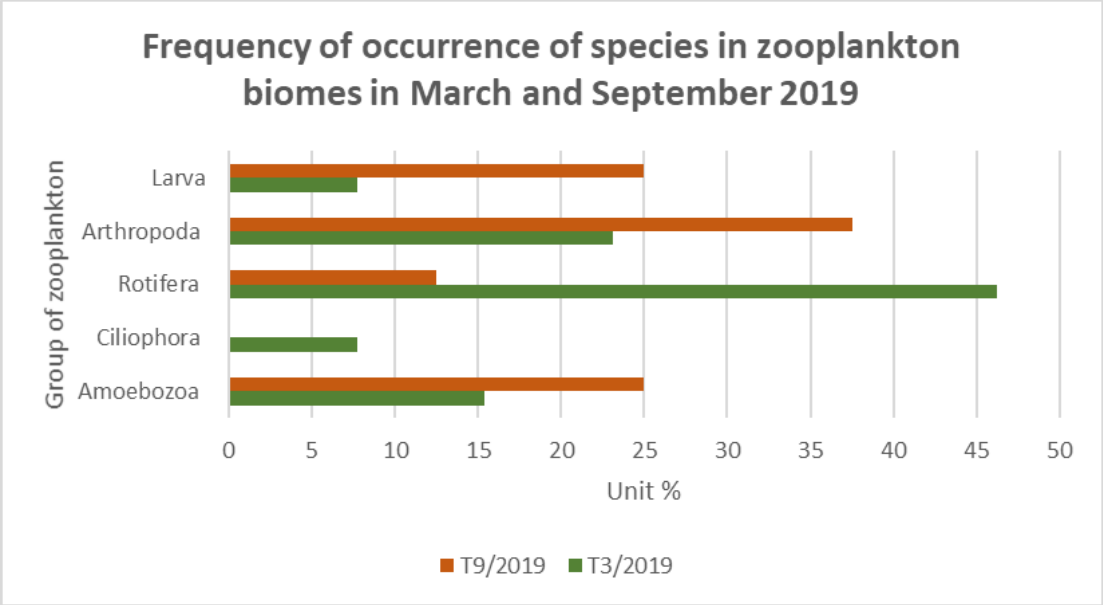

Figure 4. Species composition of zooplankton system at SH–T during rainy and dry seasons.

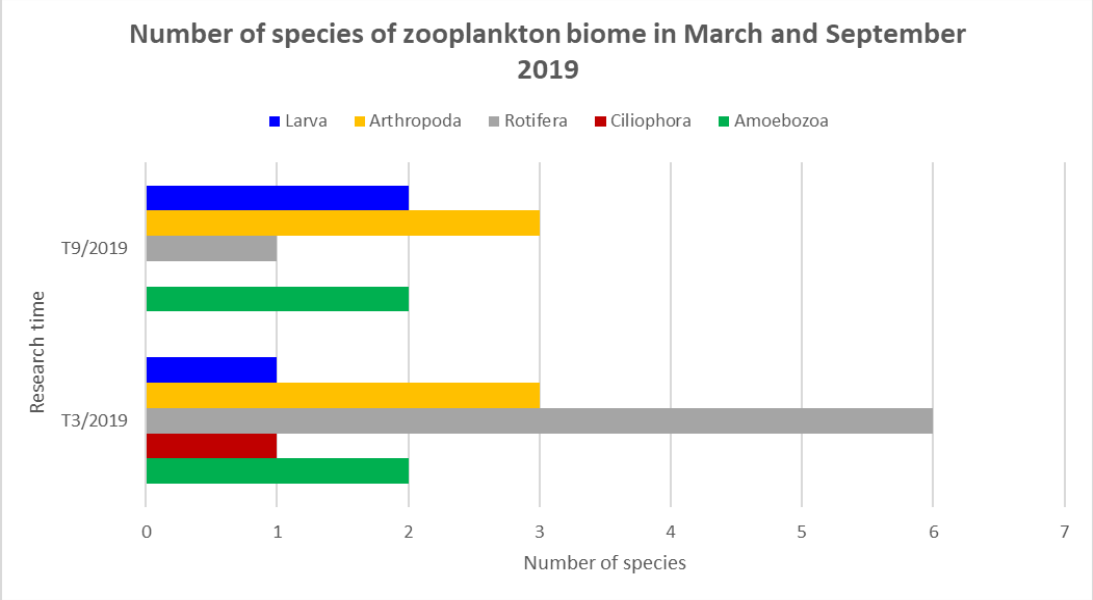

Figure 5. Number of species of zooplankton system at SH–T in rainy and dry seasons.

The comparison between the two observations in 2019 showed that the total number of species in the September monitoring period was reduced compared to the March period (05 species). The fluctuations were concentrated mainly in the Rotifera, which decreased by 5 species; the Ciliophora that decreased by 01 species and the Larval that increased by 1 species; the Arthopoda and Amoebozoa did not have much change.

Amoebozoa, Arthropoda, Larvae appeared in the whole year with a total of 03 species, accounting for 16.7% of the total number of species present in both observations. The results of two monitoring showed that the zooplankton sysytem in the upper Hau river area (SH–T) in 2019 had seasonal fluctuations, focusing mainly on the group of species adapted to the environment rich in organic matter.

- Individual density and dominant species composition: The species structure and dominant species composition in the upper Hau river area (SH–T) were different between the two observations. The number of species and density of individuals in the rainy season decreased significantly compared to the dry season.

Table 2. Number of species and density of zooplankton system in the upper Hau river area.

Location	Number of species		Density /m^3	
	March 2019	September 2019	March 2019	September 2019
SH–T	13	8	867.200	6.000

- Individual density: The total number of phytoplankton individuals detected in the upper Hau river (SH–T) area through two observations in 2019 was 867.200 individuals/m^3 and 6.000 individuals/m^3, respectively. The density of cetaceans ranged from 200–720.000 individuals/m^3 in March and from 667–3.333 individuals/m^3 in September.

- Predominant species composition: Paracalanus parvus species of biome Arthropoda predominated with the rate of 83% in March and Copepoda nauplius species of biome Larva predominated with the rate of 55.6% in September.

Table 3. The dominant species of the zooplankton system of the upper reaches of Hau river.

Location	March 2019		September 2019	
	Predominated species	Rate %	Predominated species	Rate %
SH–T	Paracalanus parvus	83.0	Copepoda nauplius	55.6

The clustering by species composition and occurrence frequency of zooplankton communities at SH–T in the rainy and dry seasons were shown above Figure 6 and Figure 7.

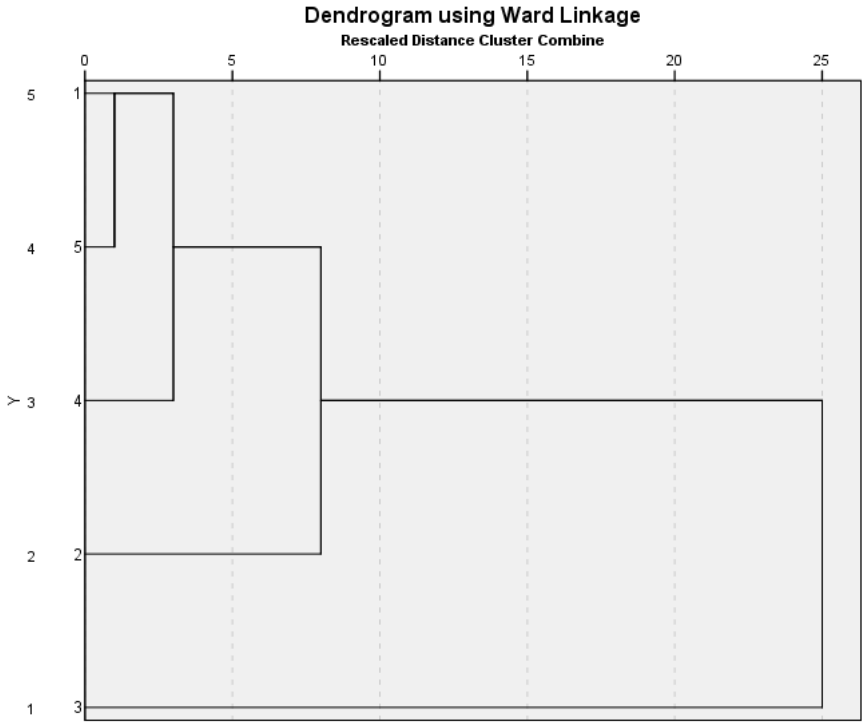

Figure 6. Clustering chart by species composition of zooplankton biome at SH–T in rainy and dry seasons. 1. Amoebozoa, 2. Ciliophora, 3. Rotifera, 4. Arthropoda, 5. Larva.

3.2.2. Diversity index H’

Calculation results showed that the diversity index H’ of the zooplankton in the upstream area of Hau river SH–T through two observations in 2019 ranged from 0.91 to 1.89. In which, the H’ index in the rainy season was higher than in the dry season, the water quality according to the index H’ of the zooplankton tended from “Heavily polluted” to “Moderately polluted” (Table 4).

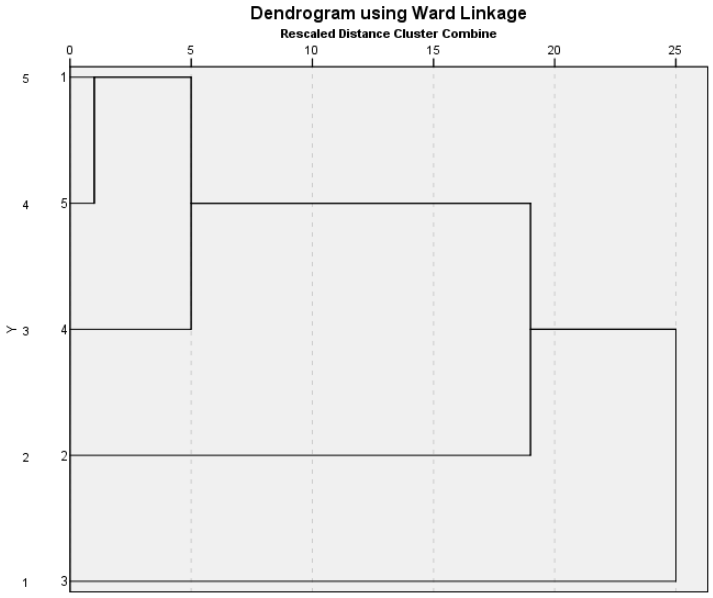

Figure 7. Clustering chart by frequency of zooplankton biomes at SH–T in rainy and dry seasons. 1.Amoebozoa, 2. Ciliophora, 3. Rotifera, 4. Arthropoda, 5. Larva.

Table 4. Diversity index H' of the zooplankton system.

Zooplankton sysytem	3–2019		9–2019	
	Diversity index H'	**Water quality**	**Diversity index H'**	**Water quality**
	0.91	Heavily polluted	1.89	Moderately polluted

3.3. Statistical analysis of water quality parameters

3.3.1. Descriptive statistical analysis of the variables

Because the parameters Ammonium (NH_4^+ by N), As, Pb, Hg had low values, most were not found in observations, these parameters were removed and not further analyzed. The results of the descriptive statistics are presented in Table 5.

Table 5. Descriptive statistics of water quality parameters at sampling locations in Hau river in the dry and rainy seasons.

Parameters	Unit	Dry season			Rainy season		
		Number of samples	**Mean values**	**Dtandard deviations**	**Number of samples**	**Mean values**	**Standard deviations**
Temperature	^oC	48	30,01	1.37	44	29.69	1.29
pH		48	7.05	0.32	44	7.04	0.36
DO	mg/l	48	5.00	0.81	44	5.04	0.74
TSS	mg/l	48	48.79	6.60	44	53.07	8.68
COD	mg/l	48	13.17	2.01	44	14.02	2.70
BOD_5	mg/l	48	8.52	1.22	44	9.02	1.70
Nitrat	mg/l	48	0.08	0.04	44	0.15	0.15
Phosphate	mg/l	48	0.07	0.03	44	0.10	0.07
Coliform	MPN/100ml	48	8.28	4.50	42	12.78	5.44

The descriptive statistics of the data in Table 5 showed that the average value of water quality parameters did not change much between the two seasons. The parameters with relatively clear diagnostic deviations are Temperature, TSS, COD, BOD_5 and Coliform, and most of these parameters in the rainy season have higher standard deviations than in the dry season. However, to determine whether the difference in standard deviations of the variables in the 2 seasons is due to random factors from the data or due to the actual difference of the environment in the 2 seasons (such as influenced by runoff, rain, washout, tides and seasonal flow characteristics, etc), the study assessed the statistical significance of the water quality difference according to each pollution parameter.

3.3.2. Evaluation of the statistical significance of the variation of water quality by each parameter between the two seasons

a. Shapiro–Wilk test

To choose a method to test the statistical significance of water quality parameters, the study conducted to determine the normal distribution of water quality parameters. The number of samples in the rainy and dry seasons was < 50, so the study applied the Shapiro–Wilk test with the significance level of 5% to determine the normal distribution of water quality parameters. The results of the Shapiro–Wilk normal distribution test are presented in Table 6 and the pattern of the distribution's evolution is shown in the Histograms in Figures 16 and 17 (Values of water quality parameters with a normal distribution will have Histograms with a symmetric bell–shaped normal curve with the highest frequencies in the middle and the lower frequencies on the sides. Mean and median values are close to each other and the slope is close to zero).

Table 6. Shapiro–Wilk normal distribution test results of water quality parameters in rainy and dry seasons.

Number	Parameter	p–value in dry season	p–value in rainy season
1	Temperature	1.53E–02	6.64E–01
2	pH	7.22E–01	4.23E–03
3	DO	6.03E–02	4.63E–03
4	TSS	1.22E–01	1.05E–09
5	COD	4.48E–02	2.56E–05
6	BOD_5	2.87E–04	1.13E–06
7	Nitrat	1.53E–01	2.24E–09
8	Phosphate	6.02E–05	9.18E–06
9	Coliform	5.14E–05	3.50E–14

The results of the Shapiro–Wilk normal distribution of the parameters from Table 6 showed that:

- Dry season: pH, DO, TSS, and Nitrate parameters were normally distributed with p–value > 0.05; Temperature, COD, BOD_5, Phosphate and Coliform parameters were not normally distributed because they had p–value < 0.05.
- Rainy season: Temperature parameter was normally distributed with p–value > 0.05; pH, DO, TSS, Nitrate, COD, BOD_5, Phosphate and Coliform parameters were not normally distributed because they had p–value < 0.05.
- Most of the water quality parameters did not have a normal distribution, so the study chose a non–parametric test method (the Wilcoxon signed–rank non–parametric test with the level of statistical significance $\alpha = 5\%$) to determine the statistical significance of the water quality parameters in 2 seasons.

b. Wilcoxon signed–rank test

The results are shown in Table 7.

Table 7. Wilcoxon signed–rank non–parametric test results.

Number	Parameters	Number of samples in dry season	Number of samples in rainy season	p–value	Statistically significant*
1	Temperature	48	44	2.1E–01	No
2	pH	48	44	9.9E–01	No
3	DO	48	44	1.0E+00	No
4	TSS	48	44	1.4E–02	Yes
5	COD	48	44	2.3E–01	No
6	BOD_5	48	44	5.7E–01	No
7	Nitrat	48	44	1.9E–04	Yes
8	Photphat	48	44	1.4E–01	No
9	Coliform	48	44	6.1E–06	Yes

*After comparing the p–value with $\alpha = 5\%$.

According to the results of the Wilcoxon signed–rank non–parametric test, the water quality parameters had significant differences and are statistically significant between the two seasons, namely TSS, Nitrate and Coliform, and all three parameters in the rainy season had higher concentration values than in the dry season. Parameters with no statistically significant differences between the two seasons were Temperature, pH, DO, COD, BOD_5 and Phosphate. Thus, in general, Hau river water quality in the rainy season showed more signs of pollution of suspended solids and harmful bacterias than in the dry season. The cause could due to natural origin such as phenomenon of erosion, erosion, geological structure or under the influence of human activities, production, untreated wastewater, excessive agricultural production, etc. For these reasons caused many bad effects leading to pollution in water by the process of decomposition of organic compounds, high concentration of Coliform bacteria in water; TSS concentration in water was mainly affected by the amount of alluvium flowing back from upstream, plus a large amount of soil, rock, and waste due to overflowing rainwater washed into the river, contributing to a significant increase in TSS concentration.

3.3.3. Correlation analysis

The results of Pearson matrix analysis are shown in Figure 8 and Figure 9.

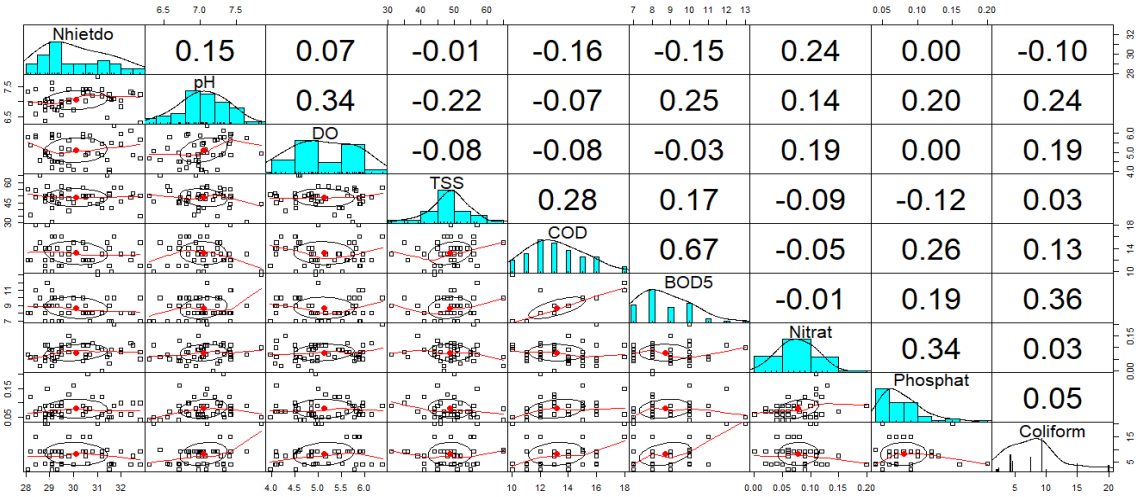

Figure 8. Correlation analysis matrix between water quality parameters in dry season.

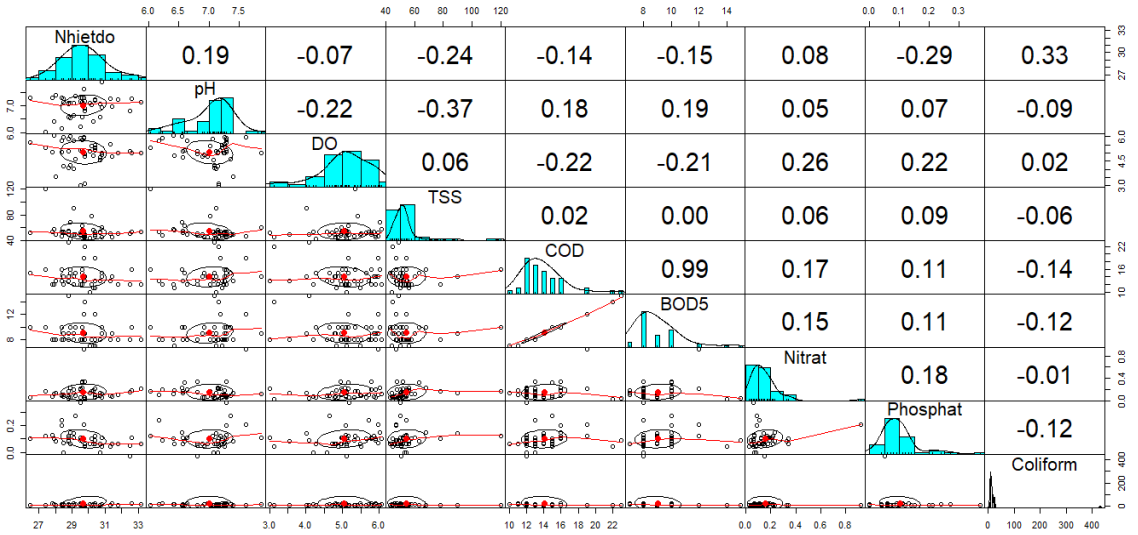

Figure 9. Correlation analysis matrix between water quality parameters in rainy season.

The results of correlation analysis of water quality parameters in Figure 8 and Figure 9 showed that the correlation coefficients between water quality parameters in the dry season were much larger in absolute values than in the rainy season, so water quality parameters in the dry season had a stronger correlation than in the rainy season.

- In the dry season: the pair of parameters COD and BOD_5 had a strong correlation ($r \geq 0.5$). Meanwhile, the pairs of parameters pH–DO, Nitrate–Phosphate, BOD_5–Coliform had an average correlation ($0.3 \leq r < 0.5$). Parameter pairs pH–Temperature, DO–Temperature, TSS–COD, TSS–BOD_5, pH–BOD_5, Nitrate–Temperature, Nitrate–DO, Nitrate–pH, pH–Phosphate, COD–Phosphate, BOD_5–Phosphate, pH–Coliform, DO–Coliform, COD–Coliform, Phosphate–Coliform had a weak correlation ($r < 0.3$). The remaining parameter pairs: TSS with pH and DO; COD with Temperature, pH and DO; BOD_5 with Temperature; Nitrates with TSS, COD; Phosphate–TSS; Coliform with Temperature had an inverse and weak correlation ($r < 0$ and $r < 0.3$). In addition, the pairs of parameters Temperature–Phosphate, DO–Phosphate had absolutely no correlation ($r = 0$) and the parameter pairs of Temperature–TSS, DO–BOD_5, BOD_5–Nitrate, Coliform–TSS, Coliform–Nitrates had no observed significance ($r < \alpha = 5\%$).

- In the rainy season: parameters COD and BOD_5 had a strong correlation ($r \geq 0.5$). Meanwhile, pair of parameters Temperature–Coliform had an average correlation ($0.3 \leq r < 0.5$). Pairs of parameters pH–Temperature, DO–TSS, COD–pH, pH–BOD_5, Nitrate–Temperature, Nitrate–DO, Nitrate–pH, Nitrate–COD, Nitrate–BOD_5, Nitrate–TSS, Phosphate–DO, Phosphate–pH, Phosphate–COD, Phosphate–BOD_5, Phosphate–TSS had a weak correlation ($r < 0.3$). Pair of parameters pH–TSS had an inverse and average correlation ($r < 0$ and $r \geq 0.3$) The remaining parameter pairs: DO with pH and Temperature; TSS with Temperature; COD with Temperature and DO; BOD_5 with Temperature and DO; Phosphate with Temperature; Coliform with pH, TSS, COD, BOD_5 and Phosphate had an inverse and weak correlation ($r < 0$ and $r < 0.3$). In addition, pair of parameters TSS–BOD_5 had absolutely no correlation ($r = 0$) and pairs of parameters COD–TSS, Coliform–nitrate had no observable significance ($r < \alpha = 5\%$).

3.4. Principal component analysis (PCA)

3.4.1. Dry season

a. Principal component analysis of water quality parameters in the dry season

In the dry season, the research based on the results of the Scree plot (Figure 10) with the Eigenvalue index > 1.0 identified the first 4 principal components PC1, PC2, PC3, PC4 with the total variance accounting for 68.6% of tuples. These 4 components were used for further analysis. From the 5th components onwards had small variance, so they were ignored.

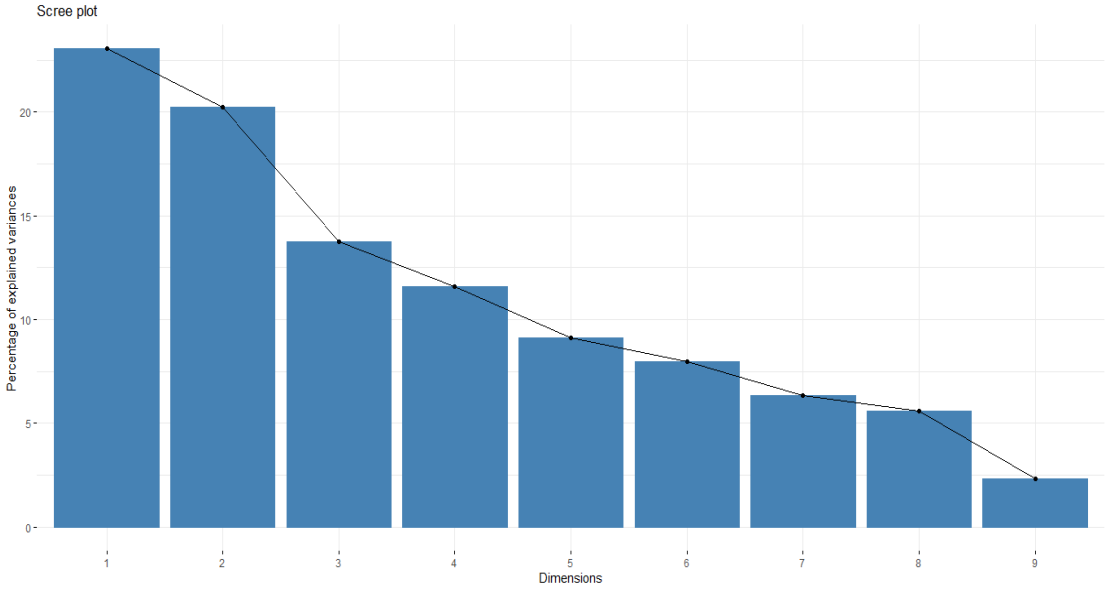

Figure 10. Screen plot analysis of principal components of water quality parameters in dry season.

The main influencing parameters in the principal components PC1, PC2, PC3, PC4 include:

- PC1 had a total variance value of 23.04%, including: COD (positive contribution with rotated component indicator of 0.88), BOD_5 (positive contribution with rotated component indicator of 0.85). The principal group of components showed pollution by organic substances of natural or artificial origin (domestic wastewater, industrial wastewater, agricultural wastewater).
- PC2 had a total variance value of 20.22%, including: DO (positive contribution with rotated component indicator of 0.73), pH (positive contribution with rotated component indicator of 0.69), Coliform (positive contribution with rotated component indicator of 0.65). The principal group of components showed that pH and dissolved oxygen were correlated with Coliform parameter. From analyzing the correlation of water quality parameters in the dry season, this study showed that Coliform parameter is positively correlated with DO and pH, which means that the increase of pH and dissolved oxygen increases the Coliform concentration in water.
- PC3 had a total variance value of 13.76%, including: Phosphate (positive contribution with rotated component indicator of 0.76), TSS (negative contribution with rotated component indicator of 0.85). The principal group of components indicated pollution of suspended solids and phosphates with a inverse correlation, if TSS concentration increases, phosphate concentration decreases and vice versa.
- PC4 had a total variance value of 11.58%, including: Temperature (positive contribution with rotated component indicator of 0.92). PC4 showed that the temperature of the water was affected by the environment or the source of the discharge.

b. Pollution characteristics of Hau river in dry season

- Principal components PC1 and PC2

The water quality characteristics of Hau river at the monitoring locations SH–T and SH–H for PC1 and PC2 in the dry season are shown in Figure 11.

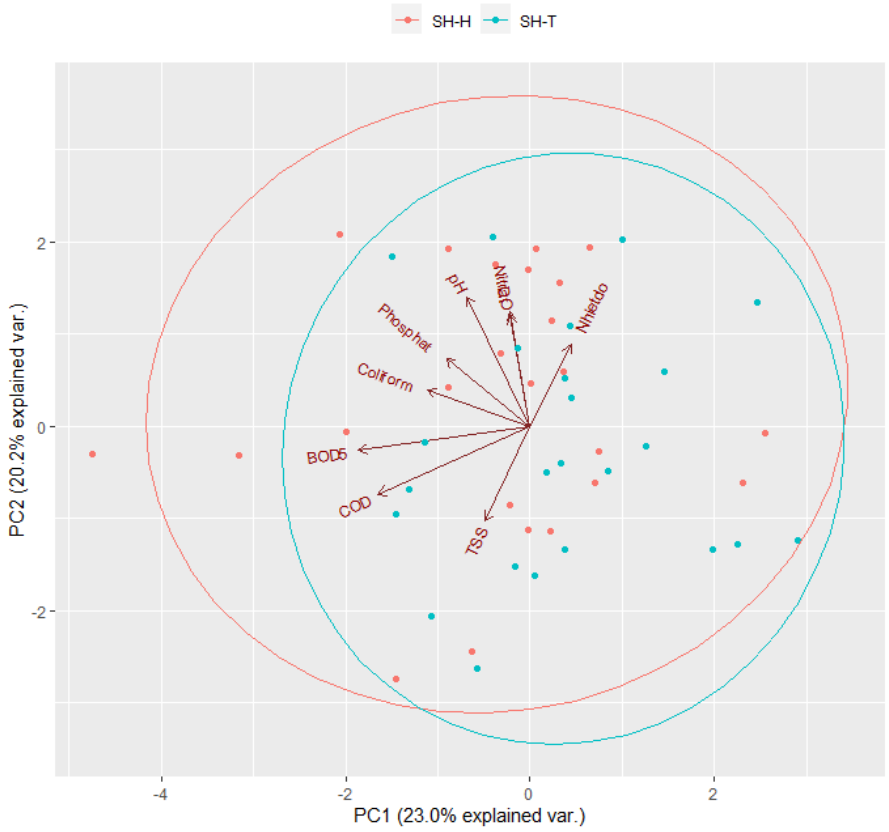

Figure 11. Water quality characteristics of Hau river at monitoring locations SH–T and SH–H corresponding to PC1 and PC2 in the dry season.

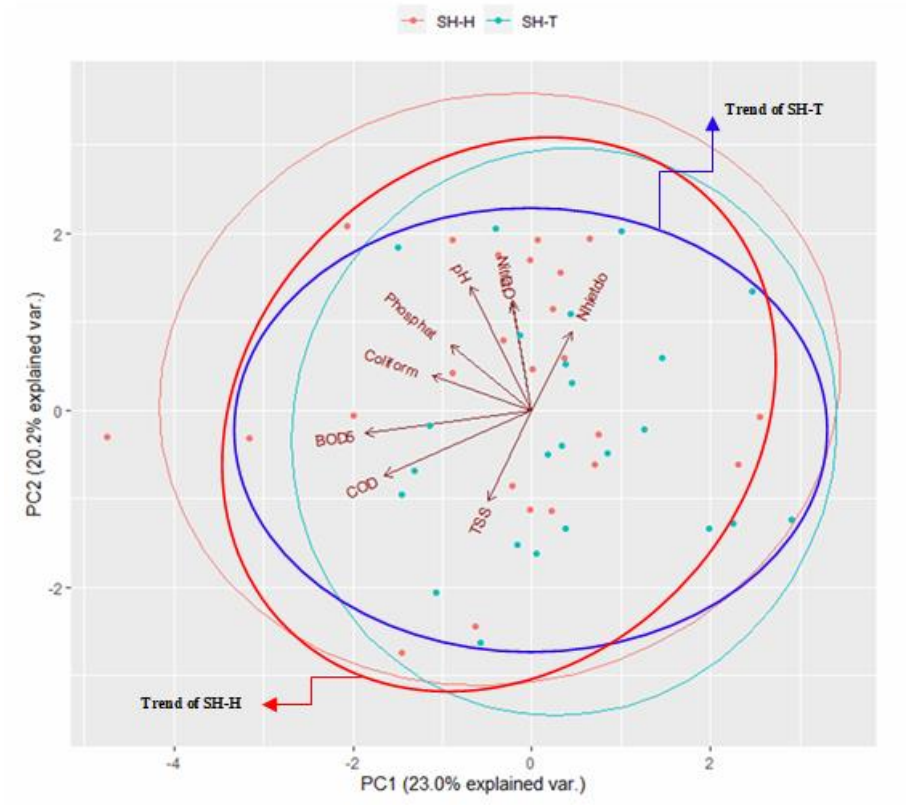

Figure 12. Water quality trends of Hau river at locations SH–T and SH–H corresponding to PC1 and PC2 in the dry season.

Analysis results from R software showed that: At the monitoring location upstream of Hau river (SH–T) was characterized by most of the main parameters of PC1 (COD, BOD_5) and PC2 (DO, pH and Coliform); however the main parameters in PC2 (vertical axis) had more influential. At the monitoring location downstream of Hau river (SH–H) was characterized by most of the main parameters of PC1 (COD, BOD_5) and PC2 (DO, pH and Coliform), however the main parameters in PC1 (horizontal axis) had more influential. However, the research team assessed that the trend of water quality in the upper Hau River (SH–T) was influenced by water quality parameters of the principal component PC1 more than PC2. Besides, the trend of water quality in the lower Hau River (SH–H) was influenced by water quality parameters of the principal component PC2 (Figure 12). In other words, in the dry season, the SH–T position of the river is affected by the parameters of COD, BOD_5 more.

In fact, from the results of sample analysis data and comparison with QCVN 08–MT:2015/BTNMT (level A1)–National technical regulation on quality surface water, DO at the location SH–T was the lowest in the 4th observation in November and only 04/48 monitoring times had values that the allowed standards. The monitoring results at SH–T location showed that the COD concentration were 1.1–2.2 times higher than the allowed standards, the highest pollution value was the 4th observation in November. The values of BOD_5 concentration at SH–T ranged from 7–14 mg/l, which were 1.75–3.50 times higher than the standard. High COD and BOD_5 concentrations reduced the DO concentration of the water, which was harmful to water organisms and the water ecosystem in general. Organic wastewater, domestic wastewater and chemical wastewater were the agents that create high BOD_5 and COD values of the aquatic environment. High levels of COD and BOD_5 in water showed that the water source contains many organic pollutants. At SH–H, except for the 4th observation in January and the 1st observation in July, the values of Coliform in the remaining observations were higher than QCVN 08–MT:2015/BTNMT, level A1 (2500 MPN/100 ml) from 1.72–9.60 times.

- Principal components PC3 và PC4

The water quality characteristics of Hau river at the monitoring locations SH–T and SH–H for PC3 and PC4 in the dry season are shown in Figure 13.

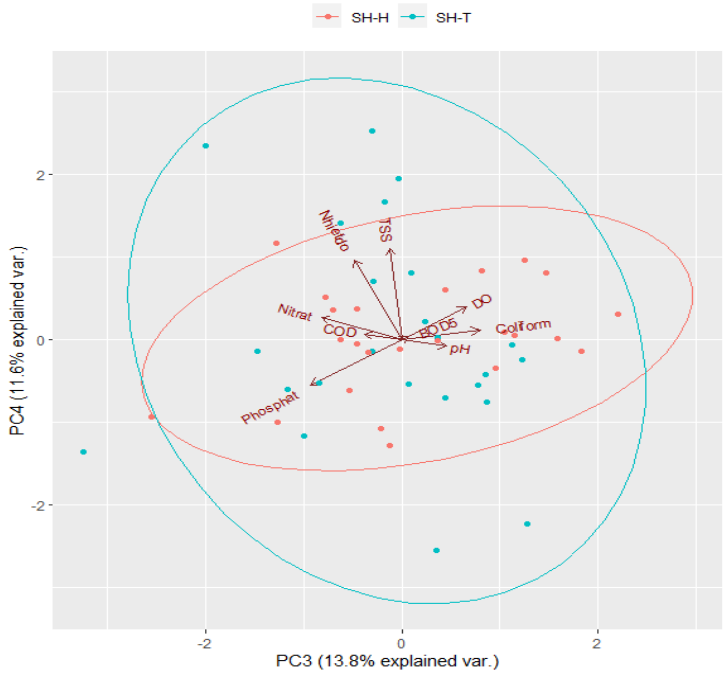

Figure 13. Water quality characteristics of Hau river at monitoring locations SH–T and SH–H corresponding to PC3 and PC4 in the dry season.

Analysis results from R software showed that: At the monitoring loction upstream of Hau river (SH–T) was characterized by most of the main parameters of PC3 (Phosphate and TSS) and PC4 (Temperature), however the Temperature parameter in PC4 (vertical axis) had more influence; At the monitoring location downstream of Hau River (SH–H) was characterized by most of the main parameters of PC3 (Phosphate and TSS) and PC4 (Temperature), but the main parameters in PC3 (horizontal axis) had more influence. This explains that the water downstream quality of Hau river showed signs of being affected by phosphates and suspended solids. However, the influence of the two principal components PC3 and PC4 will have little apparent effect because PC3 and PC4 account for very small percentages of the total variance of the principal components (13.8% and 11.6%).

3.4.2. Rainy season

a. Principal component analysis of water quality parameters in the rainy season

In the rainy season, the research based on the results of the Scree plot (Figure 14) with the Eigenvalue index > 1.0 identified the first 4 principal components PC1, PC2, PC3, PC4 with the total variance accounting for 72.14% of tuples. These 4 components were used for further analysis. From the 5th components onwards had small variance, so they were ignored.

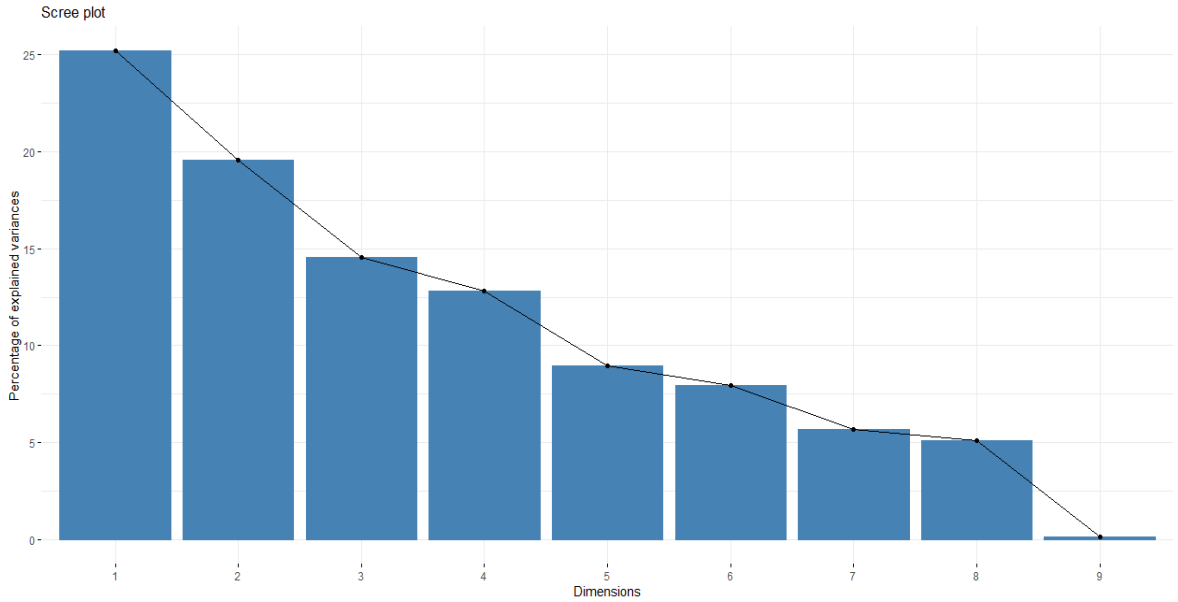

Figure 14. Screen plot analysis of principal components of water quality parameters in rainy season.

The main influencing parameters in the principal components PC1, PC2, PC3, PC4 include:

- PC1 had a total variance value of 25.2%, including: COD (positive contribution with rotated component indicator of 0.98), BOD_5 (positive contribution with rotated component indicator of 0.97). The principal group of components indicated pollution by organic substances of natural or artificial origin (domestic wastewater, industrial wastewater, agricultural wastewater).

- PC2 had a total variance value of 19.6%, including: pH (positive contribution with rotated component indicator of 0.82), TSS (negative contribution with rotated component indicator of 0.79). The principal group of components showed that the pH and total suspended solids in the water.

- PC3 had a total variance value of 14.56%, including: Coliform (positive contribution with rotated component indicator of 0.87), Temperature (positive contribution with rotated component indicator of 0.73). The principal group of components indicated harmful microorganisms that are affected by temperature (parameters Temperature and Coliform had

an average correlation with r = 0.33 (increasing temperature will increase Coliform and vice versa).

- PC4 had a total variance value of 12.82%, including: Nitrat (positive contribution with rotated component indicator of 0.83), DO (positive contribution with rotated component indicator of 0.75). PC4 showed that water environment was affected by nitrate and temperature with a rather weak correlation coefficient (r = 0.08).

b. Pollution characteristics of Hau River in rainy season

- Principal components PC1 and PC2

The water quality characteristics of Hau river at the monitoring locations SH–T and SH–H for PC1 and PC2 in the rainy season are shown in Figure 15.

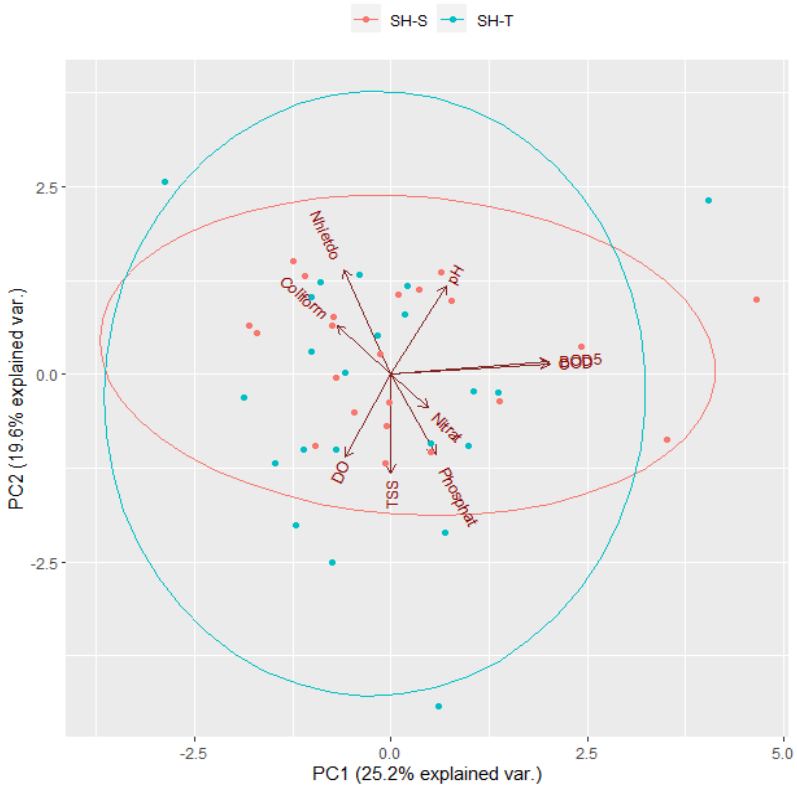

Figure 15. Water quality characteristics of Hau river at monitoring locations SH–T and SH–H corresponding to PC1 and PC2 in the rainy season.

Analysis results from R software showed that: At the monitoring location upstream of Hau River (SH–T) was characterized by most of the main parameters of PC1 (COD, BOD_5) and PC2 (pH and TSS); however the main parameters in PC2 (vertical axis) had more influence. At the monitoring location downstream of Hau river (SH–H) was characterized by most of the main parameters of PC1 (COD, BOD_5) and PC2 (pH and TSS), but the main parameters in PC1 (horizontal axis) had more influence.

However, the authors assessed that the water quality of Hau river at the upstream location of SH–T influenced very clearly by the principal component PC2 and at the same time had been greatly influenced by principal component PC1 (Figure 16).

In fact, from the results of sample analysis data and comparison with QCVN 08–MT:2015/BTNMT (level A1)–National technical regulation on quality surface water, the monitoring results at SH–T location showed that the COD concentration by the monitoring times did not reach the allowable standards according to QCVN 08–MT:2015/BTNMT, level A1 (10 mg/l). The values of BOD_5 concentration at SH–T ranged from 7–14 mg/l, which were 1.75–3.50 times higher than QCVN 08–MT:2015/BTNMT, level A1 (4 mg/l).

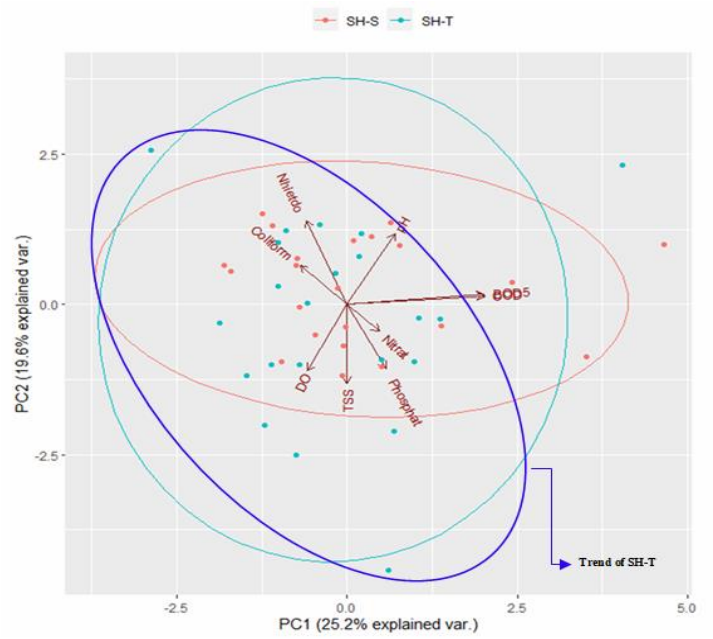

Figure 16. Water quality trends of Hau river at locations SH–T and SH–H corresponding to PC1 and PC2 in the rainy season.

- Principal components PC3 và PC4

The water quality characteristics of Hau river at the monitoring locations SH–T and SH–H for PC3 and PC4 in the rainy season are shown in Figure 17. Analysis results from R software showed that: At the monitoring location upstream of the Hau river (SH–T) was characterized by most of the main parameters of PC3 (Temperature and Coliform) and PC4 (Nitrates and DO), but PC4 (vertical axis) had more influence. In which, parameters DO and nitrate had a weak positive correlation (r = 0.26). At the monitoring location downstream of Hau river (SH–H) was characterized by most of the main parameters of PC3 (Temperature and Coliform) and PC4 (nitrate and DO), but the main parameters in PC3 (axis diaphragm) had more influence. This explains that the water downstream of Hau river showed signs of being affected by Coliform bacterias; they and Temperature had an average positive correlation (r = 0.33).

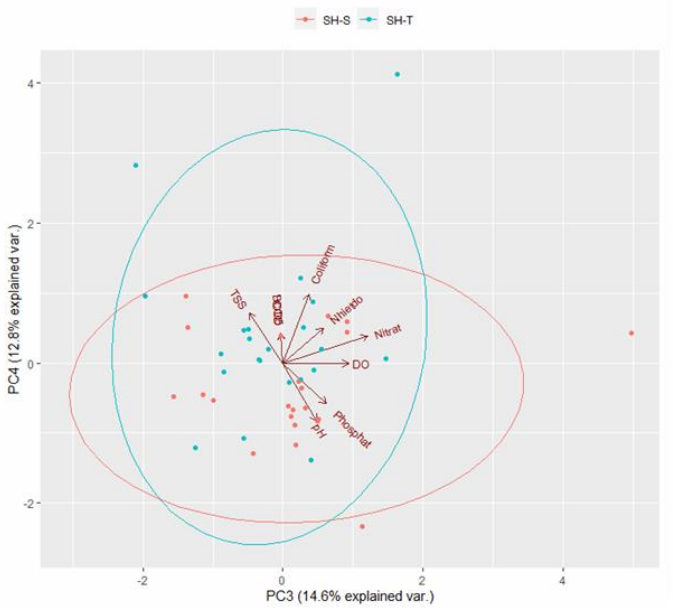

Figure 17. Water quality characteristics of Hau river at monitoring locations SH–T and SH–H corresponding to PC3 and PC4 in the rainy season.

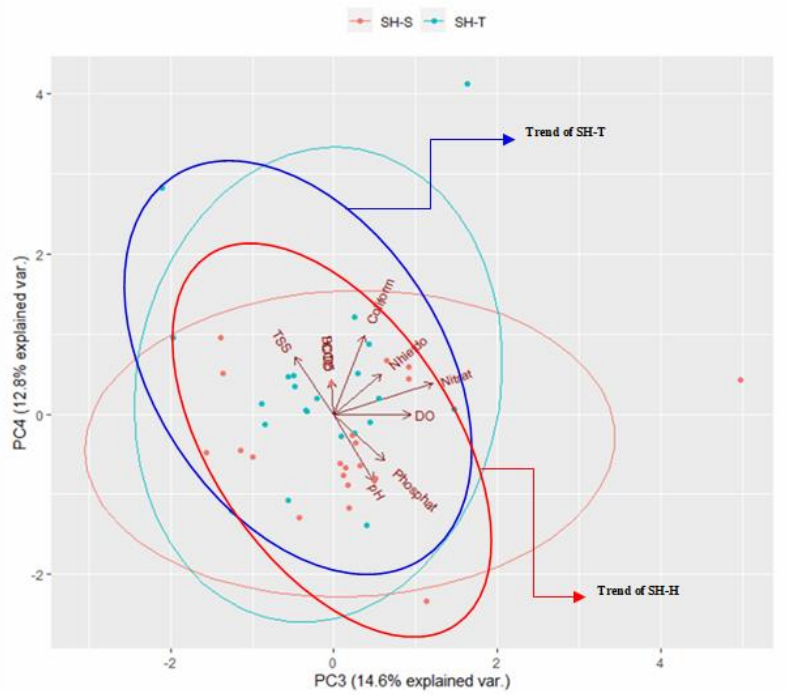

Figure 18. Water quality trends of Hau river at locations SH–T and SH–H corresponding to PC3 and PC4 in the rainy season.

The authors assessed that the water quality of Hau river at the upstream location of SH–T influenced very clearly by the principal component PC4 and at the same time had been greatly influenced by principal component PC3. Besides, the trend of water quality in the lower Hau River (SH–H) was affected by both principal components PC3 and PC4. However, the influence of the two principal components PC3 and PC4 will have little apparent effect because PC3 and PC4 account for very small percentages of the total variance of the principal components (14.56% and 12.82%).

4. Conclusion

Surface water quality in the area was continuously monitored at the upstream and downstream locations of Hau river bordering Can Tho in 2019 was not guaranteed well according to QCVN 08–MT:2015/BTNMT (level A1)–National technical regulation on surface water quality. In which, the DO concentrations in the water were lower than the permitted standards and in the polluted state of parameters TSS, COD, BOD_5, Phosphate (PO_4^{3-} by P), Ammonium (NH_4^+ by N) and especially Coliform bacteria.

The results of two monitoring sessions on zooplankton in the upper Hau river location (SH–T) in 2019 showed that the water quality according to diversity index H' was in a polluted state; Surface water quality ranges from "Heavily polluted" to "Moderately polluted" according to the diversity index H' of the zooplankton parameters. This once again proved that the assessment of water quality according to the diversity index (H') was quite similar to the results of the assessment of water quality according to the physicochemical parameters.

Besides, the results of statistical analysis on the difference of physico–chemical parameters data in the 2 rainy and dry seasons showed the difference of 3 parameters Coliform, TSS, Nitrate in 2 real seasons was caused by environmental conditions (had statistically significant). This results showed that the water quality of Hau river was affected by these parameters and the cause may be due to natural origin such as erosion, geological structure or under the influence of other activities, human activities, production, untreated wastewater, excessive agricultural production, etc. Because they had caused many bad

impacts leading to water pollution due to the decomposition of organic compounds muscle, high concentration of coliform bacteria in water; TSS concentration in water is mainly affected by the amount of alluvium from upstream, plus a large amount of soil, rock, wastes washed into the river by stormwater runoff, contributing to a significant increase in TSS concentration. This result also corresponds to the results of direct analysis of water quality parameters and is compared according to QCVN 08–MT:2015/BTNMT, level A1.

The results of analysis of main components of water quality parameters in space (SH–T and SH–H) and over time (dry season and rainy season) showed that water quality in Hau river tended to be polluted by COD, BOD_5 and Coliform. In the rainy season, the water quality of Hau River was affected by these parameters more than in the dry season. In addition, according to the results of the correlation analysis: In the dry season, the pair of parameters COD and BOD_5 had a strong correlation ($r \geq 0.5$), BOD_5–Coliform had an average correlation ($0.3 \leq r < 0.5$); In the rainy season, COD and BOD_5 parameters had a strong correlation ($r \geq 0.5$), pair of parameters Temperature–Coliform have an average correlation ($0.3 \leq r < 0.5$). This result showed the mutual influence and correlation between pollution parameters that the Hau river water quality at SH–T and SH–H tended to be affected by. The analysis results also showed that in the rainy season, water quality was more affected by these than in the dry season.

Therefore, it is recommended that people living along the river should not use it directly, it is necessary to treat the water thoroughly before putting it into use to ensure long–term health.

Authors contribution: Contructing reseach idea: H.P., N.L.N.T.; Select research methods: H.P., N.L.N.T., H.T.N.H.; Data processing: H.P., N.L.N.T., H.T.N.H.; Sample analysis: N.L.N.T., T.N.N.; Take samples: H.P., N.L.N.T., T.N.N.; Writing original draft preparation: H.P., H.T.N.H.; N.L.N.T; Writing review and editing: H.P., H.T.N.H., N.L.N.T.

Acknowledgments: This article was completed from the results of the research project on water quality of Hau river flowing through An Giang province.

Conflicts of Interest: The authors declare that this article was the work of the authors, has not been published elsewhere, has not been copied from previous research; there was no conflict of interest within the author group.

References

1. Wikipedia. Key economic region in the Mekong Delta region. https://vi.wikipedia.org/wiki/V%C3%B9ng_kinh_t%E1%BA%BF_tr%E1%BB%8Dng_%C4%91i%E1%BB%83m_v%C3%B9ng_%C4%91%E1%BB%93ng_b%E1%BA%B1ng_s%C3%B4ng_C%E1%BB%ADu_Long (In Vietnamese).
2. Luu, P.T. Using water quality index (WQI) and the biological diatom index (BDI) for assessment of the water quality in the Sai Gon River. *Ho Chi Minh City Univ. Educ. J. Sci.* **2020**, *17(9)*, 1558–1596. (In Vietnamese)
3. Lien, N.T.K. Research on biological monitoring methods in assessing water quality on Hau river route using large invertebrates. PhD thesis in aquaculture, 2017.
4. Boyd, C.E. Water quality for pond Aquaculture. Deparment of Fisheries and Allied Aquacultures. Auburn University, Alabama 36849 USA, 1998, pp. 37.
5. Quyen, L.C. Distribution of phytoplankton in Bung Binh Thien, An Giang. *Sci. J. An Giang University* **2015**, *7(3)*, 66–74.
6. Cat, L.V.; Nhung, D.H.; Cat, N.N. Quality aquaculture water and quality improvement solutions. Science and Technology Publishing Company, Hanoi, 2006, pp. 424.
7. Ba, L.H. Soil environment ecology. Ho Chi Minh City National University Publishing Company, 2007, pp. 320.

8. Linh, L.T.N.; Hung, P.Q. Current status of exploitation and protection of inland aquatic resources in An Giang province. *J. Fish. Sci. Technol.* **2015**, *2*, 47–49.
9. Nguyen, P.Q.; Y, L.H.; Cong, N.V.; Phu, T.Q. Evolution of some water quality parameters in intensive cultured catfish (Pangasianodon hypophthalmus) ponds. *Scie. J. Can Tho Univ.* **2014**, *34*, 128–136.
10. Thuong, P.V.; Bach, D.D. Textbook of environmental chemistry, Hanoi Science and Technology Publishing Company, 1999, pp. 231.
11. Department of Natural Resources and Environment of An Giang province, 5–year environmental status report of An Giang province for the period 2005–2009, 2012, pp. 152.
12. Tri, T.N.; Dat, H.D.; Sang, N.V. Research on the biodiversity of fish fauna in Bung Binh Thien wetland, An Giang province. *J. Biol.* 2012, *34*, 21–29.
13. Nguyen, T.T. Fluctuations in water quality in Hau river. Master thesis, Faculty of Fisheries, Can Tho University, 2013, pp. 70.
14. Phu, T.Q.; Yi, Y. Effects of catfish farming in rafts on water quality in Hong Ngu district, Dong Thap province. *Sci. J. Can Tho Univ.* **2005**, *3*, 8–17.
15. Van, L.T.H.; My, T.N.D. Survey of phytoplankton composition and surface water quality at some points around aquaculture areas in some Ben Tre provinces. *J. Sci. Technol. Dev. Fac. 4(1)*, 401–411.
16. Ty, D.V.; Huy, N.H.; Da, C.T.; Ut, V.N.; Viet, T.V. Assessment of water quality changes in Bung Binh Thien, An Giang province. *Can Tho Univ. Sci. J.* **2018**, *54(3)*, 125-131. Doi:10.22144/ ctu.jvn.2018.048.
17. Dung, T.D.; Quan, N.Q.; Hue, N.T.T.; Luan, P. Evaluation of water quality in La Buong river by method multivariate statistics over space and time. *VN J. Hydrometeorol.* **2021**, *731*, 36–53. Doi:10.36335/VNJHM.2021(731).36-53.
18. Climatology and Hydrology Research Centre. Department for Geography, Tourism and Hotel Management. Statistical analysis of water quality parameters of veliki bački canal (vojvodina, serbia) in the period 2000–2009. *Carpathian J. Earth Environ. Sci.* **2012**, *7(2)*, 255–264.
19. Hung, N.T.Q.; Dang, D.H.; Thai, P.V.; Ky, N.M.; Tuan, H.N.A. Research and assessment of water use and quality level of living in Trang Bang district, Tay Ninh province. *VNU Sci. J. Earth Environ. Sci.* **2018**, *34(4)*, 10–21.
20. Au, N.H.; Ngan, P.T.K.; Thuy, H.T.T.; Ngoc, P.N.H. Aplication of multivariate statistical analysis in Evaluation of underground water quality Tan Thanh district, Ba Ria – Vung Tau province. *Sci. Technol. Dev.* **2017**, *20*, M2–2017.

VIETNAM JOURNAL OF HYDROMETEOROLOGY

Research Article

Sources of sedimentary organic carbon in coastal ecosystems from the Tien Yen Bay, Quang Ninh

Luu Viet Dung[1,2*], Pham Thao Nguyen[3], Nguyen Thi Hoa[4], Nguyen Thi Tuyet Chinh[2], Nguyen Tai Tue[1,2], Tran Dang Quy[1,2], Mai Trong Nhuan[1,2]

[1] Key Laboratory of Geoenvironment and Climate Change Response, VNU University of Science, Vietnam National University, Hanoi, Vietnam; dungluuviet@gmail.com; tuenguyentai@hus.edu.vn; quytrandang@gmail.com; nhuanmt@vnu.edu.vn

[2] Faculty of Geology, VNU University of Science, Vietnam National University, Hanoi, Vietnam; dungluuviet@gmail.com; nguyenthituyetchinh97@gmail.com; tuenguyentai@hus.edu.vn; quytrandang@gmail.com; nhuanmt@vnu.edu.vn;

[3] Graduate School of Science and Engineering, Ehime University, Matsuyama Japan; thaonguyen3m@gmail.com

[4] Vietnam – Japan University, Vietnam National University, Hanoi, Vietnam; 19110009@st.vju.ac.vn

*****Correspondence: dungluuviet@gmail.com; Tel.: +84–904729009

Received: 24 October 2021; Accepted: 08 December 2021; Published: 25 December 2021

Abstract: Mangroves in Tien Yen Bay, Quang Ninh province are considered typical mangrove ecosystems in Northern Vietnam. Mangroves play a significant role in carbon storage, and mangrove sediment is the largest carbon pool in this ecosystem. The present study aims to determine the role of the carbon source from mangroves to provide the organic matter in intertidal sediments by the stable isotopes approach. The $\delta^{13}C$ of sediments ranged from –27.36 ± 0.28‰ in mangrove forest (RNM) to –26.28 ± 0.05‰ in the tidal flat with seagrass (SG1). Stable isotope mixing model results showed that mangrove materials are an important source of sedimentary organic carbon (OC), providing 64.6 ± 14.9%, 38.4 ± 14.9%, 39.8 ± 15%, and 48.8 ± 14.9% for the site RNM, SG1, SG2, and SG3, respectively. The second OC source in mangrove sediment is suspended particulate organic matter (POM). The POM in this area includes fine mangrove materials, which are exchanged with coastal waters through the tidal dynamics. The present results suggested that mangroves are important in accumulating organic carbon and fine–grained sediments in the Tien Yen Bay, contributing important values to climate change mitigation and maintaining biodiversity in this area.

Keywords: Carbon sources; Mangroves; Stable isotopes; Sediment; Tien Yen.

1. Introduction

Mangrove forests play an important role in preventing climate change, natural disasters, catastrophes such as storms, floods, coastal erosion, saline intrusion, etc. [1–2]. They also provide critical ecological functions and services such as nursing habitat, feeding zone, breeding grounds for aquatic species, waterbirds, migratory birds, and providing high economic benefits for humans [3–5]. Recently, mangrove forests have been degraded globally due to human activities such as aquaculture, urbanization, industry, and agriculture [6–7]. The Kyoto Protocol (1997) and the Paris Agreement on Climate Change (2016) were signed by 191 members of the United Nations Framework Convention on Climate Change to reduce greenhouse gas emissions. These agreements are the legal basis for implementing greenhouse gas reductions through various solutions and mechanisms such as the Clean

Development Mechanism (CDM) and the Greenhouse Gas Emission Reduction Initiative. The Reducing Emissions from Deforestation and Forest Degradation program (REDD+) plays essential roles in reducing deforestation and forest degradation, enhancing conservation, sustainable management of forests, and maintaining forest carbon stocks [8–9]. Mangroves are considered a rich carbon pool in coastal areas, with higher carbon storage than other forests on Earth [10–11]. Currently, the total global area of mangroves is 139170 km^2, from which mangroves accumulate about 6.5 billion tons of carbon, equivalent to 24 billion tons of potential CO_2 gas [12].

The largest C stock of mangrove forests is sedimentary organic carbon, which have trapped CO_2 for thousands of years [10, 13–15]. Thus, carbon accumulation in mangrove sediments plays a vital role in the global carbon cycle and reduces Greenhouse gas. In Vietnam, mangrove forests are also large carbon sinks in coastal areas and can store more than 900 tons of C/ha [14, 16, 17]. In mangrove research, the stable isotope carbon ($\delta^{13}C$) is applied to trace organic carbon sources for animals and deposited sediments [18]. Study results from the Red River Delta and Thanh Hoa province highlighted that mangrove materials are important carbon sources in mangrove sediments [19–20]. Therefore, understanding the roles of mangroves on carbon accumulation in the sediment will provide valuable information for conserving and coastal ecosystems and climate change mitigation. In the present study, we hypothesize that the mangrove materials are the primary sources of organic carbon accumulation in mangrove sediments and adjacent habitats in Tien Yen Bay, Northern Vietnam. We investigated the transect analysis of sediment grain size, total organic carbon (TOC), total Nitrogen (TN) and $\delta^{13}C$ values of sediment samples through a natural mangrove forest to seagrass beds to examine the roles of mangrove forest in organic carbon accumulation and to determine the sources of organic carbon in sediments.

2. Materials and Methods

2.1. Study site

The study was conducted in the Hai Lang and Dong Rui communes, Tien Yen District, Quang Ninh province. Sampling sites are located between the Voi Lon and the Ba Che Rivers, with natural mangrove forests and seagrass bed growth in the tidal flat along the coastline. Tien Yen Bay is a large semi-closed Bay in the Northeast of Quang Ninh Province [21], which has a high biodiversity with specific ecosystems such as mangroves, seagrass beds and estuaries. Recently, the wetlands in Hai Lang have been converted into cultivated land and aquaculture, causing the degradation of coastal ecosystems. Human activities such as exploiting marine resources, farming, sea transportation, seafood harvesting strongly affected the environment and ecosystem in this area. The mangrove forest in Hai Lang commune covered 770.81 ha, which is considered a typical mangrove ecosystem in Northern Vietnam. The mangroves have good forest quality, dominated by *Kandelia obovata, Avicennia marina, Aegiceras corniculatum,* and *Bruguiera gymnorrhiza* and *Rhizophora stylosa* [21]. Mangrove forests in this area are rich in biodiversity with high–value seafood products such as peanut worms, octopus, flower crabs, and penaeid shrimps. However, the mangrove forest ecosystem in the study area has been degraded due to the less sustainable exploitation activities. The remaining forest area is still under threat of destruction and degradation due to infrastructure and economic development impacts.

2.2. Field Sampling

Sediment samples were collected following three transects from mangrove forest to seagrass beds in Hai Lang–Dong Rui tidal flat, Tien Yen Bay, Quang Ninh (Figure 1). Four sediment samples were collected at each transect by a stainless-steel spatula in the low tide and kept in polyethylene bags. Samples were stored in a cool box with ice immediately then transported to the laboratory for further analysis. We also recorded additional information of dominant vegetation and sediment characteristics in each sampling site. The seagrass species *Halophila ovalis* and *Halophila beccarii* are distributed in tidal mudflat (SG1, SG2, SG3) adjacent to mangrove forest (RNM). Total 12 sediment samples were collected for analysis, with 09 samples in seagrass beds and 03 samples in mangrove forests. SG 01 is the sampling

zone with a distance of 300 m from the mangrove forest, SG 02 is located between the estuary and mangrove forests, SG 03 is adjacent to the mangrove forest, and the RNM zone is inside mangrove forests. The distance between each transect was approximately 200 m in length.

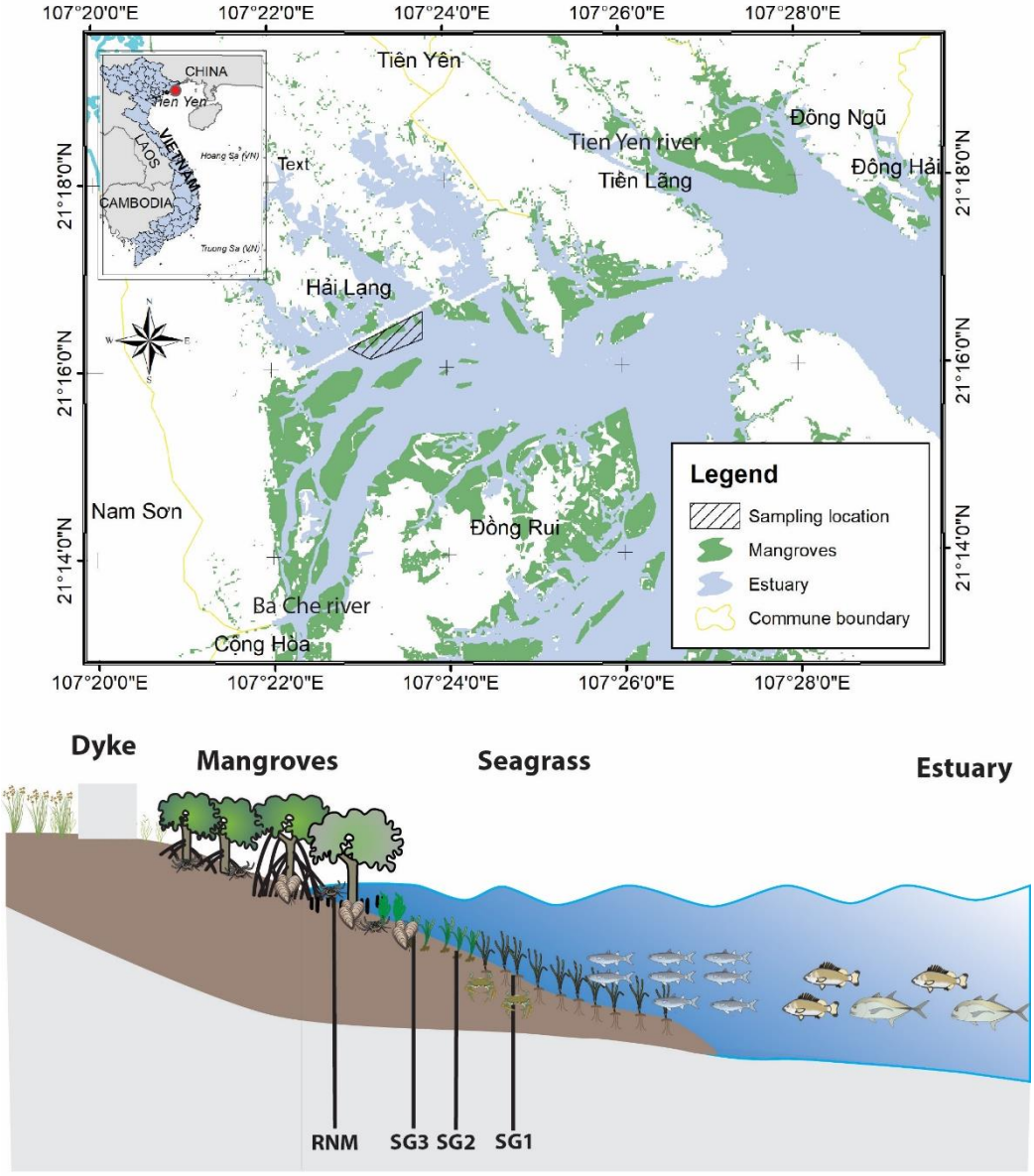

Figure 1. Map of the study area and sampling location.

2.3. Sediment grain size and organic matter content analysis

For sediment grain size analysis, approximately 1g of wet sediment sample was weighed and transferred to ceramic cups, then removed all visible root debris, shells, organic litter with a stainless steel clamp. Then 10% H_2O_2 solution was added to remove organic matter in sediment, and H_2O_2 solution was added to samples until no air bubbles existed. The remaining sample was put in the electric oven to remove the residual H_2O_2 and distilled water was added during the H_2O_2 removal process to ensure the sample was not dried. The laser particle analysis Horiba LA950 was used to determine sediment grain size, ranging from 0.01 to 3000 μm. Each sediment sample was analyzed repeatedly three times with a relative error <10%.

The organic matter (OM) content in sediment was measured by loss on ignition methods. Approximately ten cubic centimeters of fresh sediment samples were also collected to determine bulk sediment density. Fresh sediment samples were dried at 60°C in an electric oven until constant weight for bulk density measurement. Then, the dried samples were

ground until fine powder by an agate mortar and pestle. All visible branches, roots, crumbs, and other organic materials are removed during the grinding process. Approximately 2 g of finely ground sediment sample will be burned at 550°C for 3 hours to estimate OM content [14, 19].

2.4 Total organic carbon (TOC), total nitrogen (TN), and stable isotope analysis

Approximately 0.2 g of finely ground sediment sample was placed in an Eppendorf tube for stable isotope analysis. Then, 2 ml of 1N HCl were added to remove the carbonate content in 24h. After acid treatment, the milli–Q deionized water was used to wash and remove any acid residuals in the sample. This process was repeated four times in each sample before the subsample was dried at 60°C for 48 hours. Powdered samples were weighed about 10–30 mg for stable isotopes analysis depending on organic matter content. Then the samples were wrapped in 6×8 mm tin capsules before analysis by stable isotope ratio mass spectrometry (IRMS) by the method of connecting elemental analysis system (Elemental Analyzer – Euro Vector) and the stable isotope ratio mass spectrometry system (Nu – Perspective IRMS) at Key laboratory of Geoenvironment and Climate Change Response, VNU University of Science.

Analytical samples were placed in the automatic sample tray and dropped into the elemental analyzer combustion chamber. In the combustion chamber, the sediment sample was converted to CO_2 and NO_2. Then, these gases were passed through the reducing chamber and reduced to CO_2 and N_2 gas. These gases were passed through the gas chromatographic column and separated for a stable isotope mass spectrometry system. Here, the gases are ionized and pass through the isotope ratio mass spectrometry (IRMS) where carbon and nitrogen isotopes are counted by Faraday cups. The IRMS determines the stable isotopes values of the sample by comparison with standard gases. The values $\delta^{13}C$ and $\delta^{15}N$ of the sample were calculated using the formula:

$$\delta X(‰) = \left(\frac{R_{sample}}{R_{standard}} - 1\right) \times 100 \quad (1)$$

where δX is $\delta^{13}C$ or $\delta^{15}N$, R is the ratio of a heavy isotope to a light isotope ($^{13}C/^{12}C$ or $^{15}N/^{14}N$), R_{sample} is the ratio of the sample analyzed, and $R_{standard}$ is the stable isotope standards of limestone Pee Dee Belemnite (PDB).

2.5. Stable isotope mixing model and statistical analysis

The source of organic matter can come from both local and phylogenetic sources. Locally–sourced organic matter is provided by mangrove or benthic plants that settle into the sediment. Organic matter has phytoplankton origin transport of organic matter from other places too, from the mainland by the flow of phytoplankton through tidal dynamics. However, the true phytoplankton value is hard to determine in semi-closed bays and estuaries like sampling areas. Thus, we applied an average value of the suspended organic matter (POM) as a potential carbon source of sediment in the present study.

The value of $\delta^{13}C$ in organic matter can be used to distinguish organic matter in sediments and different organic matter derived from different plants. The difference in the value of $\delta^{13}C$ between terrestrial and phytoplankton is because terrestrial plants take CO_2 directly from the air during photosynthesis, and phytoplankton takes dissolved CO_2 or HCO_3^- in water. Through photosynthesis, taking CO_2 directly from the air, terrestrial C3 plants, including higher plants, create organic matter with $\delta^{13}C$ value ranging from –29.4% to –27‰ [21–22]. According to the United States Environmental Protection Agency, the organic carbon source contribution was estimated by an iso_error calculation file provided in excel format [23]. In the study area, the primary sources of organic matter include mangrove materials and suspended organic matter in the sedimentary environment. The seagrass materials (SG) were not considered potential carbon sources in sediment due to low biomass and rare abundance. For statistical analysis, the analysis of variance (ANOVA) was performed in Sigma Plot 12.0 software to determine the spatial differences in sediment characteristics.

3. Results and Discussion

3.1. Sediment characteristics

The sediment samples are sticky mud with dark gray color. The sediment composition varied spatially from mangrove to seagrass bed (Figure 2). The sand content in SG2 was highest while in RNM was highest. In contrast, the silt content was highest (Figure 2). In sampling transects, it was caused by the tidal dynamics in transporting sediments. The decreasing tidal energy from Ba Che River watershed to mangrove forests causes large sediment particles to be deposited at the edge of the forest, and the smaller particles size of sediments are transported and accumulated inside the forest during high tide [24–25]. Furthermore, mangrove roots and trunks play important roles in reducing wave and tidal current velocity, providing a stable environment for sediment deposition.

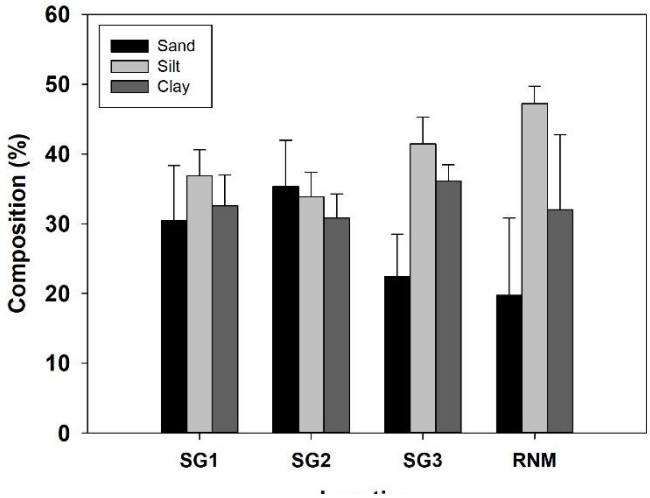

Figure 2. The grain size composition in sediment in the study area.

The bulk density of sediments at the mangrove forest was 1,431 ± 0.15 (g/cm^3), which was smaller than that of seagrass areas with average values of 1,501 ± 0.06; 1,495 ± 0.06 and 1,546 ± 0.03 g/cm^3 for SG1, SG2, and SG3 zone, respectively. This difference may be related to the increase in fine-grained sediment and organic matter content in the mangrove forests. However, the density value of sediments in this area is relatively high compared to other mangrove forests in Vietnam and Asia–Pacific regions [14, 15, 19].

3.2. TOC, TN and organic matter contents in sediments

The average TN (± SD) concentration in sediment ranged from 0.077 ± 0.002% to 0.148 ± 0.008% and tended to increase gradually from the estuary to the mangrove forest (Figure 3a). The ANOVA results showed a clear difference between the TN content in mangroves and the seagrass sediments (ANOVA, $p < 0.05$). This difference may be related to the high abundance of decomposing organic matter in mangrove forests compared to the seagrass area, which provides an important nitrogen source in sediments [26–27]. Additionally, the seagrass beds are often flooded by tides, and nitrogen in the sediment can be exchanged with the water column, leading to a decreasing trend in the TN content in the sediment. However, the TN content in sediments from Tien Yen Bay is not too high compared to the mangrove and coastal tidal flat areas in Vietnam [22, 28].

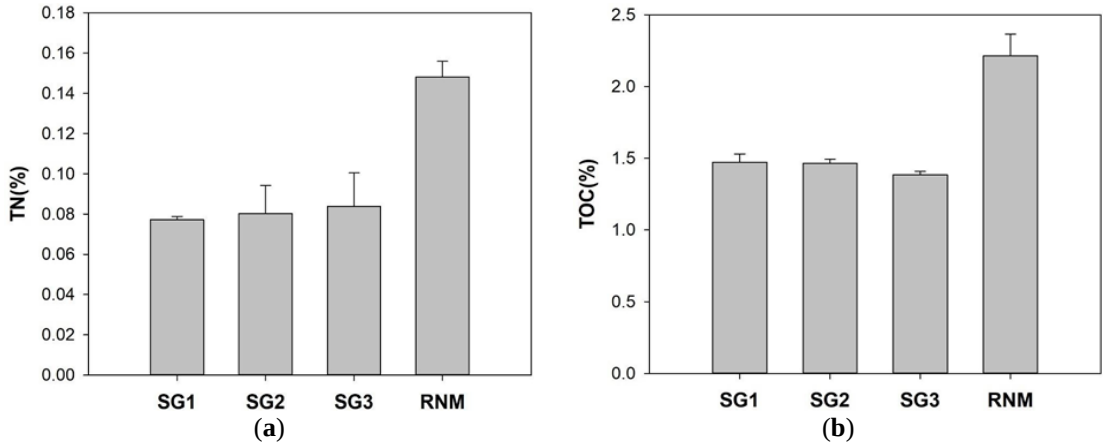

Figure 3. The TN (a) and TOC (b) content in sediments.

The OM content varied spatially with sampling location. The OM in mangrove sediment is higher than in seagrass areas, ranging from 4.3 ± 0.05% to 8.51 ± 1.53% for SG2 and RNM zone, respectively. Similarly, the TOC content in the sediment showed an increasing trend from the seagrass beds into the mangrove forests (Figure 3b). ANOVA analysis showed a statistical difference in TOC content among mangrove and seagrass sediments (ANOVA, $p < 0.05$). However, the spatial difference of TOC between the sampling locations in the seagrass bed was not observed in this area. The average TOC content in the mangrove sediment was 2.21 ± 0.15% which was lower than other sites in the Asia–Pacific region [13, 14, 20]. The increasing TOC in mangrove sediment is related directly to abundant organic matter sources from mangrove litters such as fallen branches and leaves [15, 18, 29].

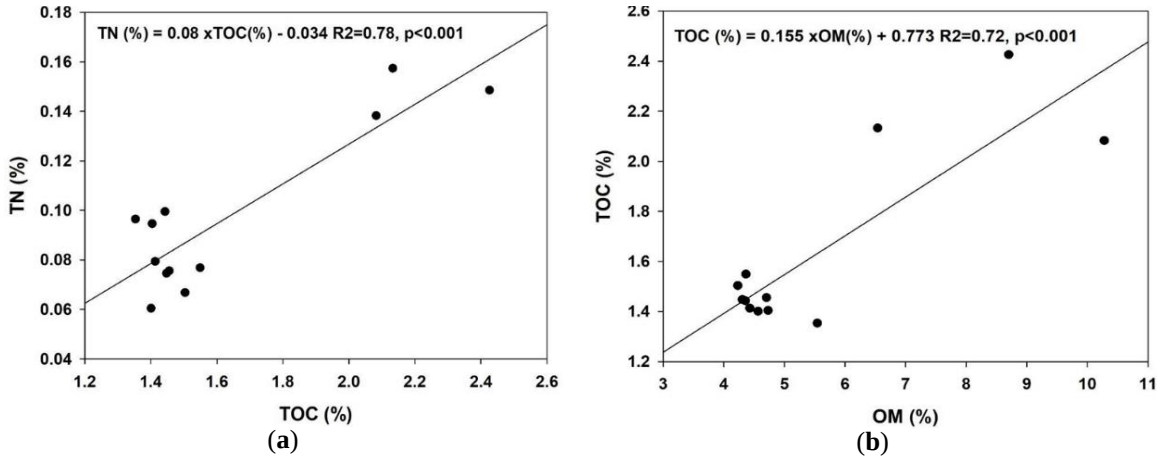

Figure 4. The relationships between TN and TOC (a) and TOC and OM (b) in sediments.

In addition, the TOC content can be affected by the sediment deposition rate and the maturity level of mangroves. When the sediment deposition rate is high, organic matter can escape the decomposition of microorganisms faster, so it is better preserved. Therefore, the sediment deposition rate is important in conserving and retaining OM in coastal areas. The maturity level of mangroves also has a positive relationship with TOC in sediments. The TOC and TN in sediment have a close relationship (Figure 4a), which indicates that the nitrogen content in mangrove sediments comes mainly from organic matter. The correlation between TOC and OM (Figure 4b) is similar to previous research in Tien Yen Bay, Red River Delta, Thanh Hoa, and Can Gio mangrove forests [14, 19, 20, 28].

3.3. Sources of sedimentary organic carbon in sediments

In the present study, the organic matter sources of sediments include mangrove (Man), seagrass (SG), and suspended organic matter (POM). The values of $\delta^{13}C$ (‰) was showed in

Table 1. The organic matter sources in the area have a clear difference in values of $\delta^{13}C$ (‰) and can be used to determine organic carbon sources in sediments. However, the $\delta^{13}C$ (‰) value of SG is significantly higher than those of sediments, mangroves, and POM, indicating that seagrass is not a significant source of OC in sediment. Thus, a stable isotope mixing model was applied for estimating OC sources in sediments.

Table 1. The $\delta^{13}C$ (‰) value of potential organic carbon sources in sediments.

Source of OM	$\delta^{13}C$ (‰)	n	Reference
POM	–25.0 ± 0,9	4	[30]
SG	–14.8 ± 1,7	8	[30]
Mangrove (Man)	–28.8 ± 1,2	39	[3]

The value of $\delta^{13}C$ (‰) at all sampling sites is showed in Figure 5. The lowest $\delta^{13}C$ was found in the mangrove forest, with an average of –27.36 ± 0.28‰. The $\delta^{13}C$ values of sediment increased gradually from SG3, SG2 to SG1, with average values of –26.71 ± 0.24, –26.34 ± 0.20 and –26.28 ± 0.05‰, respectively. Research results observed a statistically significant difference among sampling locations of the $\delta^{13}C$ value in sediment (ANOVA, $p < 0.05$). The $\delta^{13}C$ values decreased gradually from the estuary to mangrove forests, which reflected the possibility of changing the origin of OC in sediments [20, 21, 28]. The value of $\delta^{13}C$ (‰) in mangrove sediments ranged from –26.01 to –27.06, within the range of POM and Man. The stable mixing model showed that the mangrove materials contributed 64.6 ± 14.9%, 38.4 ± 14.9%, 39.8 ± 15 %, and 48.8 ± 14.9% for the RNM, SG1, SG2, and SG3 areas, respectively (Figure 5).

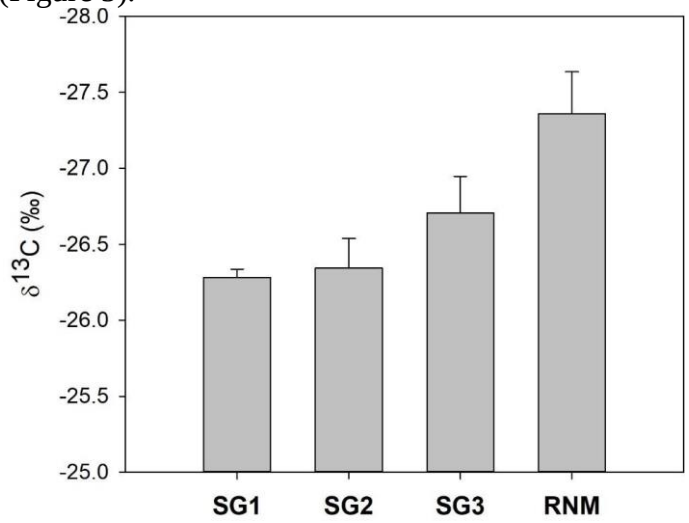

Figure 5. The value of $\delta^{13}C$ (‰) in coastal sediment.

3.4. Roles of mangrove forest in organic carbon accumulation

Research results showed that mangrove materials significantly contribute to OC sources of mangrove sediment and adjacent habitats (Figure 6). The mangrove forest biomass is significantly higher than seagrass, which provides a vital source of OC for coastal waters. The POM in coastal water and estuaries in sampling areas was higher than the previous research in Thanh Hoa, Red River Delta [4,22]. This pattern may be related to the geomorphological settings of Tien Yen Bay, causing the mangrove materials to not be accessible and exported to open water, leds to low values of $\delta^{13}C$ in POM samples [21]. The second reason may be that seagrass grows only seasonally, so it will not be a significant source of sediments [31]. Overall, mangrove materials play important roles in carbon accumulation in sediment. The mangrove materials contribute significantly to sedimentary OC accumulation in the forest and adjacent habitats. Thus, the conservation and development of mangrove forests will play important roles in carbon sequestration and climate change mitigation.

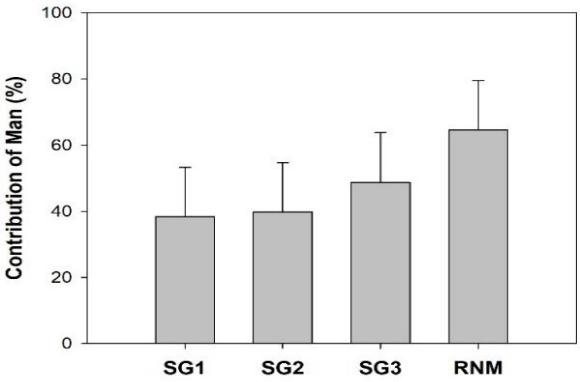

Figure 6. Contribution of mangrove materials for organic carbon buried in sediments.

4. Conclusions

The present results showed that mangroves might accumulate large amounts of organic carbon and fine–grained sediments in coastal areas. The fine–grained sediment content tends to increase from estuaries towards mangrove forests, indicating the roles of mangroves in enhancing sediment deposition and lower tidal dynamics. The values of OM, TOC, TN, and $\delta^{13}C$ in sediments varied spatially with sampling sites along mangroves and seagrass beds transect. The stable isotope mixing model results indicated that mangrove materials contribute significantly to organic carbon sources of sediment in both mangrove and seagrass beds areas. Therefore, conserving mangrove forests and adjacent ecosystems will enhance carbon storage and reduce greenhouse gas emissions from coastal areas.

Supplementary Materials: None

Author Contributions: Conceptualization, L.V.D., N.T.T., M.T.N.; Methodology, P.T.N., L.V.D., T.D.Q.; formal analysis, N.T.T.C., P.T.N.; writing–original draft preparation, L.V.D., N.T.H.; writing–review and editing, L.V.D., N.T.T., T.D.Q., P.T.N., N.T.H.; All authors have read and agreed to the published version of the manuscript.

Funding: This research was funded by the Ministry of Natural Resources and Environment under project TNMT.2018.06.16.

Acknowledgments: The authors are grateful to the staff of VNU University of Science, Vietnam, for their help with sampling and sample analysis.

Conflicts of Interest: The authors declare no conflict of interest.

References

1. Alongi, D.M. Mangrove forests: Resilience, protection from tsunamis, and responses to global climate change. *Estuarine Coastal Shelf Sci.* **2008**, *76*, 1–13, http://dx.doi.org/10.1016/j.ecss.2007.08.024.
2. Badola, R.; Hussain, S. Valuing ecosystem functions: an empirical study on the storm protection function of Bhitarkanika mangrove ecosystem, India. *Environ. Conserv.* **2005**, *32*, 85–92.
3. Tue, N.T.; Quy, T.D.; Nhuan, M.T.; Dung, L.V.; Thai, N.D. Tracing carbon transfer and assimilation by invertebrates and fish across a tropical mangrove ecosystem using stable isotopes. *Mar. Ecol.* **2017**, *38*, e12460. http://dx.doi.org/10.1111/maec.12460.
4. Van Hieu, P.; Hoang Ha, N.T.; Viet Dung, L.; Omori, K. Carbon Sources Supporting Macro–Invertebrate Communities in Restored Mangrove Forests from Hau Loc, Thanh Hoa, Vietnam. *J. Mar. Sci. Eng.* **2020**, *8*, 651.
5. Nagelkerken, I.; Blaber, S.J.M.; Bouillon, S.; Green, P.; Haywood, M.; Kirton, L.G.; Meynecke, J.O.; Pawlik, J.; Penrose, H.M.; Sasekumar, A., et al. The habitat function

of mangroves for terrestrial and marine fauna: A review. *Aquat. Bot.* **2008**, *89*, 155–185. http://dx.doi.org/10.1016/j.aquabot.2007.12.007.

6. Andreetta, A.; Huertas, A.D.; Lotti, M.; Cerise, S. Land use changes affecting soil organic carbon storage along a mangrove swamp rice chronosequence in the Cacheu and Oio regions (northern Guinea–Bissau). *Agric. Ecosyst. Environ.* **2016**, *216*, 314–321. http://dx.doi.org/10.1016/j.agee.2015.10.017.
7. Blasco, F.; Aizpuru, M.; Gers, C. Depletion of the mangroves of Continental Asia. *Wetlands Ecol. Manage.* **2001**, *9*, 255–266. http://dx.doi.org/10.1023/a:1011169025815.
8. Alexander, S.; Nelson, C.R.; Aronson, J.; Lamb, D.; Cliquet, A.; Erwin, K.L.; Finlayson, C.M.; de Groot, R.S.; Harris, J.A.; Higgs, E.S., et al. Opportunities and Challenges for Ecological Restoration within REDD+. *Restor. Ecol.* **2011**, *19*, 683–689. http://dx.doi.org/10.1111/j.1526-100X.2011.00822.x.
9. Olander, L.P.; Galik, C.S.; Kissinger, G.A. Operationalizing REDD+: scope of reduced emissions from deforestation and forest degradation. *Curr. Opin. Environ. Sustainability* **2012**, *4*, 661–669. http://dx.doi.org/10.1016/j.cosust.2012.07.003.
10. Donato, D.C.; Kauffman, J.B.; Murdiyarso, D.; Kurnianto, S.; Stidham, M.; Kanninen, M. Mangroves among the most carbon–rich forests in the tropics. *Nat. Geosci.* **2011**, *4*, 293–297.
11. Dixon, R.K.; Solomon, A.; Brown, S.; Houghton, R.; Trexier, M.; Wisniewski, J. Carbon pools and flux of global forest ecosystems. *Science* **1994**, *263*, 185–190.
12. Siikamaki, J.; Sanchirico, J.N.; Jardine, S.L. Global economic potential for reducing carbon dioxide emissions from mangrove loss. Proceedings of the National Academy of Sciences of the United States of America, **2012**, *109*, 14369–14374, http://dx.doi.org/10.1073/pnas.1200519109.
13. Bhomia, R.K.; Kauffman, J.B.; McFadden, T.N. Ecosystem carbon stocks of mangrove forests along the Pacific and Caribbean coasts of Honduras. *Wetlands Ecol. Manage.* **2016**, *24*, 187–201. http://dx.doi.org/10.1007/s11273-016-9483-1.
14. Dung, L.V.; Tue, N.T.; Nhuan, M.T.; Omori, K. Carbon storage in a restored mangrove forest in Can Gio Mangrove Forest Park, Mekong Delta, Vietnam. *For. Ecol. Manage.* **2016**, *380*, 31–40. http://dx.doi.org/10.1016/j.foreco.2016.08.032.
15. Kauffman, J.B.; Heider, C.; Cole, T.G.; Dwire, K.A.; Donato, D.C. Ecosystem Carbon Stocks of Micronesian Mangrove Forests. *Wetlands* **2011**, *31*, 343–352. http://dx.doi.org/10.1007/s13157-011-0148-9.
16. McNally, R.; McEwin, A.; Holland, T. The potential for mangrove carbon projects in Vietnam. SNV–Netherlands Development Organisation REDD+ Programme: Ha Noi, Vietnam, 2011.
17. Tue, N.T.; Dung, L.V.; Nhuan, M.T.; Omori, K. Carbon storage of a tropical mangrove forest in Mui Ca Mau National Park, Vietnam. *Catena* **2014**, *121*, 119–126. http://dx.doi.org/10.1016/j.catena.2014.05.008.
18. Bouillon, S.; Connolly, R.M.; Lee, S.Y. Organic matter exchange and cycling in mangrove ecosystems: Recent insights from stable isotope studies. *J. Sea Res.* **2008**, *59*, 44–58. http://dx.doi.org/10.1016/j.seares.2007.05.001.

19. Pham, V.H.; Luu, V.D.; Nguyen, T.T.; Koji, O. Will restored mangrove forests enhance sediment organic carbon and ecosystem carbon storage? *Reg. Stud. Mar. Sci.* **2017**, *14*, 43–52. http://dx.doi.org/10.1016/j.rsma.2017.05.003.
20. Tue, N.T.; Ngoc, N.T.; Quy, T.D.; Hamaoka, H.; Nhuan, M.T.; Omori, K. A cross–system analysis of sedimentary organic carbon in the mangrove ecosystems of Xuan Thuy National Park, Vietnam. *J. Sea Res.* **2012**, *67*, 69–76. http://dx.doi.org/10.1016/j.seares.2011.10.006.
21. Quy, T.D.; Tue, N.T. Spatial distribution of total organic carbon (TOC), total nitrogen (TN), TOC/TN ratio, and stable carbon isotopes value ($\delta^{13}C$) in surface sediments of Tien Yen Bay, northeast Vietnam. *VN J. Earth Sci.* **2011**, *33*, 616–624.
22. Tue, N.T.; Hamaoka, H.; Sogabe, A.; Quy, T.; Nhuan, M.; Omori, K. The application of $\delta^{13}C$ and C/N ratios as indicators of organic carbon sources and paleoenvironmental change of the mangrove ecosystem from Ba Lat Estuary, Red River, Vietnam. *Environ. Earth Sci.* **2011**, *64*, 1475–1486. http://dx.doi.org/10.1007/s12665-011-0970-7.
23. Phillips, D.L.; Gregg, J.W. Uncertainty in source partitioning using stable isotopes. *Oecologia* **2001**, *127*, 171–179.
24. Adame, M.F.; Neil, D.; Wright, S.F.; Lovelock, C.E. Sedimentation within and among mangrove forests along a gradient of geomorphological settings. *Estuarine Coastal Shelf Sci.* **2010**, *86*, 21–30. http://dx.doi.org/10.1016/j.ecss.2009.10.013.
25. Marchand, C.; Lallier–Vergès, E.; Baltzer, F. The composition of sedimentary organic matter in relation to the dynamic features of a mangrove–fringed coast in French Guiana. *Estuarine Coastal Shelf Sci.* **2003**, *56*, 119–130. http://dx.doi.org/10.1016/S0272-7714(02)00134-8.
26. Holmer, M.; Olsen, A.B. Role of decomposition of mangrove and seagrass detritus in sediment carbon and nitrogen cycling in a tropical mangrove forest. *Mar. Ecol. Prog. Ser.* **2002**, *230*, 87–101.
27. Melillo, J.; Aber, J.; Linkins, A.; Ricca, A.; Fry, B.; Nadelhoffer, K. Carbon and nitrogen dynamics along the decay continuum: Plant litter to soil organic matter. *Plant Soil* **1989**, *115*, 189–198. http://dx.doi.org/10.1007/bf02202587.
28. Tue, N.T.; Nguyen, P.T.; Quan, D.M.; Dung, L.V.; Quy, T.D.; Nhuan, M.T.; Thai, N.D. Sedimentary composition and organic carbon sources in mangrove forests along the coast of northeast Vietnam. *Reg. Stud. Mar. Sci.* **2018**, *17*, 87–94. http://dx.doi.org/10.1016/j.rsma.2017.12.001.
29. Bouillon, S.; Dahdouh–Guebas, F.; Rao, A.; Koedam, N.; Dehairs, F. Sources of organic carbon in mangrove sediments: variability and possible ecological implications. *Hydrobiologia* **2003**, *495*, 33–39.
30. Nguyen, P.T. The connectivity between invertebrates and fishes and coastal ecosystems in Ha Dong lagoon, northeastern Vietnam. Ehime University, Japan, 2019.
31. Huong, T.T.L.; Vermaat, J.E.; Terrados, J.; Van Tien, N.; Duarte, C.M.; Borum, J.; Tri, N.H. Seasonality and depth zonation of intertidal Halophila ovalis and Zostera japonica in Ha Long Bay (northern Vietnam). *Aquat. Bot.* **2003**, *75*, 147–157.

VIETNAM JOURNAL OF HYDROMETEOROLOGY

Research Article

Linking hydrological, hydrodynamic models for saline intrusion assessment – Applying for Ve river estuary as a case study

Bui Ta Long[1,2*], Le Thi My Diep[3]

[1] Ho Chi Minh City University of Technology; longbt62@hcmut.edu.vn
[2] Vietnam National University Ho Chi Minh City; longbt62@hcmut.edu.vn
[3] The Southern Institute of Water Resources Research; diepmoitruongqn@yahoo.com.vn

*Corresponding author: longbt62@hcmut.edu.vn; Tel.: +84–918017376
Received: 15 November 2021; Accepted: 11 December 2021; Published: 25 December 2021

Abstract: Researches on combinion of hydrological and hydrodynamic models are very important when performing risk assessment and disaster management, including saline intrusion, which is especially important for watersheds, with limited measurement data. The objective of this study is linking two types of hydrological and hydrodynamic models to simulate the scope of salinity intrusion in the Ve estuary, Quang Ngai province. Firstly, SWAT/NAM is applied to calculate flow rate, and then MIKE 21/3 model is applied for hydraulic and salt intrusion simulation. The calibration and validation are also done to show that the acceptable reliability of simulation. Simulation result showed that salinity intrusion depends on water discharge, water level, tidal regime according to dry and wet seasons; the longest distance of saline intrusion from the rivermouth is 5.47 km, occurring in the dry season.

Keywords: Rainfall–Runnoff; SWAT/NAM; MIKE 21/3; Salinity Intrusion; Ve River.

1. Introduction

The development and use of hydrological models has attracted increasing attention in the past two decades [1], and the combination of hydrological and hydrodynamic models has demonstrated is an important tool for the integrated assessment of hydrological processes in basins where measurements are very expensive [2]. Such a combination helps to solve many problems in the area including saline intrusion in the estuary. The hydrological model helps to calculate the discharge of rivers – one of the important factors to simulate the flow [3–4], thereby assessing the scope of salinity intrusion as well as the problems of flooding, bank erosion – which are very typical for many regions bordering the sea [5–6].

With a coastline stretching over 3260 km, along with many socio–economic activities, the coastal zone of Vietnam is a special important one; and saltwater intrusion has always been the subject of national studies [7–22]. In particular, saltwater intrusion in the Mekong Delta is selected in many national researches, projects and programs [23–26] . However, research on saltwater intrusion in the central coastal region is still quite modest in terms of quantity and results [8, 16, 18]. Although there have been studies done, however, when applied to the local scale it is necessary to concretize the dependence as the scope of salinity intrusion on the such factors as upstream discharge, the downstream water level, and the tidal regime. Accurate salinity intrusion forecasting plays a huge role in proactive agro–fishery and land use planning in coastal economic zones, especially in the current climate change situation [7]. Saltwater intrusion prediction would be difficult to do without calculating the water flow entering the river, leading to the need for the application of suitable hydrological

models. This shows that the linkage of hydrological – hydrodynamic models play an important role in calculating and predicting saline intrusion [25].

The study selects a typical river in Quang Ngai province as a research case study, following published articles [27–29]. The hydrological coupled models SWAT/NAM combined with the MIKE21 HD to determine the set of hydrological and hydraulic parameters for the Ve river basin was performed [27]. [28] has initially applied a set of hydrological parameters to calculate discharge for the hydraulic model and used it to simulate saline intrusion from the sea to the river. [29] helps to answer the question of how the salinity intrusion mechanism depending on water discharge, water level, seasons have not been shown. In the mentioned articles, the scope of salinity intrusion depending on water discharge, water level, seasonal regimes have not been shown. In this study, the combination of SWAT/NAM coupled hydrological models and MIKE 21/3 HD, AD hydrodynamic models was clarified with the result of determining the scope of salinity intrusion for Ve river. In addition, a number of arguments have been made to argue the dependence of salinity intrusion on the factors of discharge, tidal regime, and flow by 2–D models. The results of this study complement previous studies [28–30].

2. Methods and materials

2.1. The study area

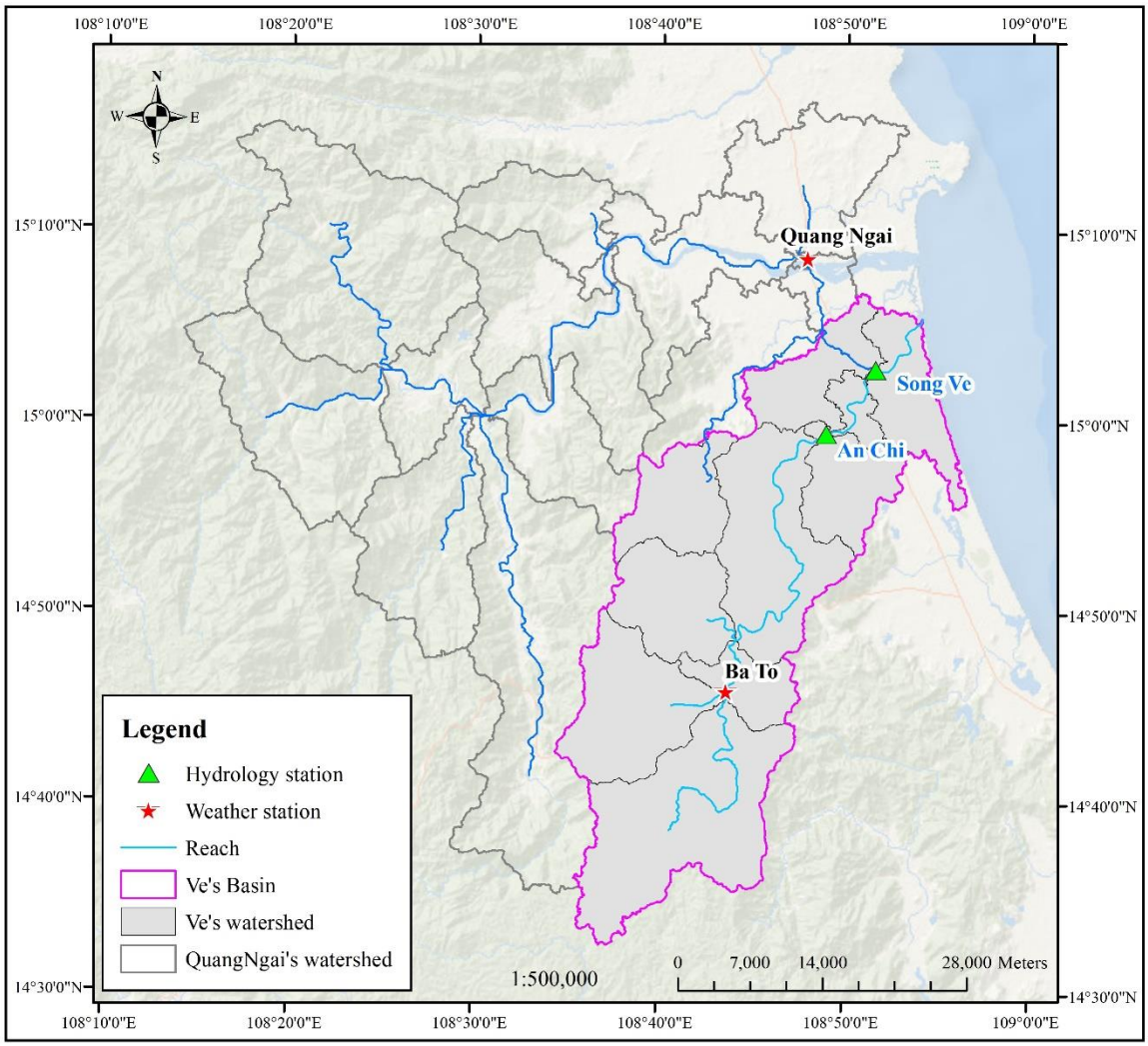

Figure 1. Focus area of the study Ve River basin.

Ve River is one of the largest river systems in Quang Ngai province, covering an area of 1,263 km^2, accounting for 24.51% of the natural area of this province [27]. The study [30], although it mentioned saline intrusion in the Tra Khuc–Ve river basin system, used a 1D hydrodynamic model combined to assess the intrusion salinity in the downstream of Tra Khuc–Ve river system. However, the scope of this study focuses on the Tra Khuc River, not mentioning the Ve River. But, research specifically for the Ve River part, in the last 2 years, has been the subject of some studies [27–29], in which the combination of hydrological and hydrodynamic models has been systematically done.

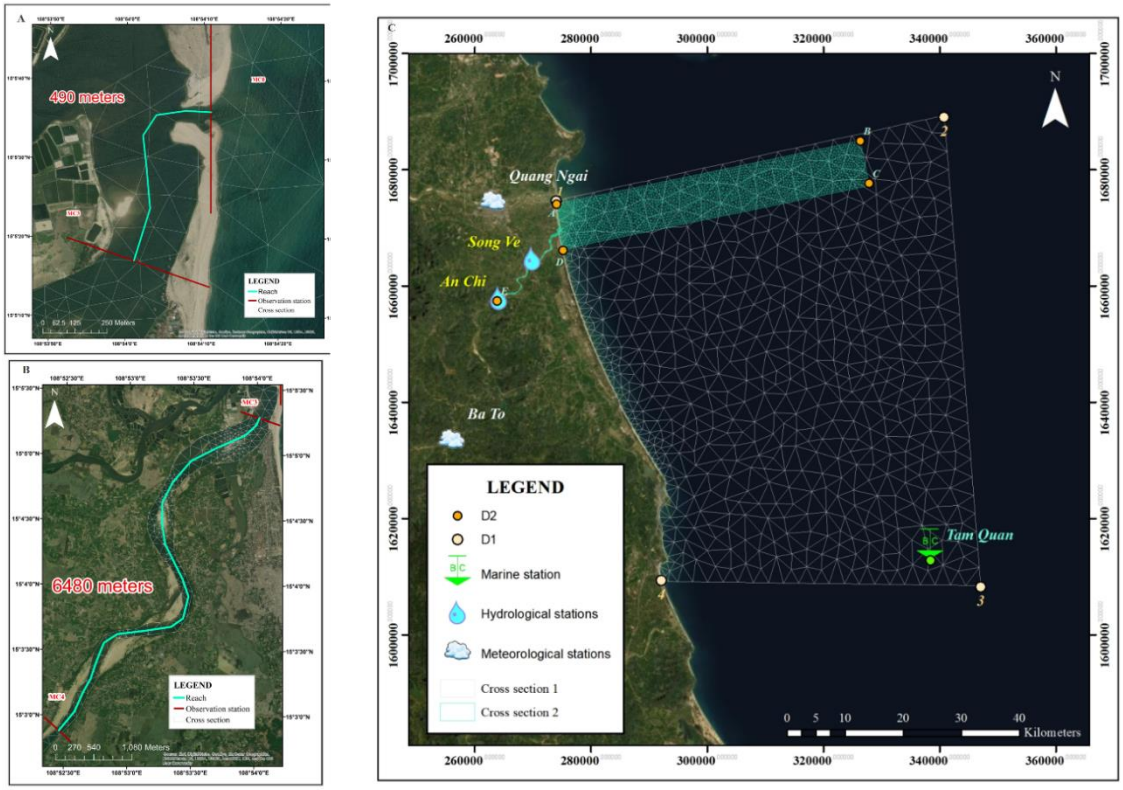

Figure 2. (A), (B) The 3 cross–sectional positions MC0, MC3, MC4 measured water level and salinity; (C) The grid domain D1 includes 4 vertices 1, 2, 3, 4 including marine station Tam Quan, Binh Dinh; The grid domain D2 with 5 peaks A, B, C, D, E was selected to simulate HD and saline intrusion AD, the four measurement stations are shown: meteorology (Quang Ngai, Ba To), discharge (An Chi), water level (Song Ve).

2.2. Hydrological models

To build hydrodynamic scenarios, hydrological models are often used, which involve the use of mathematical modelling techniques of rainfall–runnoff processes in the basins [4, 31]. Analysis of the advantages and disadvantages of these models was carried out in a series of studies [4, 32–33]. For sub–basin division, SWAT is used, input data for the SWAT model includes ASTER digital elevation model data (ASTGTM) with spatial resolution of 30 m, river Ve shapefile (line) and a raster mask layer within Quang Ngai province with 48N UTM coordinate system. Select a flow direction division area of 6838 ha with 72830 cells (default value from SWAT model). An Chi station is added to ArcSWAT using the tool to create an outlet at An Chi station location (Figures 1–2). Thus, using NAM, the discharge data extracted at the outlet of An Chi station will be compared with the actual measured data. In this study, rainfall, temperature, wind, and solar radiation data at Quang Ngai station were used to generate evaporation data. Together with the results of sub–basin division, this dataset is included in NAM to calibrate the set of hydrological parameters for the basin. The set of

measured discharge at An Chi is used for the calibration, verification steps. The linking between SWAT and NAM is shown in Figure 3. The results of calibration of the hydrological parameter set for the study basin reflected in the work [27]. To perform the calibration, first, from the initial set of parameters, NAM performs automatic calibration by the gradual trial method to increase the accuracy to a stable level with the allowed error based on the statistical indicators [34].

2.3. MIKE 21/3

The MIKE software package – a product of the Danish Hydraulic Institute – DHI Water & Environment, with modules such as MIKE 11, MIKE 21, MIKE3 HD, AD, ST, MT, SW is used to simulate the one–dimensional, two–dimensional, three–dimensional hydrodynamic processes, the transport and diffusion of dissolved and suspended substances, sediments; propagation of ocean waves, calculation of alluvial sediments in estuaries and coastal areas. Research on the application of MIKE to simulate saline intrusion has been carried out in many studies [7, 10, 17, 21–22]. 2D governing equations and numerical solution of MIKE 21 models (HD and AD) are presented in detail in [35, 37].

2.4. Data

2.4.1. Bathymetry

The MIKE 21 HD running data in this study was divided into 2 groups. The first related to the coastal area was collected, processed and transferred into the module [27–29], the second group related to the mainland and estuary includes: real data measured 19 cross–sections measured, inherited from the previous project. The section of the Ve River considered in this study is limited from the upper reaches of the river to the mouth of the Lo mouth and is 21.47 km long (Figure 1).

2.4.2. Tital factors

Song Ve is influenced by the East Sea with a semi–diurnal tidal regime with 4 main tidal components: M2 = 20h, S2 = 10h, O1 = 30, K1 = 30h, are used to analyze the tidal wave harmonic function to create tidal boundary for the model [29, 38]. This set of parameters plays an important role in the MIKE 21/3 HD and AD modules.

2.4.3. Hydrometeological data

The MIKE 21/3 FM runs for coastal waters requiring hourly data including wind speed and direction. In this study, the Weather Research and Forecasting (WRF) model was used for hourly extraction [29]. [27, 29] show that in July 2018, the average daily discharge is the lowest, and December 2018 has the highest average daily discharge. Besides, in this study, the measured meteorological data at Ba To and Quang Ngai stations, discharge measurement data at An Chi, and water level measurement at Song Ve stations are used. These datasets are used to calibrate NAM hydrological models and hydraulic models. The steps to apply these datasets are shown in Figure 3.

2.3.4. Actual measuring data for water and salinity levels

Within the framework of the thesis, field measurements were carried out with the following equipment: Acoustic Doppler Current Profiler (ADCP); NA2 Leica hydrometer, LEICA (TC805), echo sounder HONDEX PS–7; salinity meter; terrain mia; handheld GPS unit; compass. Hydrological factors were recorded from 0:00 on October 7, to 23h on October 8, 2018 and measured cross–section and elevation conduction from October 9–10, 2018. Simultaneously with measuring the water level, the salinity factor was also sampled and measured in a 24–hour mode from 0:00 on October 7 to 11 p.m. on October 8, 2018 at all 3

cross–sections: section 0, cross section 3 and section 4 [29]. Measurement of water flow by ADCP is performed at 3 cross–sections according to 24/24 mode from 0:00 on October 7 to 23:00 on October 8, 2018. This set of measured salinity data is used to calibrate the AD model.

2.5. Procedural steps

In the study [27], the hydrological – hydrodynamic package SWAT/NAM/MIKE was used to build a set of hydrological and hydraulic parameters for flow calculations.

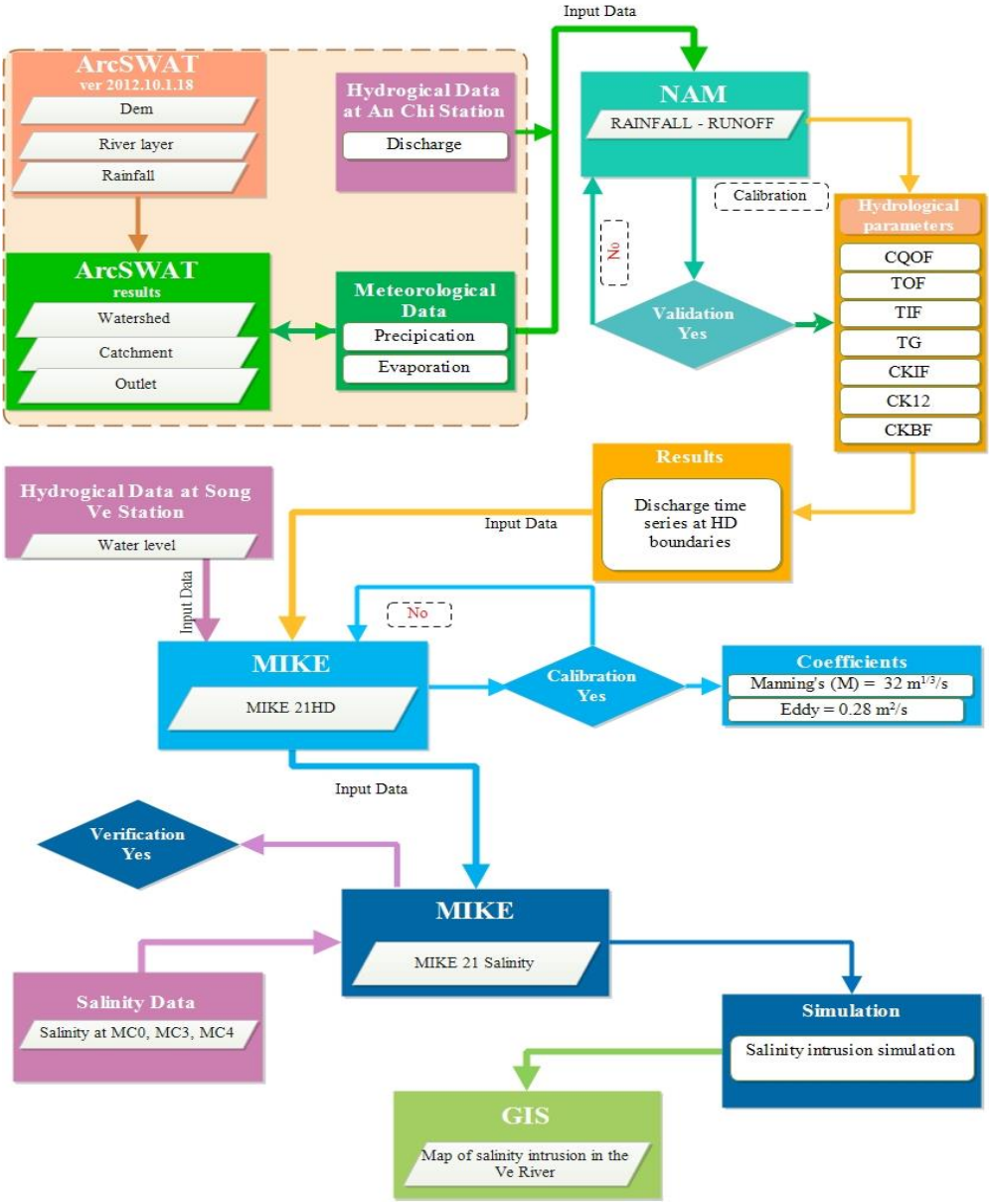

Figure 3. Linking hydrological and hydraulic models to simulate saline intrusion.

The contents and implementation sequence are shown in Figure 3, as follows: first, SWAT is used to divide the basin, determine the outlet as well as create the evaporation, precipitation dataset for NAM. The set of actual discharge measurements at An Chi is used for calibration and validation, the result of the step is the set of calibrated hydrological parameters. The second step–performing calibration and testing of the hydraulic module for the Ve River, using the discharge boundary created by NAM. Measured data of water level at the Ve station is used (Figure 3). The salinity data measured at MC0, MC3, MC4 cross–

sections are used to calibrate dispersion parameter for AD modelling (Figure 3). Third, the MIKE 21/3 AD module is used to simulate saline intrusion from the sea to the land.

The HD module is used on two domain grids D1, D2 (Figure 2). Grid D1(1234) with vertices **1**(108° 53,849'E; 15° 8.245'N), **2**(109° 31,094'E; 15° 16,491'N), **3**(109° 34.907'E; 14° 32,590'N), **4**(109° 4.328'E; 14° 32.776'N) contains Tam Quan station (Figure 2). Grid D2 (ABCDE), where B, E are the vertices located the sea with coordinates **B** (109° 22,973'E; 15° 14.079'N), **C** (109° 23,821'E; 15° 10.165'N); vertices **A** (108° 53,866'E; 15° 7,957'N), **D** (108° 54.421'E; 15° 3,722'N) are located in the coastal area; The vertice **E** (108° 48.130'E; 14° 58.928'N) is located inland and is also upstream of the Ve River (Figure 2). Hydraulic modeling for grid D1 was performed with water level boundaries obtained from the Tide Prediction of Height toolkit in MIKE 21Toolbox(.21t). The set of real data measured at Tam Quan in 2015 was selected for calibration with the result R^2 = 0.916; Nash = 0.988; PBIAS = 7.323; RSR = 0.460 and verification with results: R^2 = 0.919; Nash = 0.991; PBIAS = 7.933; RSR = 0.490. The result of this step is calibrated parameters: viscosity coefficient 0.28 (m^2/s), roughness coefficient 30 ($m^{1/3}/s$). The hydraulic model that is runs for domain D1 is used to create the water level boundaries for 3 edges AB, BC, CD, belonging to grid D2 (Figure 2). The HD model for grid D2 uses the water level boundary from 3 sides AB, BC, CD, the discharge boundary at the upstream location E, using NAM. Actual data of water level measurement at Song Ve station (Figures 1–2) in 2018 is used for calibration and verification; in which the calibration results are R^2 = 0.939; Nash = 0.970; PBIAS = –2.290; RSR = 0.490 and verification results are: R^2 = 0.901; Nash = 0.953; PBIAS = –16,763; RSR = 0.490. The result of this step is the set of parameters for the viscosity coefficient of 0.28 (m^2/s) and the Manning roughness coefficient of 32 $m^{1/3}/s$ for the Ve River.

Based on meteorological data in at Ba To station for 2018, the NAM model is applied to create a discharge boundary for the Ve River [27]. From the time series of data for discharge, the month with the smallest and largest average discharge are found, namely the months of July, December. MIKE (21 and 3) HD and AD are applied for hydraulic and saline intrusion modelling in the seleted area. From these results, the relationship between the scope of saline intrusion, the tidal regime and flow discharge has been made.

3. Results and discussions

3.1. Setup the set of hydrological parameters

The discharge data set measured at An Chi station, in the period 2013–2015 is used to calibrate, verify, validate NAM, in which the whole year of 2013 is used for calibration, two years 2014–2015 for verification and validation purposes are determined. The results for the Nash index are 92%, 90% and 93%, respectively, are shown in Figures 3a–3c.

Table 1. Calibrated hydrological parameters set for the selected basin.

Parameters	Meaning	Value
U_{max}	Upper limit of the amount of water in the surface storage (mm)	17
L_{max}	upper limit of the amount of water in this storage (mm)	172
CQOF	Overland flow runoff coefficient, dimensionless	0.185
TOF	Threshold value for overland flow	0.531
TIF	Root zone threshold value for interflow	0.114
TG	Root zone threshold value for groundwater recharge	0.404
CKIF	Time coefficient of surface water flow	655.8
CK12	Constant intrusion time of surface water flow	19
CKBF	Constant intrusion time of groundwater flow	3972

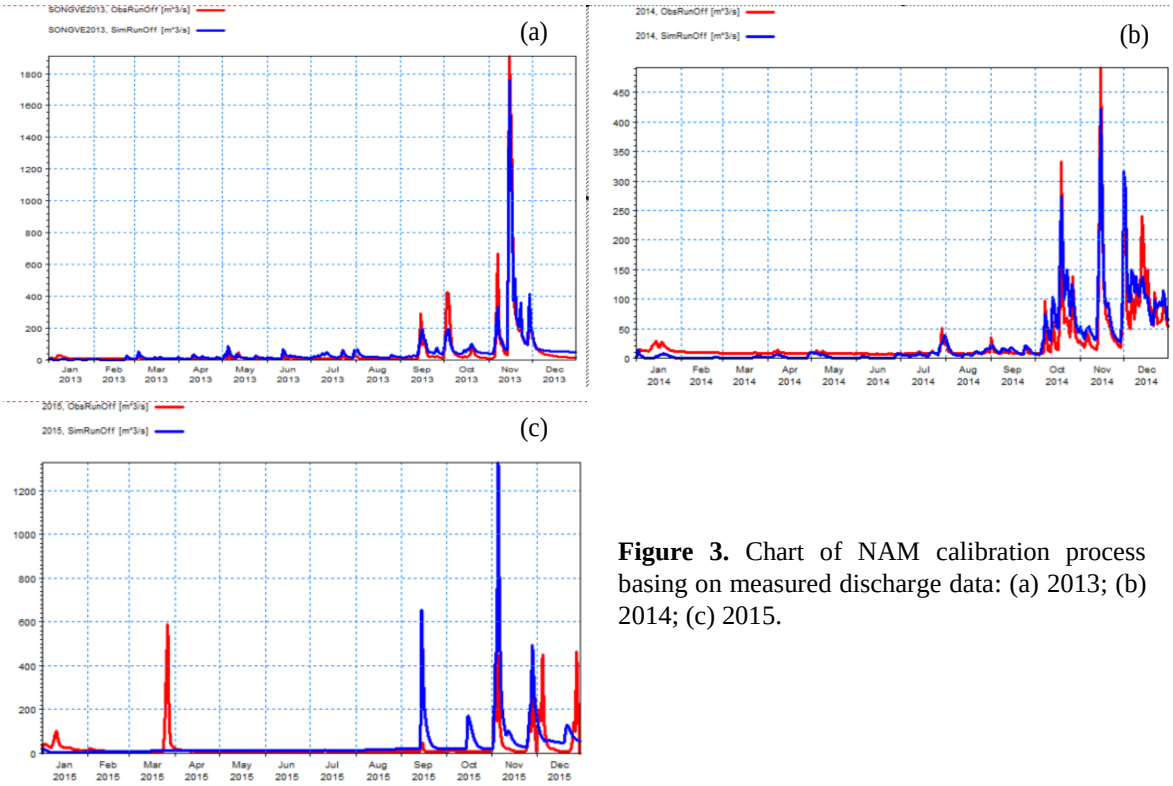

Figure 3. Chart of NAM calibration process basing on measured discharge data: (a) 2013; (b) 2014; (c) 2015.

3.2. HD and AD validation

The time series of water levels selected for validation of the MIKE 21/3 HD hydraulic model is as follows: time series for correction: October 7, 20188 00:00:00 AM – October 8, 2018 11:00:00 PM. Actual measured data of water level is done, described in 2.3.4. The results of validation of the hydraulic model are shown in Table 1 and Figure 4.

Table 1. Verification results of HD module at 3 monitoring sections.

Sections	R^2		Nash		PBIAS		RSR	
MC0	0.9098	Very good	0.8805	Very good	–4.6676	Very good	0.3457	Very good
MC3	0.9027	Very good	0.8929	Very good	–1.0879	Very good	0.3272	Very good
MC4	0.8932	Good	0.8055	Very good	–3.9384	Very good	0.4410	Very good

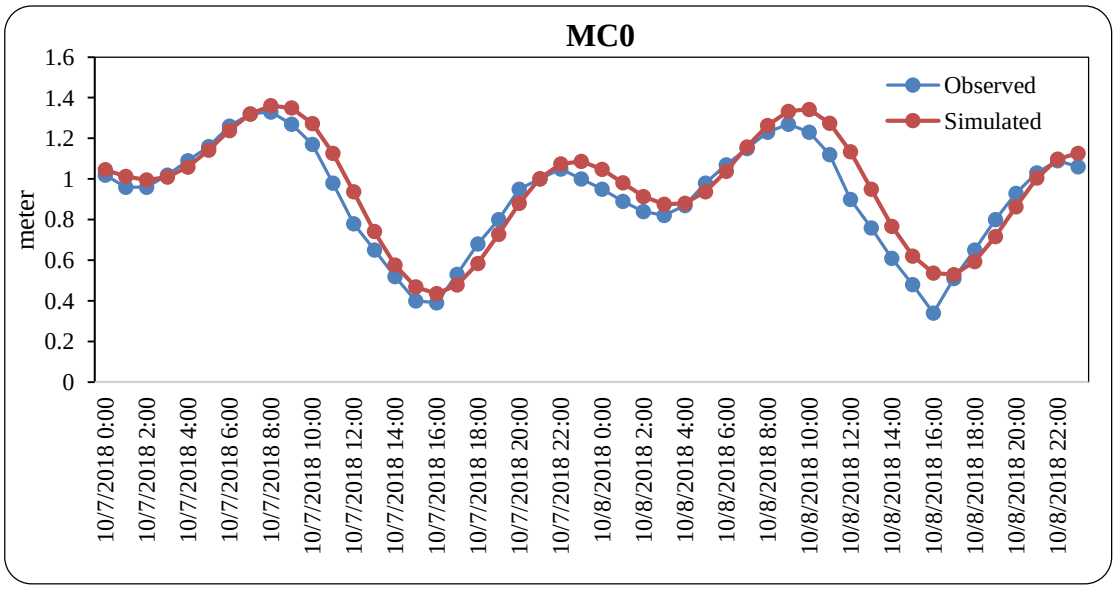

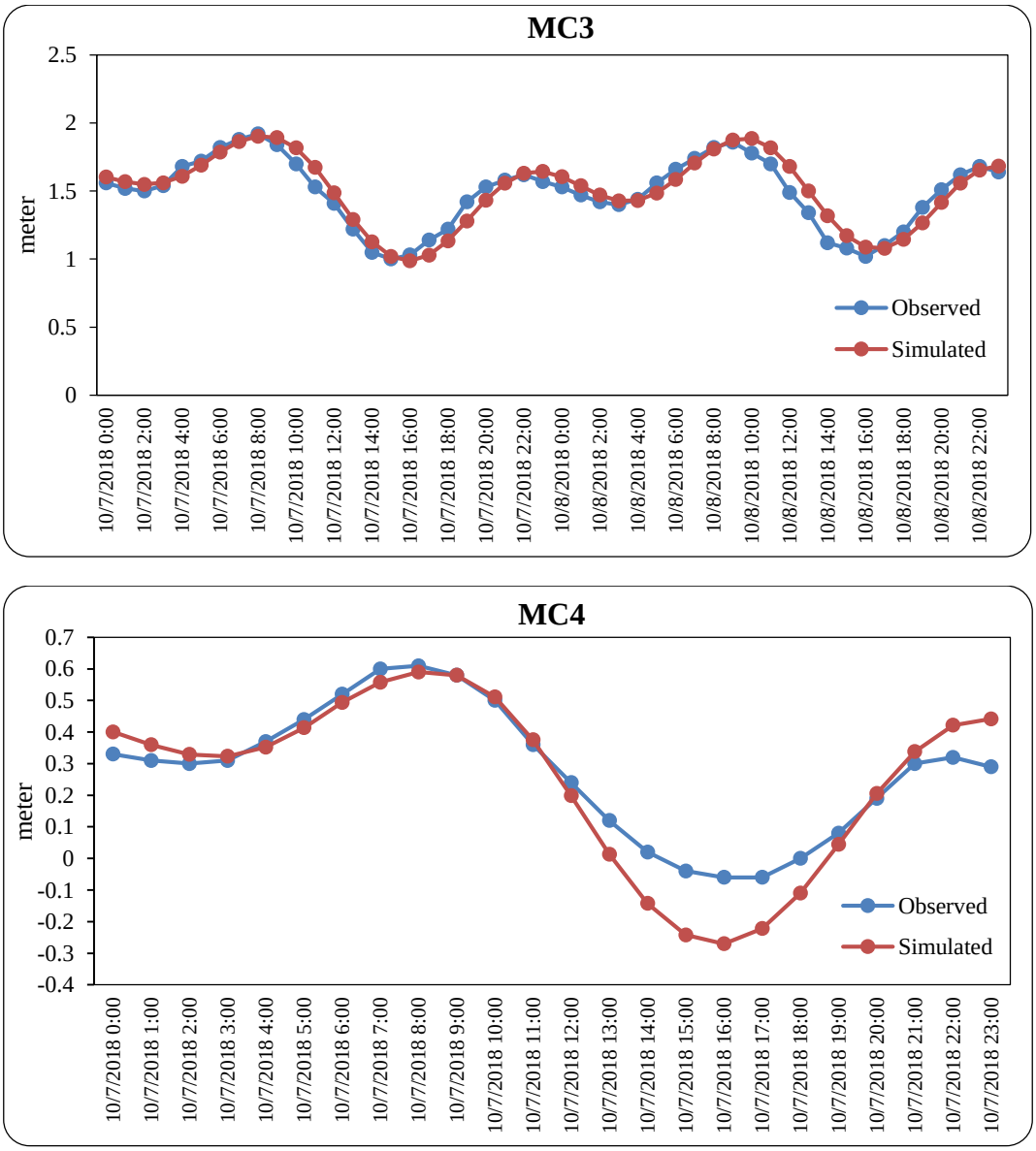

Figure 4. Results of HD verification using real data measured at 3 cross–sections MC0, MC3, MC4.

The results of the MIKE 21/3 AD calibration and verification performed, usingh 48 hours of continuous salinity measurement data for 2 days 7–8 October 2018 at 3 cross–sections MC0, MC3, MC4 (section 2.3.3) are shown in Table 2. This result allows to confirm that MIKE 21/3 AD can be applied to simulate the saline intrusion picture for this study.

Table 2. The results of calibration of the AD module using continuous monitoring data at MC0, MC3, MC4.

Sections	R^2		Nash		PBIAS		RSR	
MC0	0.876	Good	0.704	Good	–18.476	Satisfactory	0.544	Good
MC3	0.725	Good	0.845	Very good	–11.380	Good	0.563	Good
MC4	0.749	Good	0.720	Good	–0.354	Very good	0.539	Good

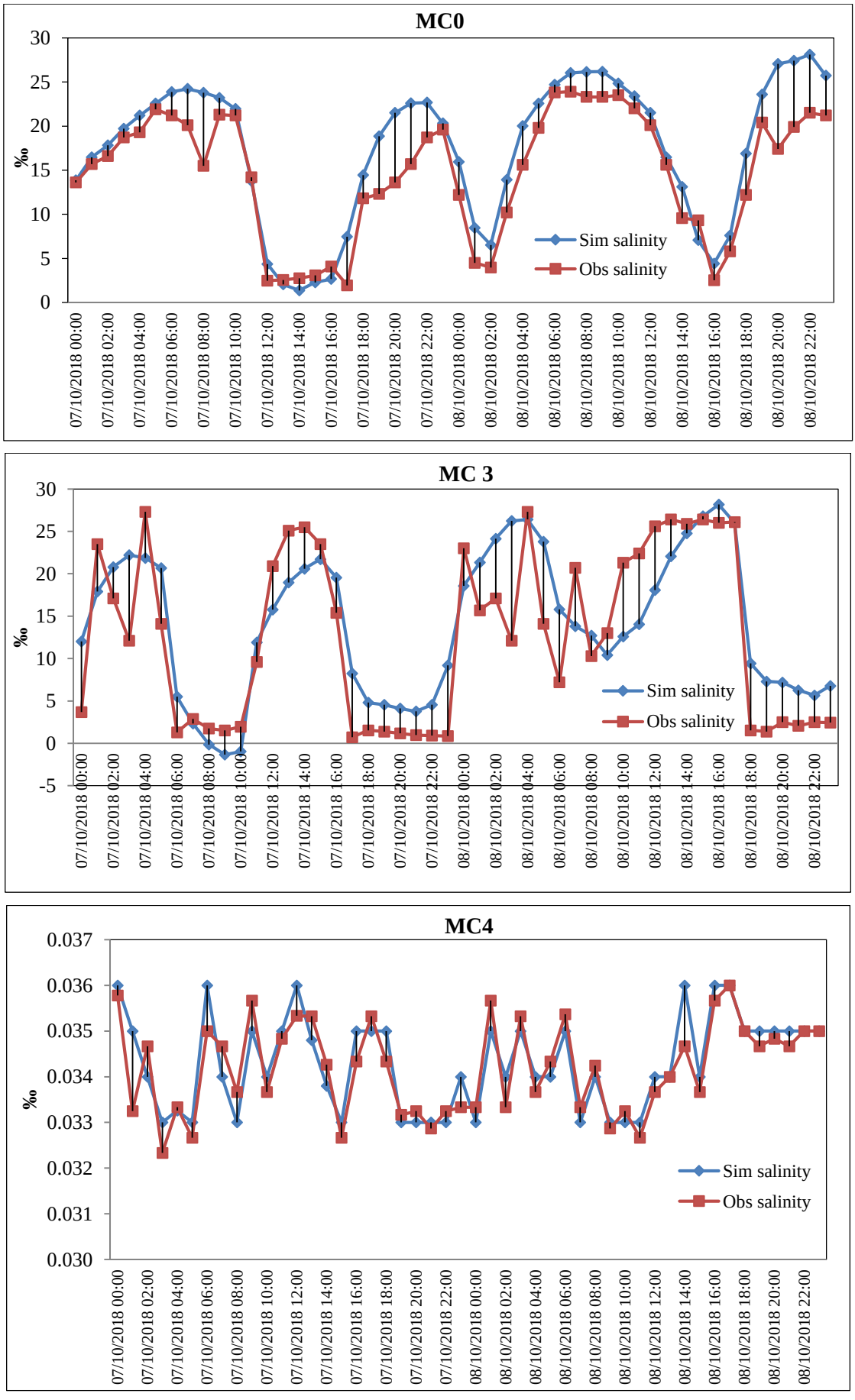

Figure 5. Results of calibration and verification of the AD using the measured data set.

3.3. Simulation of salinity intrusion

The flow discharge in the dry season is small, the selected month July, 2018 has an amplitude ranging from 2.17–13.13 m^3/s. This is the month with the smallest average one of 2018. Salinity amplitude $1^0/_{00}$ and landmark MC0 were selected for discussion. At 0 AM from July 19 to July 20, the tide is falling, the salinity reaches the mark of 5.03 km (Figure 6a), from 0–4 AM, the flow still has a direction from the sea into the river, the salinity reaches the 5.48 km (Figure 6b). This is the time when the salinity intrusion the farthest of the day. From 5 AM, when the tide rises, the flow direction is gradually changing, so the salinity decreases. At 6 AM, the flow direction changed completely from the sea to the river with great speed, the salinity decreased much, until 11 AM, the salinity intrusion slightly down, reaching 5.17 km, which is consistent with low tide in the period of 5–11 AM, currents tendency to go from river to sea (Figure 6c). At 2 PM, the tide is high, the flow is complicated, but the trend of going from the sea to the river, the salinity transmission from the sea to the river reaches the mark of 5.26 km (Figure 6d). Until 10 PM, the range of salinity transmisson is decreased to only 4.99 km (Figure 6e). The time when salinity transmits the least of the day. At 11 PM, the salinity increased slightly and spread to 5.04km (Figure 6f).

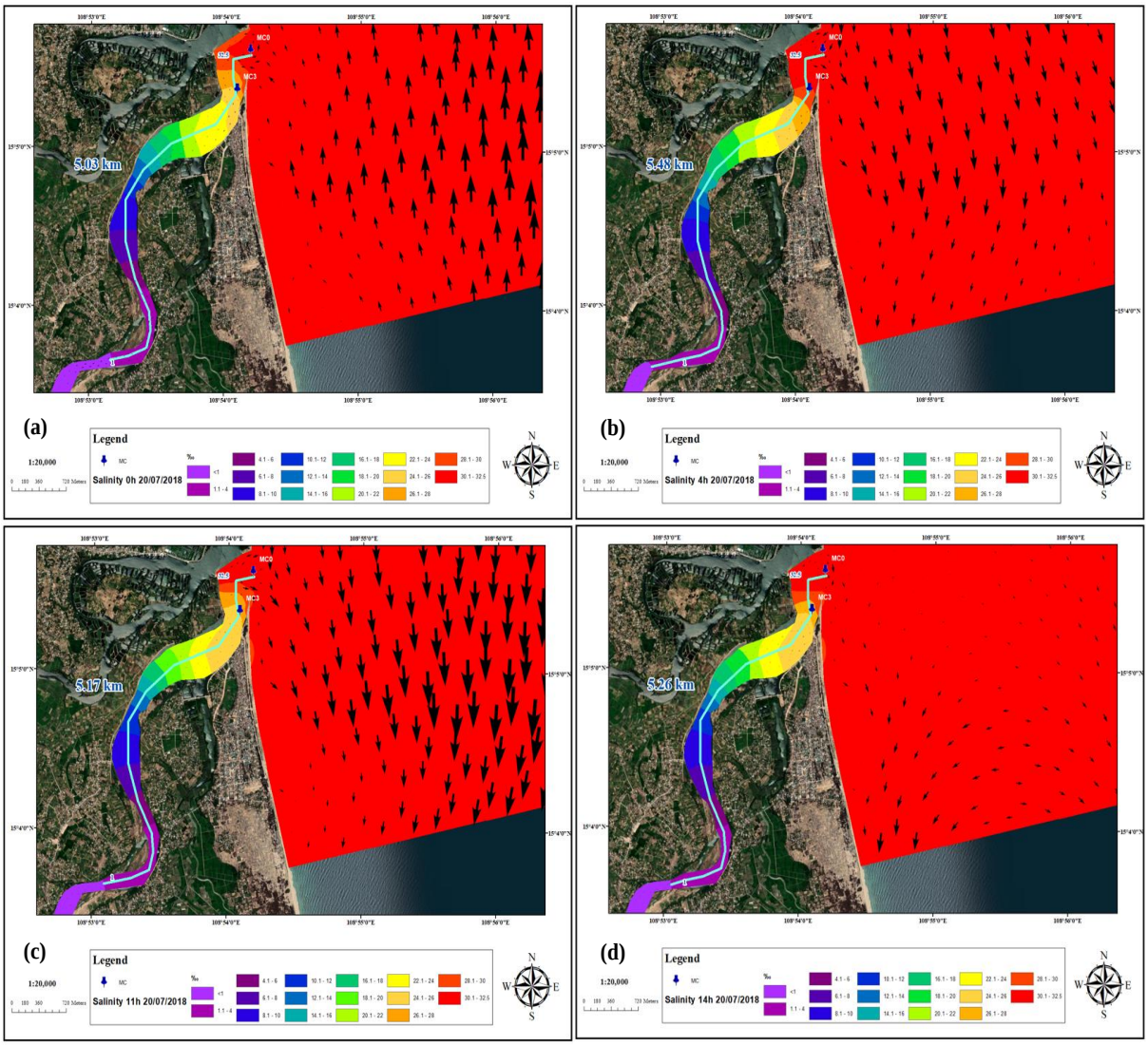

Figure 6. Results of modelling the scope of salinity intrusion in the dry season, simulation results for the day July 20, 2018: (a) At the time of 0 AM, the saline intrusion reaches the mark 5.03km; (b) At the time of 4 AM, the saline intrusion reaches the mark 5.48km; (c) At the time of 11 AM, the saline intrusion reaches the mark 5.17km; (d) At the time of 2 PM, the saline intrusion reaches the mark 5.26 km.

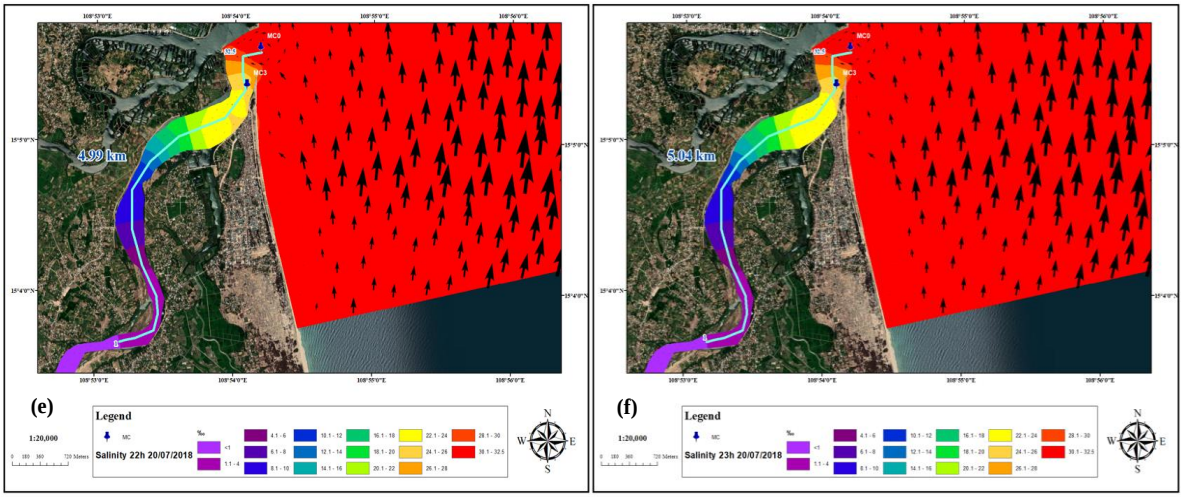

Figure 6. Results of modelling the scope of salinity intrusion in the dry season, simulation results for the day July 20, 2018: (e) At the time of 10h PM, the saline intrusion reaches the mark 4.99 km; (f) At the time of 11 PM, the saline intrusion reaches the mark 5.04km (cont.).

3.4. Discussion

The relationship S = F(Q, H) was built for July 2018, with S being the salinity at the MC3 cross–section. Correlation relationship between salinity depending on flow discharge Q, water level H is following:

$$S = 25.22229 - 0.05313 \times Q + 4.04644 \times H, R^2 = 0.7399, R = 0.8602 \quad (1)$$

The correlation coefficient is R = 0.8602, R^2 = 0.7399, showing that the two factors of discharge and water level explain about 73.99% of the variation in salinity value over time. Based on the results of univariate analysis (Table 3), the correlation coefficient R of water level (0.8563) is much larger than discharge (0.0778).

The results from the p–value show that both the above two factors, H, water level and Q, discharge, are statistically significant, respectively with p–value = 0.000001 < 0.05 and p–value = 0.033805 < 0.05. At the same time, this shows that although both above factors have an influence on the salinity changes in July 2018, the impact of water level H is much larger than the influence of flow Q.

Table 3. Summary of values in single linear regression analysis S = F(Q, H) for July 2018.

Factors	α	β	R	R^2	p–value
Discharge, Q	28.81364	–0.05080	0.0778	0.0061	0.033805
Water level, H	24.98979	4.04484	0.8563	0.7333	0.000001

The relationship S = F(Q, H) is also built for December 2018 – the month with the largest average discharge of the year. Correlation relationship between salinity depending on flow discharge Q, water level H is following

$$S = 6.36848054 - 0.0306469 \times Q + 3.91260007 \times H, R^2 = 0.456827, R = 0.67593099 \quad (2)$$

The correlation coefficient is R = 0.67593099 and both the discharge and water level factors explain about 45.69% of the change in salinity value over time in December at MC3, while based on the univariate analysis results (Table 4) the correlation coefficient R of the discharge (0.6355) is larger than the water level (0.2523). The results from the p–value show that both the above two factors, H, water level and Q, flow discharge, have an impact on MC3 salinity, respectively with p–value = 2.9256E–37 < 0.05 and p–value = 5.4118E–06 < 0.05; At the same time, this shows that although both above factors have an influence on the salinity changes in December 2018, the impact of Q discharge is more, the influence of H water level is lower.

Table 4. Summary of values in single linear regression analysis S = F(Q, H) for December 2018.

Factors	α	β	R	R^2	p–value
Discharge, Q	9.86260676	–0.0310392	0.63548934	0.4038467	2.9256E–37
Water level, H	2.29778936	4.28387584	0.25230199	0.0636563	5.4118E–06

The relationship $X_{max} = F(Q, H)$, where X_{max} is the maximum distance that salinity with the selected value $1\ ^0/_{00}$ is reached, is obtained as follows:

$$X_{max} = F(Q,H) = 6.17327 - 0.01612 \times Q - 0.40167 \times H, R^2 = 0.1451, R = 0.3809 \quad (3)$$

In given case, the correlation coefficient is R = 0.3809, showing that the two factors of flow discharge and water level only explain about 14.51% of the change in X_{max}, that is, up to 85.49% due to the impact of other factors. Based on the results of univariate analysis, Table 5, the correlation coefficient R of water level (0.368) is much larger than that of discharge (0.057). The results from the p–value show that only the water level H is statistically significant p–value = 0.041483 < 0.05, which shows that although both factors have an influence on X_{max}, but mainly due to the impact of water level H, the influence of flow rate Q is insignificant.

Table 5. Summary of values in single linear regression analysis Xmax = F(Q, H).

Factors	α	β	R	R^2	p–value
Discharge, Q	5.93374	–0.00940	0.0570	0.0033	0.760634
Water level, H	6.09630	–0.39051	0.3683	0.1356	0.041483

To construct the relationship S = F (X), the driest month of the year (with the lowest average discharge) was chosen, as well as the month of the highest salinity penetration. Landmarks 0, 1 km,…, 6 km are chosen as variable X. The average salinity S is calculated for each day of July. The functional dependence S = F (X) is shown in Figure 7. Results show that salinity gradually decreases with distance from the mouth, although salinity levels differ depending on the day of the month.

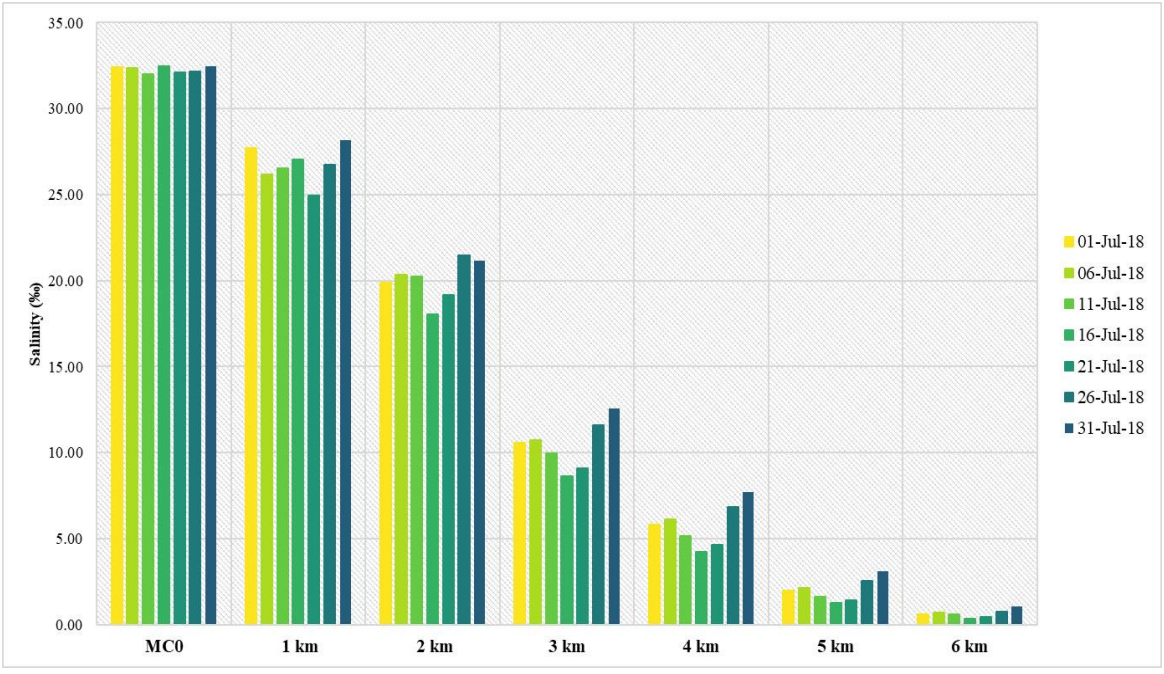

Figure 7. Relationship between salinity S depending on salinity intrusion distance for July, 2018.

4. Conclusion

In this study, the hydrological and hydrodynamic models were performed to simulate saline intrusion for the Ve estuary, Quang Ngai. The results obtained include:

First, the salinity intrusion in a specific day in July 2018 is shown. The results showed that salinity penetrated the farthest distance up to 5.47 km. A two–dimensional map of saline distribution was built for the time of change in the intrusion state: from the sea and from the river.

Second, the relationship between the salinity in the MC3 cross section and the flow rate and water level is built. The typical dry season month serves as an example. The results show that in section MC3 the effect of the water level is much greater than the comparison of the flow discharge factor.

Third, the relationship has been established between the furthest salinity intrusion distances depending on Q,H. The results show that the two factors of discharge and water level have not significantly impact on this relationship, however, the water level factor still has a larger impact.

Fourth, the relationship between salinity level and intrusion distance shows that salinity decreases with distance from the estuary, although salinity at landmarks varies by day.

Note that this study is still limited, as actual measurement data, including salinity, are limited by a 48–hour measurement sequence over 2 days October 7–8, 2018, so further monitoring of salinity is required for a longer time to improve the accuracy of the salinity intrusion modelling. In addition, due to the lack of data on the amount of water pouring in from the Tra Khuc river side, this study did not take into account this effect on saline intrusion.

Author contribution statement: Conceived and designed the experiments; Analyzed and interpreted the data; contributed reagents, materials, analysis tools or data; wrote the draft manuscript; manuscript editing: B.T.L.; Performed the experiments; contributed reagents, materials, analyzed and interpreted the data,: L.T.M.D.

Competing interest statement The authors declare no conflict of interest.

References

1. Paul, P.K.; Zhang, Y.; Ma, N.; Mishra, A.; Panigrahy, N.; Singh, R. Selecting hydrological models for developing countries: Perspective of global, continental, and country scale models over catchment scale models. *J. Hydrol.* **2021**, *600*, 126561.
2. Fleischmann, A.; Siqueira, V.; Paris, A.; Collischonn, W.; Paiva, R.; Pontes, P.; … Tanimoun, B. Modelling hydrologic and hydrodynamic processes in basins with large semi–arid wetlands. *J. Hydrol*. **2018**, *561*, 943–959.
3. Bravo, J.M.; Allasia, D.; Paz, A.R.; Collischonn, W.; Tucci, C.E.M. Coupled Hydrologic–Hydraulic Modeling of the Upper Paraguay River Basin. *J. Hydrol. Eng*. **2012**, *17(5*), 635–646.
4. Kovář, P.; Hrabalíková, M.; Neruda, M.; Neruda, R.; Šrejber, J.; Jelínková, A.; Bačinová, H. Choosing an appropriate hydrological model for rainfall–runoff extremes in small catchments. *Soil Water Res*. **2015**, *10(3*), 137–146.
5. Liu, B.; Peng, S.; Liao, Y. The characteristics and causes of increasingly severe saltwater intrusion in Pearl River Estuary. *Estuar. Coast. Shelf Sci.* **2019**, *220*, 54–63.
6. Chen, Q.; Zhu, J.; Lyu, H.; Pan, S.; Chen, S. Impacts of topography change on saltwater intrusion over the past decade in the Changjiang Estuary. *Estuar. Coast. Shelf Sci.* **2019**, *231*, 106469.
7. Thuc, T.; Hien, N.X.; Thai, T.H. Study on the effects of sea level rise and climate change on salinity intrusion in Red River Delta area. *VN J. Hydrometeorol.* **2010**, *589(1)*, 7–13.
8. Do, N.H.T.; Thien, D.Q.; An, T.T.P.; Viet, L.V. Assessment of current status and factors affecting the saltwater intrusion of Truong Giang River, Quang Nam

province. *VN J. Hydrometeorol.* **2011**, *606(6)*, 19–24.

9. Dai, H.V.; Hien, N.T.; Hien, T.D.; Khanh, N.Q. Assessment of some paramenters sensitivity for intrusion salinity simulative model in Ma river downstream. *VN J. Hydrometeorol.* **2014**, *643(*7), 24–28.
10. Hung, N.Q.; Huy, H.A. The application of Mike basin model for water balance calculation in Lam River basin. *VN J. Hydrometeorol.* **2016**, *663*, 47–54.
11. Thuong, L.D.; Huong, H.T.L. Assessing impacts of sea level rise on salt water intrusion in Ba River basin. *VN J. Hydrometeorol.* **2013**, *625*, 38–46.
12. Phung, N.K.; Bay, N.T.; Kim, T.T.; Tuan, L.N. Risk of saltwater intrusion in main rivers of Dong Nai province in the context of climate change and sea level rise. *VN J. Hydrometeorol*. **2017**, *678*, 18–28.
13. Dao, N.V.; Binh, P.T.T. Evaluation of the situation and impact of climate change on the Sality intrusion at Ben Tre province. *VN J. Hydrometeorol*. **2019**, *700*, 12–23.
14. Phung, L.T.; Phung, N.K.; Nam, B.C.; Hoang, T.X.; Tuan, L.N. Saltwater intrusion risk in main rivers of Vinh Long province in the context of climate change and sea level rise. *VN J. Hydrometeorol*. **2017**, *674*, 8–15.
15. Hoang, T.T.; Vi, V.T.T.; Long, P.T.; Tung, T.T. The impact of saltwater intrusion to take freshwater for Tan Hiep water plant. *VN J. Hydrometeorol*. **2016**, *666*, 15–20.
16. Bao, D.P. Developing technology for dry–season flow and saltwater intrusion forecasting in the Vu Gia – Thu Bon River system. *VN J. Hydrometeorol*. **2017**, *682*, 48–55.
17. Dung, D.V.; Phuong, T.D.; Oanh, L.T.; Cong, T.T. The effectiveness of the MIKE11 ad model for forecasting and warning the salinity intrusion in the MeKong delta. *VN J. Hydrometeorol*. **2018**, *693*, 48–58.
18. Son, H.T.; Lan, V.T.T.; Chung, N.D. Saline intrusion of the river in downstream Vu Gia – Thu Bon under hydropower project. *VN J. Hydrometeorol*. **2018**, *690*, 1–11.
19. Truong, T.V.; Sach, B.N.; Tuan, N.V.; Son, L.V. Assessment of saline water intrusion in the northern coastal area corresponding to water supply scenarios in the winter–spring season on the Red River system and proposing solution for saving water source released from reservoirs. *VN J. Hydrometeorol*. **2019**, *704*, 33–48.
20. Quang, H.N. Simulating saltwater intrusion on the Tra Ly riverunder climate change scenarios. *VN J. Hydrometeorol*. **2016**, *672*, 13–19.
21. Ha, L.T.; Kham, D.V.; Ha, L.H. Applying Mike 11 HD to assess the risk of salinity intrusion as sea level rise scenarios. *VN J. Hydrometeorol*. **2012**, *613*, 32–39.
22. Dai, H.V.; Thai, T.H. Researching 1–2 dimensional hydrodynamic model to predict salinity intrusion in Ma river downstream. *VN J. Hydrometeorol*. **2014**, *654*, 1–6.
23. Chau, T.V. Salinity intrusion in the Mekong delta under the impact of climate change and the proposal for mitigation measures. *VN J. Hydrometeorol*. **2013**, *634*, 21–25.
24. Ha, N.M.; Nghia, N.V. Trends change of factors affecting salinity intrusion in the Mekong Delta. *VN J. Hydrometeorol*. **2013**, *635*, 31–34.
25. Tri, D.Q. Application Mike 11 model on simulation and calculation for saltwater intrusion in southern region. *VN J. Hydrometeorol*. **2016**, *671*, 39–46.
26. Viet, L.V. The effect of ENSO on drought anhd saltwater industrion in lower Mekong Delta. *VN J. Hydrometeorol*. **2016**, *665*, 12–19.
27. Diep, L.T.M.; Anh, B.H.; Long, B.T. Applying mathematical models SWAT/NAM/MIKE to build hydrological and hydraulic parameters for flow calculation – in case of Ve river, Quang Ngai. *VN J. Hydrometeorol*. **2019**, *700*, 1–12.
28. Diep, L.T.M.; Long, B.T. Application of Mike/Swat for simulation the salt intrusion – a case study in Ve river, Quang Ngai province. *Lowl. Technol. Int.* **2020,** *22(1)*,

258–267.
29. Long, B.T.; Diep, L.T.M. Modelling the dependence between salinity intrusion and hydrological factors using MIKE 3: a case study of Ve river, Quang Ngai. *VN J. Hydrometeorol*. **2021**, *725*, 1–16.
30. Nhung, D.T.K.; Nghiem, D.V.; Hoang, N.D. Evaluation and prediction of saline intrusion patterns in the lower Tra Khuc river – Ve river. *Water Res. Environ. Eng.* **2015**, *50(9)*, 116–126.
31. Neitsch, S.L.; Arnold, J.G.; Kiniry, J.R.; Williams, J.R. Soil and water assessment tool theoretical documentation. 2002.
32. Gudmundsson, L.; Wagener, T.; Tallaksen, L.M.; Engeland, K. Evaluation of nine large–scale hydrological models with respect to the seasonal runoff climatology in Europe. *Water Resour. Res.* **2012**, *48(11)*, 1–20.
33. Devia, G.K.; Ganasri, B.P.; Dwarakish, G.S. A Review on Hydrological Models. *Aquat. Procedia* **2015**, *4*, 1001–1007.
34. Moriasi, D.N.; Arnold, J.G.; Van Liew, M.W.; Bingner, R.L.; Harmel, R.D.; Veith, T.L. Model evaluation guidelines for systematic quantification of accuracy in watershed simulations. *Trans. ASABE* **2007**, *50(3*), 885–900.
35. DHI. Mike 21 toolbox: User guide, 2014, pp. 268.
36. DHI. MIKE 11. Hydrodynamic and Transport Module, Scientific Documentation. 2005.
37. DHI, MIKE 21 & MIKE 3. Flow model FM, Hydrodynamic and Transport Module, Scientific Documentation. 2018.
38. Ninh, P.V. Hydrometeorology and marine dynamics. Publishing East Sea, Ha Noi: Natural science and technology publishing house, 2009, pp. 644.

VIETNAM JOURNAL OF HYDROMETEOROLOGY

Research article

Assessment of water resources using comprehensive sustainability indicators for water and land resources - a pilot study for the Southern Hau River basin

Le Thi Mai Van[1*], Nguyen Viet Tung[2], Le Manh Hung[3], Bui Thi Bich Ngoc[1], Doan Quang Tri[4], Truong Viet Chau[1], Bui Van Dung[2], Truong Van Hung[1], Dang Hoang Ha[1]

[1] Centre for Water Resources Warning and Forecasting (CEWAFO), National Center for Water Resources Planning and Investigation; lethimaivantnn@gmail.com; bichngoc209hunre@gmail.com; truongvietchau.tnn@gmail.com; truongvanhung888@gmail.com hadangld2@gmail.com.

[2] National Center for Water Resources Planning and Investigation; tungwr@gmail.com; dungtvb88@gmail.com

[3] University of Virginia; hml5rn@virginia.edu

[4] Vietnam Journal of Hydrometeorology, Viet Nam Meteorological and Hydrological Administration; doanquangtrikttv@gmail.com

*Corresponding author: lethimaivantnn@gmail.com; Tel.: +84–982420298

Received: 15 October 2021; Accepted: 12 December 2021; Published: 25 December 2021

Abstract: Currently, water resources planning is paying attention in Vietnam with several master plans established in some large basins across the country. However, in the context of water resources planning, the water allocation task still has inconsistency in calculation methodology. Therefore, this study aims to provide a set of indicators to estimate water and land resources to serve as the foundation for water resources allocation task. We have been used the following methods: (i) data collection, analysis and processing; (ii) field surveying; (iii) expert consultation; and (iv) mathematical modelling. We selected the Southern Hau River basin (SHRB) as our pilot study. The results indicate that the total amount of surface water from the Hau River supplying to the entire SHRB region in the dry season months (January to April) is about 487 million m^3/month. The total amount of groundwater (saltwater and freshwater) is 35.5 million m^3/day, with 16.7 million m^3/day coming from freshwater. The SHRB has a great variation in season - 3.8 billion m^3 (19%) for the dry season and 16.19 billion m^3 (81%) for the flood season. The outcomes of this study provide basis information for implementing water resources planning's steps in allocating water resources to the SHRB's sub–basins.

Keywords: Indicator; Sustainability; Water Resources; Land Resources; Southern Hau River basin.

1. Introduction

There have been a number of studies worldwide on sustainability indicators in the field of water resources. In particular, at the level of the river basin, [1] integrated issues of hydrology, environment, life and policies on water resources into a single sustainability index - Watershed Sustainability Index (WSI). The authors of this study applied the Pressure - State - Responses model to the indicators (H-Hydrology, E-Environment, L-Life and P-Policy) and placed them in a matrix frame, from which a typical WSI index for the whole basin was calculated [1]. This WSI index has a value from 0 to 1, representing the lowest and highest watershed sustainability. The study also applied the calculation method to the SF Verdadeiro

River Basin in Brazil. The results show that this basin has a WSI index of 0.65 which is equivalent to the average sustainability level [1].

[2] applied the WSI method [1] for calculating the sustainability index of the Reventazón River Basin in the province of Cartago and Limón, Costa Rica. In this study, the river basin was divided into three regions: highland, midland and lowland according to the elevations of the regions to calculate more accurately the indicators of the basin. The average WSI for the entire basin is 0.71, which equates to a fairly sustainable level. However, the research team focused on analyzing the indicators with the lowest scores, thereby making recommendations to the Commission for Conservation and Management of the Watershed of the Reventazón River (COCUMRE) for better improvement as well as to make the future WSI calculations for the watershed more accurate. The calculation method [1] was also applied to the Elqui River basin in Chile and the Motru river basin in Romania, and gave the results of 0.61 and 0.36 respectively (WSI values for the Motru river basin were calculated for an approximate period of 5 years), respectively with moderate and poor sustainability values [2–3].

In Vietnam, a number of research and projects have also developed indicators related to the assessment and use of water resources. Some notable research projects include as follows:

The Vietnam Water Sector Review Project was funded by the Asian Development Bank on behalf of international development partners with the objective of strengthening water resource management, poverty reduction and national development [4]. The project has synthesized the river basin monitoring data, the data on water exploitation and use, the relationship between the society, the population community and the river basin to build a set of indicators including 58 indicators as an approach tool to water sector management. Among these 58 indicators, there are 13 indicators on surface water resources, 3 indicators on groundwater, 15 indicators on social aspects, 12 indicators on economic aspects and 15 indicators on environmental aspects. These indicators were used to assess the current status of 16 main river basins in our country, thereby affirming that many large river basins have been in an alarming state of exploitation and over–use of water resources, which provide advanced information to the authorized managers for better planning of allocation, sharing and economical use of water resources. However, these indicators are only individual indicators and have not been placed in an overall framework for sustainable development [4].

While employing this set of indicators [5], the Department of Water Resources Management has developed the set of indicators to 81 indicators to serve the "Planning of Management of the Red River–Thai Binh River Basin" from 2013 to 2015. This set of indicators represents the factors on surface water, groundwater, social, economic, environmental and water resource management. However, this set of indicators only provides individual parameters in water resource planning and management, but it does not provide a general index of water resource use in the basin [5].

In the study [6], through the consultation method with experts in the Central Highlands provinces and experts specialized in sustainable development in various fields, a set of sustainable development indicators were synthesized and developed which include 77 regional–level indicators, 70 provincial–level indicators, and 49 district–level indicators. In this set of indicators, water resource was a topic in the field of the environment along with other topics namely land, atmosphere, natural disasters and biodiversity. Although the study has not provided specific assessment levels for each indicator, the set of indicators has demonstrated the correlation between the indicators and the topics, thereby stimulating a 'more comprehensive measure' of an overall development towards a sustainable manner.

For groundwater resources, [7] proposed a set of indicators including 6 main indicators: (i) the renewable groundwater resources per capita; (ii) the total groundwater resources exploited /supplied; (iii) the total exploited groundwater resources/total exploitable groundwater resources; (iv) the total amount of groundwater for drinking/total drinkable

water in the area; (v) the groundwater depletion indicator; and (vi) the groundwater vulnerability indicator. The groundwater resource indicators were evaluated at 3 levels: high, medium and low; then illustrated on the map with a value varying from 1–5, corresponding from less stable to very stable status. However, these indicators were still calculated separately, not integrated to provide a general index for the study area.

[8] analyzed the factors affecting the sustainability of river basins in Vietnam and included four groups of rivers based on current emerging issues in water resource planning, management and protection such as the Law on Water Resources 2012. The study proposed a set of parameters affecting the sustainability of the river basin for each specific river group. The study also proposed 35 parameters affecting the sustainability of the river basin, a basis for determining the level of sustainability, and how to calculate parameter values, thereby determining the level of sustainability of indicators (i.e., the fields) of water resources on environment, life, human activities and policies, then calculating the river basin sustainability index for Vietnam. In addition to the above studies, a number of studies have proposed statistical indicators on surface water resources, groundwater resources, water use [9], or water resource vulnerability index [10].

With a special geographical location, the hydrological regime in the southern area of the Hau River is directly affected by the upstream flow, the tidal regime of the East Sea, part of the tide in the Gulf of Thailand and the rainfall regime in the entire field. At the time of the flood, due to the upstream recedes, and the tidal regime strengthens, therefore the increase in water level and the discharge leading to a high possibility of large floods is still to occur in this flood period. The high–tide days are the time–period of temporary accumulation of water in the infield canals as well as an increase in the average water–level and vice versa. The complex hydrological–hydraulic regime in the Southern Hau River basin (SHRB) and the interweaving combination of varying degrees between flood–rain–tide and fresh–salt water are major limitations in calculating the distribution of water resources in the region.

Preliminary assessment revealed that although current indicators of sustainable use of water and land resources in the world and Vietnam are quite available, they have neither been fully complete yet nor presented the specificity in the planning of water resources distribution. Therefore, a study on a set of indicators of sustainable use of water and land resources in order to apply in the allocation of water resources would meet the urgent current needs. Within the scope of the research, this paper focuses on clarifying the general picture of the characteristics of the research area in order to propose a set of indicators for sustainable use of water and land resources and demonstrate a pilot calculation using a number of indicators to evaluate water resources in the SHRB. Specifically, in this research, the authors use Mike NAM hydrological model, Mike 11 hydraulic model, Feflow groundwater model to calculate and assess water resources (both surface water and groundwater) in the SHRB.

2. Materials and Methods

2.1. Description of the study area

The SHRB is part of the Mekong River basin with a natural area of 23,534.45 km^2 and a population of 8,737,454 people, including the area of 7 provinces and cities (An Giang, Bac Lieu, Ca Mau, Can Tho, Hau Giang, Soc Trang and Kien Giang) (Figure 1). The main terrain of the study area is the delta plain and the edged delta plain in the Southwest region with the topographical features of mainly low, flooded plains such as the Long Xuyen quadrangle region. The network of rivers and canals is quite developed due to the topography and influence of the Mekong River. The two mainstreams of the Tien and Hau Rivers strongly dominate the development of the Mekong Delta. After My Thuan River, Tien River has successive major distributaries, namely Co Chien River, Ham Luong River, Ba Lai River, Cua Dai River and Cua Tieu River. The Hau River flows in a straight line and only splits into two before discharging

into the sea about 30 km through Dinh An and Tran De estuaries. Both Tien and Hau rivers have formed many islets, curved river sections and flow diversions... Thus, the process of bank erosion and river bed sedimentation is very complicated, causing instability of the riverbed. The climate in the SHRB has the common characteristics of the Mekong Delta's climate, with a sub–equatorial monsoon climate regime with high temperature all year round and heavy rainfall with seasonal variation. A year has two seasons: The rainy season starts in May and ends in November; The dry season starts in December and ends in April of the following year. In addition, it is also influenced by the tropical monsoon climate regime and is typical of the coastal plain [11].

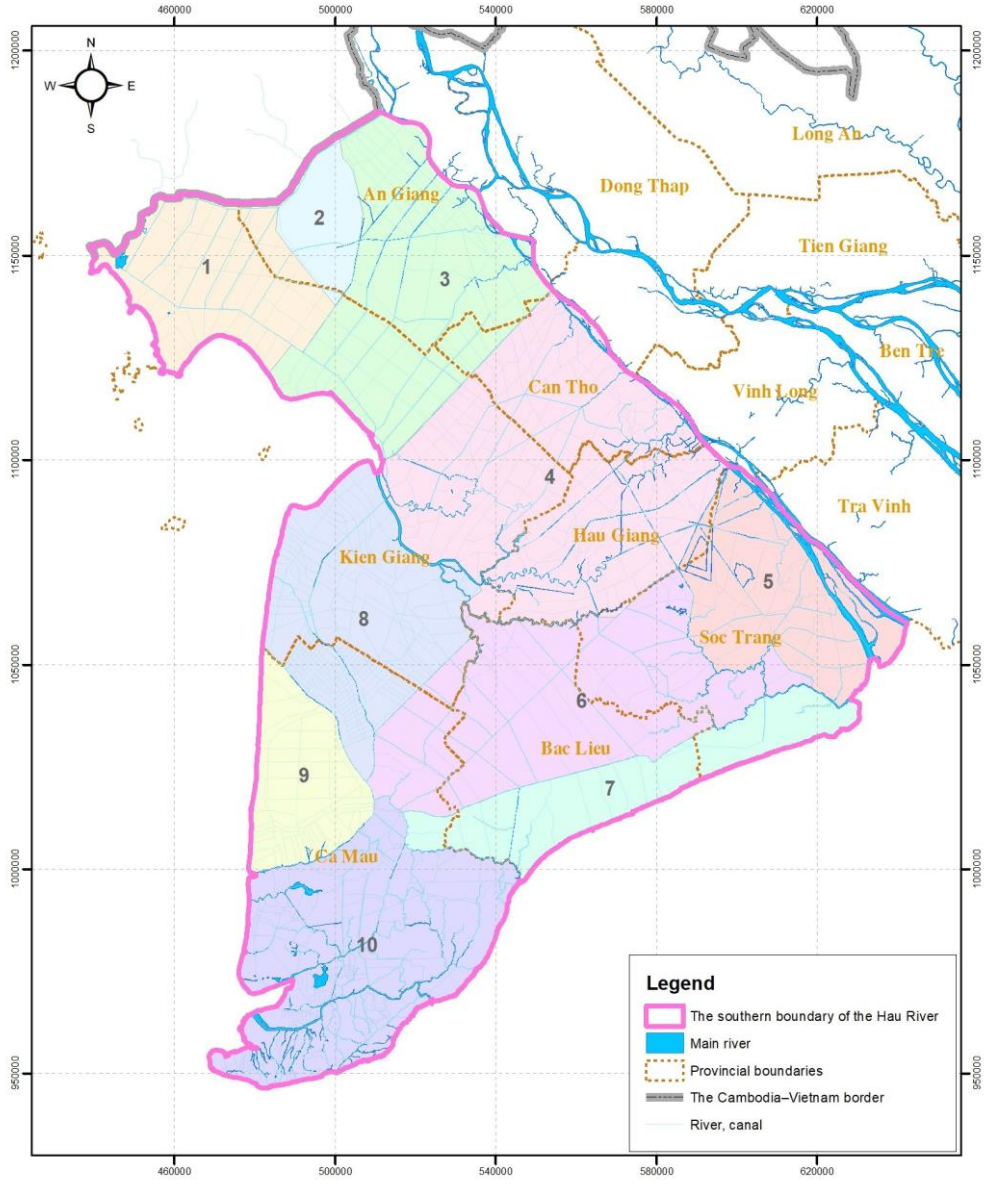

Figure 1. Map of the Southern region of Hau River.

2.2. Scientific basis for the proposed set of indicators

The basis of the proposed sustainable use indicators is:

(1) Based on the factors affecting the sustainability of water and land resources in the river basin;

(2) Based on a German study to develop an assessment framework, selecting indicators and parameters to calculate the sustainability index of water and land use in accordance with natural and social conditions in the research area.

(3) Referred to relevant domestic and foreign studies on the group of indicators and parameters affecting the sustainability of water and land resources in the river basin.

According to the approach of the research in the country and in the world, the sustainability of a system in general must ensure to be considered in three areas: environment, economy and society. However, the research proposing parameters into these three areas is still general, neither showing which specific groups of parameters affect natural resources in general and water resources - the important natural resources in the river basin in particular, nor which groups of parameters reflect human exploitation and use of natural resources... Therefore, the paper chose a set of indicators examining areas that affect river basin sustainability, including: Natural resources (mainly water resources); environment (soil environment, forests, ecosystems, etc.); life and policies of the river basin.

In addition, since the study targeted the integrated indicators on land and water resource sustainability, the research team proposed to also take land resource indicators into account. The assessment method is based on the land suitability classification, comparing the appropriateness between the requirements of the usage types in economic, social and environmental conditions related to the optimally effective use of land. The three main groups of criteria in FAO's sustainable land use assessment include environmental, social and economic performance.

In fact, many factors are affecting the sustainability of water and land resources that can be selected, however, it is not possible to choose all of these parameters as they will make the application process complicated; moreover, due to the lack of data for calculation, they cannot be also totally quantifiable. Therefore, only the dominant indicators were selected [12–16]. The indictor selection was based on the following principles:

The selected indicators need to ensure:

(1) Their representativeness and significance in the fields of water and land resources;

(2) To be based on a clear scientific basis, i.e the parameters can be qualified (quantitatively) and verified through actual data;

(3) To be widely accepted (previously consulted with experts to exclude non–representative indicators and add more relevant ones);

(4) To be understandable, reliable, highly sensitive, independent and not overlapping.

The selected set of indicators needs to ensure:

(1) The representativeness: a set of indicators will provide an overview of the current stress and status and their pressure on the fields of water and land resources.

(2) The number of parameters is reasonable, neither too much nor too little so that their accessibility to policymakers is greater at an acceptable cost.

2.3. Collect, analyze and process data

A range of documents on economic, social and environmental aspects related to water and land use issues in the study area were collected. The collection was carried out through many management and research agencies as well as through a variety of other sources such as seminars, surveys, interviews, etc. The collected data for calculation will be updated to 2020 and in accordance with the requirements of each mathematical model:

- Groundwater model FEFLOW: collected data includes: DEM map; data on the bottom elevation of aquifers and weak permeable layers (397 boreholes in the study area and vicinity); conductivity of aquifers; specific yield for the subterranean basins is taken according to the general survey of the projects implemented in the Mekong Delta and has been corrected by the German expert BGR through the software TTIM; Hydrometeorological data and data on the current status of exploitation and use of ground water resources in the region.

- With the hydrological model MIKE NAM: input data includes (precipitation and evaporation) from 20 meteorology stations in the area; Soil data, land use map of the study

area to conduct analysis, evaluation and selection of suitable parameters for calculation based on TCVN 10406-2015, ground flow coefficient is referenced from the model FEFLOW.

- The MIKE11 hydraulic model includes: Topographic map of the land surface with 17,796 elevation points; Cross-sectional data: 12,316 cross-sections/3,553 rivers, about 625 flood plains including embankments and sluices; System of works: about 15,000 km of main canals and grade I canals, nearly 27,000 km of grade II canals, about 50,000 grade III and inland canals, 450 km of sea dykes, 1,290 km of river dykes and about 7,000 km of embankments, 80 wide sluices over 5 m (the largest is Lang The sluice-dam at 100 m and Ba Lai sluice with 84 m), over 800 culverts 2-4 m wide and tens of thousands of small culverts and culverts, over 1,000 large and medium-sized electric pumping stations. thousands of small pumps to actively irrigate and drain; Data of 21 water level measurement stations, 4 flow measurement stations in the area [17].

2.4. Mathematical Modelling Methods

The mathematical modelling method used to solve the problem of water resource allocation in the SHRB is diagrammed in Figure 2.

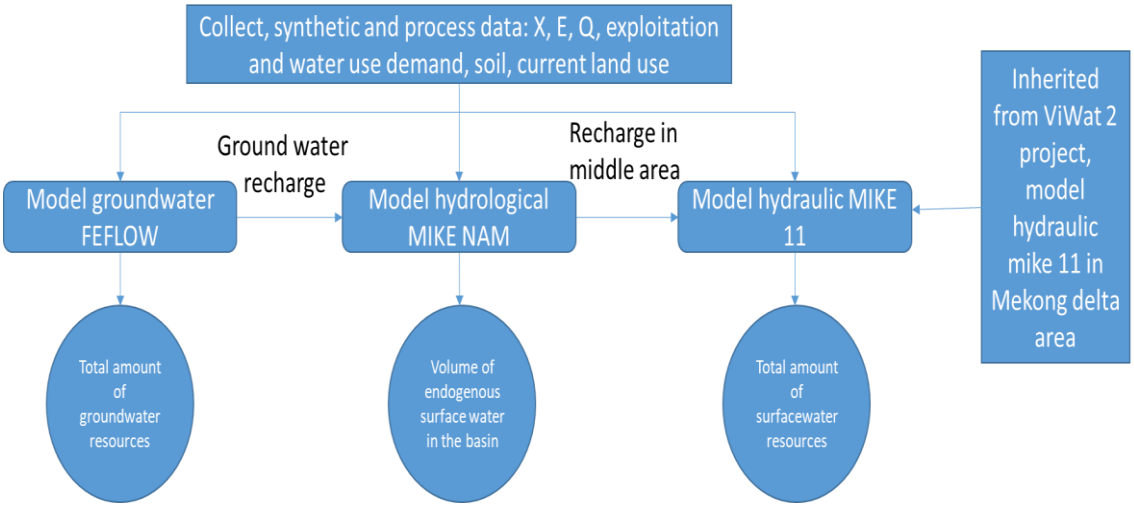

Figure 2. The calculation process of water resource assessment indicators.

The research team used the FEFLOW model to calculate the groundwater resource assessment index. Calculation results of groundwater recharge from the model combined with the current land use and soil characteristics determine a set of parameters for the Mike NAM hydrological model to calculate the amount of endogenous surface water in the basin. To calculate the total amount of surface water resources, the research team used the Mike 11 hydraulic model with the amount of middle–zone recharge determined from the hydrological model. The results are extracted at predefined allocation locations.

Accordingly, the SHRB area is divided into 7 regions, in which each region will have basic and relatively uniform characteristics of nature, environment, development form..., with relatively similar problems of water source system that need to be solved; especially the areas in the region are related to each other through the system of focal irrigation works (Table 2).

Within each region, it can be divided into a number of sub–regions if there are relative differences in natural conditions, construction measures, water source conditions and exploitation methods between regions. Thus, in each sub–region, there will be a higher homogeneity of exploitation methods, water source conditions and a closer relationship between irrigation works. Accordingly, the calculation area was divided into 66 sub–basins to serve the calculation (Figure 3).

Table 2. The statistics of regions and sub–regions for calculation in the SHRB.

No.	Region	Sub–region	Area (km^2)
1	N1 (freshwater)	11TLV	4228.4
2	M3 (saltwater)	6TLV	426.02
3	L1 (brackish water)	2TLV	1249.57
4	M1 (saltwater)	4TLV	749.21
5	M2 (saltwater)	27TLV	6730.18
6	N4 (freshwater)	9TLV	4517.75
7	L2 (brackish water)	7TLV	2462.76

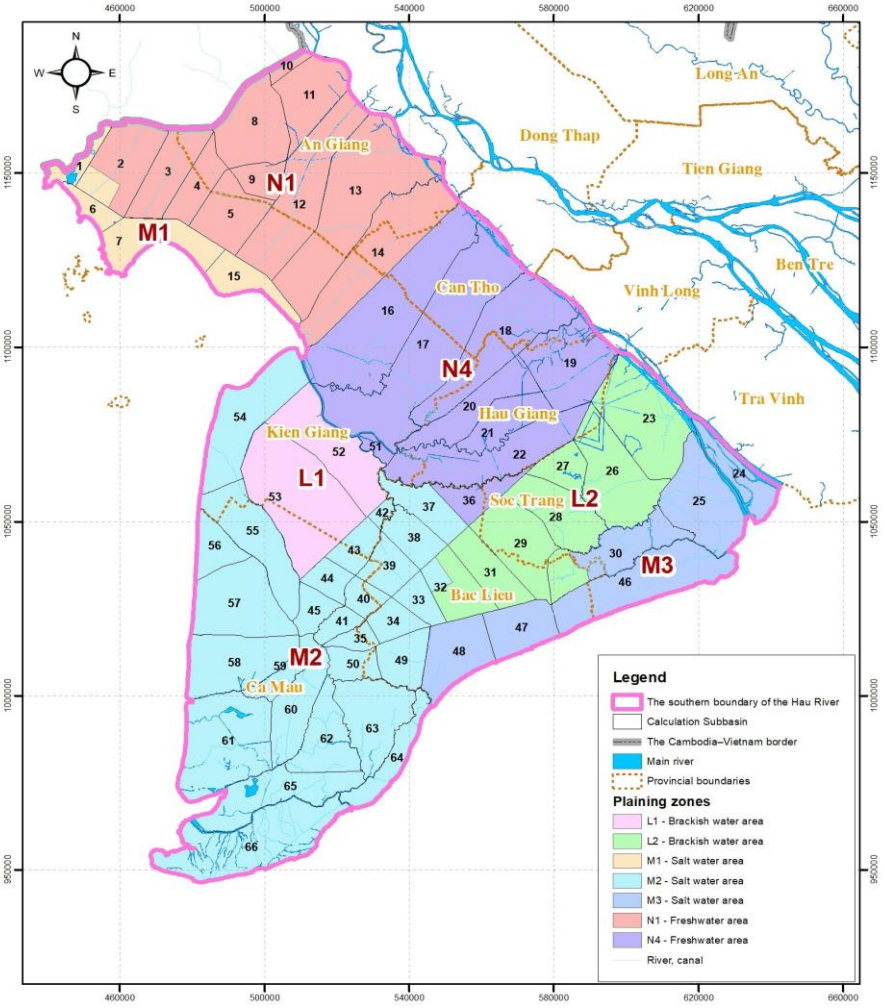

Figure 3. The demarcation of regional and sub–regional boundaries in the Southern Hau River area.

In addition, the analysis of regional flow characteristics and the assessment of locations and water sources in the SHRB, including surface water, groundwater at the representative points and locations in the sub–regions showed that the main distribution points and locations are the beginning of the main canals taking water from the Hau River, including 27 points (Table 3). Calculation results from these 27 points were used to calculate the allocation of water resources for 7 planning regions in the SHRB.

Table 3. Table of points (locations) distributed in the southern area of Hau River (names of rivers and channels for distribution of water resources from the mainstream of Hau river).

No.	Sub–region	Region	River (channel)
1	1	1	C. Vinh Te

No.	Sub–region	Region	River (channel)
2	10	10	C. Muoi Chau Phu
3	142	142	C. Dao
4	143	143	C. Can Thao
5	149	149	C. No. 1
6	25	25	C. Ba Chieu
7	33	33	C. Thom Rom
8	27	27	C. Thot Not
9	144	144	C. Chac Ca Dao
10	6	6	C. Tri Ton
11	12	12	C. Ba The
12	20	20	C. Tron
13	148	148	C. Nang Mau
14	36	36	C. O Mon
15	18	18	C. Rach Gia – Long Xuyen
16	150	150	C. Dai Ngai
17	48	48	C. Cai Con
18	75	75	C. Mac Can Dung
19	22	22	C. Cai San
20	147	147	C. KH9
21	146	146	C. Kh8
22	145	145	C. Kien Hao
23	1	46	C. Can Tho
24	41	132	Quan lo–Phung Hiep 132
25	53	159	Chac Bang
26	39	158	Quan lo–Phung Hiep 158
27	53	89	C. Lang thu 7

The lacking documents on natural and socio–economic characteristics were collected, especially the situation of exploitation, use and pollution of water and land resources in the SHRB. The research team also conducted a survey to take samples of the current state of the water and land environment and assess their pollution status in the study area.

2.5. Proposing a set of indicators for sustainable use of water and land resources in the group of water resource assessment

Based on the scientific basis mentioned above, the research team decided that water resources need to be evaluated via the three basic characteristics of quantity, quality and dynamics. Water quantity is a characteristic that indicates the abundance of water resources in a territory. Water quality is the characteristics of the dissolved substance content in the water that serves a specific water use requirement in terms of benefits and harms, according to the standards of water users. To accurately assess water resources, we need to evaluate the main factors: quantity, quality and dynamics of water in the study area. Overall, water and land resources maintain a close relationship with each other, interacting with each other in the process of movement. The characteristics of land resources affecting water resources are as follows: Soil thickness; Topographic; Soil structure; The composition of the soil; Proportion of soil; Reaction of the soil, etc. The research team realized that the natural cover index of the land has included these above factors that can represent land resources in the water resource assessment group.

Therefore, the research team proposes a set of indicators for sustainable use of water and land resources in the water resource assessment group, including: The total amount of surface water resources; the quality of surface water; the total amount of groundwater resources; the quality of groundwater; the amount of surface water transferred to the basin; natural cover index of the land.

3. Results and Discussion

3.1. Calculation results of the water resource assessment index in the Southern Hau River area

With its special location, the SHRB is greatly affected by saline intrusion and complicated hydrological regimes, so it is very difficult to assess the quantity of surface water resources, which causes big challenges for the planning of sustainable use of water resources in the region. This is also the reason why it is necessary to consider the groundwater reserve in the regional water resource allocation planning since the groundwater is an important water source that can ensure the essential needs of water users. Therefore, within the scope of the article, the research team selects a number of indicators in the water resource assessment group for a pilot calculation for the SHRB: The total amount of surface water resources; The total amount of groundwater resources; The amount of surface water transferred to the basin (the amount of endogenous water).

3.2.1. Total amount of surface water resources

The entire hydraulic network system of rivers and canals was calculated in the model with the time period. The calculation results have determined the flow process and water level on nodes along the main canals of the SHRB. These results extracted from the model were outputs to calculate the average monthly flowrate value in the period 2000–2019.

The results show that the average amount of surface water from Hau River supplying to the entire SHRB in the dry season months (I–VI) is about 487 million m^3/month, of which the surface water mainly flows along the axis canals of the Long Xuyen Quadrangle and a number of canals in the Can Tho and Hau Giang areas to supply the Ca Mau Peninsula area. The calculation results of the total average amount of water for many years are presented in Table 4.

Table 4. The total monthly average volume of water at the beginning of the main canals taking water from the Hau River to the SHRB (million m^3).

River	I	II	III	IV	V	VI	VII	VIII	IX	X	XI	XII	Average Drought season (I–VI)	Average year
Vinh Te	37.8	30.4	25.4	18.9	15.6	-10.0	-528.1	-2169.1	-3443.7	-3175.5	-1282.9	-202.6	**19.7**	**-820.3**
Muoi Chau Phu	9.9	6.9	5.6	4.2	3.6	6.4	9.6	14.9	16.3	6.9	5.7	10.0	**6.1**	**8.4**
Dao	9.2	6.4	5.1	3.8	3.5	4.8	-19.8	-73.8	-100.6	-114.4	-57.4	-7.2	**5.5**	**-28.4**
Can Thao	9.8	6.8	5.5	4.1	3.7	5.8	-6.1	-30.3	-44.8	-55.9	-29.0	2.0	**6.0**	**-10.7**
Chac Bang	-75.7	-61.5	-68.3	-65.8	-44.6	-49.0	-43.8	9.5	16.7	-39.9	-63.3	-79.8	**-60.8**	**-47.1**
No. 1	58.2	51.4	53.7	47.2	25.3	-5.4	-25.4	-29.4	-28.1	-21.7	21.1	49.1	**38.4**	**16.3**
Ba Chieu	32.7	23.6	20.1	15.9	10.2	11.5	19.1	47.8	79.7	74.5	49.8	39.5	**19.0**	**35.4**
Thom Rom	72.4	60.2	60.3	50.9	42.7	43.9	60.4	87.3	106.5	110.2	95.2	83.7	**55.1**	**72.8**
Thot Not	17.5	12.8	10.8	8.3	2.4	-0.5	-3.0	9.6	19.2	6.4	16.0	18.8	**8.6**	**9.9**
Chac Ca Dao	125.3	89.3	75.6	58.4	53.4	96.1	197.7	367.0	458.6	427.7	266.4	177.5	**83.0**	**199.4**
Tri Ton	95.4	67.8	56.5	42.5	37.3	68.2	105.5	172.4	216.5	160.8	89.7	103.1	**61.3**	**101.3**
Ba The	61.6	43.5	35.8	26.7	23.4	45.2	84.9	145.9	179.6	158.3	99.5	77.7	**39.4**	**81.9**
Tron	19.8	14.5	12.5	10.0	7.2	10.1	19.3	39.4	67.2	61.2	32.7	24.4	**12.4**	**26.5**
Nang Mau	8.8	7.0	6.3	5.6	1.8	0.2	-0.8	3.8	9.6	8.8	8.4	8.7	**5.0**	**5.7**
O Mon	122.7	92.5	84.3	71.6	44.3	46.7	73.5	152.8	214.8	198.1	175.5	148.6	**77.0**	**118.8**
Rach Gia Long Xuyen	22.9	20.6	18.4	15.3	5.6	-4.8	-43.4	-134.5	-190.6	-170.3	-58.5	4.0	**13.0**	**-42.9**
Dai Ngai	27.4	17.7	13.8	11.9	-4.0	-6.4	-0.3	13.7	32.7	22.0	32.7	32.6	**10.1**	**16.1**
Cai Con	36.6	21.4	11.9	4.6	-23.0	-26.8	-17.2	13.1	45.4	29.5	43.6	45.7	**4.1**	**15.4**
Mac Can Dung	14.2	9.3	7.6	5.9	5.3	10.0	29.1	74.4	102.4	82.3	40.2	22.6	**8.7**	**33.6**
Cai San	78.9	57.6	49.4	39.2	27.9	39.3	74.4	166.2	255.5	245.8	146.9	101.2	**48.7**	**106.8**
KH8	6.0	3.7	2.8	2.1	1.2	2.8	7.2	15.6	21.8	20.8	14.0	9.3	**3.1**	**8.9**
KH9	33.7	28.7	25.6	20.3	15.9	16.3	22.2	30.0	35.1	37.1	36.0	36.0	**23.4**	**28.1**

River	I	II	III	IV	V	VI	VII	VIII	IX	X	XI	XII	Average Drought season (I–VI)	Average year
Quan lo–Phung Hiep	-27.5	-22.7	-23.0	-17.0	-6.1	-0.8	7.9	14.4	10.3	-3.1	-21.2	-26.0	**-16.2**	**-9.6**
Quan lo–Phung Hiep	-13.2	-11.1	-11.5	-10.0	-4.7	1.9	6.1	7.6	4.5	3.1	-6.5	-12.8	**-8.1**	**-3.9**
Kien Hao	89.0	65.2	55.2	42.3	36.8	64.3	116.3	202.8	248.9	209.8	132.5	108.6	**58.8**	**114.3**
Can Tho	-77.9	-57.6	-50.4	-43.7	-11.6	-2.1	-1.7	-26.3	-55.8	-56.1	-74.5	-82.3	**-40.5**	**-45.0**
C. Lang thu 7	2.5	1.8	1.6	1.8	3.6	5.7	10.9	12.9	13.0	17.4	8.4	4.5	**2.9**	**7.0**
Total	**825.0**	**610.5**	**518.6**	**401.7**	**258.7**	**304.6**	**14.9**	**-1073.7**	**-1930.1**	**-1927.6**	**-317.6**	**705.2**	**486.5**	**-64.1**

3.2.2. The total amount of groundwater resources

The results of calculating the total amount of groundwater including saltwater and freshwater in the SHRB are shown in Table 5; and the results of the total amount of groundwater resources for freshwater are in Table 6. In which, the total amount of groundwater resources including freshwater and saltwater is 88.9 million m^3/day, of freshwater is 42.1 million m^3/day (accounting for 47% of the total water volume). Details of the modular map of the total exploitable amount of groundwater are shown in Figure 4.

Table 5. The total groundwater resources in the SHRB (saltwater and freshwater) (m^3/day).

Region	Total of saltwater and freshwater (m^3/day)							
	qh	**qp_3**	**qp_{2-3}**	**qp_1**	**n_{2-2}**	**n_{2-1}**	**n_{1-3}**	**Total**
N1	111278	1814233	3409345	2709881	1882600	2052550	810487	12790375
M3	198474	886165	1975837	1767120	2598646	2722782	1101243	11250267
L1	22060	386848	952755	920791	1181145	884639	227607	4575845
M1	8901	205623	384512	321012	113906	85908	0	1119862
M2	584084	1919270	5400694	4038280	5019888	6375347	899539	24237103
N4	372125	2966739	4375352	4605879	2190091	5230813	2122419	21863419
L2	226677	1130740	2309181	2056924	2772262	2927494	1657792	13081072
Total	**1523600**	**9309618**	**18807678**	**16419889**	**15758539**	**20279533**	**6819087**	**88917943**

Table 6. The total groundwater resources in the SHRB (freshwater) (m^3/day).

Region	Total of freshwater (m^3/day)							
	qh	**qp_3**	**qp_{2-3}**	**qp_1**	**n_{2-2}**	**n_{2-1}**	**n_{1-3}**	**Total**
N1	15373	144448	1081316	546536	302882	14920	810487	2915962
M3	43981	443337	1563195	1371107	930790	474414	1101243	5928067
L1	0	0	891581	767917	735450	464714	227607	3087267
M1	0	0	2282	0	0	0	0	2282
M2	0	0	3047078	2487622	1735494	1818395	991790	10080379
N4	310	1141842	3074336	2217133	850108	3723651	2122419	13129799
L2	0	189328	1856024	1067605	1032582	1169629	1657792	6972961
Total	**59663**	**1918955**	**11515812**	**8457920**	**5587306**	**7665723**	**6911338**	**42116717**

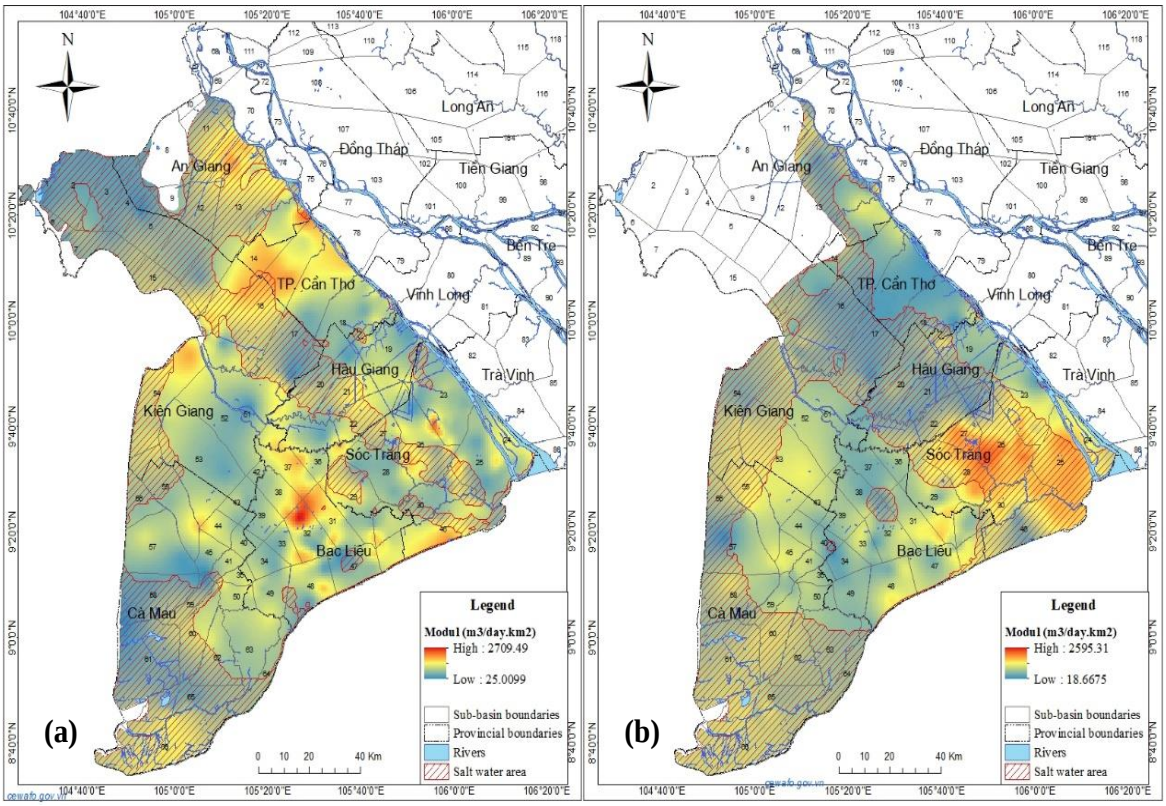

Figure 4. A modular map of total groundwater volume TCN qh(a) and qp3(b).

3.2.3. The amount of surface water transferred to the basin

The calculation results from the NAM model show that the total amount of surface water resources from endogenous rain in the above 66 sub–basins in the SHRB is 19.95 billion m^3. In which, the area M2 with 7.98 billion m^3 accounts for the largest proportion with 40% of the total water volume of the whole region; the area M1 has the lowest total amount of endogenous water from the rain with only 0.64 billion m^3 accounts for 3% of the total water volume of the whole region (Figure 5).

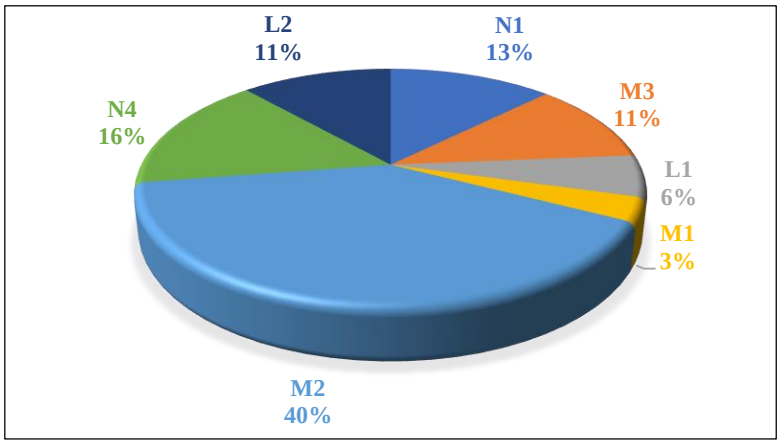

Figure 5. The percentage of total calculated water volume across regions.

Statistical data also show that there is a large difference in total water volume between the dry season and the flood season in the SHRB. Specifically, the amount of water volume in the dry season accounts for only 19% of the total annual water amount, equivalent to 3.8 billion m^3, while in the flood season, it accounts for 81% of the total annual water amount with a volume of 16.19 billion m^3 (Figure 6).

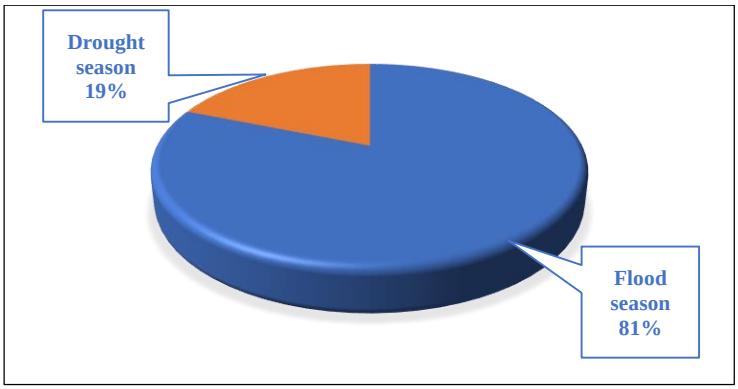

Figure 6. The percentage distribution of the total water volume in the dry–flood season in the region.

3.2. Result of index hierarchy

3.2.1. Index of total surface water resources

According to the viewpoint of the International Water Resources Association (IWRA), in the countries with average water resources, the average standardized amount of water is 10,000 m^3/person/year. Thus, the total water volume per capita of Vietnam is lower than the standard level; specifically, even if the calculation is taken the amount of endogenous water in the territory, each Vietnamese person will only have about 3,222 m^3/year. While nearly two–thirds of Vietnam's surface water flows from abroad, in the case that upstream countries do not have a fair share and reasonable use of water resources in inter–national rivers, Vietnam will face the risk of water crisis, which threatens its stable economic and social development, food security and water security [20–24].

Thus, if based on the viewpoint of the International Water Resources Association (IWRA), but now, if the total water resources per person of 3,222 m^3/year or more is considered sufficient, and the level below this threshold is considered a water shortage status, there is a hierarchy of sustainability levels. This study implemented a hierarchy of sustainability levels of total water according to the Falkenmark indicator. The levels of hierarchy are clearly shown in Table 7.

Table 7. The classification of total surface water resources index.

No.	Water level per capita	Rating of water resources
1	> 4000 m^3/person/year	Threshold of water sufficiency for using
2	1700–4000 m^3/person/year	The upper threshold of insufficiency when it happens sporadically or only locally
3	1000–1700 m^3/person/year	Water shortage threshold
4	500–1000 m^3/person/year	Threshold of water scarcity, restrictions on economic development, human health and social welfare
5	< 500 m^3/person/year	Life threatening threshold

3.2.2. Surface water quality index

There have been many in–depth studies on surface water quality index in the country and the world [25–26]. Almost studies have shown that the WQI surface water quality index hierarchies are representative and reliable. Since the research topic determines the index of sustainable use of water and land resources in the southern area of Hau River, the team focused on examining and evaluating the existing studies on the hierarchy of water quality indicators in the country.

Decision No.1460/QD–TCMT on the promulgation of Technical Guidelines for the calculation and publication of Vietnam's water quality index by the Vietnam Environment Administration has specified the method of calculating the water quality index as well as provided an assessment of water quality in the context of Vietnam. Therefore, the research team decided to choose the hierarchical level of water quality classification used in the study as the level given in Decision No. 1460/QD–TCMT.

Table 8. WQI Water Quality Index Hierarchy.

WQI Value	Rating of water quality	Color
91–100	Well–used for domestic water supply purposes	Blue
76–90	Used for domestic water supply purposes but need appropriate treatment measure	Green
51–75	Used for irrigation and other equivalent purposes	Yellow
26–50	Used for navigation and other equivalent purposes	Orange
0–25	Severely polluted water that needs future treatment measures	Red

In Table 8, the water quality index is calculated on a scale from 0 to 100 with five specific levels of assessment and alarming.

3.2.3. Index of the total amount of groundwater resources

This index can rank the degree of sustainability for potential reserves through the change in groundwater reserves per capita [7]. This index represents the change of the amount of groundwater resources (shown in potentially exploitable reserves) during the study period. The specific calculation formula is:

$$A = (Q_{kttn\ nc} - Q_{kttn\ nn})/Q_{kttn\ nn} \times 100 \quad (1)$$

where A is the level of change; $Q_{kttn\text{-}nc}$ is the potentially exploitable reserves per capita in the study period (m^3/day); $Q_{kttn\ nn}$ is the potentially exploitable reserves per capita over a period of many years (m^3/day).

The data on groundwater reserves over a period of many years were collected from reports on groundwater resources at the National Center for Water Resources Planning and Investigation. The population data were collected from the Statistical Yearbook in the SHRB. Figure 7 shows the variation of the parameter from the smallest to the largest range towards the mean value over a multi–year period for that parameter.

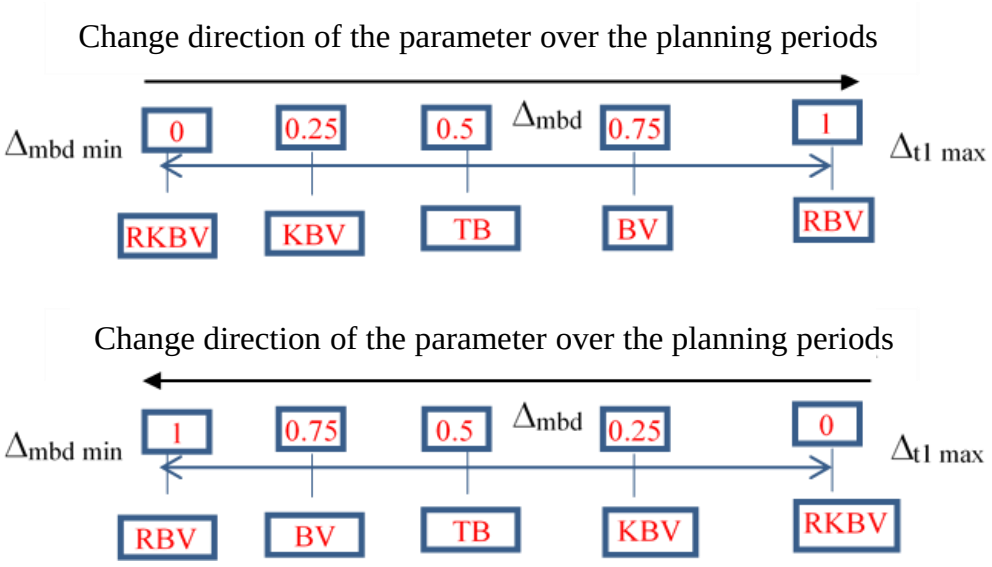

Figure 7. The hierarchy of the total groundwater resource index.

Abbreviated term: RKBV: very unsustainable; KBV: less sustainable; TB: average; BV: sustainable; RBV: very sustainable.

This "variable level" hierarchy was divided into 4 equal levels from the smallest to the largest with scores of 0.25, 0.5, 0.75, 1, respectively, depending on the specific value and the changing tendency of the parameters over the planning period to score the parameters. If this level of change achieves the "expected value" (that is the value of the parameter given in the planning period), that means the value is considered sustainable when it satisfies the needs and wants for the following years.

3.2.4. Groundwater quality index

According to Circular No. 19/2013–BTNMT dated July 18, 2013, regulating techniques for monitoring groundwater resources, types of groundwater quality samples include comprehensive analysis samples, iron samples, microscopic samples and samples with organic pollution origins and a number of other groundwater quality parameters. Since it is not possible to consider all the groundwater quality parameters within the scope of the study, only one representative parameter was selected to examine the level of groundwater quality change. Depending on the characteristics of groundwater resources of each specific study area, the appropriate representative parameters are determined. For the SHRB, the selected representative parameter was the pH index, since the pH data at the groundwater resource monitoring works are complete, easy to collect, measurable and able to demonstrate the sustainability of the groundwater quality. The pH is the acidity of the water, and the pH value is also the representation value for the presence of H+ ions in the groundwater environment. Water source with the pH > 7 often contains many carbonate and bicarbonate ions as it flows through many layers of limestone soil; Water source with the pH < 7 often contains many acid–based ions. If the pH is too small (below 6.0) or too large (above 8.5), health problems will occur, affecting daily life activities, irrigation, agriculture, fisheries... The most obvious evidence of the relationship between the pH and health is that a prolonged usage of water with high or low pH will cause growth retardation, stunting and susceptibility to disease for both humans and organisms. When the water has the pH > 8.5 with the presence of organic compounds, the disinfection with chlorine will form trihalomethane compounds that cause cancer. According to the standard, the pH of the water for domestic usage is 6.0–8.5 and that of drinking water is 6.5–8.5. Thus, if the pH parameter that is between 6.0 and 8.5 is considered to be sustainable; the pH that is either below 6.0 or above 8.5 is considered unsustainable. The groundwater quality index was also used a quantitative assessment method of water quality based on the RQ_2 ratio, which was calculated by the average concentration through the measured pH parameters over a period of many years and the pH level limit which is determined according to the national technical regulation on groundwater quality QCVN 09:2015–MT/BTNMT. If the RQ_2 coefficient is between 0.01 and 0.1, the groundwater quality is considered to be good. If the value of this ratio is greater than 1, it demonstrates that the quality of groundwater is poor, exceeding the allowable standard.

Table 9. The classification of groundwater index.

Index	Threshold	Score	Existing research
Ground water quality index	$RQ_2 \geq 1$	0.25	EPA [12]
	$0.5 \leq RQ_2 < 1$	0.50	
	$0.1 \leq RQ_2 < 0.5$	0.75	
	$0.01 \leq RQ_2 < 0.1$	1.00	

4. Conclusions

This study has conducted an overall water resources assessment for the SHRB as proposing a set of indicators of sustainable use of water and land resources. These indicators were estimated by using a range of the hydrological-hydraulic- and groundwater model.

- The set of indicators for sustainable use of water and land resources includes six indicators: (i) the total amount of surface water resources; (ii) the quality of surface water; (iii) total amount of groundwater resources; (iv) the groundwater quality; (v) the amount of surface water transferred to the basin; (vi) the natural cover index of the land.

- With a special geographical position, the hydrological regime in the SHRB is directly affected by the upstream flow. Therefore, the assessment of the quantity of surface water resources is very difficult, which causes big challenges for the planning of sustainable use of water resources in the region. It is also the reason why it is necessary to consider the groundwater reserve in the regional water resource allocation planning since this is an important source of water that can ensure the essential needs of water users.

- Within the scope of this study, we selected a number of indicators in the group of water resources assessment to conduct the pilot calculation for the SHRB. The results showed that the total amount of surface water from the Hau river supplying for the entire SHRB in the dry season months (I–VI) reached the average of about 487 million m^3/month; The total amount of groundwater including freshwater and saltwater is 35.5 million m^3/day, only 16.7 million m^3/day of freshwater; The total amount of surface water resources from endogenous rain in the SHRB is 19.95 billion m^3, of which that of the Ca Mau Peninsula area is 16.8 billion m^3, accounting for 84.2% of the total water volume of the whole region; The Long Xuyen Quadrangle area has the lowest total amount of endogenous water from the rain with only 3.15 billion m^3, accounting for 15.8% of the total amount for the whole region. There is a large difference in total water volume between the dry season and the flood season in the SHRB; in particular, the water volume in the dry season accounts for only 19% of the total water volume, equivalent to 3.8 billion m^3, while the water volume in the flood season accounts for 81% of the total water volume with a value of 16.19 billion m^3.

Although the models have been established to ensure the most reliable results for the years of calibration and verification, the errors in the calculation of water resources in the area are unavoidable as the direction of the flow is not clearly determined yet, the hydrological data is not long enough, it is not possible to ensure the appropriateness for the entire multi–year data series due to the fluctuations of the riverbed and reservoir topography, and the regulation and activity coordination process of irrigation works and canals in the region are still inadequate and difficult to control when the activity operations in many locations are still spontaneous. Therefore, in order to improve the quality of calculations, it is necessary to include the measured additional cross–sections for the hydraulic models of the flow and updated rules of reservoir operation and irrigation works in the area.

Author's contribution: Developing research ideas: L.T.M.V., B.T.B.N.; Selecting of research methods: L.V.M.V., B.T.B.N.; Collecting, analyzing, calculating and processing of data: Writing the draft paper: N.H.A., B.T.B.N., L.T.M.V., D.Q.T.; T.V.C; D.H.H; Editing the final paper: N.H.A., B.T.B.N., L.T.M.V., D.Q.T; L.M.H; T.V.H.

Acknowledgements: This study was funded by "Research on Integrated Indicators of sustainable use of water and land resources in the distribution of water resources in the South Hau River basin" - grand number: ĐL.CN–45/18. The authors also thank anonymous reviewers for their constructive comments

Disclaimer: The authors declare that this paper is the work of the research team, has not been published anywhere, and has not been copied from previous studies; there is no conflict of interest among the author group.

References

1. Chaves, H.M.L.; Alipaz, S. An integrated indicator based on basin hydrology, environment, life, and policy: The watershed sustainability index. *Water Resour. Manage.* **2007**, *21*, 883–895.
2. Catano, N.; Marchand, M.; Staley, S.; Wang, Y. Development And Validation Of The Watershed Sustainability Index (WSI) For The Watershed Of The Reventazón River, 2009, pp. 67.
3. Mititelu–Ionuș, O. Watershed Sustainability Index Development and Application: Case Study of the Motru River in Romania. *Pol. J. Environ. Stud.* **2017**, *26(5)*, 2095–2105.
4. Department of Water Resources Management. Report on Vietnam Water Sector Assessment Project, 2009.
5. Ministry of Natural Resources and Environment. Master plan for socio–economic development in the Red River Delta in the period 2010–2013, 2013.

6. Y, T.V.; Tri, N.D.; Can, L.T.; Chi, T.T.; Chinh, N.T.; Hau, N.X.; Hieu, N.V.; Tuan, D.Q.; Thinh, N.V.; Tuan, N.T.; Hennessy, J. Establishing a sustainable development indicator set including economic, social, and environmental fields in Tay Nguyen provinces. *VN J. Earth Sci.* **2014**, *36*, 241–251.
7. Hoan, H.V. Research on assessing the sustainability of groundwater resources in Ho Chi Minh City, Binh Duong and Dong Nai, 2012.
8. Van, L.T.M. Research on determining the sustainability index of the river basin and its pilot application in the Cau River basin. Ministry of Natural Resources and Environment, 2016.
9. Huong, H.T.L. Research on the scientific basis and propose solutions for integrated management of water resources in the Lo River basin. Hanoi Water Resources University, 2009.
10. Dung, N.K. Research on scientific and practical basis to determine content, methods of calculation, synthesis and statistics of water resource indicators, 2012.
11. Southern Institute of Water Resource Planning. The Mekong Delta Irrigation Master Plan in the context of climate change and sea–level rise, 2009.
12. Chuong, H.V.; Mai, L.Q. Evaluation of multi–criteria land for the development of land use types for rubber trees in the hilly areas of Huong Tra district, Thua Thien Hue province. *J. Soil Sci.* **2012**, *39*, 123–127.
13. Dinh, L.C. Integration of GIS and multi–criteria group decision analysis in land adaptation assessment. *J. Agric. Rural Dev.* **2011**, 82–89.
14. Trang, N.T.T. Research on sustainable land use in Ba Lat estuary area, Giao Thuy district, Nam Dinh province. Hanoi University of Agriculture, 2013.
15. Binh, N.V. Assessment of the current status to propose directions for sustainable agricultural land use in Huong Tra town, Thua Thien Hue province. Hue University, 2017.
16. Tuan, T.V.; Huan, N.C.; Thu, D.T.T.; Chinh, N.T.; Nhu, T.T.Q. Research and evaluation of land use system for sustainable agricultural land use planning (Case study: Dai Thanh commune, Quoc Oai district, Hanoi city). *VNU Sci. J. Earth Environ. Sci.* **2015**, *31*, 24–35.
17. Vietnam Mekong River Commission. Study of the Impacts of Hydroelectric Plants on the Mainstream of the Mekong River, Main Report, 2016.
18. Chinh, N.H. and et al. The results of groundwater monitoring in the Southern Delta in the National Monitoring Project – Southern Federation of Hydrogeology–Engineering Geology, 2000.
19. Dung, N.H. and et al. Project Result Report: N–Q stratigraphic division and study of the geological structure of the Southern Delta. General Department of Geology and Minerals of Vietnam, Archives Library of the Southern Federation of Hydrogeology–Engineering Geology, 2004.
20. Dung, N.Q. et al. Result Report: Result of water survey in the Remoted Southern region. General Department of Geology and Minerals of Vietnam, Archives Library of the Southern Federation of Hydrogeology– Engineering Geology, 2003.
21. DHI. Research Project on Impacts of Hydroelectric Plants on the Mainstream of the Mekong River, Volume 1–Model–Design and Simulation, 2016.
22. Vietnam Institute of Meteorology Hydrology and Environment. Impact of climate change on water resources and adaptation measures in the Mekong Delta, 2010.
23. Thai, T.H. Research on the effects of climate change on the change of water resources in the Mekong Delta, 2013.
24. Develop a plan for sustainable irrigation management in the Mekong Delta. Institute of Irrigation & Environment– University of Water Resources, 2013.
25. Report on the formulation of water resources planning tasks in the Mekong River Basin. National Center for Planning and Investigation of Water Resources, 2018.
26. Chaurasia, A.K.; Pandey, H.K.; Tiwari, S.K.; Prakash, R.; Pandey, P.; Ram, A. Groundwater Quality assessment using Water Quality Index (WQI) in parts of Varanasi District, Uttar Pradesh, India. Journal of the Geological Society of India, **2018**, *92(1)*, 76–82. https://doi.org/10.1007/s12594–018–0955–1.

Table of content